RTD-TDR-63-1049

SUMMARY REPORT
A RESEARCH STUDY TO ADVANCE THE STATE-OF-THE-ART OF SOLID PROPELLANT GRAIN DESIGN

TECHNICAL DOCUMENTARY REPORT NO. RTD-TDR-63-1049

OCTOBER 15, 1963

ROCKET RESEARCH LABORATORY
AIR FORCE SYSTEMS COMMAND
UNITED STATES AIR FORCE
EDWARDS, CALIFORNIA

PROJECT NO. 3059, TASK NO. 30531

(PREPARED UNDER CONTRACT NO. AF 33(616)-6530 BY
THIOKOL CHEMICAL CORPORATION, ELKTON DIVISION, ELKTON, MARYLAND)

SUMMARY REPORT
A RESEARCH STUDY TO ADVANCE THE STATE-OF-THE-ART OF SOLID PROPELLANT GRAIN DESIGN

TECHNICAL DOCUMENTARY REPORT NO. RTD-TRD-63-1049

OCTOBER 15, 1963

ROCKET RESEARCH LABORATORY
AIR FORCE SYSTEMS COMMAND
UNITED STATES AIR FORCE
EDWARDS, CALIFORNIA

PROJECT NO. 3059, TASK NO. 30531

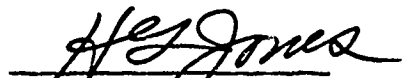

H. G. Jones
General Manager

(PREPARED UNDER CONTRACT NO. AF 33(616)-6530 BY
THIOKOL CHEMICAL CORPORATION, ELKTON DIVISION, ELKTON, MARYLAND)

SUMMARY REPORT
A RESEARCH STUDY TO ADVANCE THE STATE-OF-THE-ART OF SOLID PROPELLANT GRAIN DESIGN

TECHNICAL DOCUMENTARY REPORT NO. RTD-TDR-63-1049

OCTOBER 15, 1963

ROCKET RESEARCH LABORATORY
AIR FORCE SYSTEMS COMMAND
UNITED STATES AIR FORCE
EDWARDS, CALIFORNIA

PROJECT NO. 3059, TASK NO. 30531

H. G. Jones
General Manager

(PREPARED UNDER CONTRACT NO. AF 33(616)-8530 BY
THIOKOL CHEMICAL CORPORATION, ELKTON DIVISION, ELKTON, MARYLAND)

FOREWORD

This report has been prepared by the Elkton Division of Thiokol Chemical Corporation for the Air Force Systems Command, Rocket Propulsion Laboratory (DGSMD), at Edwards, California. Lt. Harold W. Gale is the Air Force Project Officer.

The report number assigned to this document by Thiokol Chemical Corporation is E92-63. The principal contributors to this report are Messrs. W. G. Andrews, D. H. Frederick, F. E. Moore, D. Saylak, A. Stornelli, D. D. Thomas, and R. H. Thompson. Mr. James F. Hoebel is the Program Manager.

ABSTRACT

The work conducted under Contract AF 33(616)-6530 during the period from July 1, 1962, to July 31, 1963, is reported. This program was a research study to advance the state-of-the-art of solid propellant grain design and consisted primarily of theoretical and applied analyses of solid propellant grain designs. Heat transfer factors, effect of strain on burning rate, and analyses of propellant stresses were specifically considered.

An analytical study was undertaken to develop a two-dimensional heat transfer analysis for solid propellant motors subjected to a nonlinear circumferentially variant and time dependent, external thermal environment, including convection, radiation, or known heat flux, or any combination of these.

Finite difference equations representing the irregular external boundary condition, the temperature of the case, the case-propellant interface, the propellant interior points, and the heat flow across the irregular internal boundary were developed. These equations were programmed and incorporated into a numerical solution. The program further considers temperature dependent thermal properties and the internal heat generation due to the exothermic polymerization reaction of propellant.

A study was performed to evaluate the apparent approaches to solid propellant grain design through digital techniques and then to implement the best approach into a FORTRAN language computer program. The Elkton-Moore Method, a vectorial approach to the geometrical portion of the problem, was conceived and developed and

has served as the theoretical base for the Advanced Grain Design Analysis program. Program AGDA evaluates motors with arbitrary center perforations, with or without head- and aft-end webs, and, in addition, considers two-dimensional temperature variations existing in the grain and accounts for their effect on propellant burning rate. Motors are described to the program in terms of readily available parametric values, which are the standard configuration dimensions stated on all fully loaded case drawings.

Four propellants, including two hydrocarbons, one polyurethane, and a polyvinyl plastisol type, were subjected to tensile strains ranging from 0 to 12 percent and burned in the strained condition in a strand burner at pressures ranging from 500 to 1500 psi. Results established that not all propellants are affected to the same degree by strain. A correlation between percent change in burning rate and volumetric change index is given. The latter term is a representation of the departure from incompressibility that the material experiences due to strain. To achieve these data, an optical technique for measuring Poisson's ratio was developed and is described in this report. In addition to linear burning rate, the mass burning rate of the four propellants was investigated.

A study was undertaken to find a method by which the effects of internal pressurization thermal shrinkage, and axial acceleration loads upon propellant structural stability could be determined. Nominal effort was expended in specifying a means for analytically characterizing the viscoelastic properties of a solid propellant by means of linear differential operators and the time dependent elastic modulus, E(t). The method and its

accuracy are illustrated. Major effort was directed toward the development of a technique for structurally analyzing axisymmetric grains having arbitrary end geometries and straight-through ports. The analysis is formulated in terms of two stress functions, ϕ and ψ, and a coupled pair of elliptic partial differential equations. The pertinent boundary conditions are specified, the solution by means of finite difference equations is outlined, and a corresponding computer program is discussed.

HEADQUARTERS
AIR FORCE FLIGHT TEST CENTER
AIR FORCE SYSTEMS COMMAND
UNITED STATES AIR FORCE
EDWARDS AIR FORCE BASE, CALIFORNIA 93523

REPLY TO
ATTN OF: FTKR-2/M.J. Brown/30411

SUBJECT: Contract AF 33(616)-6530

TO: Thiokol Chemical Corporation
Elkton Division
Attn: C. W. Kramer
Elkton, Maryland

The final report under the above contract is approved for publication and distribution in accordance with the terms of the contract, subject to the minor changes requested by the Project Officer at the 21 August review.

MARION J. BROWN
AF Contracting Officer
Directorate of Procurement

Copy to: PACMD (REHPAC-2)

OCT 7 1963

TABLE OF CONTENTS

		Page
I.	INTRODUCTION	1
II.	HEAT TRANSFER ANALYSIS	4
	A. Two-Dimensional Heat Transfer Analysis	4
	B. Advanced Grain Design Analysis-Program AGDA	35
III.	EFFECTS OF STRAIN ON BURNING RATE	98
IV.	PROPELLANT SLUMP ANALYSIS	139
	A. Characterization of Propellant Time-Dependent Material Properties	140
	B. Stress Analysis of Axisymmetric Grain Designs having Arbitrary End Geometries and Straight-Through Ports	151
V.	CONCLUSIONS AND RECOMMENDATIONS	192
REFERENCES		198
DISTRIBUTION LIST		200

LIST OF APPENDIXES

I. Two-Dimensional Heat Transfer Program

- A. Glossary
- B. List of Functions and Subroutines (Transfer Vector) used by Two-Dimensional Heat Transfer
- C. Card Input Format (Two-Part Program)
- D. Flow Charts
- E. Input Format (Revised Input for One-Part Loading when Grid Size is within Specified Limitations)

II. Elliptical Case, Constant Web

III. Pictorial Representation of the Insignificance of Surface Normal Bending Resulting from a Nonuniform Grain Temperature

IV. Determination of Linear Viscoelastic Model Constant from Uniaxial Creep and Stress Relaxation Tests

LIST OF ILLUSTRATIONS

		Page
1.	Propellant Interior Nodal Point	8
2.	Outer Surface Nodal Point	13
3.	Case-Propellant Interface Point	14
4.	Typical Internal Boundary Nodal Point	18
5.	Segment of Grain With Partial Grid Illustrating Typical Nodal Points	21
6.	Nodal Network and Boundary Conditions for Test Case 1	25
7.	Nodal Network and Boundary Conditions for Test Case 2	26
8.	Nodal Network and Boundary Conditions for Test Case 3	27
9.	Nodal Network and Boundary Conditions for Test Case 4	28
10.	Temperature Distribution Through Grain After 12 Hours for Test Case 2	30
11.	Temperature Distribution Through Grain After 12 Hours for Test Case 3	31
12.	Isotherm Plot for Test Case 4	32
13.	Nodal Network for 180° Star Grain Configuration	34
14.	Isotherm Plot for 180° Star Configuration (Adiabatic Internal Boundary)	36
15.	Isotherm Plot for 180° Star Configuration (Heated Internal Boundary)	37
16.	Isotherm Plot for 180° Star Configuration (Cooled Internal Boundary)	38

LIST OF ILLUSTRATIONS (Continued)

		Page
17.	Random Collection of Rocket Motors Amenable to Straightforward Solution by Program AGDA	40
18.	Typical Rocket Motor Evaluated by Program AGDA	41
19.	Simplified Computer Program Flow Chart	43
20.	Grain Representation	48
21.	Sample Element of Grain	48
22.	Volume Element	52
23.	Calculation of Elemental Surface and Volume for Various "End" Conditions	53
24.	Representation of a Shell Within the Grain	56
25.	Comparison of Elemental Surface Regression Between Uniform and Nonuniform Temperature Grains	60
26.	Simplified Program AGDA	62
27.	Program AGDA with Variable Temperature	64
28.	Schematic Diagram of a Rocket Motor Illustrating Complete Program Capabilities	66
29.	Example of a Typical Pseudo-Rectangular Grid	68
30.	The AGDA Input Generator Considers Any of These Three Half Star Point Cross Sections	70
31.	Schematic Representation of Cross Sections of Generalized Solid Propellant Rocket Amenable to Solution with AGDA Showing Required Input Parameters	71
32.	AGDA Input Data Sheet	73
33.	Schematic of Solid Propellant Rocket Motor for Which Full Computer Output is Presented in Tables II - XI	78

LIST OF ILLUSTRATIONS (Continued)

		Page
34.	Location within a Solid Propellant Rocket Motor of the Periphery Points	90
35.	Definition of Normals $\vec{S}$ and $\vec{H}$ Together With Their Associated Angles	91
36.	Grain Temperature Profile Used in the Variable Temperature Test Case	93
37.	Comparison of Solutions, Grain Temperature Test Cases	96
38.	Propellant Strand Burner	103
39.	Method of Preparing Strained Propellant Strands	105
40.	Test Jig for Nonuniform Strain Versus Burning Rate Test	107
41.	Window Bomb Internal Assembly	108
42.	Window Bomb Test Arrangement	109
43.	Apparatus for Measuring Cross Sectional Area of a Specimen During a Tensile Test	111
44.	Linear Burning Rate Versus Pressure	124
45.	Mass Burning Rate Versus Pressure	131
46.	Poisson's Ratio Versus Strain	133
47.	n-Element Wieckert Model	142
48.	Input Strain Versus Time	144
49.	Relaxation Modulus Versus Log (Time), TP-H-1011	147
50.	Relaxation Modulus Versus Log (Time), TP-H-1011	148
51.	Relaxation Modulus Versus Log (Time), TP-H-1011	149
52.	Stress Versus Log (Time), TP-H-1011	150

LIST OF ILLUSTRATIONS (Continued)

		Page
53.	Axial Cross Section of Cylindrical Grain with Arbitrary Head and Aft End	154
54.	Nondimensional Coordinate System	155
55.	Finite Difference Molecule	161
56.	Irregular Interior Nodes	163
57.	Cylindrical Grain with Fully Loaded Head End and Conical Aft End	167
58.	Axial Cross Section of Fully Loaded Cylindrical Grain with Arbitrary Head and Aft End	168
59.	Nondimensional Coordinate System	169
60.	Irregular Interior Nodes	170
61.	Block Diagram - Stress Analysis of Axisymmetric Grain Designs Having Arbitrary End Geometries and Straight-Through Ports	184

LIST OF TABLES

		Page
I.	Input Data Quantities Required by the AGDA Input Generator	72
II.	Reproduction of Input Data to Program AGDA for Rocket Shown in Figure 33	80
III.	Reproduction of AGDA "Point Periphery Tape" Output	81
IV.	Reproduction of Page 2 of AGDA "Point Periphery Tape" Output	82
V.	Reproduction of Page 3 of AGDA "Point Periphery Tape" Output	83
VI.	Check Results	84
VII.	Page 1 of Summarization of Program AGDA Output	85
VIII.	Page 2 of Summarization of Program AGDA Output	86
IX.	Page 3 of Summarization of Program AGDA Output	87
X.	Page 1 of New Program AGDA Output	88
XI.	Page 2 of New Program AGDA Final Output	89
XII.	Final Page of Output, Test Case 1	94
XIII.	Computer Output for Variable Temperature Test Case	95
XIV.	Burning Rate of Hydrocarbon "A" (0% Strain)	113
XV.	Burning Rate of Hydrocarbon "A" (4% Strain)	114
XVI.	Burning Rate of Hydrocarbon "A" (8% Strain)	115
XVII.	Burning Rate of Hydrocarbon "A" (12-1/2% Strain)	116

LIST OF TABLES (Continued)

		Page
XVIII.	Burning Rate of Polyurethane Propellant (0% Strain)	117
XIX.	Burning Rate of Polyurethane Propellant (10% Strain)	118
XX.	Linear Burning Rate of Hydrocarbon "B" (Mod) (0% Strain)	119
XXI.	Linear Burning Rate of Hydrocarbon "B" (Mod) (5% Strain)	120
XXII.	Linear Burning Rate of Hydrocarbon "B" (Mod) (10% Strain)	121
XXIII.	Burning Rate of Plastisol Propellant (0% Strain)	122
XXIV.	Burning Rate of Plastisol Propellant (10% Strain)	123
XXV.	Mass Burning Rate Versus Strain, Hydrocarbon "A"	127
XXVI.	Mass Burning Rate Versus Strain, Polyurethane Propellant	128
XXVII.	Mass Burning Rate Versus Strain, Hydrocarbon "B" (Mod)	129
XXVIII.	Mass Burning Rate Versus Strain, Plastisol Propellant	130
XXIX.	Poisson's Ratio Versus Strain	134

LIST OF SYMBOLS

Area A - Heat Transfer Analysis

T	Temperature, °R
θ	Time, hours
K	Thermal Conductivity, BTU/hr-ft-°R
ρ	Density, lb/ft^3
C_p	Specific Heat at Constant Pressure, BTU/lb-°F
$\dot{q}$	Internally Generated Heat, BTU/lb-hr
Q	Heat of Polymerization per Unit Mass, BTU/lb-hr
P	Polymer Fraction
R	Gas Constant
B, A, n	Empirical Constants
r, ϕ	Polar Coordinates
Δ	Finite Difference
h_o	Outer Boundary Film Coefficient, $BTU/hr\text{-}ft^2\text{-}°R$
$\mathcal{F}$	Gray-Body Shape Factor (Dimensionless)
E	Heat Flux per Unit Time, $BTU/hr\text{-}ft^2$
σ	Stephan Boltzman Constant, $BTU/hr\text{-}ft^2\text{-}°R^4$
T_{conv}	Environmental Convective Temperature, °R
T_{os}	Outer Surface Temperature, °R
T_{rad}	Environmental Radiant Temperature, °R
h_i	Internal Boundary Film Coefficient, $BTU/hr\text{-}ft^2\text{-}°R$

LIST OF SYMBOLS (Continued)

T_c	Internal Environmental Temperature, °R
T_{is}	Internal Surface Temperature, °R
T_{if}	Propellant-Case Interface Temperature
n	Direction Normal to Internal Boundry

Subscripts

j	r
k	ϕ
j+1	$r + \Delta r$
j-1	$r - \Delta r$
k+1	$\phi + \Delta\phi$
k-1	$\phi - \Delta\phi$
1	forward difference
2	backward difference

Area B - Effects of Strain on Burning Rate

A	Cross Sectional Area, $in.^2$
L	Length, in.
L_o	Original Length, in.
r	Linear Burning Rate, in./sec
r_c	Linear Burning Rate in Unstrained Condition, in./sec
V	Volume, $in.^3$

LIST OF SYMBOLS (Continued)

V_o	Original Volume, $in.^3$
W	Width, in.
W_o	Original Width, in.
$\dot{w}$	Mass Burning Rate, lb/sec
$\dot{w}_o$	Mass Burning Rate in Unstrained Condition, lb/sec
α	Principal Extension Ratio $(1 + \epsilon_1)$
ϵ	Strain, in./in.
ϵ_1	Longitudinal Strain, in./in.
ϵ_2	Lateral Strain, in./in.
ν	Poisson's Ratio, in./in.
ν_i	Poisson's Ratio, Incompressible Material,
ρ	Density, $lb/in.^3$

Area C - Propellant Slump Analysis

(r, θ, z)	Cylindrical Coordinates
(ρ, θ, η)	Dimensionless Cylindrical Coordinates
u	Radial Displacements, in.
u_ρ	Radial Displacement, (dimensionless)
w	Axial Displacement, in.
u_η	Axial Displacement (dimensionless)

LIST OF SYMBOLS (Continued)

σ_r	Radial Stress, psi
σ_ρ	Radial Stress (dimensionless)
σ_z	Axial Stress, psi
σ_η	Axial Stress (dimensionless)
σ_θ	Tangential Stress, psi
σ_ϑ	Tangential Stress (dimensionless)
τ_{rz}	Shear Stress, psi
$\tau_{\rho\eta}$	Shear Stress (dimensionless)
ϵ_r	Radial Strain, in./in.
ϵ_ρ	Radial Strain (dimensionless)
ϵ_z	Axial Strain, in./in.
ϵ_η	Axial Strain (dimensionless)
ϵ_θ	Tangential Strain, in./in.
ϵ_ϑ	Tangential Strain (dimensionless)
γ_{rz}	Shear Strain, in./in.
$\gamma_{\rho\eta}$	Shear Strain (dimensionless)
δ	Liner Coefficient of Thermal Expansion, in./in.
Ξ	Acceleration Constant
f_z	Body Force, Mass Density x Acceleration in "g," lb/in.^{3}
ϕ, Φ	Stress Functions
Ψ, ψ	Stress Functions

LIST OF SYMBOLS (Continued)

l	Length of Cylinder, in.
a	Port Radius, in.
b	Case Radius, in.
c	Minor Axis of Elliptical Case Equation (head), in.
d	Minor Axis of Elliptical Case Equation (aft), in.
H	$\frac{c + 1}{b}$
E	Elastic Modulus, psi
ν	Poisson's Ratio
α	$\frac{a}{b}$
γ	$\beta \div H$
κ	d/b
s	Arc Length
h	Nodal Dimension
$P_i(z)$	Internal Pressure, psi
$\pi_i(n)$	Normal Surface Force (dimensionless)
$f_1(n)$	Equation of Case (aft)
$f_2(n)$	Equation of Case (head)
X	$X'(\rho,\eta)$
A	Irregular Nodal Dimension, % h
B	Irregular Nodal Dimension, % h
C	Irregular Nodal Dimension, % h
K_i	Constants
K_i^*	Constants

I. INTRODUCTION

This Summary Report is submitted in partial fulfillment of continuation studies under Contract AF 33(616)-6530, Supplement No. 4, Project 3059, Task 30831, "A Research Study to Advance the State-of-the-Art of Solid Propellant Grain Design." Effort on this contract supplement was initiated on July 1, 1962, and was terminated on July 31, 1963. This report summarizes the results of work performed during this period.

The work performed under Contract AF 33(616)-6530 has been continuing since May 1959. Previous reports under this contract that have been published and distributed in accordance with SPIA or CPIA listings are identified below:

Report Title	Thiokol Report Number	Period Covered
Quarterly Report No. 1	E248-59A	May 1959 to Aug 1959
Quarterly Report No. 2	E299-59	Aug 1959 to Nov 1959
Quarterly Report No. 3	E40-60	Nov 1959 to Feb 1960
Quarterly Report No. 4	E132-60	Feb 1960 to May 1960
Quarterly Report No. 5	E181-60	May 1960 to Aug 1960
Interim Summary Report	E217-60	May 1959 to Dec 1960
Quarterly Report No. 6	E99-61	March 1961 to June 1961
Quarterly Report No. 7	E156-61	June 1961 to Sept 1961
Quarterly Report No. 8	E11-62	Sept 1961 to Dec 1961
Annual Summary Report	E70-62	March 1961 to March 1962

Report Title	Thiokol Report Number	Period Covered
Quarterly Report No. 1 (9)	E173-62	July 1962 to Oct 1962
Quarterly Report No. 2 (10)	E13-63	Oct 1962 to Jan 1963
Quarterly Report No. 3 (11)	E74-63	Jan 1963 to April 1963

The objective of this program has been to advance the state-of-the-art of solid rocket propellant grain design from a thermal-structural as well as a ballistic standpoint. Previous studies under this contract have included:

1) The development of an IBM-650 computer program to compute theoretical burning surface area as a function of time.

2) The adaptation of photoelastic principles to determine experimentally strains in scale rocket grains under thermal loading.

3) The development of an analytical method of calculating the temperature at any point in a rocket grain subjected to motor curing, environmental conditioning, or aerodynamic heating.

4) A mathematical study of the combined internal and external loads imposed on a system of concentric elastic cylinders to determine the contribution of the propellant to the reduction of the effect of chamber pressure on the motor case wall.

5) The development of a generalized three-dimensional computer program to evaluate the ballistic properties of internal burning, singly connected solid propellant grains, including consideration of head- and aft-end web effects on the burning surface.

6) The development and application of the PhotoStress technique as a two-dimensional experimental method for propellant strain analysis through the extension of the previous photoelastic studies. This effort at Thiokol-Elkton represented the first application of the PhotoStress technique to solid propellant grains in the industry.

7) The analysis of the effect of propellant defects on ballistic performance through window bomb and motor tests. High-speed motor pictures were utilized to analyse the effects.

8) A heat transfer analysis in which numerical and electrical analog techniques were used to simulate the thermal conditioning history of a motor grain.

The current program has been divided into three interdependent areas of investigation. Each area is described in separate sections of this report:

- Area A - Heat Transfer Analysis
- Area B - Effect of Strain on Burning Rate
- Area C - Propellant Slump Analysis

II. HEAT TRANSFER ANALYSIS

A. TWO-DIMENSIONAL HEAT TRANSFER ANALYSIS

The application of solid propellant rocket motors to system requirements where the motor is subjected to nonuniform environmental conditions, either natural or induced, leads to many complex problems not easily solved by routine techniques. For example, a mission may be undertaken where the vehicle is subjected to heating on a portion of the circumference and cooling on the remaining portion depending upon the attitude of the system with respect to the sun, or where variations in the angle of attack may cause circumferential variations in aerodynamic convective heating. Alternatively, a propulsion system nestled on the side of a larger vehicle could well be subjected to aerodynamic or radiation heating on a portion of the body and conductive cooling on the alternate side. These and other possible missions naturally lead to grain environments and associated effects upon performance, both structural and ballistic, which previously were not traceable because of the complexity of the problem.

Previous efforts under the original Air Force Contract AF 33(616)-6530 resulted in the development of a two-dimensional (r, ϕ) thermal analysis for solid propellant grains subjected to a uniform external environment. This analysis has been extended under continued Air Force support to consider nonlinear circumferentially variant and time dependent boundary conditions having environmental temperatures, film coefficients, and other pertinent thermal parameters of arbitrary magnitude.

Further, the analysis will consider the internal heat generation within the propellant due to polymerization. Thus, the analysis will provide the capability to predict adverse temperature gradients due not only to environment but also to curing.

The solution within the analysis to the two-dimensional temperature field existing in a circular grain having a star or similar irregular internal perforate and subjected to a nonlinear external boundary condition is obtained through the use of finite difference techniques. Having represented the heat conduction equation and boundary functions in finite difference notation, the solution is obtained by "marching out" in finite time steps from a specified initial thermal configuration to the time at which the temperature profile through the grain is desired. With each time step thermal properties and boundary parameters are adjusted for the change in time and temperature.

This solution was programmed for the IBM-7070 digital computer in the FORTRAN II language.

1. The Heat Conduction Equation

The transient temperature field in a solid having a circular cross section, variable thermal properties, and internal heat generation may be expressed by the following partial differential equation:

$$\frac{\partial T}{\partial \theta} = \frac{1}{\rho C_p}\left[\frac{\partial K}{\partial r}\frac{\partial T}{\partial r} + \frac{1}{r^2}\frac{\partial K}{\partial \phi}\frac{\partial T}{\partial \phi}\right] + \frac{K}{\rho C_p}\left[\frac{\partial^2 T}{\partial r^2} + \frac{1}{r}\left(\frac{\partial T}{\partial r}\right) + \frac{1}{r^2}\frac{\partial^2 T}{\partial \phi^2}\right] + \frac{\dot{q}}{C_p} \qquad (1.1)$$

where

T = Temperature, °R

θ = Time, hr

K = $K(T)$ = Thermal Conductivity, BTU/hr-ft-°R

ρ = Density, lb/ft^3

C_p = $C_p(T)$ = Specific Heat at Constant Pressure, BTU/lb-°R

r = Radial Coordinate, in.

ϕ = Angular Coordinate, radians

The internally generated heat $\dot{q}$ is considered for this analysis to be the exothermic heat of polymerization experienced within a solid propellant grain during curing. This may be expressed as

$$\dot{q} = Q\left[B(1-P)^n \exp(-A/RT)\right] \text{ BTU/lb-hr} \qquad (1.2)$$

where

Q = Heat of polymerization per unit mass BTU/lb-hr.

P = Polymer Fraction

R = Gas Constant

B, A, n = Empirical Constants

To account for the extremes of thermal environment experienced by solid propellant rocket motors and to permit more accurate representation of thermal properties, both the thermal conductivity, K, and specific heat, C_p, are considered to be functions of temperature of the following form

$$f(t) = A + BT + CT^2 + DT^3 + ET^4 \qquad (1.3)$$

where each parameter has a separate set of coefficients. This will provide for an extreme variation in thermal properties with temperature.

In order to compensate for the variation in thermal properties during cure, a relationship between cure temperature and the necessary parameters must be obtained experimentally.

Having defined at this point the analytical expression for the heat conduction within the propellant, equation 1.1 can now be expressed in finite difference notation for the single nodal point illustrated in Figure 1. This produces the following relationship in accordance with technique outlined in the literature.[1,2]

$$\frac{T'_{j,k} - T_{j,k}}{\Delta\theta} = \frac{1}{\rho C_p}\left\{\left[\left(\frac{K_{j+1,k} - K_{j-1,k}}{\Delta r_1 + \Delta r_2}\right)\left(\frac{T_{j+1,k} - T_{j,k}}{\Delta r_1} + \frac{T_{j,k} - T_{j-1,k}}{\Delta r_2}\right)\right.\right.$$

$$\left.+\left(\frac{K_{j,k+1} - K_{j,k-1}}{r_j^2\,(\Delta\phi_1 + \Delta\phi_2)}\right)\left(\frac{T_{j,k+1} - T_{j,k}}{\Delta\phi_1} + \frac{T_{j,k} - T_{j,k-1}}{\Delta\phi_2}\right)\right] +$$

$$\left[\left(K_{j+1,k} - K_{j-1,k}\right)\left(\frac{\dfrac{T_{j+1,k} - T_{j,k}}{\Delta r_1} - \dfrac{T_{j,k} - T_{j-1,k}}{\Delta r_2}}{\Delta r_1 + \Delta r_2}\right)\right. \qquad (1.4)$$

$$+\left(\frac{K_{j+1,k} + K_{j-1,k}}{4\,r_{j,k}}\right)\left(\frac{T_{j+1,k} - T_{j,k}}{\Delta r_1} + \frac{T_{j,k} - T_{j-1,k}}{\Delta r_2}\right) +$$

$$\left.\left.\left(\frac{K_{j,k+1} + K_{j,k-1}}{r_{jk}^2}\right)\left(\frac{\dfrac{T_{j,k+1} - T_{j,k}}{\Delta\phi_1} - \dfrac{T_{j,k} - T_{j,k-1}}{\Delta\phi_2}}{\Delta\phi_1 + \Delta\phi_2}\right)\right] \right.$$

$$\left. + \rho Q\left[B(1-P)^n \exp\left(-A/\mathcal{R}T_{j,k}\right)\right]\right\}$$

A-6559

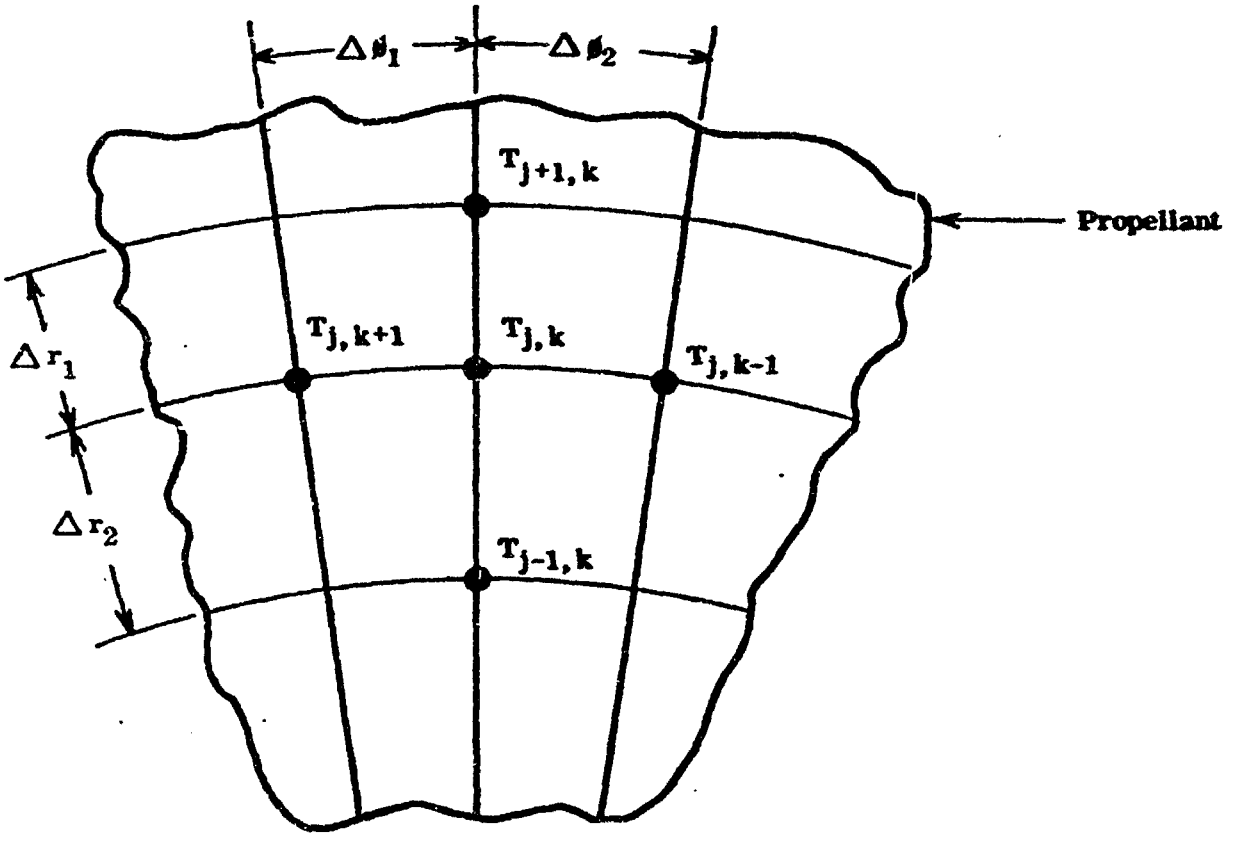

FIGURE 1. PROPELLANT INTERIOR NODAL POINT

where

$T'_{j,k} = T(r, \phi, \theta + \Delta\theta)$

$T_{j,k} = T(r, \phi, \theta)$

$T_{j+1,k} = T(r + \Delta r, \phi, \theta)$

$T_{j,k+1} = T(r, \phi + \Delta\phi, \theta)$

$T_{j,k-1} = T(r, \phi - \Delta\phi, \theta)$

$T_{j-1,k} = T(r-\Delta r, \phi, \theta)$

Δr_1 and $\Delta\phi_1$ = Forward differences in r and ϕ respectively

Δr_2 and $\Delta\phi_2$ = Backward differences in r and ϕ respectively

While this equation primarily represents an energy balance for an internal node it is, at the same time, the basic relationship for the analysis. By making appropriate substitutions within this equation and by performing certain necessary adjustments, this relationship can be adapted to satisfy the following nodal points within the grain as well:

1) External surface

2) Case-propellant interface

3) Internal surface

To illustrate the manner in which this is performed, each of the above will be discussed separately.

2. External Surface Nodal Point

The boundary condition at the outer surface of the grain resulting from

the external environment to which the motor is exposed is considered to be any combination of convection, radiation, or known flux. Since the outer boundary is circular, the heat flow into or from the motor may be expressed in terms of the radial gradient at the surface alone.

Thus

$$\frac{\partial T}{\partial r} = \frac{h_o}{K} (T_{conv} - T_{os}) + \frac{\mathcal{F}\sigma}{K} (T_{rad}^4 - T_{os}^4) + \frac{E}{K} \qquad (1.5)$$

where

h_o	=	$h_o(\phi,\theta)$	=	Outer Boundary Film Coefficient, BTU/hr-ft^2-°R
$\mathcal{F}$	=	$\mathcal{F}(\phi,\theta)$	=	Gray-Body Shape Factor (Dimensionless)
E	=	$E(\phi,\theta)$	=	Heat Flux per Unit Time, BTU/hr-ft^2
σ	=	Stephan Boltzmann Constant, BTU/hr-ft^2-°R^4		
T_{conv}	=	$T_{conv}(\phi,\theta)$	=	Environmental Convective Temperature, °R
T_{os}	=	$T_{os}(\phi,\theta)$	=	Outer Surface Temperature, °R
T_{rad}	=	$T_{rad}(\phi,\theta)$	=	Environmental Radiant Temperature, °R

To simulate a nonlinear circumferentially variant, external environment, about all or a portion (thermally symmetric) of the motor, each of the principal boundary parameters, h_o, $\mathcal{F}$, T_{conv} T_{rad}, and E, are considered to be functions of angular position ϕ of the following form

$$f(\phi) = a + b\phi + c\phi^2 + d\phi^3 + e\phi^4 + f \sin\phi + g \cos\phi \qquad (1.6)$$

Each parameter naturally has a separate set of coefficients. Furthermore, to give added versatility, the outer surface of the motor may be divided into two separate "zones" for which each boundary parameter may have a different functional relationship. Thus, for example, a particular motor may have the following circumferential variation in external film coefficient.

$$\underline{\text{Zone I}} \qquad \phi = \phi_0 \text{ to } \phi_1$$

$$h_{o_I} = a_I + b_I \phi + c_I \phi^2$$

$$\underline{\text{Zone II}} \qquad \phi = \phi_1 \text{ to } \phi_2$$

$$h_{o_{II}} = a_{II} + g_{II} \cos \phi$$

To permit the external environment to be time dependent, the coefficients of each boundary parameter function, $f(\phi)$, are considered to be functions of time.

This is accomplished within the analysis and resulting computer program by establishing a table for each boundary parameter with ten time entries for each coefficient. This is illustrated below.

Time	$f(\phi)$						
θ min.	$[h_o, \mathcal{F}, E, T_{conv}; T_{rad}]$ a	b	c	d	e	f	g
θ_1	a_1	b_1	c_1	d_1	e_1	f_1	g_1
θ_2	a_2	b_2	c_2	d_2	e_2	f_2	g_2
.	.	.	.	.	.	.	.
.	.	.	.	.	.	.	.
.	.	.	.	.	.	.	.
θ_{10}	a_{10}	b_{10}	c_{10}	d_{10}	e_{10}	f_{10}	g_{10}

Intermediate values of the coefficient, and, consequently, the boundary parameters would be obtained by linear interpolation. Likewise, separate tables are permitted for each "zone."

Having defined the manner in which the external boundary conditions are simulated, the finite difference equation for the gradient at the outer surface can be written as follows:

$$\frac{T_{j+1,k} - T_{j,k}}{\Delta r_1} = \frac{h_o}{K_{j,k}} (T_{conv} - T_{os}) + \frac{\mathcal{F}\sigma}{K_{j,k}} (T_{rad}^4 - T_{os}^4) + \frac{E}{K_{j,k}} \qquad (1.7$$

Substituting this relationship into the basic equation 1.1, with $T_{j,k} = T_{os}$, gives the following expression for T'_{os} in accordance with the nomenclature illustrated in Figure 2.

$$T'_{os} = T_{os} + \frac{\Delta\theta}{\rho_c (C_p)_c} \left\{ \left[\frac{K_{j,k} - K_{j-1,k}}{2 \quad \Delta r_2} \right] \left[\frac{h_o}{K_{j,k}} \left[T_{conv} - T_{os} \right] + \frac{E}{K_{j,k}} + \right.\right.$$

$$\frac{\mathcal{F}\sigma}{K_{j,k}} (T_{rad}^4 - T_{os}^4) + \frac{T_{j,k} + T_{j-1,k}}{\Delta r_2} \Bigg] + \left[\frac{K_{j,k+1} - K_{j,k-1}}{r_j^2 (\Delta\phi_1 + \Delta\phi_2)} \right]$$

$$\left(\frac{T_{j,k+1} - T_{j,k}}{\Delta\phi_1} + \frac{T_{j,k} - T_{j,k-1}}{\Delta\phi_2} \right) + \left(\frac{K_{j,k} + K_{j-1,k}}{2 \quad \Delta r_2} \right)$$

$$\left[\frac{h_o}{K_{j,k}} \left[T_{conv} - T_{os} \right] + \frac{\mathcal{F}\sigma}{K_{j,k}} \left[T^4_{rad} - T^4_{os} \right] - \frac{T_{j,k} - T_{j-1,k}}{\Delta r_2} \right] \qquad (1.8$$

$$+ \left[\frac{K_{j,k} + K_{j-1,k}}{4 \, r_{j,k}} \right] \left[\frac{h_o}{K_{j,k}} (T_{conv} - T_{os}) + \frac{\mathcal{F}\sigma}{K_{j,k}} \left[T^4_{rad} - T^4_{os} \right] + \frac{E}{K_{j,k}} \right.$$

$$\left. + \frac{T_{j,k} - T_{j-1,k}}{\Delta r_2} \right] + \left[\frac{K_{j,k+1} + K_{j,k-1}}{r_{j,k}^2} \right]$$

$$\left. \left[\frac{\dfrac{T_{j,k+1} - T_{j,k}}{\Delta\phi_1} - \dfrac{T_{j,k} - T_{j,k-1}}{\Delta\phi_2}}{\Delta\phi_1 + \Delta\phi_2} \right] \right\}$$

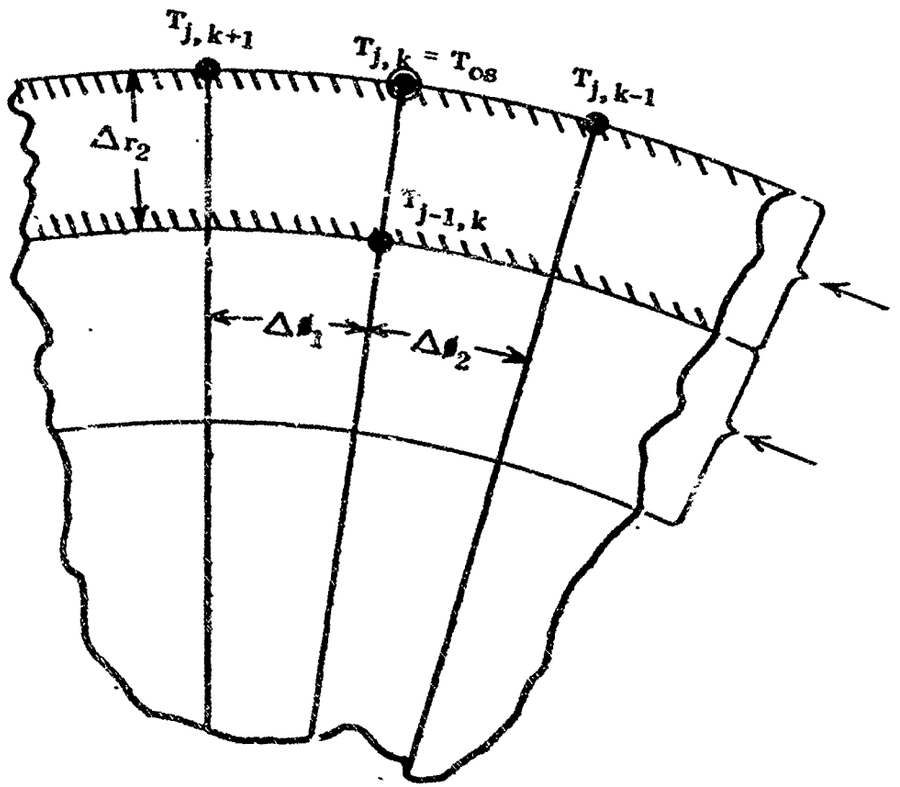

FIGURE 2. OUTER SURFACE NODAL POINT

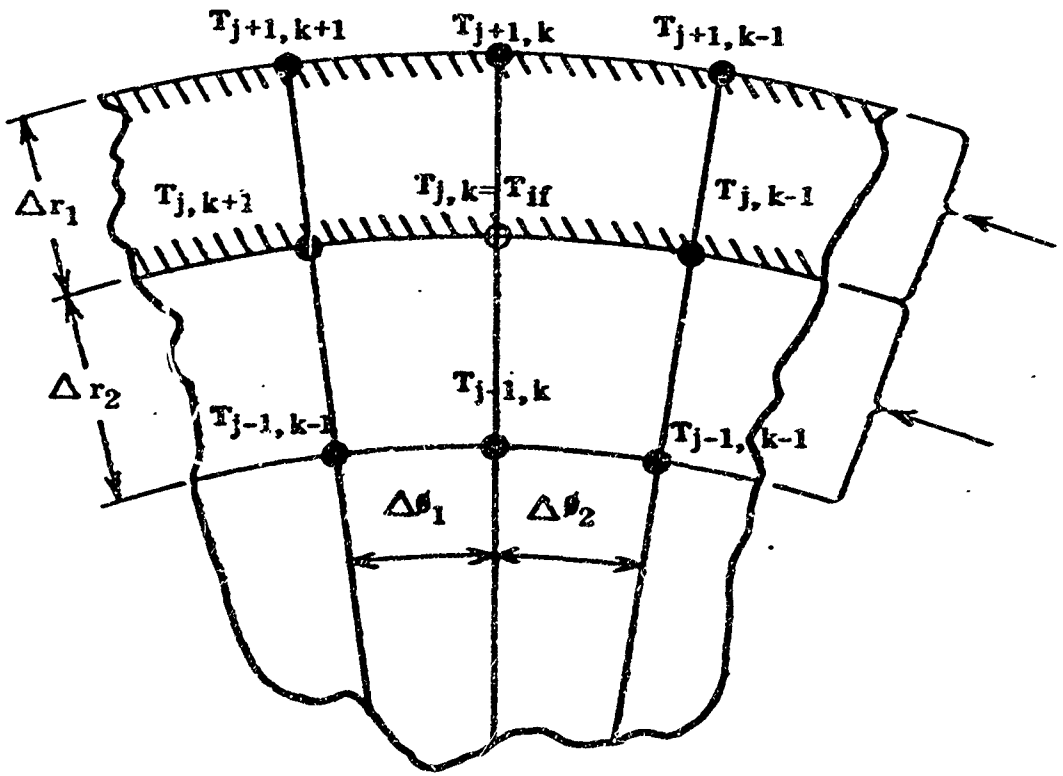

FIGURE 3. CASE-PROPELLANT INTERFACE POINT

3. Case-Propellant Interface

As can be seen from Figure 3, the case-propellant interface nodal point is influenced in its thermal response by the characteristics of both the case material and the propellant. Consequently, the finite-difference expression for the interface temperature can be obtained by substituting into the basic equation 1.1 for ρC_p, $K_{j,k+1}$ and $K_{j,k-1}$ the following relationships:

$$\rho C_p = \frac{\rho_2 (C_p)_2 \, 2r_j \, \Delta r_2 - \Delta r_2^2 + \rho_1 (C_p)_1 \, 2r_j \, \Delta r_1 + \Delta r_1^2}{2r_j \, \Delta r_2 - \Delta r_2^2 + 2r_j \, \Delta r_1 + \Delta r_1^2} \tag{1.9}$$

$$K_{j,k+1} = \frac{\Delta r_1 \, K_{j+1,k+1} + \Delta r_2 \, K_{j-1,k+1}}{\Delta r_1 + \Delta r_2} \tag{1.10}$$

$$K_{j,k-1} = \frac{\Delta r_1 \, K_{j+1,k-1} + \Delta r_2 \, K_{j-1,k-1}}{\Delta r_1 + \Delta r_2} \tag{1.11}$$

These relationships permit the proper proportioning of each material and corresponding thermal properties adjacent to the interface. Upon making these substitutions into the general expression, the finite difference notation for the interface becomes the following:

$$T_{if} = T_{if} + \frac{\Delta\vartheta\left[2r_j \, \Delta r_2 - \Delta r_2^2 + 2r_j \, \Delta r_1 + \Delta r_1^2\right]}{\rho_2 (C_p)_2 \left[2r_j \, \Delta r_2 - \Delta r_2^2\right] + \rho_1 (C_p)_1 \left[2r_j \Delta r_1 + \Delta r_1^2\right]}$$

$$\left\{\left(\frac{K_{j+1,k} - K_{j-1,k}}{\Delta r_1 + \Delta r_2}\right)\left(\frac{T_{j+1,k} - T_{j,k}}{\Delta r_1} + \frac{T_{j,k} - T_{j-1,k}}{\Delta r_2}\right) + \right.$$

$$\left.\left(\frac{\Delta r_1 (K_{j+1,k+1} - K_{j+1,k-1}) + \Delta r_2 (K_{j+1,k-1} - K_{j-1,k-1})}{r_{j,k}^2 \, (\Delta r_1 + \Delta r_2) \, (\Delta\vartheta_1 + \Delta\vartheta_2)}\right)\right.$$

$$\left(\frac{T_{j,k+1} - T_{j,k}}{\Delta\phi_1} + \frac{T_{j,k} - T_{j,k-1}}{\Delta\phi_2}\right)+\left(\frac{K_{j+1,k} + K_{j-1,k}}{\Delta r_1 + \Delta r_2}\right)$$

$$\left(\frac{T_{j+1,k} - T_{j,k}}{\Delta r_1} - \frac{T_{j,k} - T_{j-1,k}}{\Delta r_2}\right)+\left(\frac{K_{j+1,k} + K_{j-1,k}}{4r_{j,k}}\right)$$

$$\left(\frac{T_{j+1,k} - T_{j,k}}{\Delta r_1} + \frac{T_{j,k} - T_{j-1,k}}{\Delta r_2}\right)+ \tag{1.12}$$

$$\left(\frac{\Delta r_1 (K_{j+1,k+1} - K_{j+1,k-1}) + \Delta r_2 (K_{j+1,k-1} - K_{j-1,k-1})}{r_{j,k}^2 (\Delta r_1 + \Delta r_2)(\Delta\phi_1 + \Delta\phi_2)}\right)$$

$$\left.\left(\frac{T_{j,k+1} - T_{j,k}}{\Delta\phi_1} - \frac{T_{j,k} - T_{j,k-1}}{\Delta\phi_2}\right)\right\}$$

In this expression, all forward differences in r and terms subscripted with a 1 refer to the case material. Likewise, all backward differences in r and terms subscripted with a 2 refer to the propellant. This nomenclature is in accordance with Figure 3.

4. Internal Surface

The internal surface of a rocket motor, being in most cases irregular or noncircular, experiences heat flow at the boundary which is not precisely radial. Therefore, the boundary condition at the internal surface of the grain is expressed in terms of the gradient normal to the surface, as follows:

$$\frac{\partial T}{\partial n} = \frac{h_i}{K_{j,k}} (T_c - T_{is}) \tag{1.13}$$

where

h_i = Internal Boundary Film Coefficient, BTU/hr-ft^2-°R

T_c = Internal Environmental Temperature, °R

T_{is} = Internal Surface Temperature, °R

n = Direction Normal to Internal Boundary

Since all finite differences within the basic equation 1.1 are expressed with respect to the radial and circumferential directions, the normal derivative (1.13) at the internal boundary must be resolved as shown in Figure 4 to obtain the following radial and circumferential boundary gradients.

$$\frac{\delta T}{\delta \phi} = \frac{\delta T}{\delta n}\left[1 + r^2 \left(\frac{d\phi}{dr}\right)^2\right]^{-1/2} = \frac{h_l}{K_{i,j}} (T_c - T_{j,k}) \left[1 + r^2 \left(\frac{d\phi}{dr}\right)^2\right]^{-1/2} \qquad (1.14)$$

$$\frac{\delta T}{\delta r} = \frac{\delta T}{\delta n}\left[1 + \frac{1}{r^2} \left(\frac{dr}{d\phi}\right)^2\right]^{-1/2} = \frac{h_l}{K_{i,j}} (T_c - T_{j,k}) \left[1 + \frac{1}{r^2} \left(\frac{dr}{d\phi}\right)^2\right]^{-1/2} \qquad (1.15)$$

These derivatives expressed in either forward or backward finite difference notations, depending upon the grain geometry, must be substituted into the general heat conduction equation (1.1) together with other modifications necessary to simulate an internal boundary nodal point. In summary, the various types of points that may exist and the necessary nodal substitutions that are required for their simulation are presented below. Iterations are assumed to begin at $\phi = 0$ and $r = r_o$ progressing in a counterclockwise direction and with increasing r.

1) Internal surface implies $\frac{\partial T}{\partial n} = \frac{h}{K_{j,k}} (T_c - T_{j,k})$

a) Entering propellant on constant ϕ:
Replace backward differences in r

$$\frac{T_{j,k} - T_{j-1,k}}{\Delta r_2} \text{ with } \frac{h_l}{K_{j,k}} (T_{j,k} - T_c) \left[1 + \frac{1}{r_j^2} \left(\frac{\Delta r}{\Delta \phi}\right)^2\right]^{-1/2}, \ \Delta r_2 \text{ with } \Delta r_1, \text{ and } K_{j-1,k} \text{ with } K_{j+1,k}$$

b) Leaving propellant on constant ϕ implies:
Replace forward differences in r

$$\frac{T_{j+1,k} - T_{j,k}}{\Delta r_1} \text{ with } \frac{h_l}{K_{j,k}} (T_c - T_{j,k}) \left[1 + \frac{1}{r_j^2} \left(\frac{\Delta r}{\Delta \phi}\right)^2\right]^{-1/2}, \ \Delta r_1 \text{ with } \Delta r_2, \text{ and } K_{j+1,k} \text{ with } K_{j-1,k}$$

A-6560

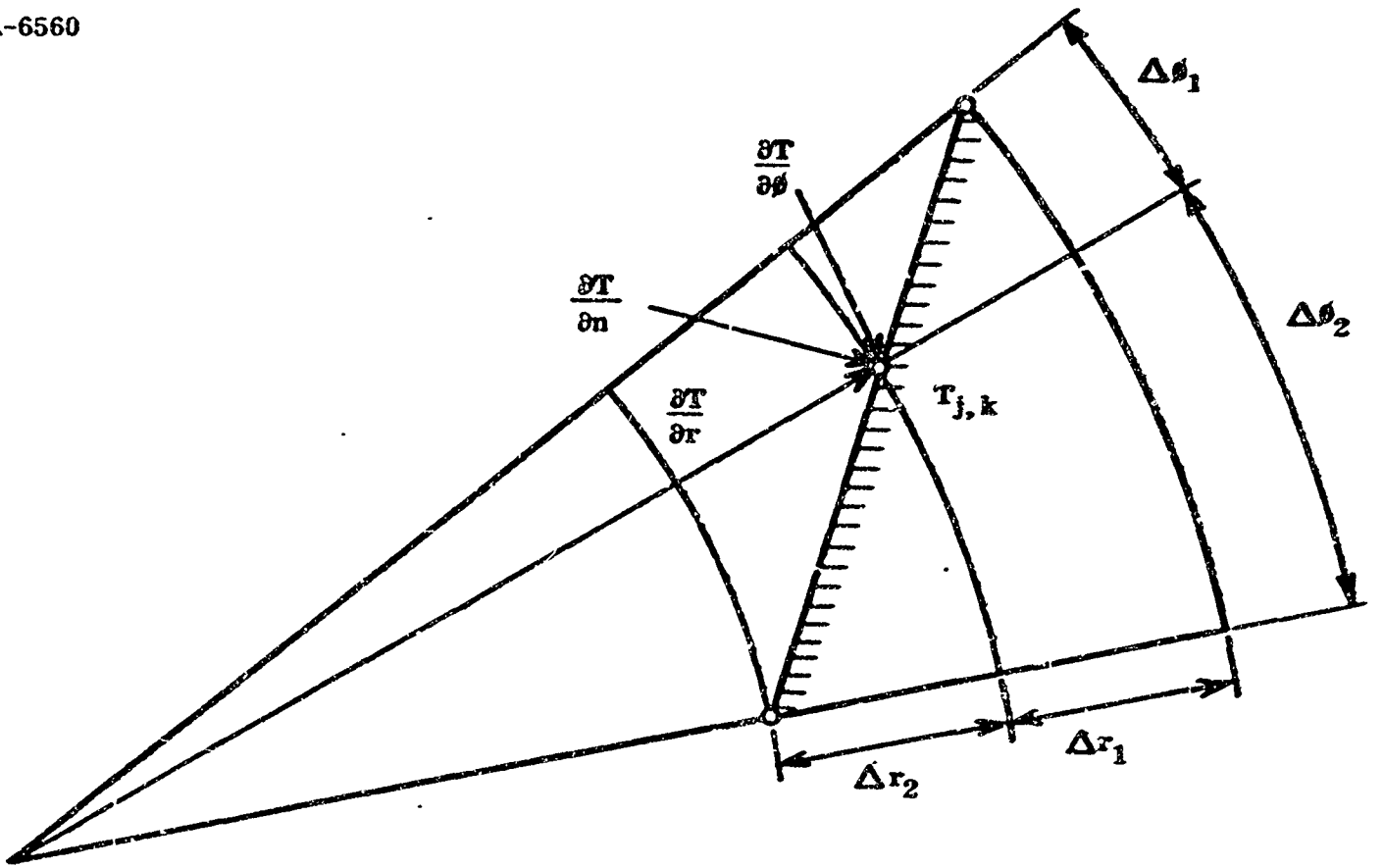

FIGURE 4. TYPICAL INTERNAL BOUNDARY NODAL POINT

c) Entering propellant on constant r implies:
Replace backward differences in ϕ

$$\frac{T_{j,k} - T_{j,k-1}}{\Delta\phi_2} \text{ with } \frac{h_i}{K_{j,k}} (T_{j,k} - T_c)\left[1 + r_j^2\left(\frac{\Delta\phi}{\Delta r}\right)^2\right]^{-1/2}, \ \Delta\phi_2 \text{ with } \Delta\phi_1, \text{ and } K_{j,k-1} \text{ with } K_{j,k+1}$$

d) Leaving propellant on constant r implies:
Replace forward differences in ϕ

$$\frac{T_{j,k+1} - T_{j,k}}{\Delta\phi_1} \text{ with } \frac{h_i}{K_{j,k}} (T_c - T_{j,k})\left[1 + r_j^2\left(\frac{\Delta\phi}{\Delta r}\right)^2\right]^{-1/2}, \ \Delta\phi_1 \text{ with } \Delta\phi_2, \text{ and } K_{j,k+1} \text{ with } K_{j,k-1}$$

2) $\phi = 0$ implies $\frac{\delta T}{\delta \phi} = 0$ and consequently the following substitutions:

Replace $T_{j,k-1}$ with $T_{j,k+1}$

$K_{j,k-1}$ with $K_{j,k+1}$

and $\Delta\phi_2$ with $\Delta\phi_1$

3) $\phi = \phi_{max}$ implies $\frac{\delta T}{\delta \phi} = 0$ and consequently the following substitutions:

Replace $T_{j,k+1}$ with $T_{j,k-1}$

$K_{j,k+1}$ with $K_{j,k-1}$

and $\Delta\phi_1$ with $\Delta\phi_2$

4) Propellant-case interface implies the following substitutions:

Replace ρ_c with $\dfrac{\rho_2 c_2\left[2r_j \Delta r_2 - \Delta r_2^2\right] + \rho_1 c_1\left[2r_j \Delta r_1 + \Delta r_1^2\right]}{2r_j \Delta r_2 - \Delta r_2^2 + 2r_j \Delta r_1 + \Delta r_1^2}$

$K_{j,k+1}$ with $\dfrac{\Delta r_1 K_{j+1,k+1} + \Delta r_2 K_{j-1,k+1}}{\Delta r_1 + \Delta r_2}$

and

$K_{j,k-1}$ with $\dfrac{\Delta r_1 K_{j+1,k-1} + \Delta r_2 K_{j-1,k-1}}{\Delta r_1 + \Delta r_2}$.

5) External surface implies the following substitutions:

$$\text{Replace} \quad \frac{T_{j+1,k} - T_{j,k}}{\Delta r_1} \text{ with } \frac{h_o}{K_{j,k}} (T_{conv} - T_{j,k}) + \frac{\mathcal{F}\sigma}{K_{j,k}}$$

$$(T_{rad}^4 - T_{j,k}^4) + \frac{E}{K_{j,k}}, \quad \Delta r_1 \text{ with } \Delta r_2, \text{ and } K_{j+1,k} \text{ with } K_{j-1,k}$$

6) Internal point implies no change in basic equation.

The above substitutions may be performed separately or in combinations as required to describe completely the nodal point condition. For the internal surface, the values of $\Delta\phi$ and Δr used in the directional derivative are those which best describe the boundary geometry. How well the geometry is simulated depends upon the fineness of the grid and the proper selection of $\Delta\phi$ and Δr.

Typical nodal points are illustrated on a hypothetical grain configuration given in Figure 5 and identified as follows:

Point No.		Identification
1	$\phi = 0$,	Internal surface, and, entering propellant on constant ϕ, adiabatic along constant r
2	$\phi = 0$,	Adiabatic along constant r
3	$\phi = 0$,	Propellant-case interface, adiabatic along constant r
4	$\phi = 0$,	External surface, adiabatic along constant r
5		Internal surface, entering propellant on constant ϕ
6		Internal point
7		Propellant-case interface
8		External surface

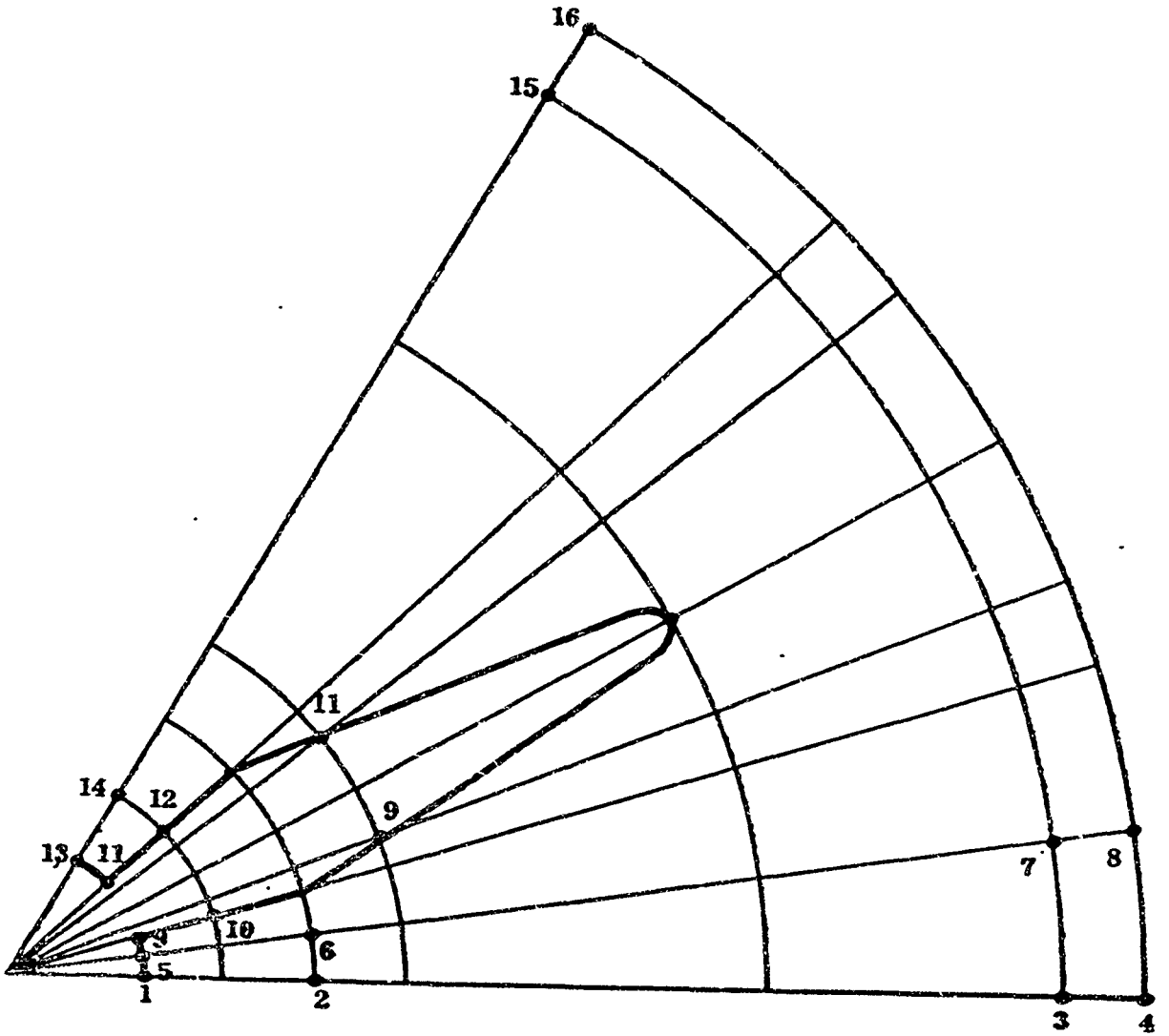

FIGURE 5. SEGMENT OF GRAIN WITH PARTIAL GRID ILLUSTRATING TYPICAL NODAL POINTS

Point No.	Identification
9	Internal surface, entering propellant on constant ϕ, leaving propellant on constant r
10	Internal surface, leaving propellant on constant r
11	Internal surface, entering propellant on constant r, entering propellant on constant ϕ
12	Internal surface, entering propellant on constant r
13	$\phi = \phi_{max}$, internal surface, entering propellant on constant ϕ
14	$\phi = \phi_{max}$
15	$\phi = \phi_{max}$, propellant case-interface
16	$\phi = \phi_{max}$, external surface

Each nodal point is identified within the program by a code which directs the substitutions and modifications of the basic equation.

5. Description of Computer Program

The method outlined in the previous sections for the modification of the basic heat conduction equation to obtain the finite difference equations representing the temperatures at various nodal points throughout a propellant grain has been programmed for the IBM-7070 digital computer in the FORTRAN II language.

Basically, there are two separate programs. The main program is capable of considering a grid configuration consisting of 30 nodal points on any radial line and as many circumferential points (radial lines) as are required to describe the

grain completely. Each nodal point must be formed by the intersection of a radial and a circumferential line. Consequently, whenever a radial line passes through a boundary line, a circumferential line must also be constructed through the same point (see Figure 5), and conversely.

In the iterative process, temperature computation begins at the internal surface on the first radial line and progresses in the direction of increasing r until the case surface is reached. The value of ϕ is then incremented, and computation begins again at the inner surface. This process is repeated until the entire configuration is scanned. At this point, time is incremented, the program is reoriented at the initial starting point, and computations proceed as before using the newly computed temperatures. This is a "marching" procedure where the program advances in time computing new temperatures based upon the previous values. By the nature of the finite difference equations, the program requires three complete radial lines and the corresponding nodal data in memory at all times. Therefore, in order to have the capability of considering an unlimited number of radial lines, the use of magnetic tape for the storage of intermediate temperatures and data was required. This, while necessary, resulted in extremely long computation times.

As a result, the program was revised, whereby all the nodal temperature data were retained in memory together with the newly computed and the previous temperatures for each node. This was made possible by limiting the number of circumferential points (radial lines) to 27 while retaining the original number of 30 radial points (circumferential lines). The effect was a significant reduction in

running time and input cards required. The latter was reduced to approximately one-half while the former was reduced by approximately one-third.

The glossary, flow chart, subroutine identification and input formats for both programs are contained in Appendix I to this report.

6. Test Cases

In order to evaluate the performance of the program and to demonstrate the utility and versatility of the analysis, numerous preliminary test runs were performed. There was sufficient variation among these test cases so that each particular routine within the program was used. Each test case is described below and illustrated in Figures 6 through 9, respectively.

1) A center perforated grain with a thin steel case wall. The center perforation was extremely small in order to approximate an end burning grain. The external boundary conditions were as follows:

$q = E \cos \phi = 400 \cos \phi$ BTU/hr-ft^2; $\phi = 0°$-$90°$

$q = \mathcal{F}_o \sigma (T_{rad}^4 - T_{os}^4) = 0.3\sigma (100^4 - T_{os}^4)$ BTU/hr-ft^2; $\phi = 90°$-$180°$

The internal boundary condition was adiabatic.

2) Same as (1) without the case wall.

3) Same as (2) with the following external boundary conditions:

$q = E \cos \phi = 120 \cos \phi$ BTU/hr-ft^2; $\phi = 0°$-$90°$

$q = \mathcal{F}_o \sigma (T_{rad}^4 - T_{os}^4) = 0.3\sigma (100^4 - T_{os}^4)$ BTU/hr-ft^2; $\phi = 90°$-$180°$

4) A 30° segment of a star grain with no case wall. The external boundary condition was:

$q = h_o (T_{conv} - T_{os}) = 8.5 (580 - T_{os})$ BTU/hr-ft^2, $\phi = 0°$-$30°$

A4868

Case Properties

Thermal Conductivity	=	22 BTU/hr-ft-°R
Specific Heat	=	0.11 BTU/lb-°R
Density	=	490 lb/ft^3
Initial Temperature	=	530°R

Propellant Properties

Thermal Conductivity	=	0.14 BTU/hr-ft-°R
Specific Heat	=	0.39 BTU/lb-°R
Density	=	100.22 lb/ft^3
Initial Temperature	=	530°R

σ = Stefan-Boltzmann Constant
= 0.173×10^{-8} BTU/hr-ft^2-°R^4

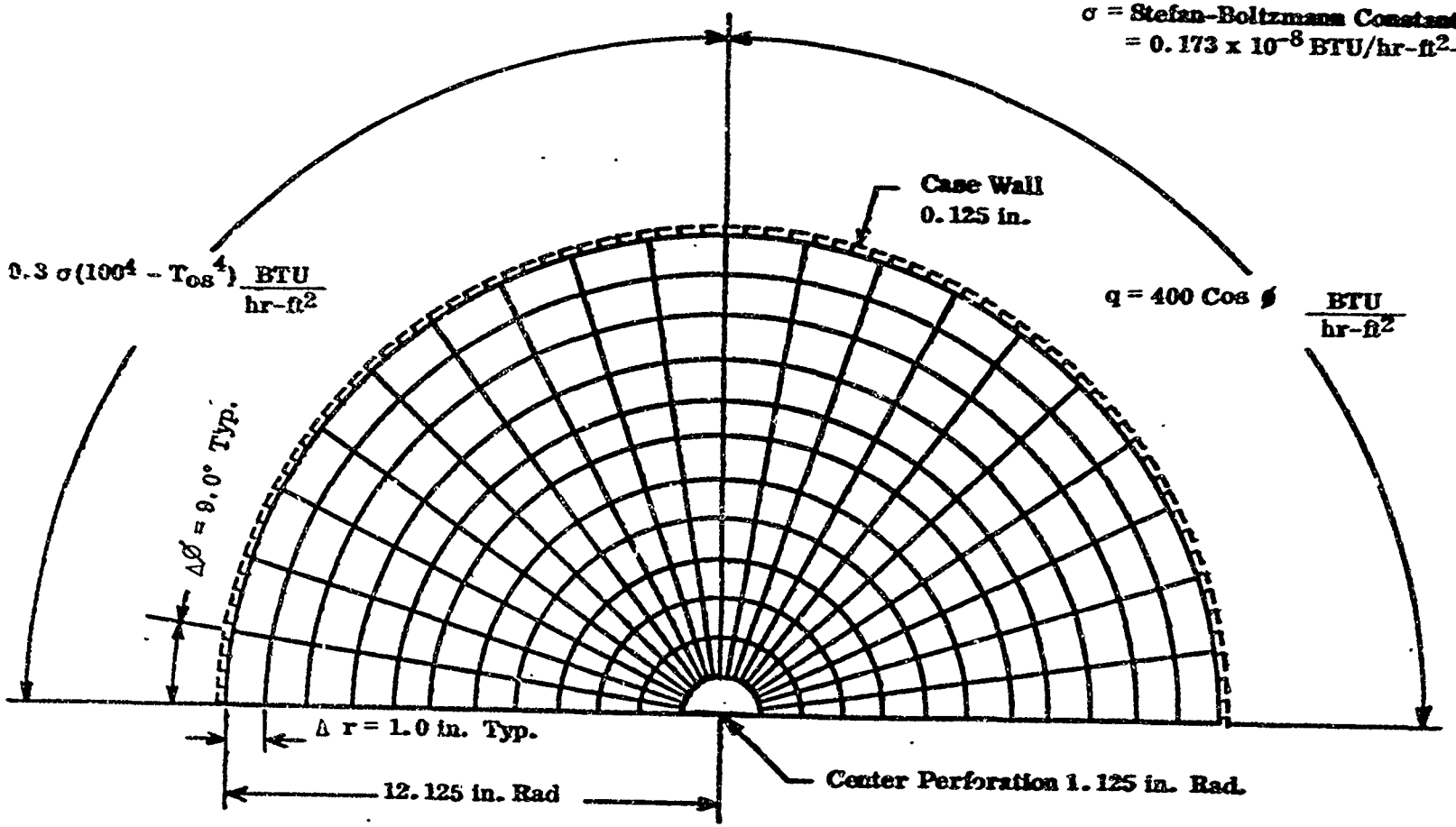

FIGURE 6. NODAL NETWORK AND BOUNDARY CONDITIONS FOR TEST CASE 1

A4870

No Case Wall

Propellant Properties

Thermal Conductivity	=	0.14 BTU/hr-ft-°R
Specific Heat	=	0.39 BTU/lb-°R
Density	=	100.22 lb/ft^3
Initial Temperature	=	530°R

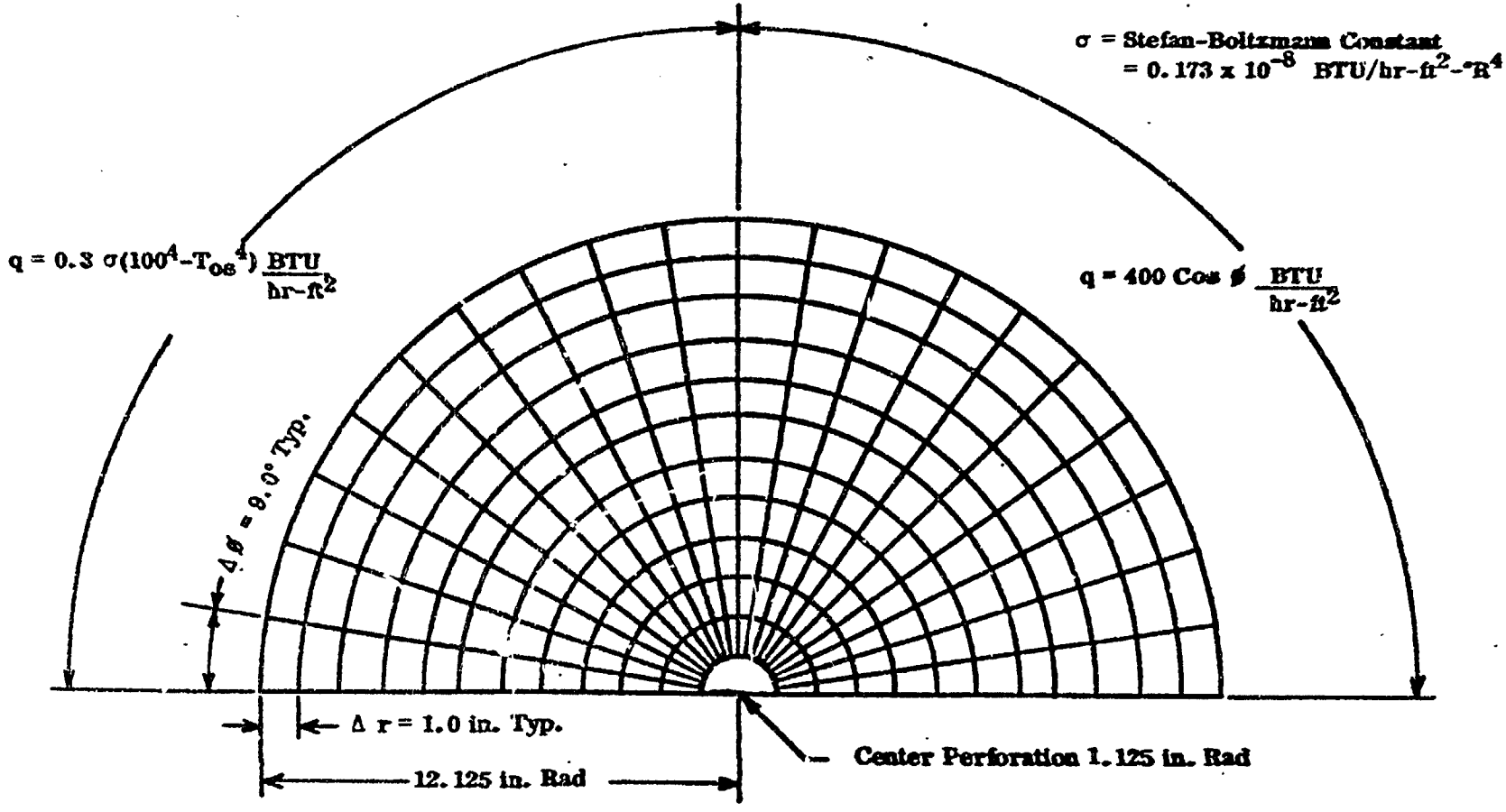

FIGURE 7 NODAL NETWORK AND BOUNDARY CONDITIONS FOR TEST CASE 2

A4871

No Case Wall

Propellant Properties

Thermal Conductivity	=	0.14 BTU/hr-ft-°R
Specific Heat	=	0.39 BTU/lb-°R
Density	=	100.22 lb/ft^3
Initial Temperature	=	530°R

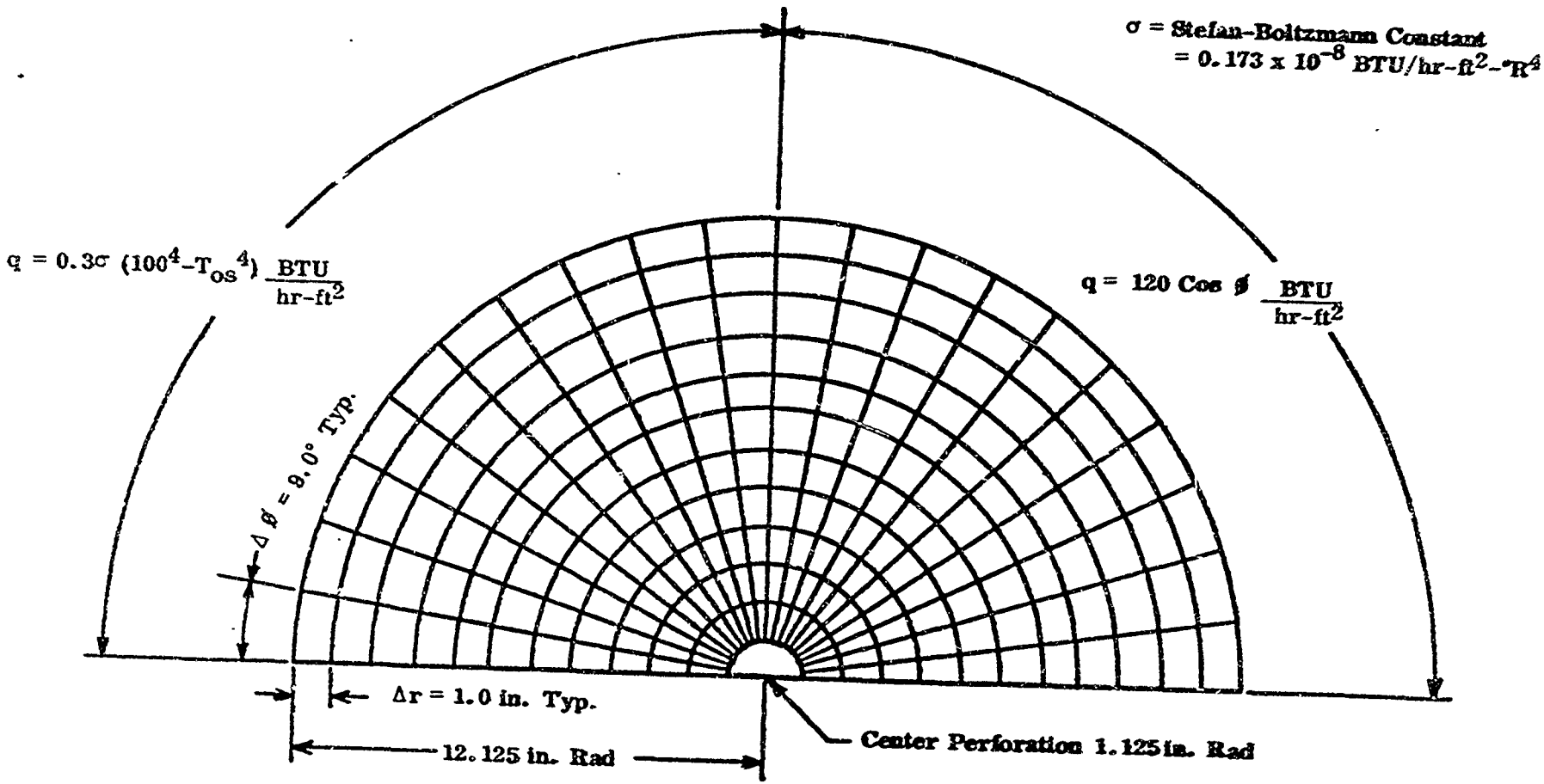

FIGURE 8. NODAL NETWORK AND BOUNDARY CONDITIONS FOR TEST CASE 3

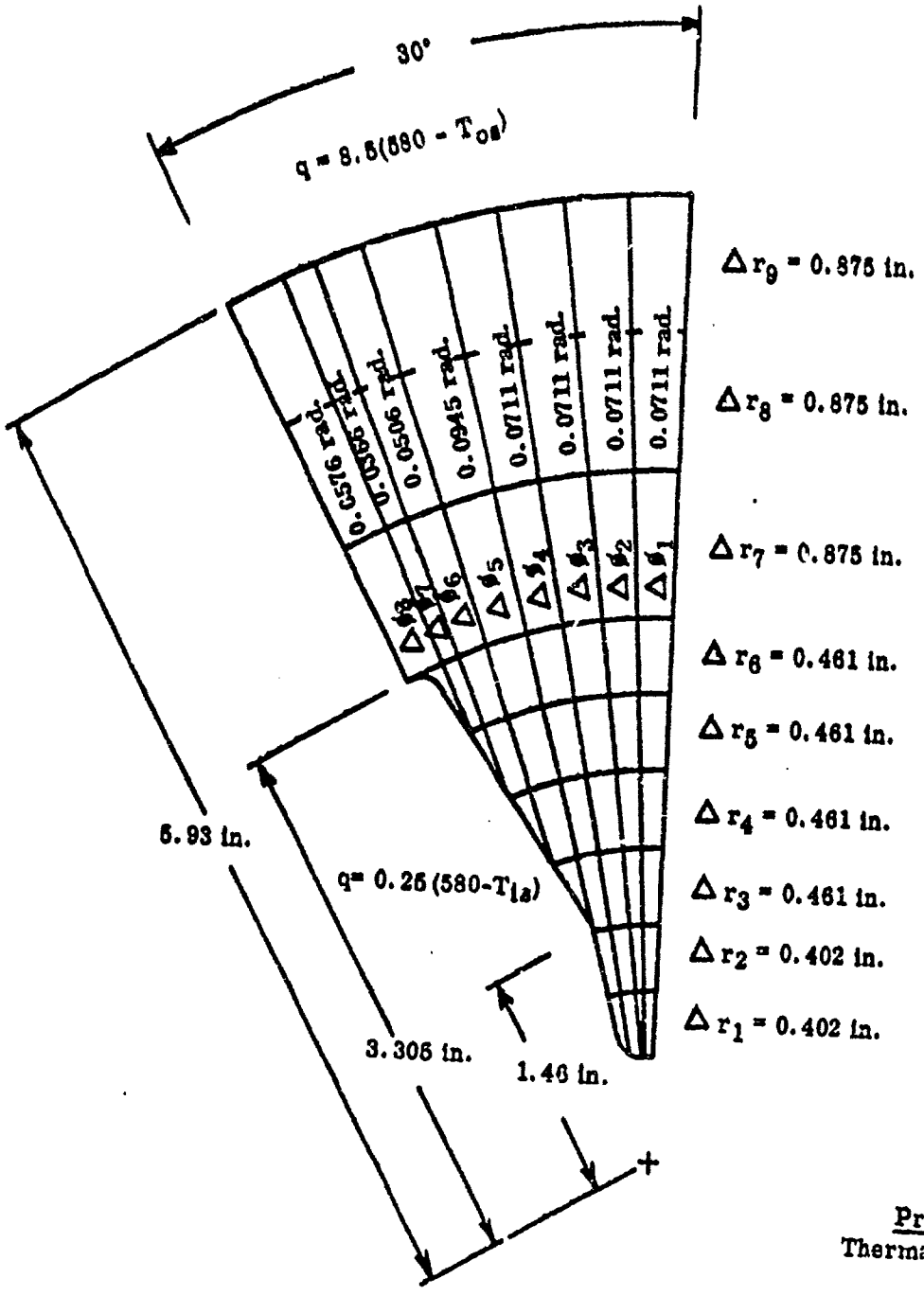

Propellant Properties

Thermal Conductivity = 0.249 $\frac{BTU}{hr\text{-}ft\text{-}°R}$

Specific Heat = 0.237 $\frac{BTU}{lb\text{-}°R}$

Density = 108.84 $\frac{lb}{ft^3}$

Initial Temperature = 460°R

FIGURE 9. NODAL NETWORK AND BOUNDARY CONDITIONS FOR TEST CASE 4

The internal boundary condition was:

$$q = h_i (T_{conv} - T_{os}) = 0.25 (580-T_{os}) \text{ BTU/hr-ft}^2$$

Test case 1 evaluated the external surface and case-propellant interface nodal point relationships. A significant result obtained from this case was the severe stability requirements imposed on the solution by a thin case wall having a relatively higher thermal diffusivity than the propellant. These stability requirements resulted in small iteration times, and, consequently, long computation times. Since the validity of the case wall and case-propellant temperatures was demonstrated within the program, the remaining test cases were evuluated without a case material. The capability exists to consider a case wall, but unless it contains sufficient thermal resistance or capacity to grossly affect the gradients within the grain it is not analytically necessary or economically feasible to do so.

The results of test cases 2 and 3 are presented in Figures 10 and 11 corresponding to 12 hours of exposure. Intermediate profiles corresponding to every 0.5 hours were also obtained for these configurations.

Test case 4 illustrates the effect of a small thermally symmetric star segment upon the temperature gradient through a grain subjected to uniform internal and external convection. The results of this test case, presented in Figure 12 in the form of an isotherm plot, show the heat sink effect obtained within the grain as heat enters from both boundaries. At the center of this sink is the point within the grain which responds last and slowest to the thermal environment. Consequently, this is a region of low thermal gradients.

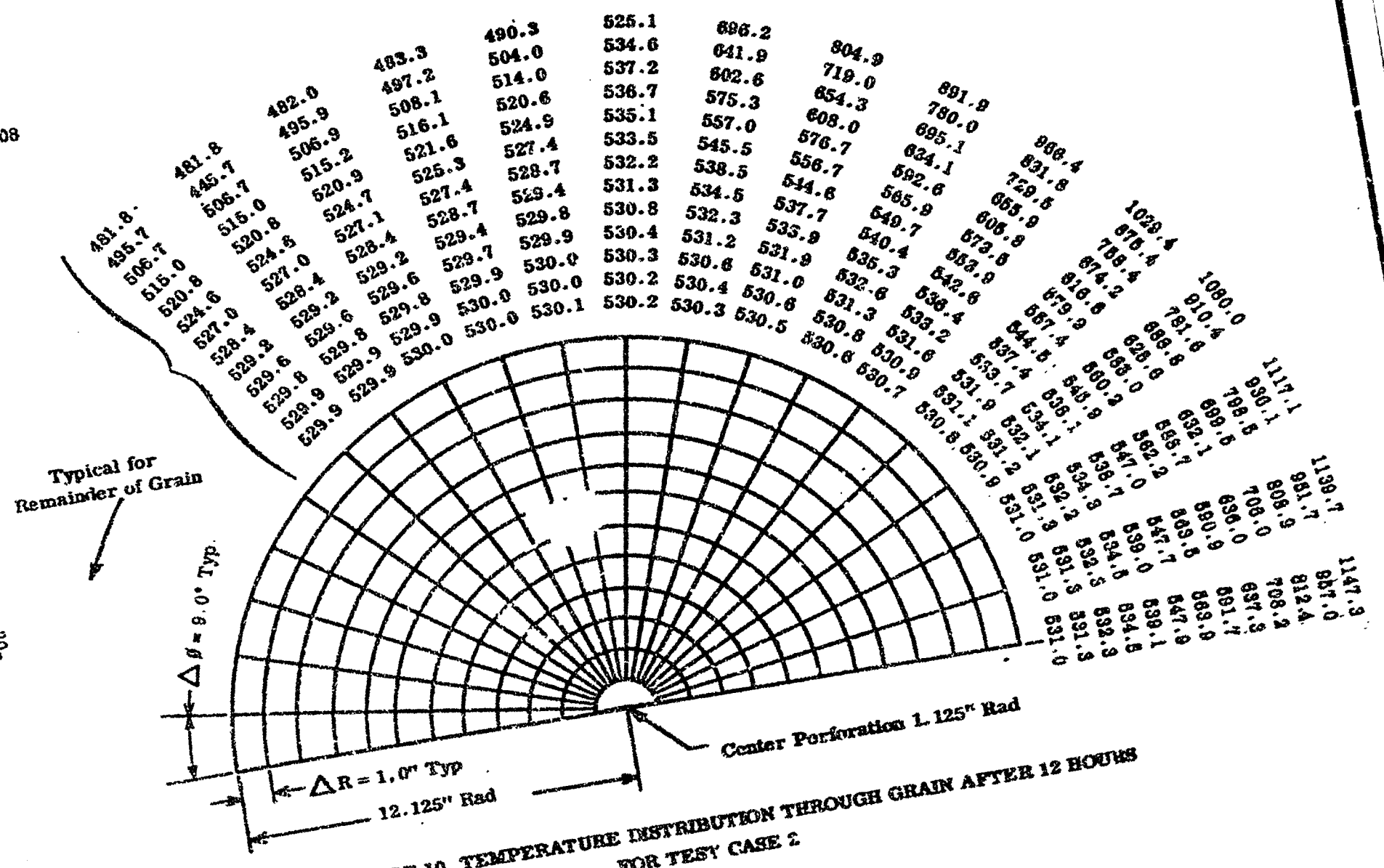

FIGURE 10. TEMPERATURE DISTRIBUTION THROUGH GRAIN AFTER 12 HOURS FOR TEST CASE 2

A-6209

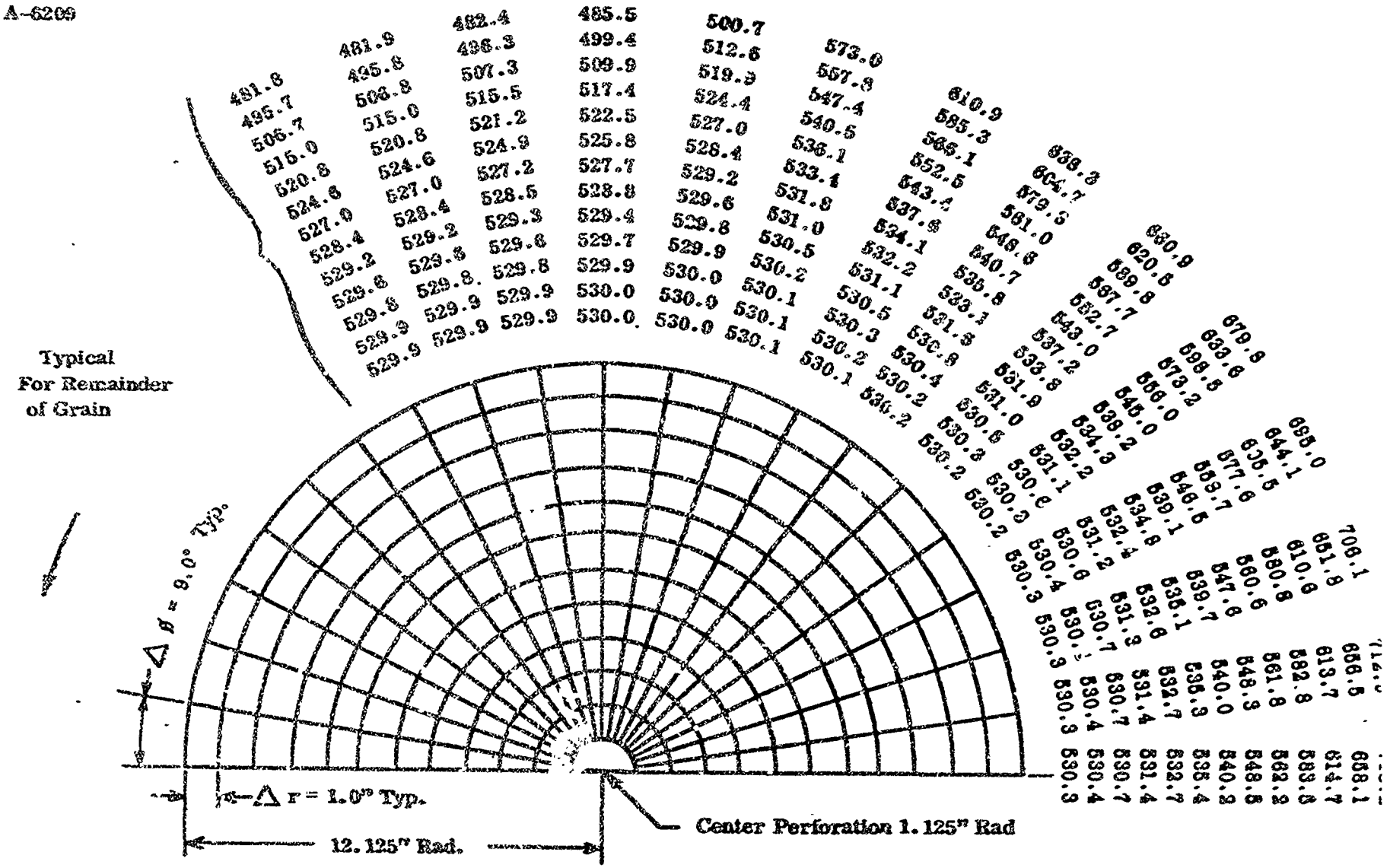

FIGURE 11. TEMPERATURE DISTRIBUTION THROUGH GRAIN AFTER 12 HOURS FOR TEST CASE 3

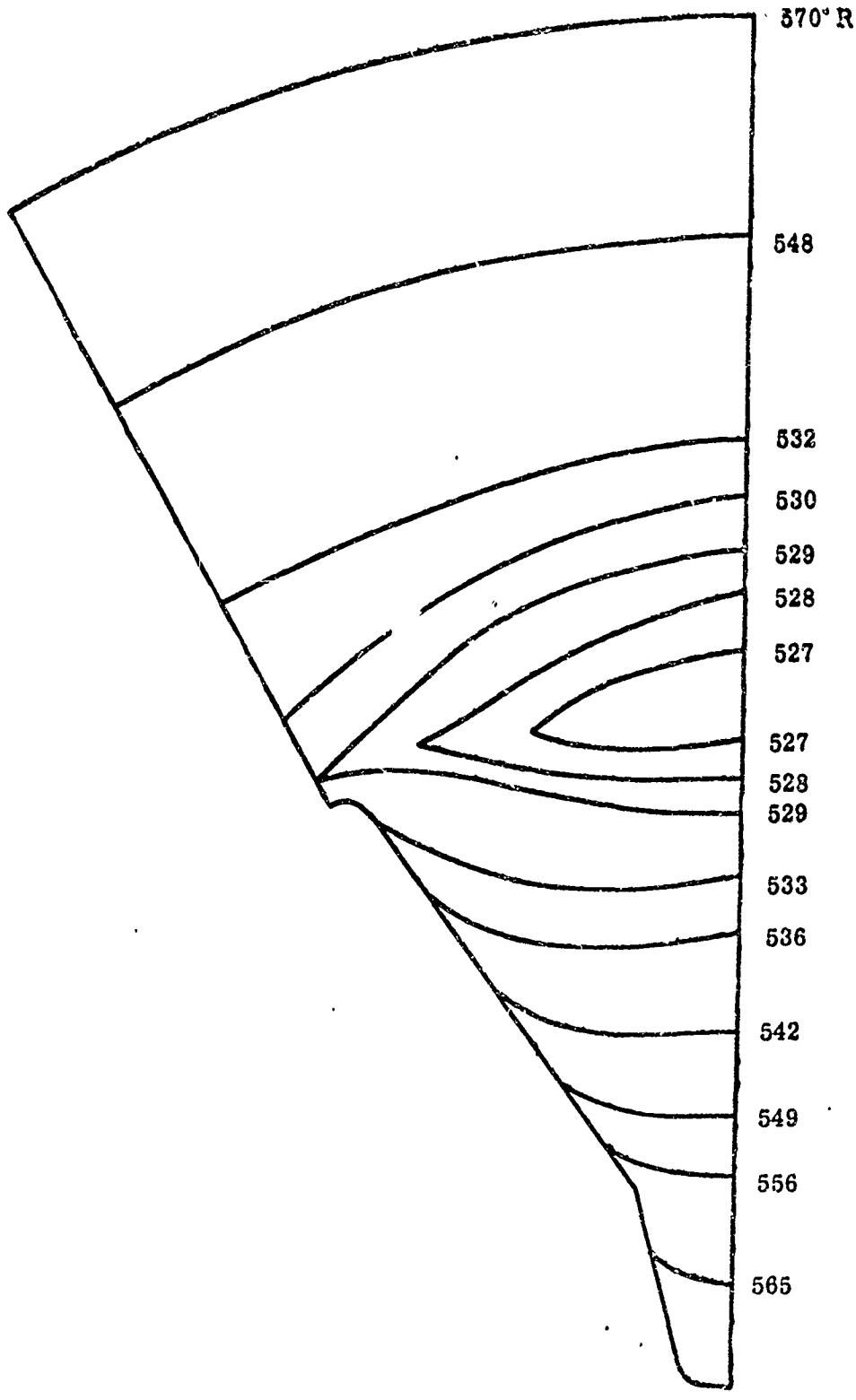

FIGURE 12. ISOTHERM PLOT FOR TEST CASE 4

To demonstrate more extensively the effects of a nonuniform external environment and an irregular internal boundary upon the thermal profile within a propellant grain, the 180° star configuration illustrated in Figure 13 was evaluated for the following three separate sets of boundary conditions. The initial temperature of the grain was considered to be 540°R.

1) External Boundary Condition

ϕ = 0° to 90°

$q = 400 \cos \phi$ BTU/hr-ft^2

ϕ = 90° to 180°

$q = 0.3 \sigma (100^4 - T_{os}^4)$ BTU/hr-ft^2

Internal Boundary Condition

$q = 0$ (adiabatic)

2) External Boundary Condition

Same as (1) above

Internal Boundary Condition

$q = h (T_c - T_{is}) = 5(650 - T_{is})$ (heated)

3) External Boundary Condition

Same as (1) above

Internal Boundary Condition

$q = h(T_c - T_{is}) = 5(300 - T_{is})$ (cooled)

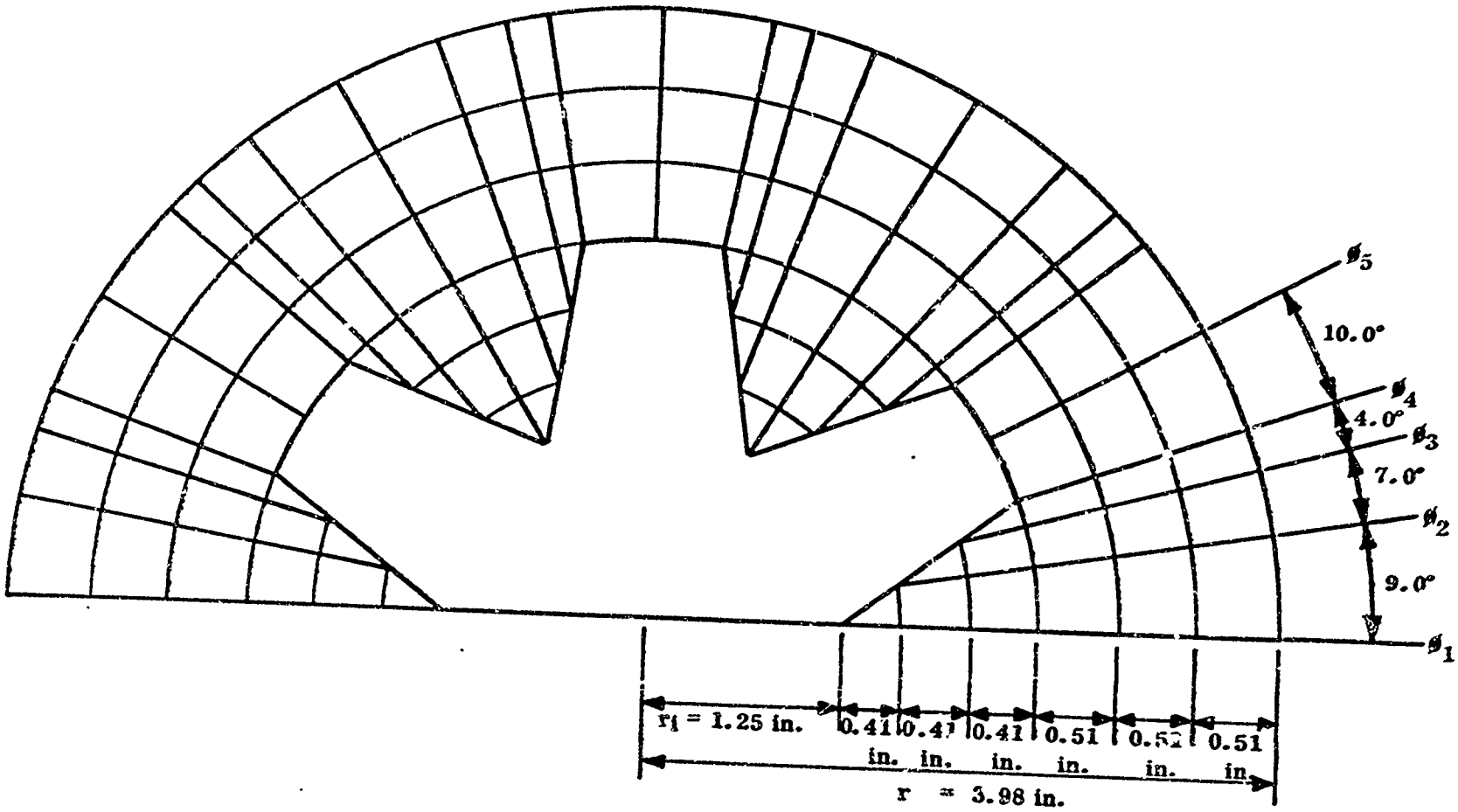

FIGURE 13. NODAL NETWORK FOR 180° STAR GRAIN CONFIGURATION

The isotherms existing within the grains for the above three environments are illustrated in Figures 14 through 16. These demonstrate the effect of the irregular internal boundary together with the response of the grain to either heating or cooling from the inside. The resolution of the solution is sufficient to outline clearly the "sink" and "source" effects, respectively, for both internal environments.

While these test cases are fictitious, they do illustrate the capability of the program to predict temperature profiles through a grain when subjected to adverse environments for subsequent evaluation of the effects upon ballistic performance and/or structural integrity.

B. ADVANCED GRAIN DESIGN ANALYSIS - PROGRAM AGDA

The Thiokol-Elkton Advanced Grain Design Analysis (AGDA) computer program represents the most general truly three-dimensional grain design computer program available today. The present computer program provides the rocket designer with all fundamental geometrically derivable rocket motor performance parameters. These parameters including burning surface area, chamber volume, propellant weight, center of gravity travel, and moments and products of inertia. With these fundamental parameters, interpretation in terms of ballistic performance tradeoffs is immediately and easily available.

The approach utilized in program AGDA represents an entirely new concept in the analysis of solid propellant rocket motor grain design. This new concept, which will be described later, yields results of extremely high accuracy through use of vector algebra and calculus techniques.

A-6391

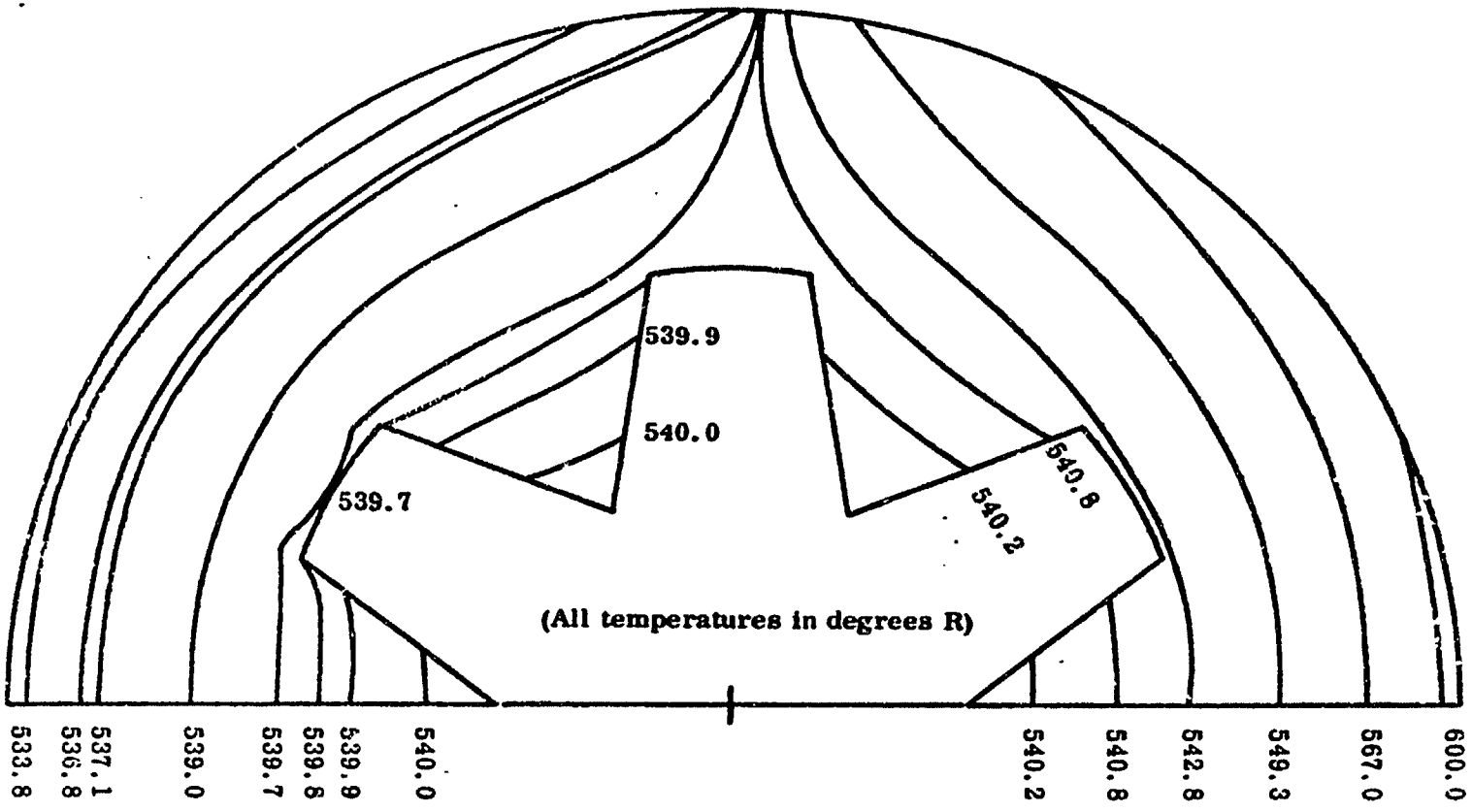

FIGURE 14. ISOTHERM PLOT FOR 180° STAR CONFIGURATION (ADIABATIC INTERNAL BOUNDARY)

A-6562

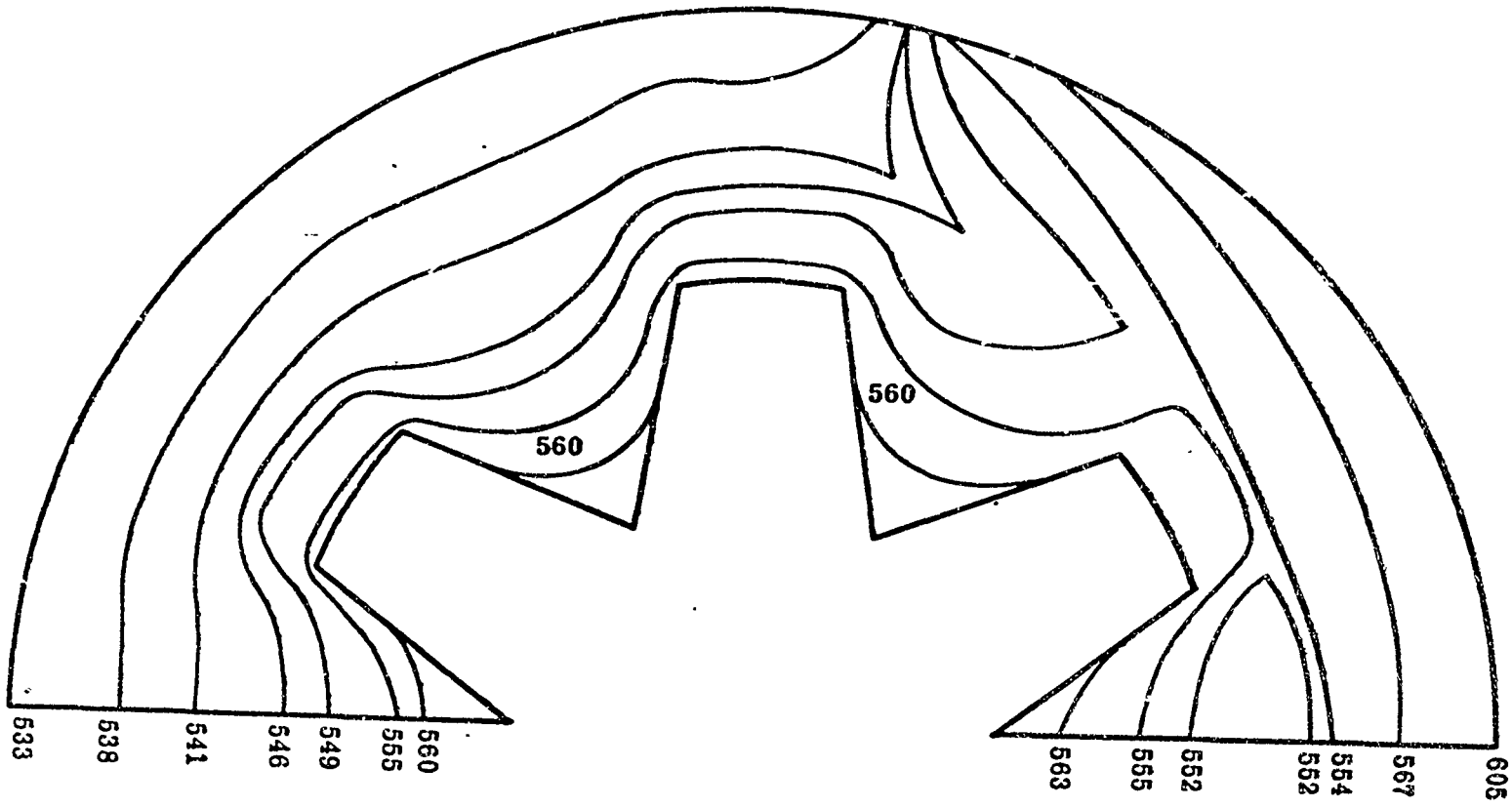

FIGURE 15. ISOTHERM PLOT FOR 180° STAR CONFIGURATION (HEATED INTERNAL BOUNDARY)

A-6561

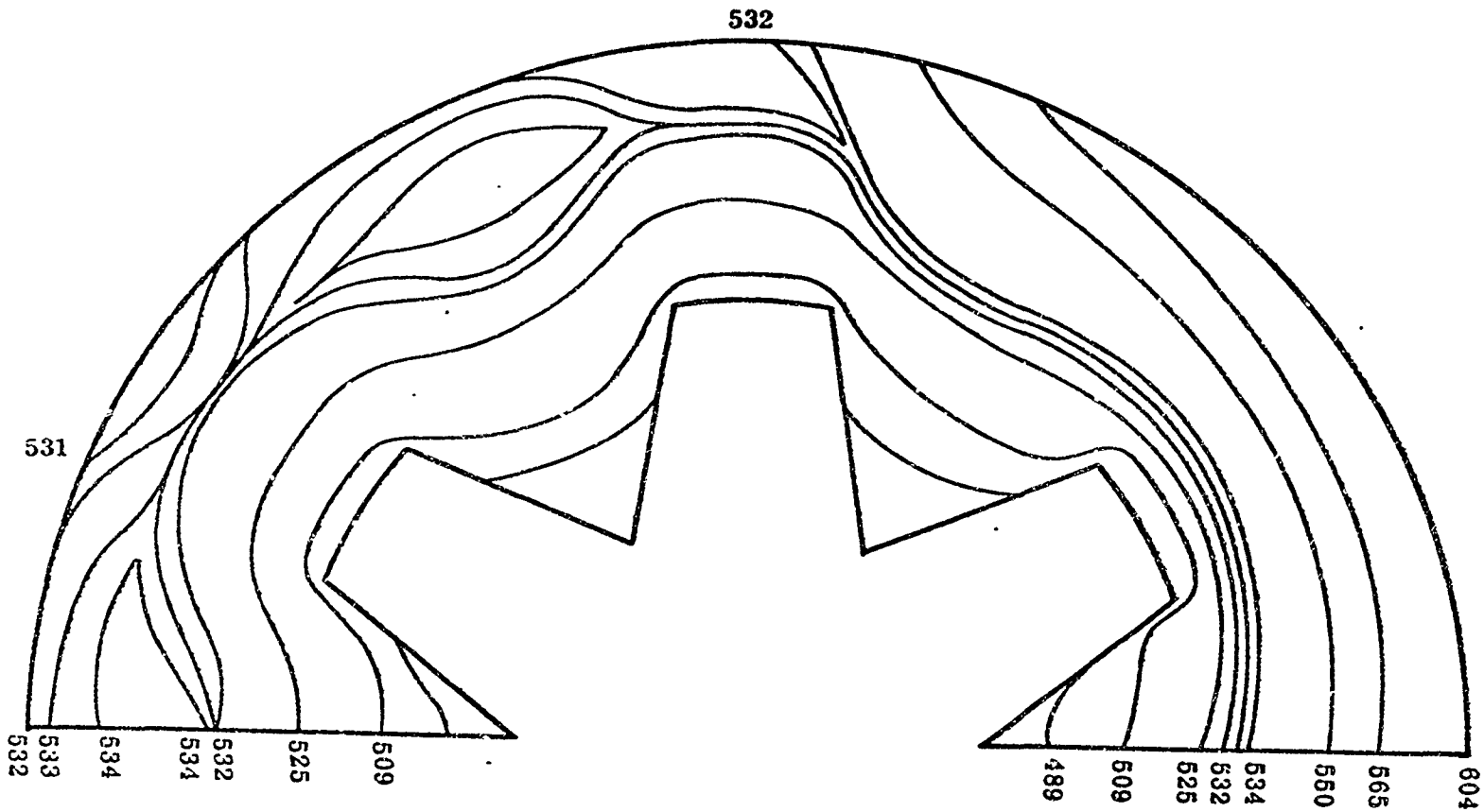

FIGURE 16. ISOTHERM PLOT FOR 180° STAR CONFIGURATION (COOLED INTERNAL BOUNDARY)

The entire system, both analysis and programming, is completely modular in design, thus readily permitting the inclusion of additional capabilities and techniques. Figures 17 and 18 are representative of the wide class of solid propellant rocket motors which may be handled today by Program AGDA.

1. Description of Program AGDA

Because of the uniqueness of the Elkton Advanced Grain Design Analysis, a brief description of the theory of the program is presented herein.

The three most salient characteristics of the Advanced Grain Design Analysis are the conceptual simplicity of the Elkton-Moore method (upon which it is based), its generality, and the accuracy it affords. In addition to providing chamber volume and burning surface area as functions of burning distance, this method permits calculation of propellant mass, the components of the inertia tensor, and propellant center of gravity.

Briefly, the Elkton Advanced Grain Design Analysis can be summarized in the following eight steps:

1) The chamber and case of the rocket motor are represented as mathematical surfaces.

2) The surface representing the outside of the chamber is divided into a large number of pseudo-rectangular elements.

3) Normals to this surface are constructed at the corners of a "rectangle" such that they travel through the propellant and intersect the case.

4) If the angle between any pair of normals emanating from the same point as calculated in Step 3 exceeds a given small value, new normals are constructed between those already calculated in such a way as to reduce the angular separation between successive normals to a tolerable value.

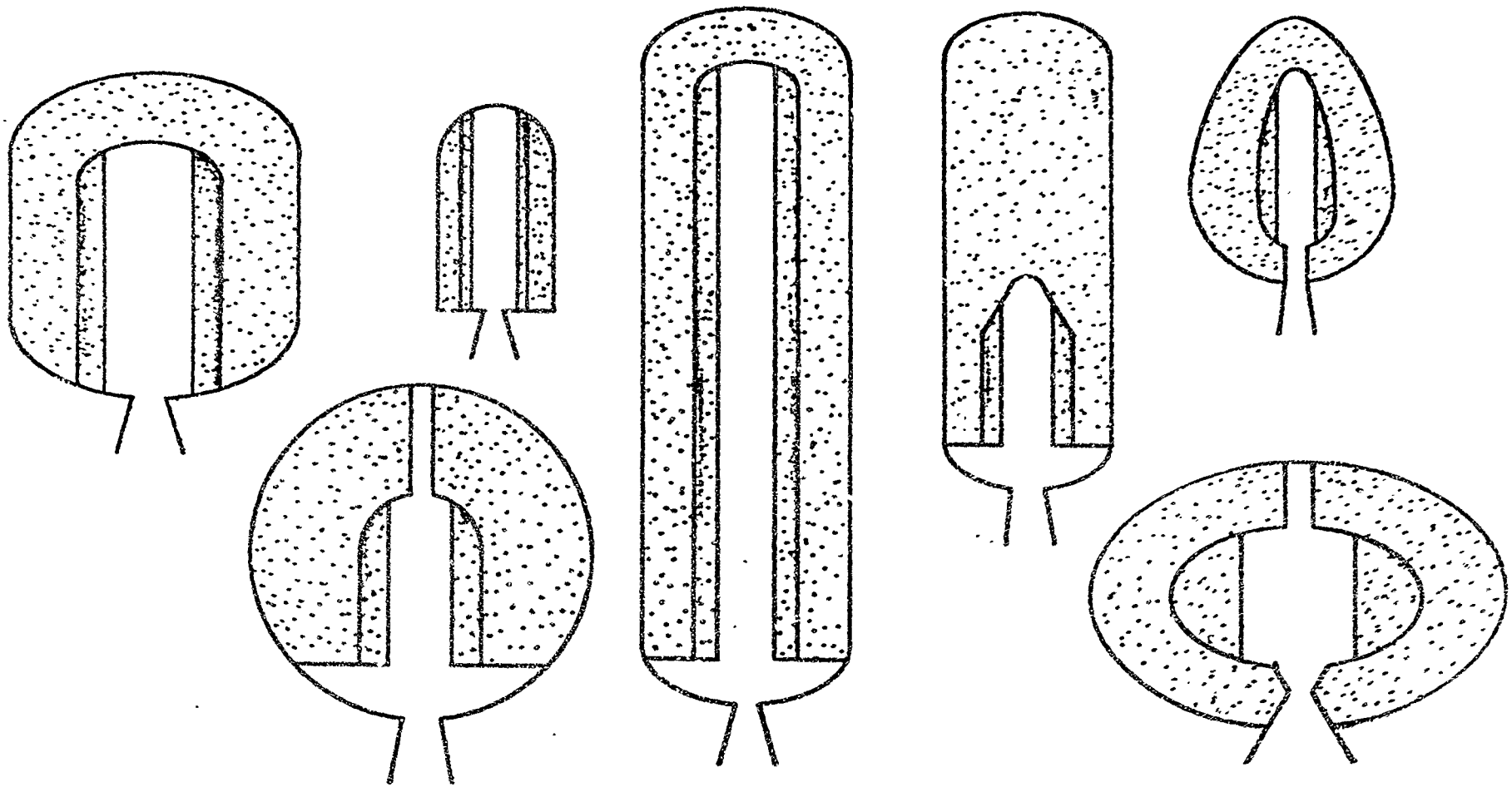

FIGURE 17. RANDOM COLLECTION OF ROCKET MOTORS AMENABLE TO STRAIGHTFORWARD SOLUTION BY PROGRAM AGDA
(All may have either simple or complex star perforations.)

A-6192

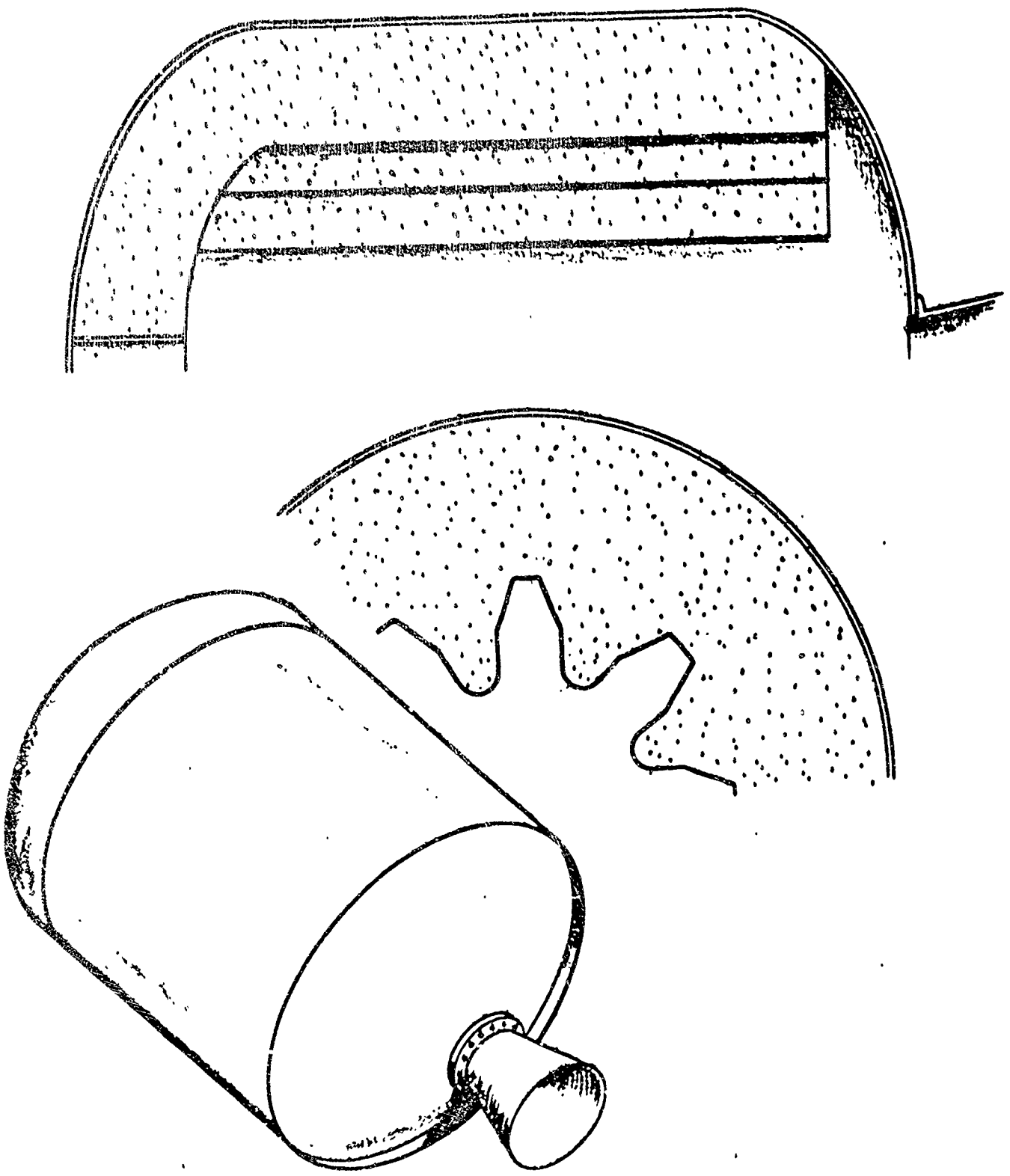

FIGURE 18. TYPICAL ROCKET MOTOR EVALUATED BY PROGRAM AGDA

5) Each of the normals constructed in Steps 3 and 4 is divided into a number of equal increments beginning at the chamber surface.

6) Surface area between each set of four points of corresponding burning distance is calculated. Volume and moments and products of inertia are calculated for regions of propellant between successive sets of points.

7) Steps 5 and 6 are repeated for all sets of four normals calculated in Step 4; then, Steps 3, 4, and 5 are repeated for each of the pseudo-rectangular areas. On each pass through these "loops," values of surface area, volume, etc., corresponding to the same burning distance are added together.

8) The quantities summed in Step 6 are converted to the following motor parameters:

   a) Burning Surface Area

   b) Chamber Volume

   c) Unconsumed Propellant Mass

   d) Moments of Inertia of Unconsumed Propellant

   e) Products of Inertia of Unconsumed Propellant

   f) Center of Gravity of Unconsumed Propellant

These steps are shown in a generalized flow chart of the program in Figure 19.

Theoretical aspects and derivation of the mathematics behind the Advanced Grain Design Analysis are presented in the next section of the report. Following this derivation, the method of application to a generalized solid propellant rocket motor is presented. A knowledge of the eight steps outlined above is all that is necessary

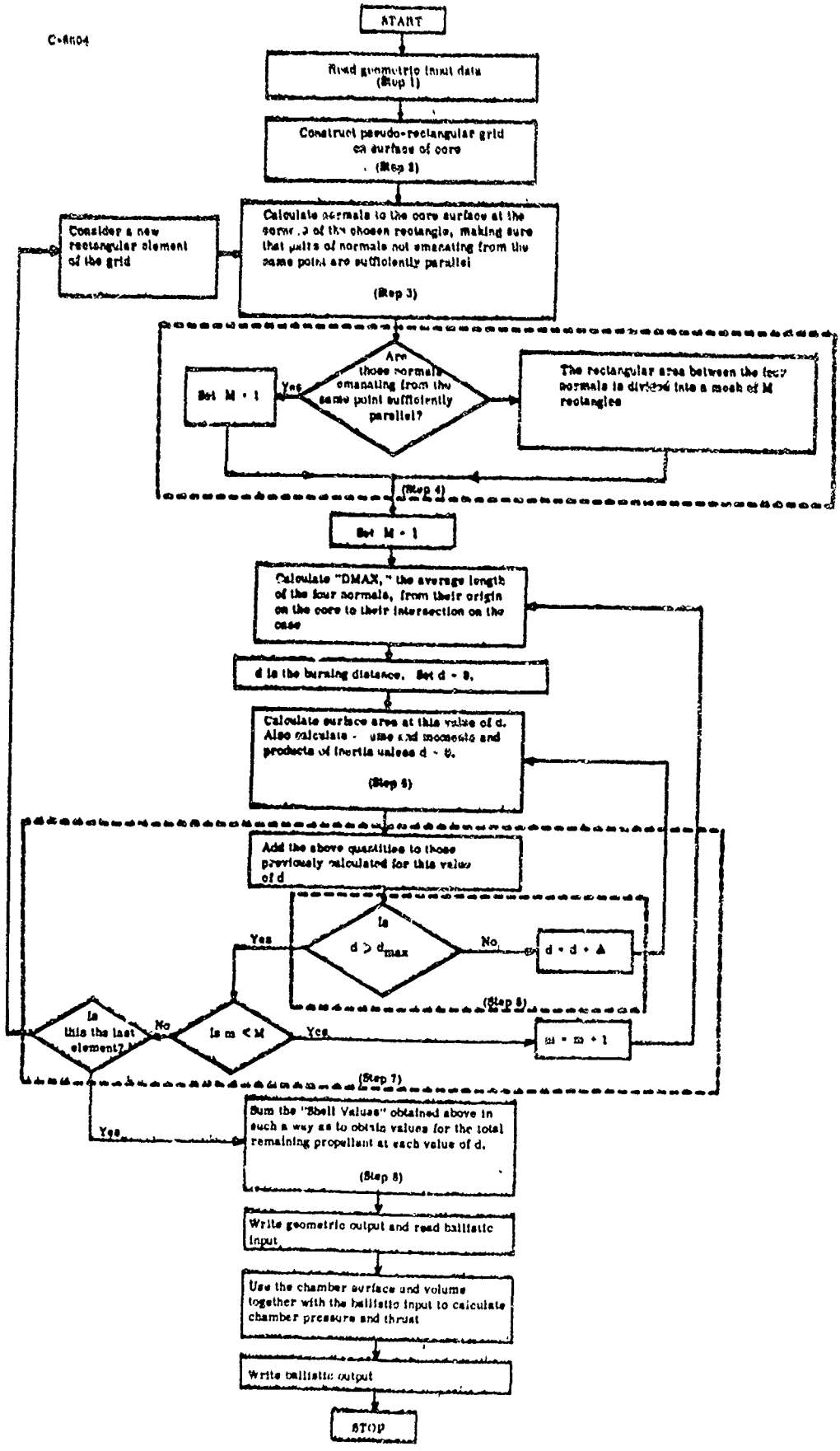

FIGURE 19. SIMPLIFIED COMPUTER PROGRAM FLOW CHART

to ensure comprehension of the majority of the section concerning application. A study of the deviation, however, will provide more insight into the method.

2. Theoretical Aspects of the Advanced Grain Design Analysis - Uniform Temperature

a. Representation of Grain and Definition of Surface Normals

Given a general grain design with inner and outer web limiting surfaces represented by ϕ (x, y, z) = 0 and ψ (x, y, z) = 0 respectively (see Figure 20), an x-y mesh is constructed on that portion of the plane $z = z_0$ intercepted by the projection of ϕ (x, y, z) = 0.

The regression of the total surface is obtained by considering the regression of each of the surface elements of ϕ (x, y, z) = 0 corresponding to a block of the x-y mesh. Since burning proceeds in a direction normal to the instantaneous burning surface, the regression of any surface element is bounded by the normals to that surface evaluated around the perimeter of the element or approximately by the normals at the corners of the element. To illustrate this, only a single representative element, such as the one shown in Figure 21, will be considered. With respect to this figure, the unit normals, $\overline{N}_i$, are defined by:

$$\overline{N}_i = \left(\frac{\nabla \phi(x, y, z)}{\nabla \phi(x, y, z)} \right) \quad P_i (0) \qquad (1.1$$

$$i = 1, 2, 3, 4$$

where P_i (0) represents the corners of any rectangular element.

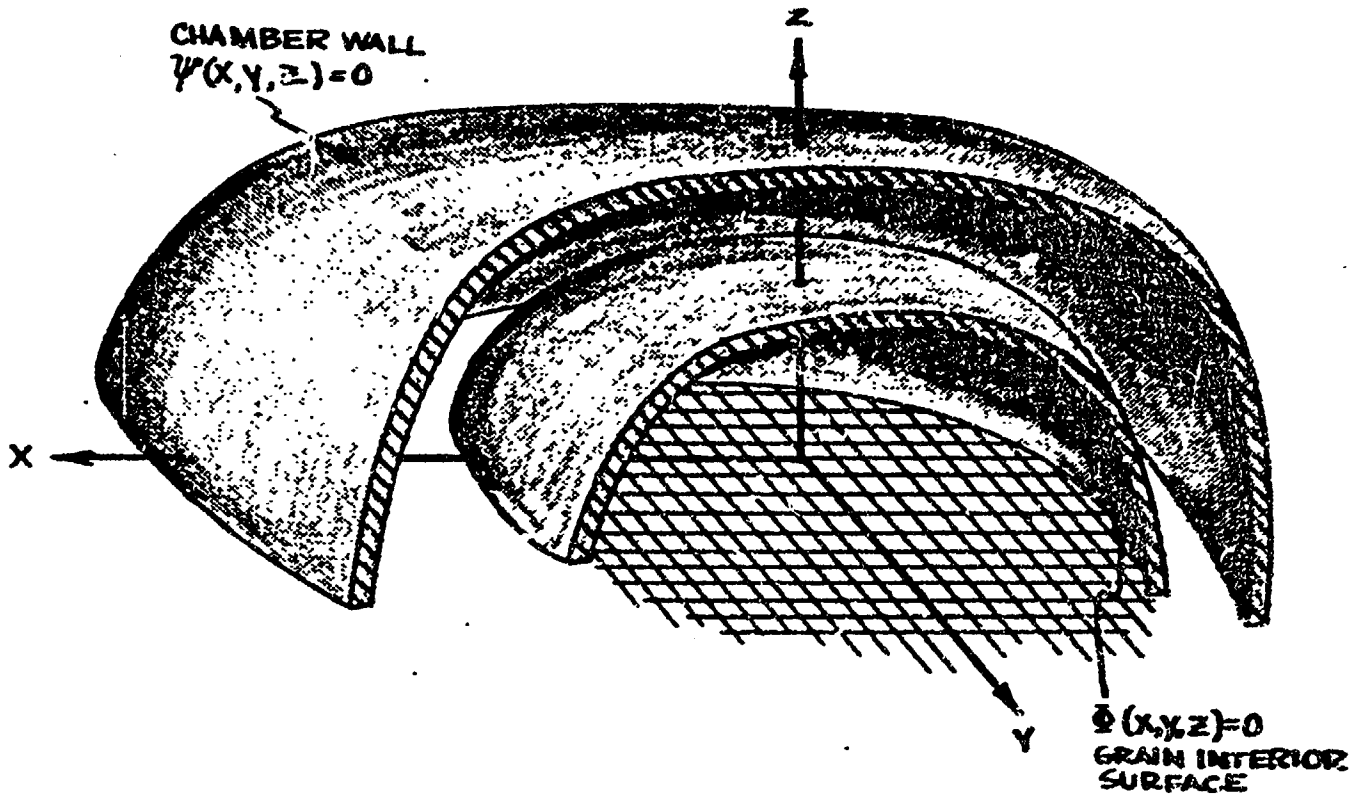

FIGURE 10 GRAIN REPRESENTATION

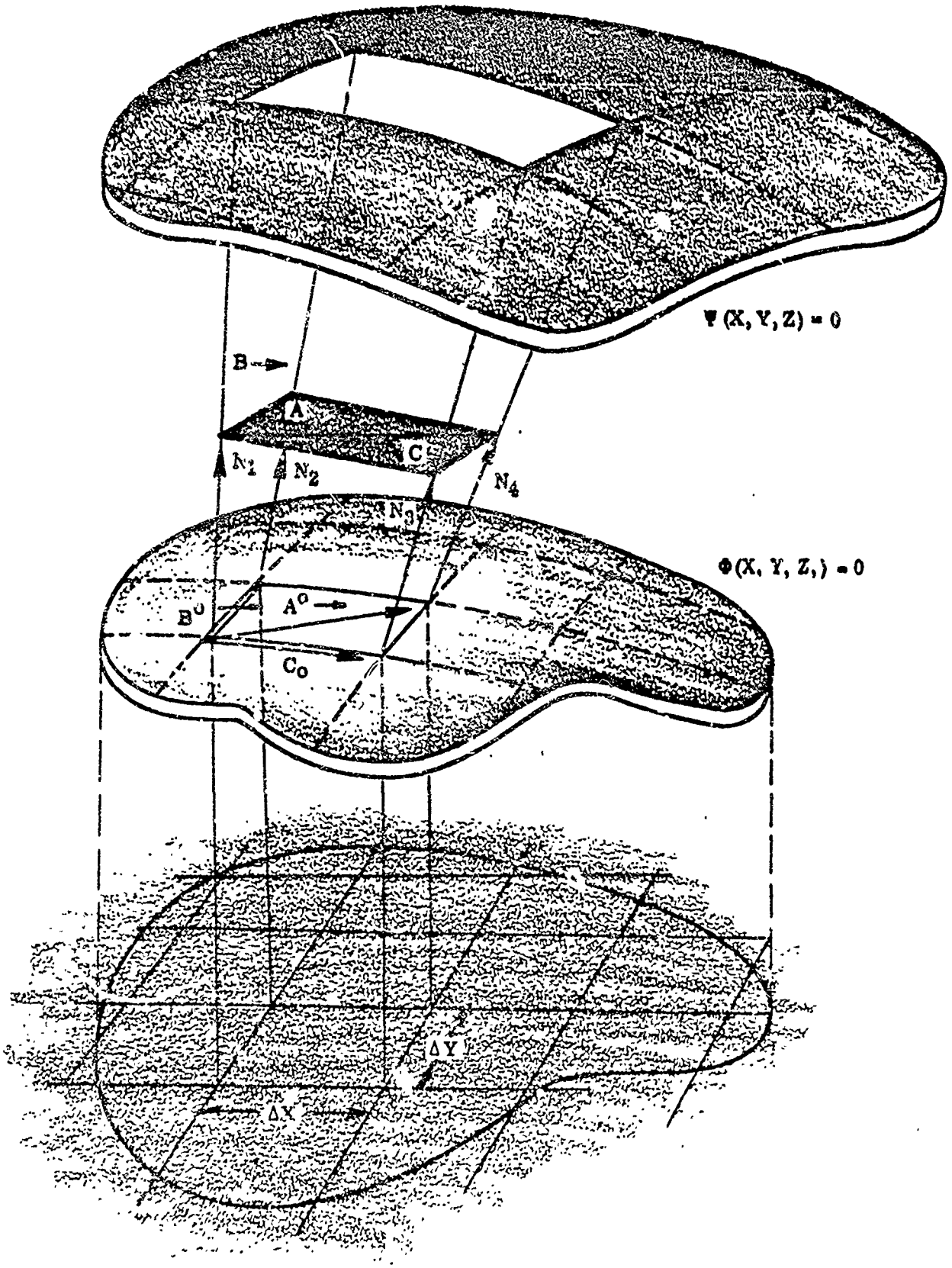

FIGURE 21. SAMPLE ELEMENT OF GRAIN

b. Control of Accuracy

Since the accuracy of the entire calculation is directly related to the angular separation of the normals, a criterion must be established for their selection. If θ_0 is the maximum permissible angular separation between any two adjacent normals, reducing θ_0 reduces the error until, as θ_0 approaches zero, the error approaches zero. Thus there exists a value of θ_0 which will ensure any predetermined degree of accuracy.

The angular separation of consecutive normals is considered under two separate conditions, each of which is handled in a completely independent manner.

The first of these to be considered is the case of normals emanating from the same point.

Initially the surface curvature is assumed to be minimal and normals are constructed for the coordinates as dictated by the specified mesh interval size. The angle between these normals is then compared with the maximum permissible angle. If the latter has been exceeded, a new coordinate is determined using the following variable mesh relationship:

$$dR = \frac{\frac{\partial \kappa}{\partial Z}\left(\frac{\partial \psi}{\partial Z}\right)^2 + \left(\frac{\partial \psi}{\partial R}\right)^2 \, d\theta}{\frac{\partial \psi}{\partial R}\frac{\partial \psi}{\partial Z}\frac{\partial}{\partial R}\left(\frac{\partial \psi}{\partial Z}\right) - \frac{\partial \psi}{\partial Z}\frac{\partial^2 \psi}{\partial Z^2} + \frac{\partial \psi}{\partial Z}\frac{\partial \psi}{\partial R}\frac{\partial}{\partial R}\left(\frac{\partial \psi}{\partial Z}\right) - \frac{\partial \psi}{\partial Z}\frac{\partial^2 \psi}{\partial R^2}} \qquad (1.17)$$

where:

Ψ (R, Z) = equation of the core head

$d\theta$ = maximum allowable angle between normals

dR = maximum allowable mesh increment, because of $d\theta$

The other condition is that of normals emanating from the same point. Stated mathematically, the problem is to find a vector, $\vec{N}$, in the plane of two other vectors (say $\vec{N}_1$ and $\vec{N}_2$), a fixed angle θ away from $\vec{N}_1$. One should be able to express $\vec{N}$ as follows:

$$\vec{N} = L_1 \vec{N}_1 + L_2 \vec{N}_2 \tag{1.18}$$

From the theory of linear algebra, this is always possible when $\vec{N}_1$ and $\vec{N}_2$ are co-planar but not co-linear.

Proof that the vector $\vec{N}$ is in the plane of $\vec{N}_1$ and $\vec{N}_2$ may be demonstrated by calculation of the triple vector product of $\vec{N}_1$, $\vec{N}_2$, and $\vec{N}$. Since this triple product represents the volume enclosed by a parallelopiped of sides parallel to the given vectors, a calculated value of zero (volume) shows that all three vectors are co-planar.

To this effect:

$$\begin{aligned}
\vec{N} \cdot (\vec{N}_1 \times \vec{N}_2) &= (L_1 \vec{N}_1 + L_2 \vec{N}_2) \cdot (\vec{N}_1 \times \vec{N}_2) \\
&= L_1 \vec{N}_1 \cdot (\vec{N}_1 \times \vec{N}_2) + L_2 \vec{N}_2 \cdot (\vec{N}_1 \times \vec{N}_2) \\
&= L_1 \vec{N}_2 \cdot (\vec{N}_1 \times \vec{N}_1) + L_2 \vec{N}_1 \cdot (\vec{N}_2 \times \vec{N}_2) \\
&= L_1 \vec{N}_2 \cdot (0) + L_2 \vec{N}_1 \cdot (0) \\
&= 0.
\end{aligned} \tag{1.19}$$

Application of the law of cosines shows that L_1 and L_2 are given by:

$$L_2 = \frac{\sin \theta}{\sin \Psi}$$

$$L_1 = \cos \theta - L_2 \cos \Psi$$

where θ = angle between $\vec{N}_1$ and $\vec{N}$

Ψ = angle between $\vec{N}_1$ and $\vec{N}_2$.

The derivation holds for $0 < \Psi < \pi$, provided that $\theta \neq \Psi$.

Thus by use of the angular control variable θ_0, one may directly control the accuracy of the resultant motor evaluation for both situations. By choosing a large value of θ_0 one obtains relatively inexpensive answers suitable for preliminary design purposes; by choosing a small value of θ_0, answers of extremely high accuracy may be obtained.

c. Maximum Burning Distance

Since burning along the i^{th} normal proceeds only to the outer web limiting surface, a maximum burning distance, $d\,max_i$, must be calculated. This is accomplished by the simultaneous solution of a scalar equation of the normal $\vec{N}_i$ and the equation of the case $\Psi(x, y, z) = 0$.

The coordinates x_i, y_i, and z_i of a point $P_i(d)$, a distance d along the i^{th} normal from the inner web limiting surface, $\phi(x, y, z) = 0$, are:

$$\begin{aligned} x_i &= x_i^\circ + d \cos \alpha_i \\ y_i &= y_i^\circ + d \cos \beta_i \\ z_i &= z_i^\circ + d \cos \gamma_i \end{aligned} \qquad (1.20)$$

where x_1^*, y_1^*, z_1^* are the coordinates of P_1 (0) in Figure 20 and cos α_1, cos β_1, and cos γ_1 are the direction cosines of $\vec{N}_1$. Thus, d max$_1$ is the value of d obtained by solving:

$$\psi(x_1, y_1, z_1) = 0$$

d. Elemental Surface, Volume and Mass

The burning surface area S of the surface element in Figure 21 is calculated by considering the following vector cross products:

$$S = 1/2\,|\bar{B} \times \bar{A}| + 1/2\,|\bar{A} \times \bar{C}| = 1/2\,|(\bar{A} \times (\bar{C}-\bar{B})|$$

where

$$\vec{A} = \vec{A}_o + d\,(\vec{N}_4 - \vec{N}_1)$$

$$\vec{B} = \vec{B}_o + l\,(\vec{N}_2 - \vec{N}_1)$$

$$\vec{C} = \vec{C}_o + d\,(\vec{N}_3 - \vec{N}_1)$$

By substituting (1.23) into (1.22), the equation of burning surface area as a function of burning distance, d, is obtained.

$$S(d) = 1/2\,\left|(\vec{A}_o + d\,(\vec{N}_4 - \vec{N}_1)\right| \times \left|(\vec{C}_o - \vec{B}_o) + d\,(\vec{N}_3 - \vec{N}_2)\right|$$

This expression may be reduced to:

$$S(d) = 1/2\,\left|\vec{C}_1 + \vec{C}_2 d + \vec{C}_3 d^2\right|$$

where $\vec{C}_1$, $\vec{C}_2$, and $\vec{C}_3$ are constant vectors defined by:

$$\vec{C}_1 = \vec{A}_o \times (\vec{C}_o - \vec{B}_o)$$

$$\vec{C}_1 = \vec{A}_o \times (\vec{N}_3 - \vec{N}_2) + (\vec{N}_4 - \vec{N}_1) \times (\vec{C}_o - \vec{B}_o)$$

$$\vec{C}_3 = (\vec{N}_4 - \vec{N}_1) \times (\vec{N}_3 - \vec{N}_2)$$

Note that the only variable in the elemental surface area equation (1.25) is the burning distance, d; the vectors $\vec{C}_1$, $\vec{C}_2$, and $\vec{C}_3$ have been determined by the inner web limiting surface.

The volume of propellant consumed as a result of the surface element burning out the distance from $d_{k-1} = \sum_{j=1}^{k-1} \Delta j$ to $d_k = \sum_{j=1}^{k} \Delta j$ is given by the approximation (Figure 22);

$$V_k = \frac{S_k + S_{k-1}}{2} \Delta_k \tag{1.27}$$

To retain over-all program accuracy especially with respect to the volume dependent parameters,* an extremely accurate method of evaluation of the propellant volumes adjacent to the case was needed. This requirement is attributable to the random manner in which each of the four normals may intersect the case and the significant variations in the respective maximum burning distances which result.

The technique employed in the program approximates the exact three-dimensional solution in the following manner: given d_{max_1}, d_{max_2}, d_{max_3}, d_{max_4}, which are the maximum burning distances along each of the normals $\vec{N}_1$, $\vec{N}_2$, $\vec{N}_3$, and $\vec{N}_4$, respectively, the two larger and two smaller values are independently averaged to obtain D_{max_L} (larger maximum burning distance) and D_{max_S} (smaller maximum burning distance). Using these parameters the various shapes of remaining propellant volumes may be extremely well approximated by use of the trapezoidal rule. Pictorial representation of these shapes, the applicable logic conditions which exist, and the respective equations for surface and volume evaluation are shown in Figure 23.

*Propellant volume, mass, and moments and products of inertia

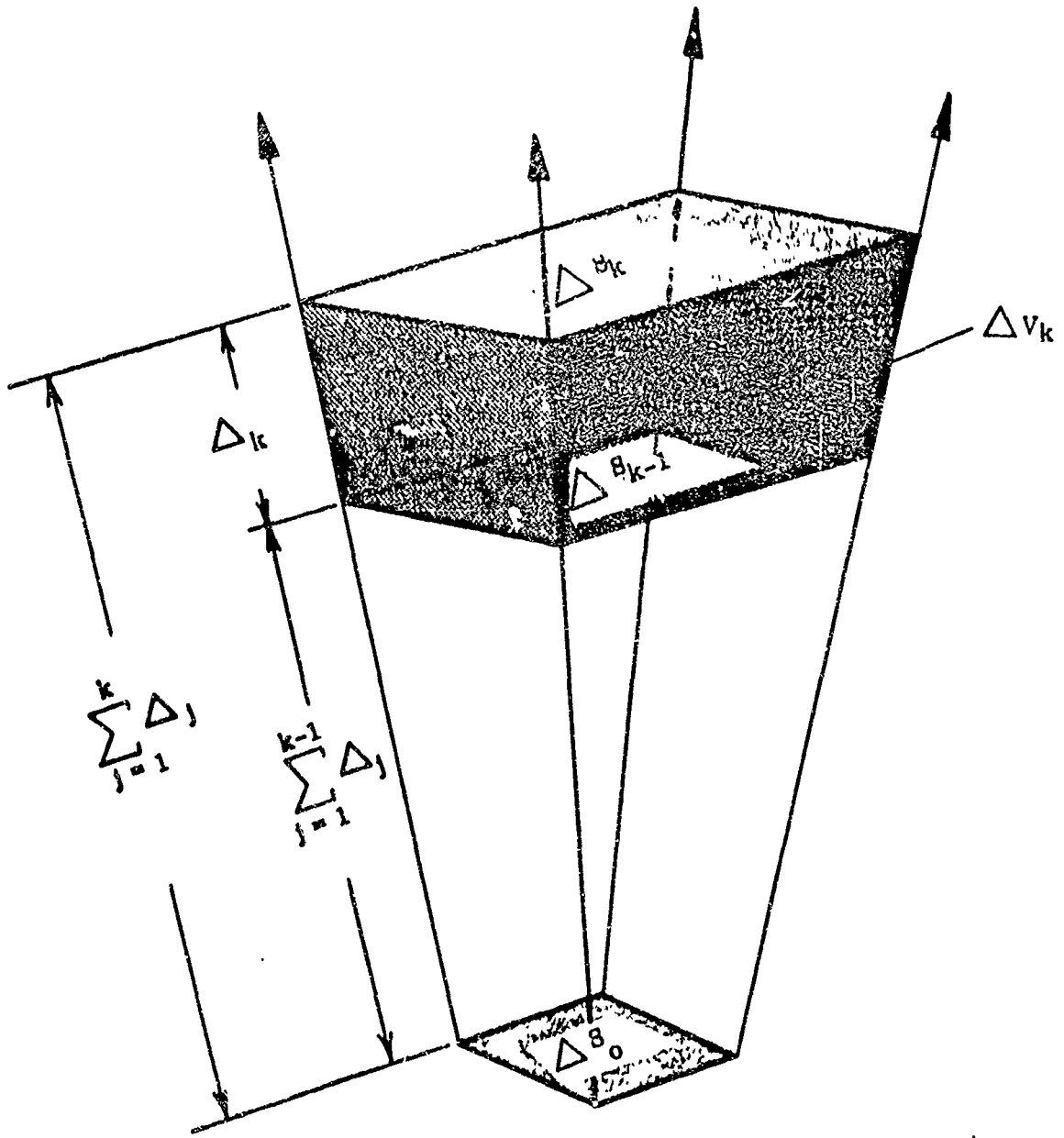

FIGURE 22. VOLUME ELEMENT

A-6599

		CRITERIA	FORMULAE
1.	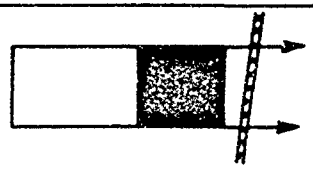	$D_{max_S} > d_k$	$S_k = S(d_k) =$ S (d) for the K^{th} burning shell $V_k = \frac{S_k + S_{k-1}}{2} \cdot \Delta_k$
2.	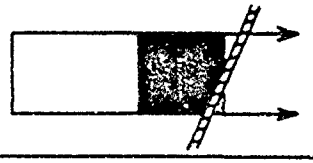	$D_{max_L} > d_k$ $d_{k-1} < D_{max_S} < d_k$	$S_k = \frac{D_{max_L} - d_k}{D_{max_L} - D_{max_S}} \cdot S(d_k)$ $V_k = \left(\frac{D_{max_L} + D_{max_S}}{2} - d_{k-1}\right) \cdot S_{k-1} - \left(\frac{D_{max_L} - d_k}{2}\right) S$
3.	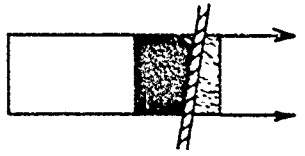	$d_{k-1} < D_{max_L} < d_k$ $d_{k-1} < D_{max_S} < d_k$	$S_k = 0$ $V_k = \left(\frac{D_{max_L} + D_{max_S}}{2} - d_{k-1}\right) \cdot S(d_{k-1})$
4.	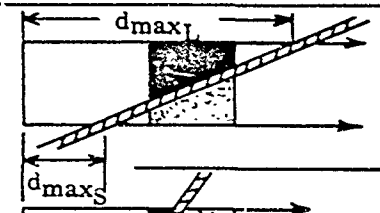	$d_k < D_{max_L}$ $D_{max_S} < d_{k-1}$	$S_k = \frac{D_{max_L} - d_k}{D_{max_L} - D_{max_S}} \cdot S(d_k)$ $V_k = \frac{S_k + S_{k-1}}{2} \cdot \Delta k$
5.	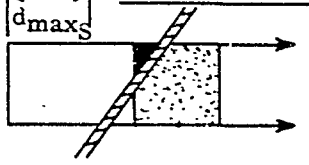	$d_{k-1} < D_{max_L} < d_k$ $D_{max_S} < d_{k-1}$	$S_k = 0$ $V_k = \frac{D_{max_L} - d_{k-1}}{2} \cdot S_{k-1}$
6.	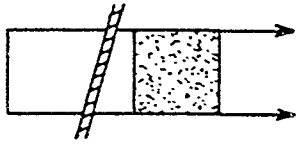	$D_{max_L} < d_{k-1}$	$S_k = 0$ $V_k = 0$

NOTE: S_k is the surface addition to the k^{th} shell summation.
$S(d_k)$ is the surface at the k^{th} shell independent of intersection of the normals with the case.

FIGURE 23. CALCULATION OF ELEMENTAL SURFACE AND VOLUME FOR VARIOUS "END" CONDITIONS

e. Elemental Moments and Products of Inertia

Since the increments Δ, Δx, Δy, and Δz as well as the maximum angle between normals, θ_o, may be arbitrarily assigned any value, sufficiently small values can be chosen so that the mass of any block can be treated as if it were concentrated as its center of mass.

If the eight corners of the volume element under consideration have coordinates (x_j, y_j, z_j), $j = 1, 2 \ldots 8$, the coordinates of the center of mass $\bar{X}_k$, $\bar{Y}_k$, $\bar{Z}_k$ are approximated by:

$$\bar{X}_k \simeq 1/8 \sum_{j=1}^{8} x_j, \quad \bar{Y}_k \simeq 1/8 \sum_{j=1}^{8} y_j, \quad \bar{Z}_k \simeq 1/8 \sum_{j=1}^{8} z_j \tag{1.28}$$

The moments and products of inertia of the k^{th} shell are:

$$\begin{aligned} (I_{xx})_k &= (\bar{Y}_k^2 + \bar{Z}_k^2)\, M_k & (I_{xy})_k &= -\bar{X}_k \bar{Y}_k M_k \\ (I_{yy})_k &= (\bar{X}_k^2 + \bar{Z}_k^2)\, M_k & (I_{xy})_k &= -\bar{X}_k \bar{Z}_k M_k \\ (I_{zz})_k &= (\bar{X}_k^2 + \bar{Y}_k^2)\, M_k & (I_{yz})_k &= -\bar{Y}_k \bar{Z}_k M_k \end{aligned} \tag{1.29}$$

Because of the cylindrical symmetry in most practical rocket systems, the only first moment to be considered is:

$$I_z = \bar{Z}_k M_k \tag{1.30}$$

This will be used to calculate the Z coordinate of the center of mass.

f. Total Surface, Moments and Products, Mass, and the Center of Mass

To review briefly, we have calculated an elemental burning surface area S_k, an elemental mass M_k, moments and products of inertia $(I_{xx})_k$, $(I_{yy})_k$, $(I_{zz})_k$, $(I_{xy})_k$, $(I_{xy})_k$, $(I_{yz})_k$, and first moment $(I_z)_k$ at each value of burning distance, $d = \Delta_1; \Delta_1 + \Delta_2, \Delta_1 + \Delta_2 + \Delta_3 \ldots\ldots, \sum_{j=1}^{k} \Delta_j = D_{max}$,

the average maximum distance between the inner and outer web limiting surfaces for this element.

As the analysis continues from block to block of the x-y mesh, these quantities are summed for corresponding values of k. Thus, after all the blocks of the mesh have been considered, the area, moments, and mass for the "shells" within the web, as shown in Figure 24, are derived.

Finally, since only the moments of inertia, products of inertia, and mass of the unconsumed portion of propellant are of interest, the shells must be added in the following manner:

$$(I_{xx})_j = \sum_{k=j}^{K_{max}} (I_{xx})_k \qquad (1.31)$$

where $(I_{xx})_j$ = xx moment of inertia of the unconsumed propellant after burning $\sum_{i=1}^{j} \Delta i$ units;

$(I_{xx})_k$ = xx moment of inertia of the k^{th} shell

k_{max} = total number of shell required to evaluate the motor.

Since chamber volume $(V_c)_j$ is defined as the volume of the case minus the volume of propellant, the equation becomes:

$$(V_c)_j = V - \frac{M_j}{\rho} \qquad (1.32)$$

where V = volume of case

ρ = density of propellant

M_j = mass of remaining propellant.

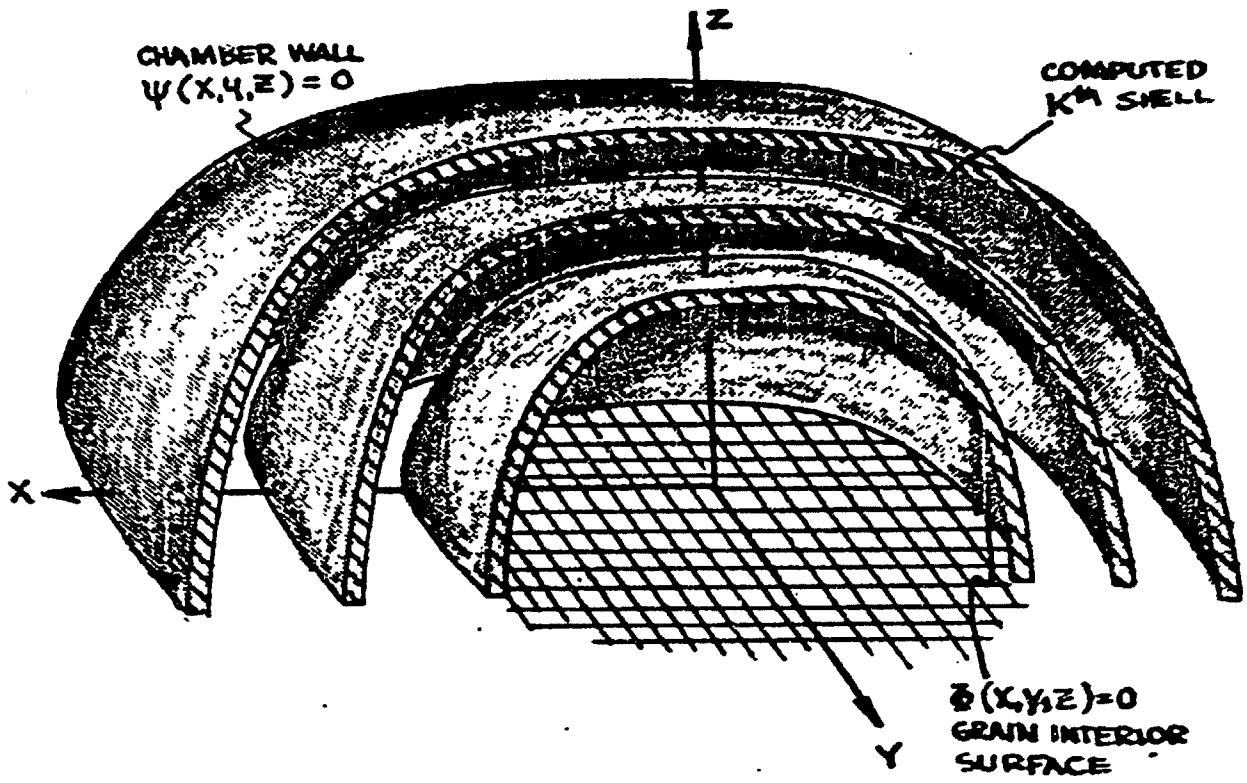

FIGURE 24. REPRESENTATION OF A SHELL WITHIN THE GRAIN

The Z coordinate $(Z_o)_j$ of the center of mass after burning a distance d_j is given by:

$$(Z_o)_j = \frac{(I_z)_j}{M_j} \tag{1.33}$$

where $(I_z)_j$ and M_j are defined as in equation, 1.31.

Using this method, moments and products of inertia, total mass of propellant, center of mass, and burning surface area of a solid propellant rocket grain for an arbitrary number of burning distances can be calculated. The general analysis as presented here is applicable for calculations of the head-end, aft-end, and straight-through portions of virtually any solid propellant grain configuration. The application of this analysis, via digital techniques, is purely restricted to the ingenuity of the programmer, the sophistication of the electronic data processing equipment available, and the order of priority of grain designs to be considered.

3. Theoretical Aspects of Nonuniform Temperature Grain Design Analysis

a. Preliminary Considerations

One of the more salient characteristics of Program AGDA is the fact that the propellant in the rocket motor under consideration is divided into literally thousands of small elements during the analysis. Since the coordinates of each small element are known in addition to its volume and surface area, a "handle" is readily available for the consideration of geometrically dependent propellant properties. The most important of these properties is grain temperature.

The effect of initial grain temperature on solid propellant rocket performance is well understood, provided that the entire grain is at the same

temperature. In general, a warmer motor burns for a shorter time and at a higher chamber pressure than an identical motor at a lower grain temperature. The total impulse, to a first approximation, is independent of the initial grain temperature, as is the progressivity or regressivity characteristics of the pressure-time or thrust-time trace.

When a nonuniform temperature gradient exists within the grain of a solid propellant rocket motor, no simple method exists to predict motor performance. The slope and shape of the pressure-time and thrust-time curves may be altered appreciably from that of the corresponding curves obtained at a uniform grain temperature. The principal purpose of this study area has been to examine in detail the effect of a nonuniform temperature gradient within the grain of a solid propellant rocket motor through a generalization of the Thiokol-Elkton Advanced Grain Design Analysis computer program.

b. Derivation of Technique of Nonuniform Temperature Grain Design Analysis

The burning rate, r, of a solid propellant rocket grain at temperature T_g is

$$r = r_c e^{\pi_k (T_g - T_{go})} f(P_c) \tag{1.34}$$

In this equation, r_o is the burning rate at grain temperature T_{go} and chamber pressure P_{co}, and π_k is the temperature sensitivity coefficient. The function $f(P_c)$ is usually of the form $(P_c/P_{co})^n$.

If dx is an increment of burn distance such that $r = \frac{dx}{dt}$ and

$r_o = \frac{dx_o}{dt}$, equation 1.34 may be written as

$$dx = dx_o e^{\pi_k (T_g - T_{go})} f(P_c) \tag{1.35}$$

The value of "dx" is required to perform a surface regression analysis which, in turn, is required to compute "P_o." However, P_o was required initially to compute dx. In order to avoid this difficulty, the surface regression analysis may be performed at the effective chamber pressure P_{co}. Since $f(P_o) = 1$ when $P_o = P_{co}$, the equation for dx becomes

$$dx = dx_o e^{\pi_k (T_g - T_{go})} \tag{1.36}$$

After the entire surface regression analysis has been completed using dx's from equation 1.36, the equilibrium chamber pressure may be defined as

$$P_c \alpha \left(\frac{A_s}{A_t}\right)^{\frac{1}{1-n}} \tag{1.37}$$

Since $r = \frac{dx}{dt}$ or $dt = \frac{dx}{r}$, formulas (1.35), (1.36) and (1.37) may be used to compute dt.

$$dt = \frac{dx_o e^{\pi_k (T_g - T_{go})} f(P_{co})}{r_o e^{\pi_k (T_g - T_{go})} f(P_c)} = \frac{dx_o}{r_o f(P_c)} \tag{1.38}$$

In application of equation (1.38), dx_o is chosen to be a fixed distance, say 5% of the web thickness; r_o is determined by experimentation with the propellant under consideration. Finally, if $f(P_c)$ has its usual form, the equation for dt may be expressed as

$$dt = \frac{dx_o}{r_o} \frac{P_{co}^{n}}{} P_c^{-n} \tag{1.39}$$

Figure 25 is intended to illustrate much of the foregoing theory.

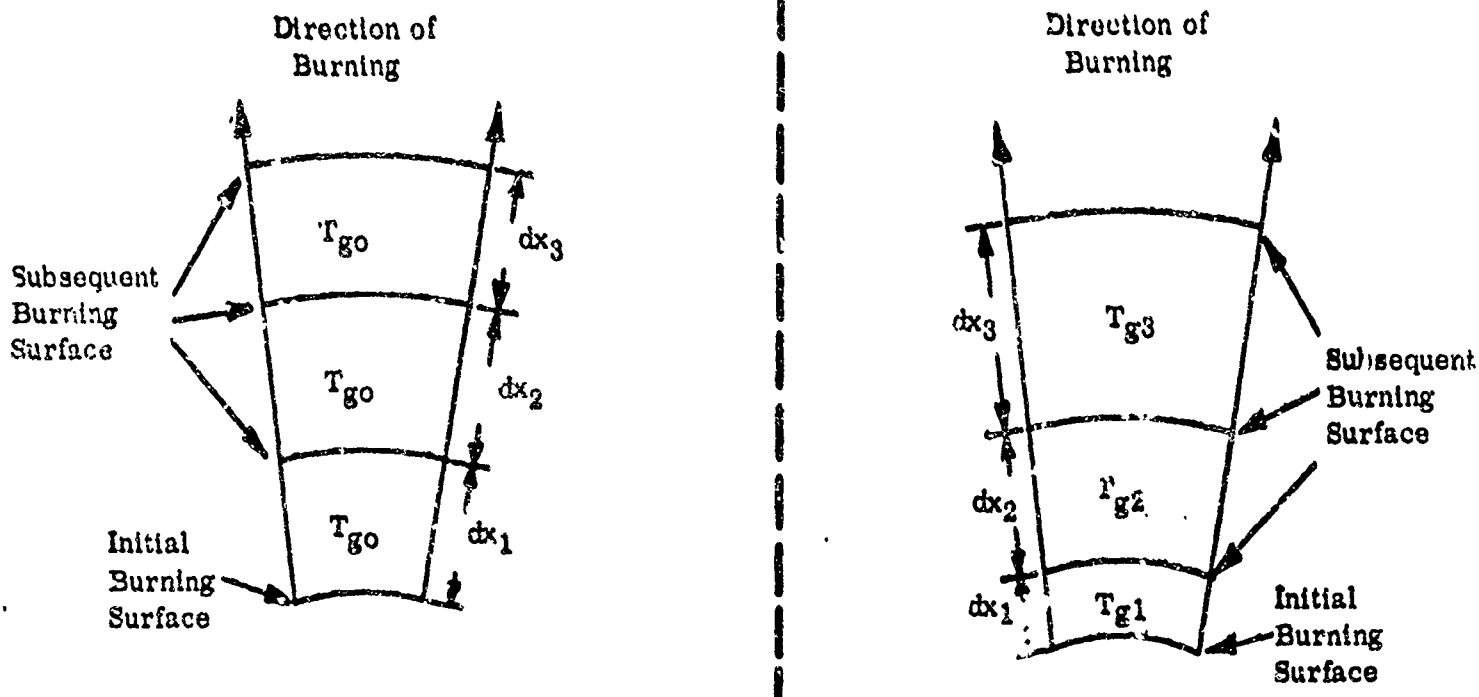

Uniform Grain Temperature

$$dx_0 = dx_1 = dx_2 = dx_3$$

when $T_{g0} = T_{g1} = T_{g2} = T_{g3}$

Nonuniform Grain Temperature

$$dx_1 < dx_2 < dx_3$$

when $T_{g1} < T_{g2} < T_{g3}$

Actual distance between burning surface calculations $= dx = dx_o e^{\pi_k (T_g - T_{gc})}$

Time corresponding to above Burn distance $= dt = \dfrac{dx_o}{r_o f(P_c)}$

FIGURE 15. COMPARISON OF ELEMENTAL SURFACE REGRESSION BETWEEN UNIFORM AND NONUNIFORM TEMPERATURE GRAINS

c. Incorporation of Variable Grain Temperature Effect Within the Framework of Program AGDA

The actual incorporation of the foregoing theory within the framework of Program AGDA may best be understood through a brief review of the program as previously described. A simplified Program AGDA for the uniform temperature condition is shown in Figure 26.

In order to proceed to the variable temperature case, only two modifications to this logic diagram are required. The first modification simply provides the computer memory with a table of grain temperatures for various coordinates. Each temperature is immediately translated to the corresponding value of Δ (incremental burning distance) by the formula

$$\Delta = \Delta_o e^{\pi_k (T_g - T_{go})} \tag{1.40}$$

where Δ_o = 5 percent of the web distance

π_k = temperature sensitivity coefficient

T_g = grain temperature at this point

T_{go} = reference grain temperature

The second modification involves two steps:

1) The coordinates of the center of the block of propellant under consideration are computed.

2) These coordinates are used to find the appropriate value of Δ to use for this particular block by the formula

$$\Delta = \Delta_{(i,j)} + \frac{\bar{x} - x_i}{x_{i+1} - x_i} (\Delta_{i+1,j} - \Delta_{ij}) + \frac{\bar{y} - y_j}{y_{j+1} - y_j} (\Delta_{i,j+1} - \Delta_{i,j}) \tag{1.41}$$

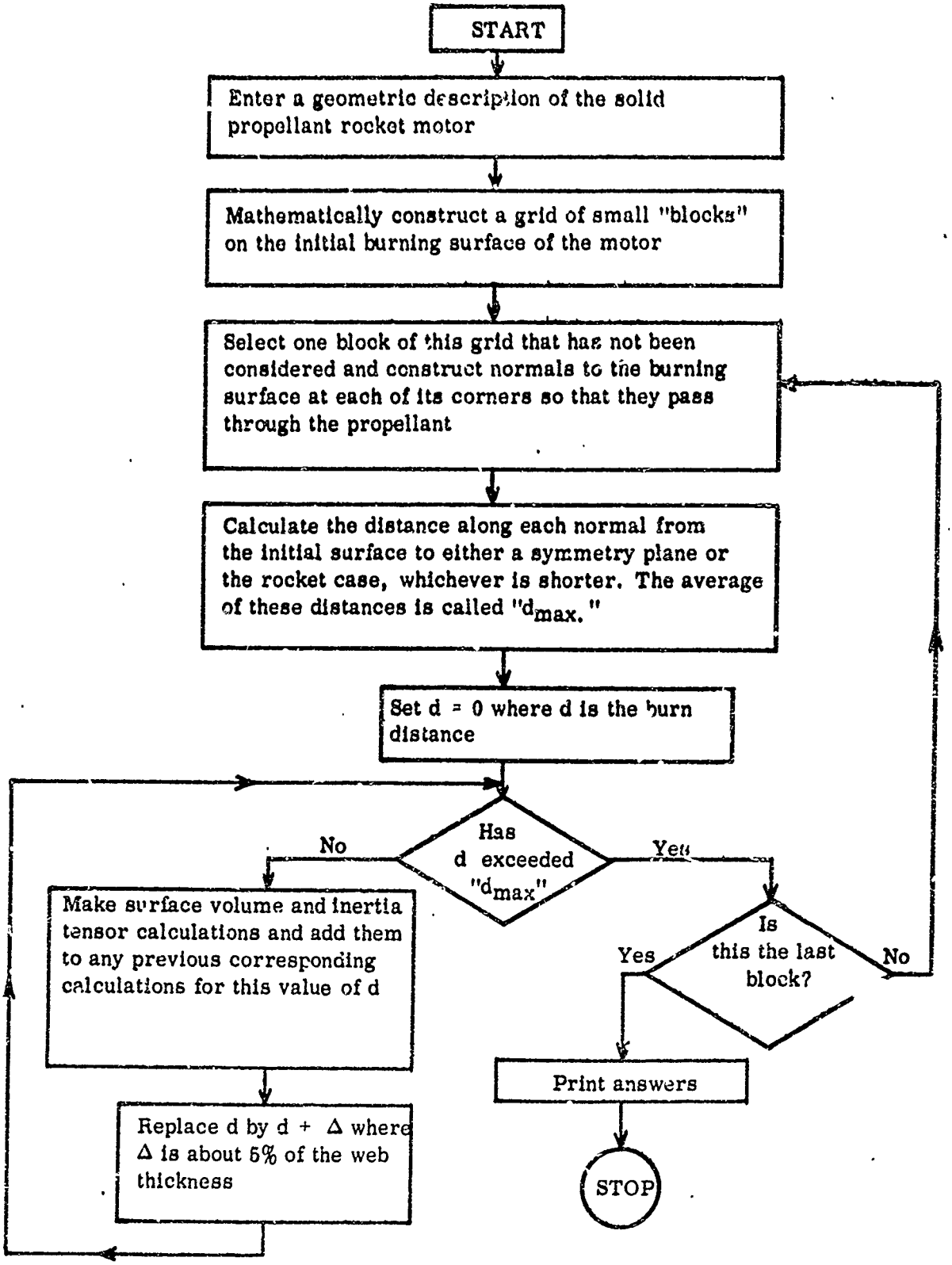

FIGURE 26. SIMPLIFIED PROGRAM AGDA

where

$\bar{x}$, $\bar{y}$ are coordinates of the center of the block

x_i, y_j are coordinates for which values of Δ are known exactly from the table

$\Delta_{i,j}$ is value of Δ associated with (x_i, y_j).

These modifications are shown in proper perspective in the logic diagram of Program AGDA with variable temperature, which is shown in Figure 27. An example illustrating the importance of inclusion of the variable grain temperature capability within Program AGDA is given in Section 4 (d) of this report.

The approach derived is not only unique but extremely desirable in that it manages to maintain both the simplicity of the Advanced Grain Design Program and the separation of the program from the heat transfer analysis. Since the latter is an extremely complex analysis, this separation is quite desirable. Further, the approach undertaken can be extended to consider effects, similar to temperature, which cause a positional variation of burning rate. In principle, the only requirement necessary is knowledge of the positional variation and the associated effect upon ballistic characteristics.

4. Application of the Theoretical Aspects of Program AGDA

a. Mathematical Representation of the Rocket Motor

Before an outline of the application of Program AGDA to a real problem is given, it is desirable to outline the philosphy by which the present program was devised.

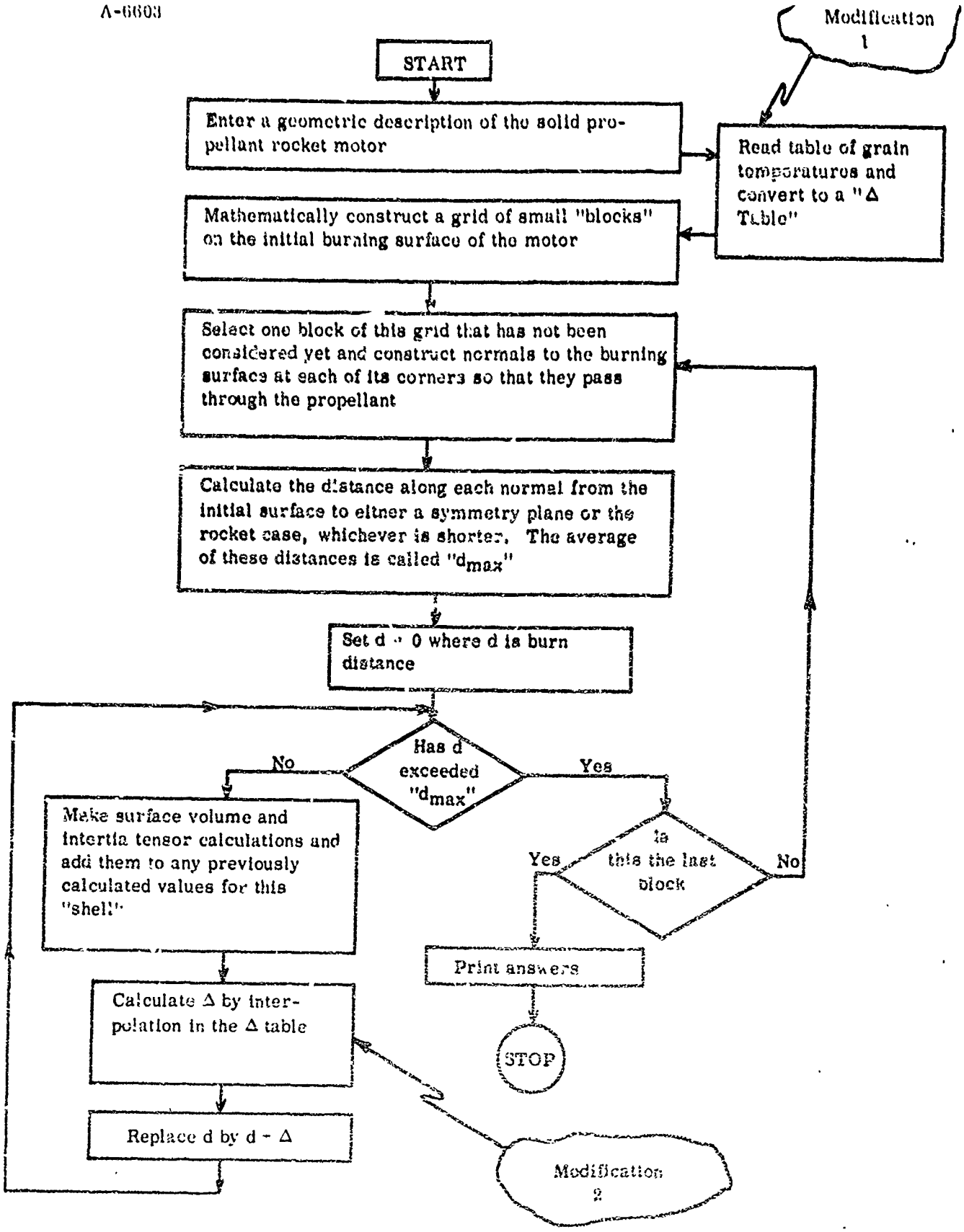

FIGURE 27. PROGRAM AGDA WITH VARIABLE TEMPERATURE

The first step in applying the Advanced Grain Design Analysis used above is to select a generalized mathematical model of a rocket motor. If this model is too simple, the resulting program will be too specific and have limited applicability. If the model is too complex, however, program utilization will suffer because of the quantity of input data required. The model selected according to this criterion is described below.

The case is divided into three sections: head end, aft end, and straight-through portion. Both the head- and aft-end equations must be either concave or convex ellipses of revolution. When one considers the totality of possible ellipses, this requirement is reasonably general.

The straight-through portion of the case must be cylindrical; however, both the length and radius are arbitrary. Note that the arbitrary length feature allows the length of this section to equal zero when spherical and elliptical motors are considered.

The surface of the chamber is divided into a head end and a straight-through portion. As shown in Figure 28, the head-end inner surface may be divided into as many as five general conic sections of revolution,* thus allowing for any configuration from a perfectly flat or a spherical head to a head with extremely complex curvature.

*The equation of a general conic section is: $Ax^2 + Bxy + Cy^2 + Dx + Ey + F = 0$. Thus the equation of a general conic section of revolution about the Z axis is $A(x^2+y^2) + Bz\sqrt{x^2+y^2} + cz^2 + D\sqrt{x^2+y^2} + ez + f = 0$.

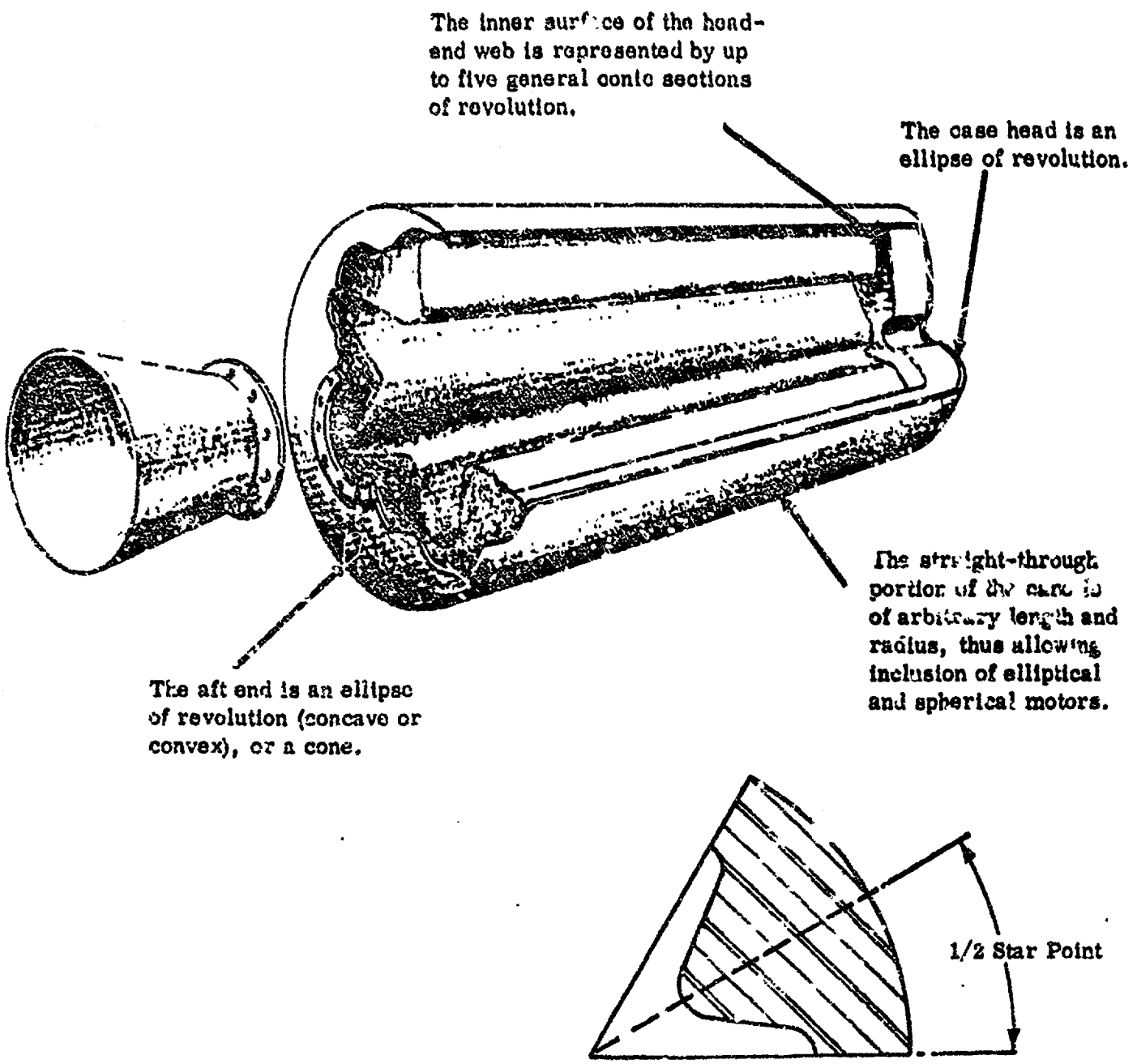

FIGURE 38. SCHEMATIC DIAGRAM OF A ROCKET MOTOR ILLUSTRATING COMPUTER PROGRAM CAPABILITIES

The straight-through portion of the chamber is considered to have any number of symmetrical sections (N star points). As shown in Figure 28, the surface representing one-half of one symmetrical section (star point) may consist of up to ten general conic sections. This is sufficient to fit virtually any singly perforated grain.

The second major step in applying the AGDA technique is to introduce a pseudo-rectangular grid on the surface of the chamber described above. Two techniques are used: one for the head-end, and the other for the straight-through portion. The head-end grid is formed by projecting an x-y mesh upward from the x-y plane (which is perpendicular to the rocket axis) to the chamber head surface. The grid for the straight-through portion is obtained from the points defining the periphery of this portion together with points equally spaced along the motor axis. Both grids are shown in Figure 29.

Once the surface is defined and the grid is superimposed, the remaining steps of Program AGDA involve simple vector integration, differentiation, multiplication, and addition. The mathematics involved are identical to those described in Section B-2 of this report.

b. Input Generator

One of the most significant innovations of the program is the input data generator. An extremely simple method of description of the geometrical peculiarities of an arbitrary motor was achieved. All parameters, other than several control and identification words, are directly obtainable from a standard engineering drawing or sketch. For example, cross sections of several classes of rocket motors

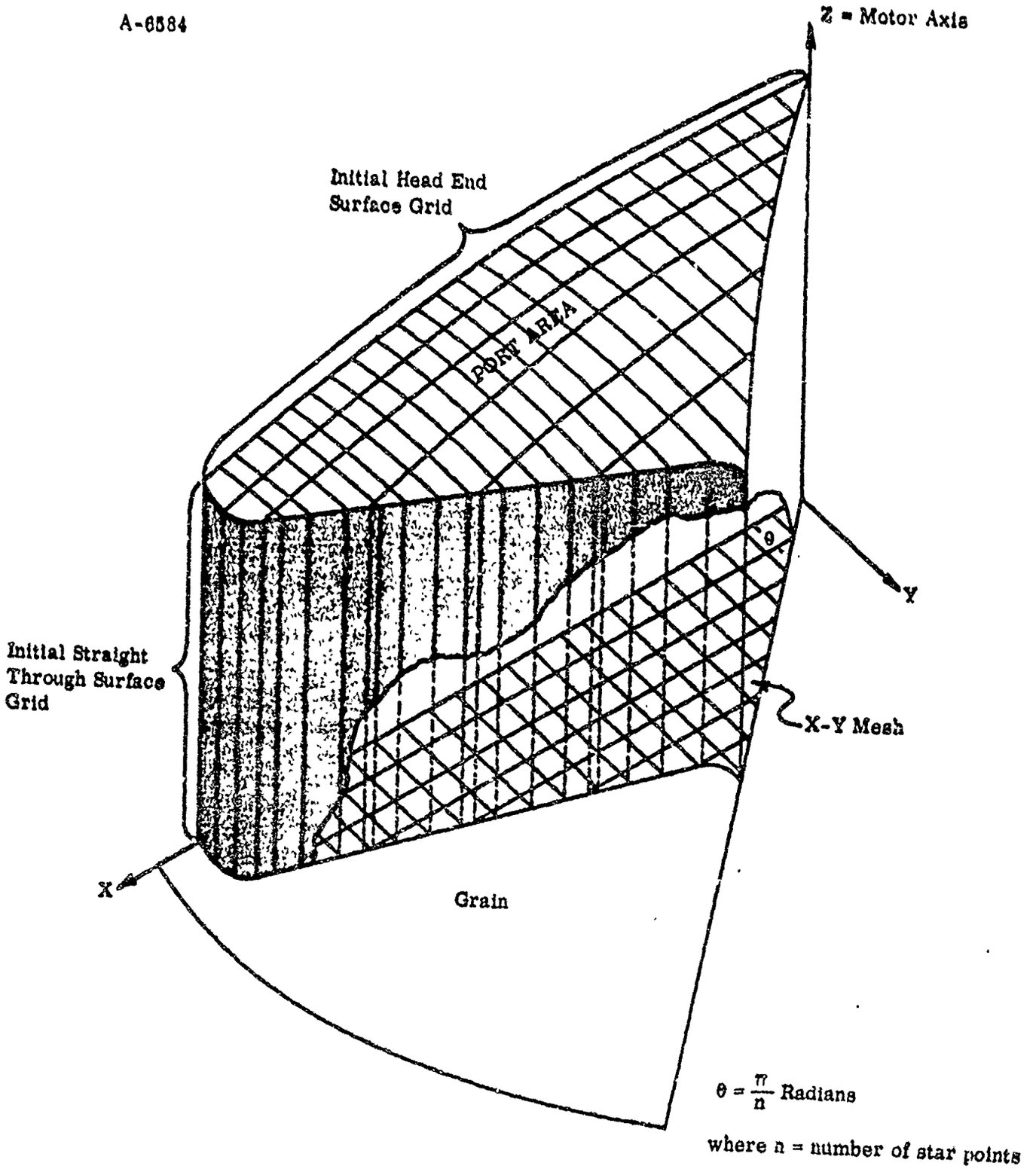

NOTE: The pseudo-rectangular grid is superimposed on a half star point of the inner surface of the grain. The X - Y mesh is visible through the cutaway portion of the star point.

FIGURE 23. EXAMPLE OF TYPICAL PSEUDO-RECTANGULAR GRID

readily specified to AGDA through the input generator are shown in Figure 30.

In rare instances, there may be need for the evaluation of a motor configuration which is not amenable to specifications using the input generator. To accommodate this possibility, the original input option (specification of all mathematical functions in generalized elliptical form) may be utilized.

The frequent engineering requirement for a grain of uniform head web thickness has called for individual consideration. Since the case head is usually an ellipse of revolution and ellipses do not burn into ellipses, a special iterative technique was devised to permit rapid calculations of the core head coordinates a constant distance from the case head. Amplification of the theory behind this technique is given in Appendix II.

A sample input data sheet describing the parameters required by the input data generator section of AGDA is shown in Figure 32. Reference is made to the sketch of a generalized rocket motor (see Figure 31) and Table I.

c. System of Checks and Balances

In extremely complex, and sometimes continuing, programs such as the Advanced Grain Design Analysis Computer Program, the need for extensive checking under a wide range of conditions is of paramount importance. To this end, the best programming practices have been exercised in the writing of the program, and to a certain extent, several novel programming innovations have been included to reduce significantly the "lost" computer time following an indication of system difficulty.

1. Simple Star

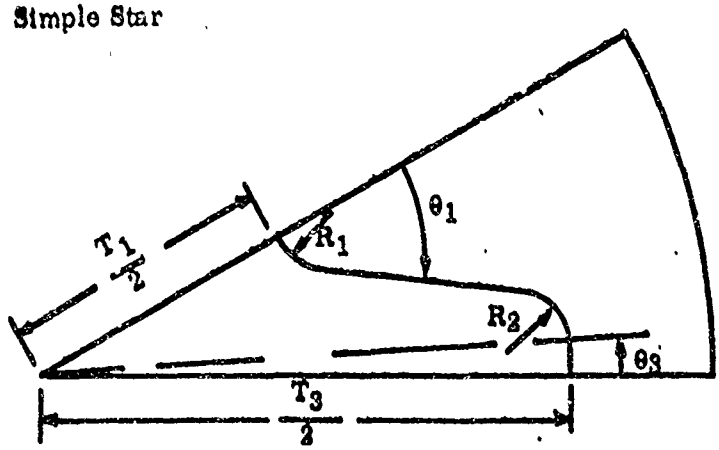

2. Broken Back Star

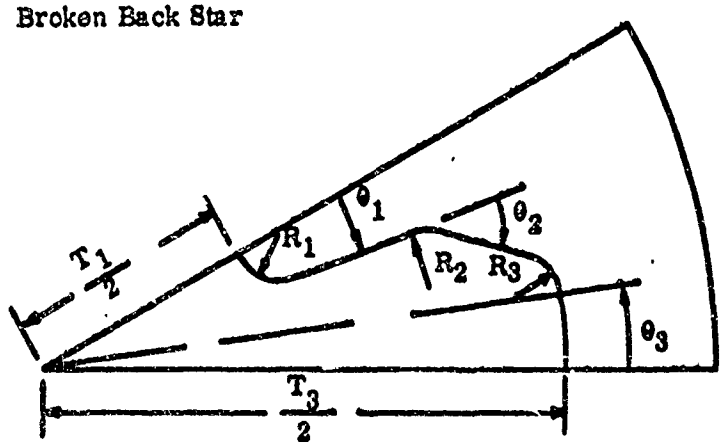

3. Wagon Wheel

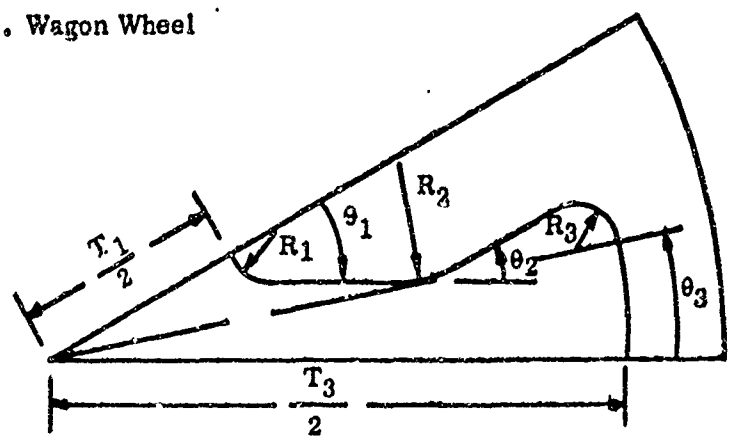

FIGURE 30. THE AGDA INPUT GENERATOR CONSIDERS ANY OF THESE THREE HALF STAR POINT CROSS SECTIONS

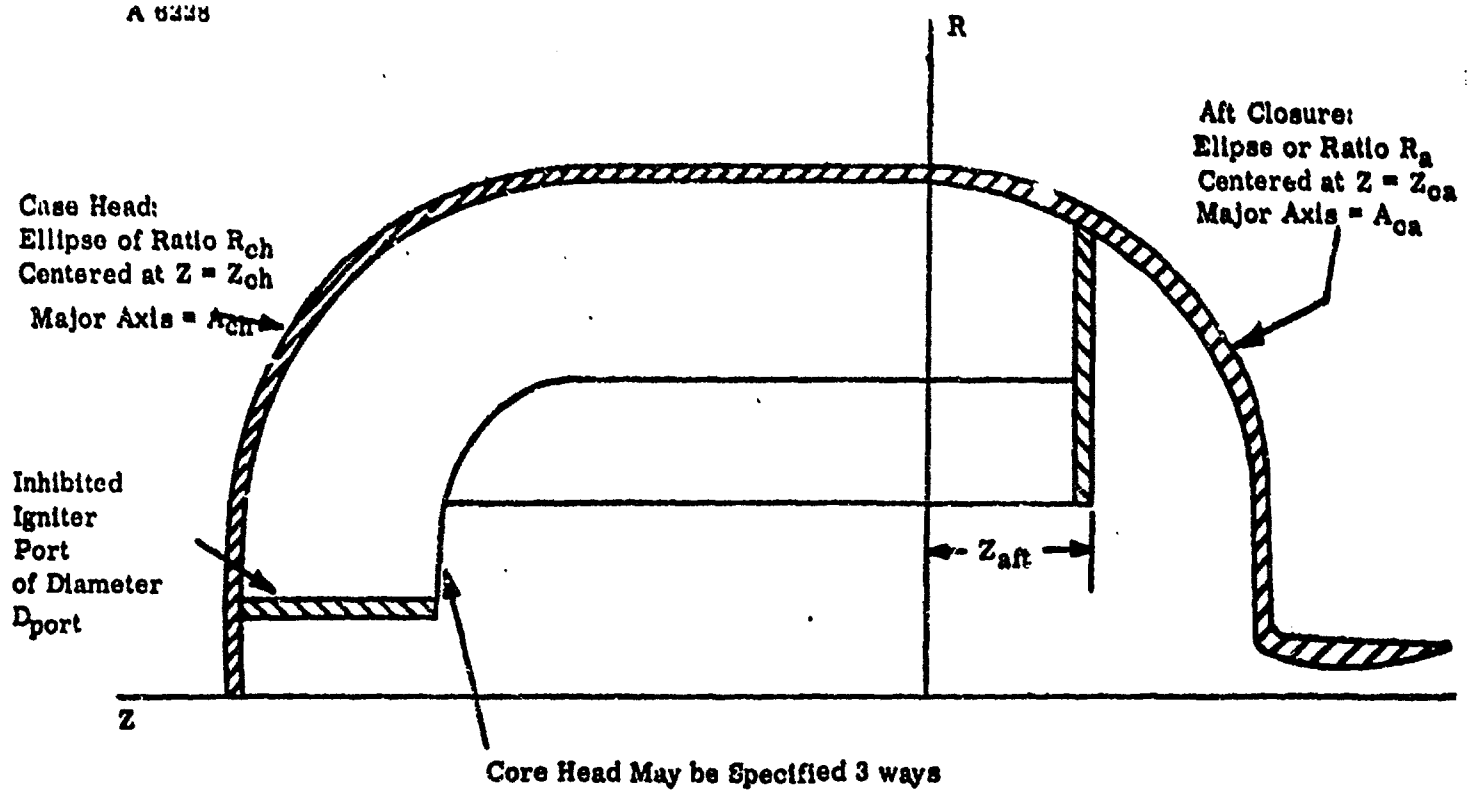

(1) Constant Distance from Case Head
(2) Ellipse of Ratio R_{core}, centered at Z_{core} with Major Axis = A_{core}
(3) As General Conic Section(s), up to five
$AR^2 + BRZ + CZ^2 + DR + EZ + F = 0$

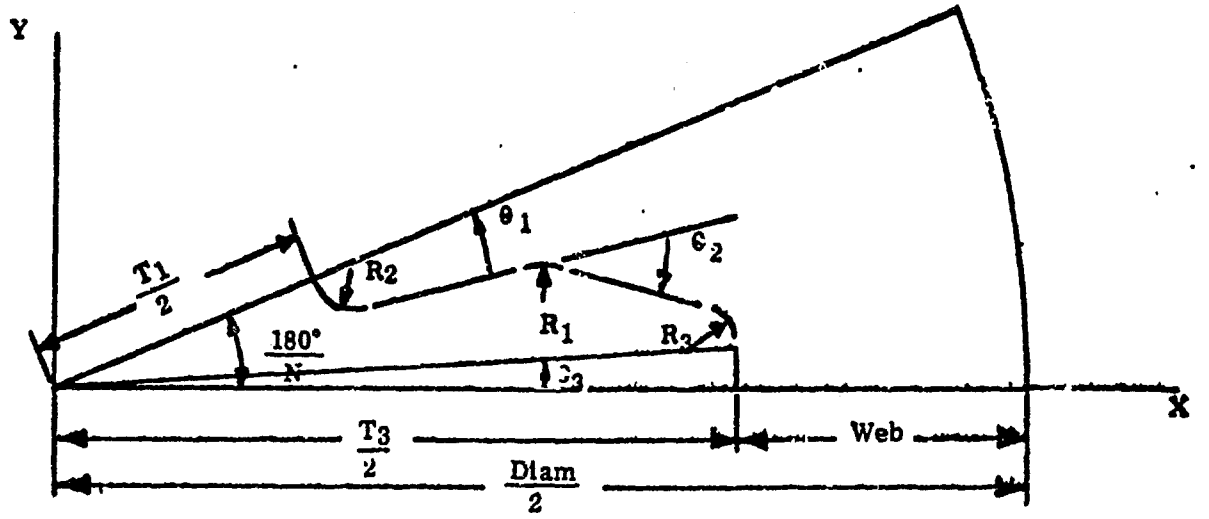

FIGURE 31. SCHEMATIC REPRESENTATION OF CROSS SECTIONS OF GENERALIZED SOLID PROPELLANT ROCKET AMENABLE TO SOLUTION WITH AGDA SHOWING REQUIRED INPUT PARAMETERS

TABLE I

INPUT DATA QUANTITIES REQUIRED BY THE AGDA INPUT GENERATOR*

RCH	Ellipse ratio of case head ellipse
ZCH	Z translation of center of case head ellipse
ACH	Major axis of case head ellipse
RCA	Ellipse ratio of case aft ellipse
ZCA	Z translation of center of case aft ellipse
ACA	Major axis of case aft ellipse
PORT	Diameter of igniter port
AFTCUT	Distance from Z = 0 to aft cutback
R1, R2, R3	Fillet radii in grain cross section
T1	Least port diameter
T3	Greatest port diameter
SN	Number of star points
HWEB	Head-end web thickness along transverse motor axis
ZNPCT	Percent web between printouts
ZEND	Type of run
ZRND	Control parameter for core rounds
ZNCORE	Number of core head equations used

* See Figure 32

NAME	NAME CARD							
CONT.	P[illegible]WEB BET. PRINTS	TYPE OF RUN*						
CASE	ACH	RCH	ZCH	CASE DIAM.	ACA	RCA	ZCA	
ST. THRU	R1	R2	R3	T_1 INNER CORE DIA	T_3 OUTER CORE DIA	N NO. STAR PTS.		
ST. THRU	θ1 DEGREES	θ1 MINUTES	θ2 DEGREES	θ2 MINUTES	θ3 DEGREES	θ3 MINUTES		
MISC.	INERT WT. LBS.	INERT C.G. IN.	PROP. DENSITY LB/CU.IN.	PORT DIAM. (IGNITER PORT) IN.	AFT CUTBACK IN.	HEAD WEB IN.		
GRID	ΔX X GRID SIZE	ΔY Y GRID SIZE	ΔZ Z GRID SIZE	$\Delta\theta$ MAX. ANGULAR NORMAL SEP.				

*TYPE OF RUN – -1.0 CHECK INPUT DATA
0.0 FULL RUN
1.0 ST. THRU ONLY
2.0 COMPUTES PROFILE
3.0 AFT END ONLY

KEYPUNCH – (1) ALL NUMERICAL INPUT IS F10
(2) COL. 1 ON NAME CARD IS BLANK

AGDA INPUT DATA

(This information is all that is needed to specify a rocket motor such as shown in Figure 1 to Program AGDA.)

FIGURE 32. AGDA INPUT DATA SHEET

The least complex, and probably the most frequently used, is the input data check option. In this type of run, the previously described input is processed by the input generator portion of the program; and the first two pages of program output are produced in entirety. Contained within the input generator portion of the program is a series of data compatibility checks. If the specified data fail to meet the requirements on one or more of these controls, the problem will be terminated as an input data check run regardless of the run type requested in the input data.

Probably the most crucial check is that which is made on the continuity of segment equations describing the central perforation. Since a primary control variable is the terminal (maximum) value of x for which a specific segment equation is valid, one of the coordinates assumed to be common to consecutive segments is immediately available. The y^- and y^+ values are then obtained from the left and right segment equations and the following requirements imposed:

$$\frac{y^- - y^+}{y^-} \leq 0.0001$$

Before this check was inserted, occasional difficulty was experienced in the transition from a given segment to an adjacent arc segment. Essentially, the incremented value x was not valid for the particular equation, since it was external to the curve. . In general engineering work, a certain tolerance is unconditionally associated with each set of calculated values; but, unfortunately, this flexibility is not available in the exact analytical representations from the computer.

Several of the numerous additional checks accomplished in this section of the program are:

1) Case equation check requiring zero coefficients for the radial translation terms to assure a surface of revolution about the transverse motor axis

2) Comparison of successive x coordinate cutoff values for the segment equations to assure a half star point specification which is a singly defined function in x

3) Evaluation of the need for the head-end web thickness, HWEB, for use in the inhibited igniter port calculation. If the latter is requested, PORT$\neq$ 0, the value of HWEB on the transverse motor axis will be calculated if the input value was zero. A note to this effect along with the computer value are included as output

4) For the constant head-end web option, installed for use with elliptical case equations, the ellipse ratio is compared with unity. If an identical comparison is found, the calculational option is altered and the appropriate spherical head-end case equation generated.

The next option in order of increasing complexity is the "Point Periphery Tape" option. This run will include all the check features mentioned above, and in addition, a great number of checks to assure proper flow, minimum degree of calculation sufficient for the particular option and the analysis, and the credibility of certain key parametric evaluations.

Another critical check occurs in the routine which calculates the maximum burning distance along a specific normal. If this value exceeds a predetermined large value (actually out of conceivable range), pertinent parameters are noted as output and the problem is terminated.

Of the numerous additional checks made in this part of the program there are two which are probably most significant: the variable mesh check and the point periphery generation check.

The function of the variable mesh check is to assure the fineness of grid structure required to meet the input tolerances in the most expedient manner.

The point periphery generation check assures that a minimal number of calculations will be done. The number of x grid evaluations is somewhat less than in the complete analysis, effecting a relatively small saving. On the other hand, the number of y grid evaluations per x grid is reduced to one, the required periphery point, as opposed to the five to twenty that might be required for the full analysis of the head end. Most significant, though, is the fact that this option involves no surface regression calculations.

The program output associated with the Point Periphery Tape Option, in addition to that mentioned above, includes the following:

1) The coordinates of each grid point on the half star point periphery, at the intersection of the core head and the straight-through section. Values are tabulated in cartesian and polar coordinates.

2) A point-wise tabulation of the point periphery vectors in terms of:

   a) The angle between the straight-through normal and the y axis, (S, Y)

   b) The angle between the head-end normal and the Z axis, (H, Z)

   c) The angle between the straight-through and head-end normals, (S, H).

3) Component and total check results for initial surface and initial chamber volume. The only parameters, other than input, supplied by the main program for these analyses are the points as described in 1) above.

4) Initial port area

5) Surface area depletion for core rounds (if requested).

Thus, throughout Program AGDA a series of checks and balances has been established which will ensure that the program:

1) Will not proceed any farther than necessary with faulty input data.

2) May be "saved" in the event of some electro-mechanical failure in the computer tape units.

3) Will provide a completely independent set of check results to help substantiate the actual program output.

With respect to the latter, the rocket engineer is assured that if the "check results" and the actual computer results agree, his answers are correct.

d. Uniform Temperature Example

For a complete appreciation of the versatility and ease of use of Program AGDA, reference is made to the following problem. The particular motor under consideration is illustrated in Figure 33.

For ease in handling of the data and to ensure the reliability of the input, the data are used immediately in the input generator program. Any inconsistencies in the input data are immediately noted in the output.

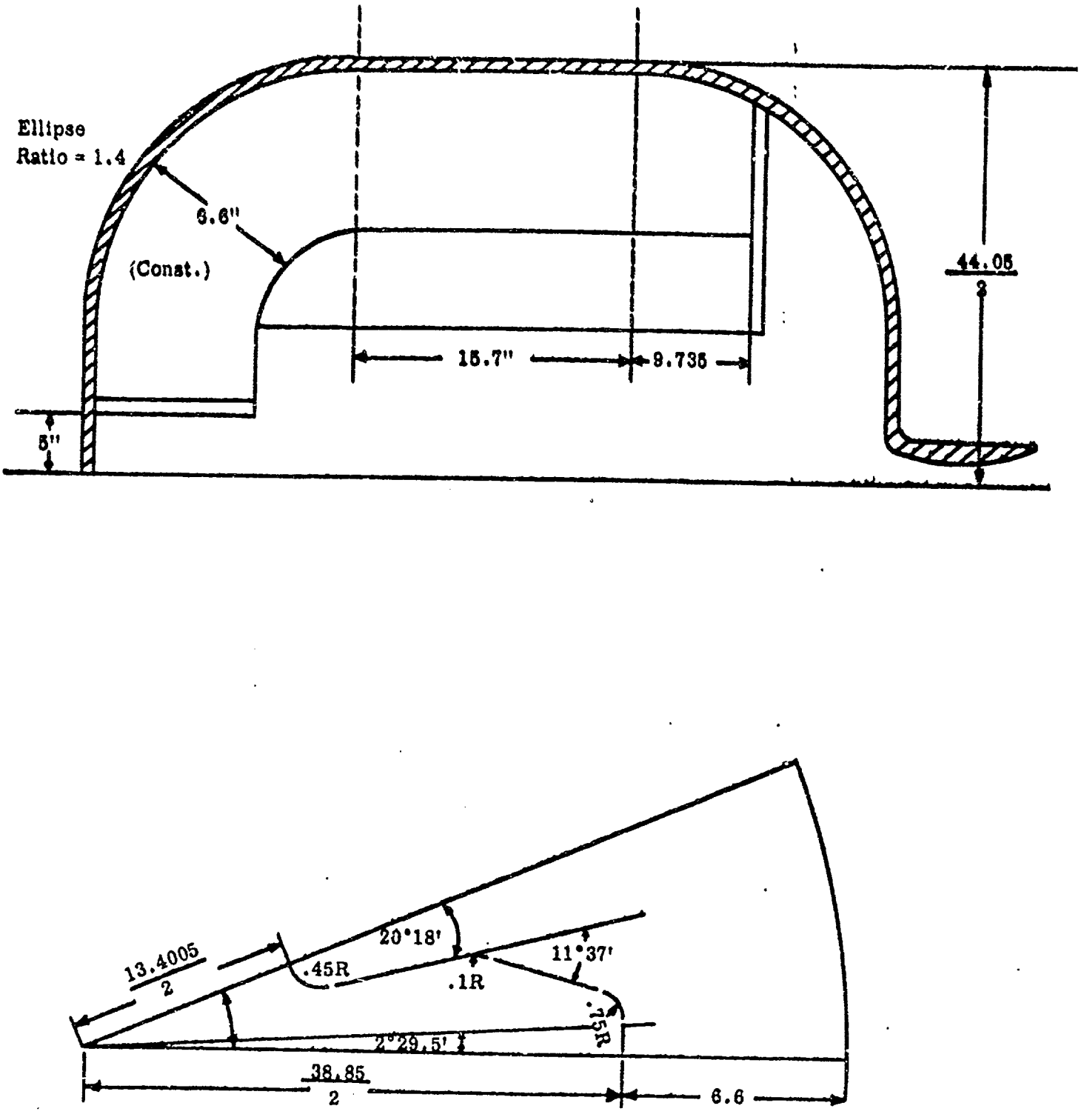

FIGURE 33. SCHEMATIC OF SOLID PROPELLANT ROCKET MOTOR FOR WHICH FULL COMPUTER OUTPUT IS PRESENTED IN TABLES II - XI

The program output for the complete rocket motor evaluation under consideration is shown in Tables II to XI.

Table II - the first page of computer output simply lists the input data "exactly as it appears on the input data cards," but with variable names printed above each word.

Tables III, IV, and V are the "Point Periphery Tape" output. This tape contains the coordinates and direction cosines which describe the head-end normals emanating from the point of intersection of the core surface of revolution and the straight-through star design. For output purposes, the direction cosines are expressed as angles relative to the coordinate axes. This is shown pictorially in Figures 34 and 35.

At the conclusion of the Point Periphery Tape output, the supplementary check results are printed (see Table VI). These results are obtained from Point Periphery Tape data only, and no use is made of the bulk of the Advanced Grain Design Analysis program. Initial surface area and initial chamber volume are calculated.

The next three pages of output (see Tables VII, VIII, and IX) are in the original output format. Table VI shows burning surface, chamber volume, and the first moment of the propellant along the Z axis. Table VIII shows the moments of inertia, while Table IX shows the products of inertia.

The final two pages of computer output (Tables X and XI) represent the new output data format. These pages are identical except that Table X is independent of propellant density, while Table XI utilizes this quantity for determination

GENERALIZED GRAIN DESIGN PROGRAM

GRAIN DESIGN INPUT GENERATOR

COMPLETE SOLID PROPELLANT ROCKET MOTOR EVALUATION TEST CASE

INPUT

CONTROL PARAMETERS

ZNPCT	ZEND	ZRND	ZNCORE
1.0			

CASE PARAMETERS

AC	RC	ZC	DIAM	ACA	RCA	ZCA
22.025	1.4	15.7	44.05	22.025	1.4	

CROSS SECTION PARAMETERS

R1	R2	R3	T1	T3	SN
.45	0.1	0.75	13.4005	30.85	8.0

THET1D	THET1M	THET2D	THET2M	THET3D	THET3M
0.0	18.0	11.0	37.0	2.0	29.5

CASER	CASECG	PROPD	PORT	AFTCUT	HWEB
705.76	-0.66	0.0632	10.0	9.735	6.6

DELX	DELY	DELZ	DELTHD	DELTHM
.3	0.3	0.5	5.0	

TABLE II. REPRODUCTION OF INPUT DATA TO PROGRAM AGDA FOR ROCKET SHOWN IN FIGURE 33
(Blank spaces indicate zero)

GENERALIZED GRAIN DESIGN PROGRAM

COMPLETE SOLID PROPELLANT ROCKET MOTOR EVALUATION TEST CASE

CHECK OUTPUT AND CORE ROUND CORRECTION

X	Y	Z	R	THETA	(S,Y)	(R,Z)	(S,H)
0.000000	0.000000	24.832141	0.000000	22.5000	90.0000	0.0000	90.0000
0.300000	0.124264	24.829965	0.324718	22.5000	90.0000	0.7676	90.0000
0.600000	0.248528	24.823436	0.649435	22.5000	90.0000	1.5363	90.0000
0.724264	0.300000	24.819454	0.783938	22.5000	90.0000	1.8548	90.0000
0.900000	0.372792	24.812545	0.974153	22.5000	90.0000	2.3059	90.0000
1.200000	0.497056	24.797279	1.298871	22.5000	90.0000	3.0776	90.0000
1.448528	0.600000	24.781306	1.567876	22.5000	90.0000	3.7189	90.0000
1.500000	0.621320	24.777620	1.623588	22.5000	90.0000	3.8519	90.0000
1.800000	0.745584	24.753543	1.948306	22.5000	90.0000	4.6294	90.0000
2.100000	0.869848	24.725020	2.273024	22.5000	90.0000	5.4110	90.0000
2.172792	0.900000	24.717425	2.351813	22.5000	90.0000	5.6013	90.0000
2.400000	0.994113	24.692014	2.597741	22.5000	90.0000	6.1972	90.0000
2.700000	1.118377	24.654485	2.922459	22.5000	90.0000	6.9889	90.0000
2.897056	1.200000	24.627350	3.135751	22.5000	90.0000	7.5122	90.0000
3.000000	1.242641	24.612385	3.247176	22.5000	90.0000	7.7867	90.0000
3.300000	1.366905	24.565657	3.571894	22.5000	90.0000	8.5916	90.0000
3.600000	1.491169	24.514243	3.896612	22.5000	90.0000	9.4042	90.0000
3.621320	1.500000	24.510409	3.919689	22.5000	90.0000	9.4623	90.0000
3.900000	1.615433	24.458071	4.221330	22.5000	90.0000	10.2258	90.0000
4.200000	1.739697	24.397063	4.546047	22.5000	90.0000	11.0566	90.0000
4.345585	1.800000	24.365692	4.703627	22.5000	90.0000	11.4637	90.0000
4.500000	1.863961	24.331139	4.870765	22.5000	90.0000	11.8952	90.0000
4.800000	1.988225	24.260193	5.195482	22.5000	90.0000	12.7516	90.0000
5.069849	2.100000	24.192010	5.487565	22.5000	90.0000	13.5301	90.0000
5.100000	2.112489	24.184130	5.520200	22.5000	90.0000	13.6179	90.0000
5.400000	2.236753	24.102825	5.844918	22.5000	90.0000	14.4981	90.0000
5.700000	2.361017	24.016152	6.169636	22.5000	90.0000	15.3937	90.0000
5.794113	2.400000	23.987831	6.271502	22.5000	90.0000	15.6781	90.0000
6.000000	2.485281	23.923967	6.494353	22.5000	90.0000	16.3061	90.0000
6.190224	2.564077	23.862589	6.700251	22.5000	67.5003	16.8941	73.1059
6.200973	2.540124	23.862342	6.701067	22.2756	64.1570	16.8965	73.1373
6.213159	2.516738	23.861594	6.703530	22.0512	60.7989	16.9035	73.2318
6.226756	2.494008	23.860341	6.707649	21.8276	57.4261	16.9154	73.3899
6.241735	2.472022	23.858581	6.713430	21.6059	54.0383	16.9320	73.6118
6.258063	2.450867	23.856312	6.720871	21.3870	50.6354	16.9535	73.8974
6.275703	2.430629	23.853541	6.729963	21.1718	47.2166	16.9798	74.2463
6.294610	2.411390	23.850258	6.740690	20.9612	43.7816	17.0105	74.6580
6.306948	2.400000	23.847974	6.748154	20.8335	41.6435	17.0321	74.9444
6.313560	2.394236	23.846708	6.752288	20.7678	40.5265	17.0440	75.1030
6.333531	2.378125	23.842719	6.765286	20.5802	37.2590	17.0815	75.6017
6.354496	2.363106	23.838291	6.779667	20.3991	33.9750	17.1236	76.1536

TABLE III. REPRODUCTION OF AGDA "POINT PERIPHERY TAPE" OUTPUT

GENERALIZED GRAIN DESIGN PROGRAM

COMPLETE SOLID PROPELLANT ROCKET MOTOR EVALUATION TEST CASE

X	Y	Z	R	THETA	(S,Y)	(H,Z)	(S,H)
6.376430	2.349228	23.833432	6.795420	20.2250	30.6698	17.1686	76.7583
6.399276	2.336561	23.828146	6.812507	20.0586	27.3432	17.2180	77.4144
6.422972	2.325173	23.822445	6.830885	19.9007	23.9954	17.2712	78.1206
6.447448	2.315128	23.816332	6.850504	19.7520	20.6262	17.3281	78.8749
6.472635	2.306491	23.809828	6.871310	19.6133	17.2353	17.3886	79.6756
6.498455	2.299316	23.802949	6.893241	19.4851	13.8230	17.4523	80.5205
6.524826	2.293660	23.795703	6.916230	19.3680	10.3884	17.5194	81.4076
6.551664	2.289572	23.788119	6.940205	19.2627	6.9313	17.5893	82.3344
6.578879	2.287099	23.780214	6.965089	19.1696	3.4515	17.6620	83.2994
6.606375	2.286284	23.772009	6.990800	19.0893	-0.0512	17.7373	84.2968
6.623244	2.286614	23.766868	7.006851	19.0468	-2.1998	17.7844	84.9216
6.923244	2.298138	23.672172	7.294707	18.3633	-2.1998	18.6373	84.8961
7.223244	2.309663	23.572312	7.583522	17.7319	-2.1998	19.5112	84.8689
7.523244	2.321188	23.467124	7.873190	17.1469	-2.1998	20.4075	84.8401
7.823244	2.332713	23.356410	8.163620	16.6034	-2.1998	21.3278	84.8093
8.123244	2.344238	23.239977	8.454735	16.0973	-2.1998	22.2739	84.7767
8.423244	2.355763	23.117592	8.746465	15.6249	-2.1998	23.2479	84.7420
8.723244	2.367287	22.988992	9.038752	15.1831	-2.1998	24.2522	84.7051
8.790053	2.369846	22.959484	9.103912	15.0885	-2.2002	24.4802	84.6968
8.796120	2.369896	22.956809	9.109782	15.0789	1.2763	24.5008	83.2958
8.802218	2.369575	22.954161	9.115587	15.0670	4.7762	24.5212	81.9012
8.810253	2.368580	22.950736	9.123088	15.0478	9.4166	24.5476	80.0930
9.110253	2.318826	22.821029	9.400727	14.2802	9.4166	25.5395	80.0219
9.410253	2.269072	22.684520	9.679956	13.5568	9.4166	26.5690	79.9461
9.710253	2.219317	22.540878	9.960642	12.8741	9.4166	27.6394	79.8653
10.010253	2.169563	22.389695	10.242663	12.2288	9.4166	28.7544	79.7791
10.310253	2.119809	22.230522	10.525915	11.6182	9.4166	29.9135	79.6870
10.429692	2.100000	22.164814	10.639007	11.3842	9.4166	30.3967	79.6485
10.610253	2.070054	22.062839	10.810299	11.0397	9.4166	31.1369	79.5884
10.910253	2.020300	21.886056	11.095730	10.4909	9.4166	32.4158	79.4828
11.210253	1.970546	21.699459	11.382127	9.9596	9.4166	33.7628	79.3695
11.510253	1.920792	21.502233	11.669419	9.4740	9.4166	35.1866	79.2476
11.810253	1.871037	21.293379	11.957543	9.0023	9.4166	36.6984	79.1161
12.110253	1.821283	21.071704	12.246439	8.5527	9.4166	38.3119	78.9738
12.238580	1.800000	20.972610	12.370240	8.3668	9.4166	39.0372	78.9093
12.410253	1.771529	20.835731	12.536055	8.1239	9.4166	40.0441	78.8194
12.710253	1.721774	20.583648	12.826341	7.7145	9.4166	41.9170	78.6511
13.010253	1.672020	20.313044	13.117253	7.3233	9.4166	43.9599	78.4668
13.310253	1.622266	20.020780	13.408749	6.9490	9.4166	46.2119	78.2637
13.610253	1.572511	19.702569	13.700794	6.5907	9.4166	48.7283	78.0382
13.910253	1.522757	19.352159	13.993352	6.2473	9.4166	51.5909	77.7858

TABLE IV. REPRODUCTION OF PAGE 2 OF AGDA "POINT PERIPHERY TAPE" OUTPUT

GENERALIZED GRAIN DESIGN PROGRAM

COMPLETE SOLID PROPELLANT ROCKET MOTOR EVALUATION TEST CASE

X	Y	Z	R	THETA	(S,Y)	(H,Z)	(S,M)
14.047468	1.500000	19.178724	14.127326	6.0950	9.4166	53.0480	77.6597
14.210253	1.473003	18.959952	14.286392	5.9180	9.4166	54.9280	77.5900
14.510253	1.423248	18.809560	14.579385	5.6020	9.4166	58.9621	77.1718
14.783834	1.377875	18.021092	14.847904	5.3247	9.4166	63.6179	76.3234
14.828248	1.369126	17.931825	14.891320	5.2753	12.8753	64.5032	73.6635
14.872167	1.357677	17.840472	14.934009	5.2161	16.3431	63.4207	70.4782
14.915425	1.343554	17.747043	14.975814	5.1472	19.8200	66.3712	67.2500
14.957859	1.326786	17.651610	15.016587	5.0690	23.3062	67.3550	63.9841
14.999306	1.307408	17.554289	15.056177	4.9816	26.8020	68.3718	60.6838
15.039606	1.285478	17.455135	15.094442	4.8854	30.3076	69.4218	57.3465
15.078603	1.261048	17.354268	15.131242	4.7806	33.8236	70.5046	53.9730
15.116142	1.234188	17.251702	15.166441	4.6677	37.3504	71.6207	50.5536
15.152073	1.204966	17.147496	15.199909	4.5469	40.9891	72.7701	47.1178
15.157753	1.200000	17.130406	15.205179	4.5265	41.4655	72.9600	46.5542
15.186250	1.173473	17.041721	15.231520	4.4186	44.4400	73.9524	43.6357
15.218533	1.139780	16.934473	15.261154	4.2831	48.0054	75.1668	40.1153
15.247043	1.106174	16.832222	15.287116	4.1495	51.3725	76.3390	36.7720
15.273603	1.070854	16.728827	15.311095	4.0105	54.7490	77.5379	33.3994
15.298086	1.033945	16.624559	15.332986	3.8665	58.1331	78.7600	30.0018
15.320389	0.995584	16.519368	15.352703	3.7181	61.5234	80.0054	26.5813
15.340396	0.955933	16.413635	15.370150	3.5658	64.9168	81.2683	23.1432
15.357996	0.915242	16.307463	15.385242	3.4104	68.3041	82.5481	19.8974
15.363869	0.900000	16.268152	15.390206	3.3525	69.5520	83.0242	18.4245
15.373234	0.873366	16.200389	15.398021	3.2515	71.7089	83.8476	16.2224
15.386031	0.830378	16.092272	15.408421	3.0892	75.1359	85.1679	12.7148
15.396291	0.786414	15.982956	15.416361	2.9240	78.5853	86.5094	9.1753
15.403937	0.741617	15.872899	15.421778	2.7564	82.0575	87.8650	5.6072
15.408868	0.696139	15.762443	15.424584	2.5867	85.5527	89.2295	2.0140
15.410416	0.670597	15.707111	15.424999	2.4917	87.5083	89.9121	0.0869
15.413326	0.600000	15.707111	15.424999	2.2292	87.7707	89.9121	0.0869
15.422082	0.300000	15.707111	15.424999	1.1144	88.8856	89.9121	0.0869
15.423409	0.221540	15.707111	15.424999	0.8229	89.1771	89.9121	0.0869
15.425000	0.000000	15.707111	15.424999	0.0000	90.0000	89.9121	0.0869

TABLE V. REPRODUCTION OF PAGE 3 OF AGDA "POINT PERIPHERY TAPE" OUTPUT

GENERALIZED GRAIN DESIGN PROGRAM

COMPLETE SOLID PROPELLANT ROCKET MOTOR EVALUATION TEST CASE

SUPPLEMENTARY CHECK RESULTS

	TOTAL	HEAD END	TOP SECT. ST. THRU	CENTER SECT. ST. THRU	AFT END
SURFACE	4022.39	509.56	878.05	2634.79	0.00
VOLUME	9434.28		2899.71	6534.57	0.00

PORT AREA = 416.0262

TABLE VI. CHECK RESULTS
(These results are based only upon "Point Periphery Tape" data and therefore serve to validate the majority of AGDA.)

COMPUTED TRACE OF INTERNAL GEOMETRY

COMPLETE SOLID PROPELLANT ROCKET MOTOR EVALUATION TEST CASE

WEB BURNOUT (PERCENT)	CHAMBER SURFACE (SQ-IN)	CHAMBER VOLUME (CU-IN)	FIRST I MOMENT (IN**4)
0	5.5747E 03	1.7151E 04	3.8688E 05
5	5.7019E 03	1.9012E 04	3.7302E 05
10	5.6624E 03	2.0901E 04	3.5862E 05
15	5.5267E 03	2.2747E 04	3.4420E 05
20	5.4046E 03	2.4546E 04	3.2976E 05
25	5.4202E 03	2.6331E 04	3.1509E 05
30	5.4407E 03	2.8123E 04	3.0001E 05
35	5.4533E 03	2.9920E 04	2.8449E 05
40	5.4620E 03	3.1720E 04	2.6850E 05
45	5.4666E 03	3.3522E 04	2.5201E 05
50	5.4663E 03	3.5325E 04	2.3499E 05
55	5.4621E 03	3.7127E 04	2.1741E 05
60	5.4524E 03	3.8926E 04	1.9921E 05
65	5.4373E 03	4.0722E 04	1.8039E 05
70	5.4150E 03	4.2511E 04	1.6089E 05
75	5.3858E 03	4.4292E 04	1.4066E 05
80	5.3518E 03	4.6060E 04	1.1971E 05
85	5.3232E 03	4.7818E 04	9.7932E 04
90	5.3015E 03	4.9568E 04	7.5305E 04
95	5.2695E 03	5.1309E 04	5.1799E 04
100-	5.2273E 03		
100+	4.4455E 03	5.3027E 04	2.7563E 04
105	2.4510E 03	5.4002E 04	1.7304E 04
110	1.8014E 03	5.4692E 04	1.0595E 04
115	1.2943E 03	5.5193E 04	5.9546E 03
120	8.7868E 02	5.5546E 04	2.8386E 03
125	5.0963E 02	5.5771E 04	9.6954E 02
130	1.6718E 02	5.5878E 04	1.2255E 02

WEB THICKNESS =	6.600
HEIGHT =	15.700
DIAMETER =	44.050
CASE VOLUME =	55894.089
INHIBITED PORT DIAMETER =	10.000

TABLE VII. PAGE 1 OF SUMMARIZATION OF PROGRAM AGDA OUTPUT

COMPUTED TRACE OF MOMENTS OF INERTIA

COMPLETE SOLID PROPELLANT ROCKET MOTOR EVALUATION TEST CASE

WEB BURNOUT (PERCENT)	I-XX (IN**5)	I-YY (IN**5)	I-ZZ (IN**5)
0	1.3464E 07	1.3464E 07	1.0534E 07
5	1.3054E 07	1.3054E 07	1.0280E 07
10	1.2619E 07	1.2619E 07	1.0000E 07
15	1.2171E 07	1.2171E 07	9.7007E 06
20	1.1710E 07	1.1710E 07	9.3811E 06
25	1.1230E 07	1.1230E 07	9.0394E 06
30	1.0726E 07	1.0726E 07	8.6734E 06
35	1.0199E 07	1.0199E 07	8.2833E 06
40	9.6484E 06	9.6484E 06	7.8691E 06
45	9.0732E 06	9.0732E 06	7.4313E 06
50	8.4736E 06	8.4736E 06	6.9701E 06
55	7.8491E 06	7.8491E 06	6.4859E 06
60	7.1994E 06	7.1994E 06	5.9794E 06
65	6.5245E 06	6.5245E 06	5.4513E 06
70	5.8240E 06	5.8240E 06	4.9026E 06
75	5.0975E 06	5.0975E 06	4.3345E 06
80	4.3465E 06	4.3465E 06	3.7491E 06
85	3.5690E 06	3.5690E 06	3.1464E 06
90	2.7642E 06	2.7642E 06	2.5266E 06
95	1.9318E 06	1.9318E 06	1.8905E 06
100	1.0789E 06	1.0789E 06	1.2447E 06
105	6.8974E 05	6.8974E 05	8.3811E 05
110	4.2827E 05	4.2827E 05	5.4197E 05
115	2.4406E 05	2.4406E 05	3.2124E 05
120	1.1819E 05	1.1819E 05	1.6209E 05
125	4.0706E 04	4.0706E 04	5.8056E 04
130	4.0489E 02	6.3055E 01	8.5904E 01

TABLE VIII. PAGE 2 OF SUMMARIZATION OF PROGRAM AGDA OUTPUT

COMPUTED TRACE OF PRODUCTS OF INERTIA

COMPLETE SOLID PROPELLANT ROCKET MOTOR EVALUATION TEST CASE

WEB BURNOUT (PERCENT)	I-XY (IN**5)	I-XZ (IN**5)	I-YZ (IN**5)
0	8.2441E-02	3.4223E-02	1.2320E-01
5	8.0341E-02	3.3352E-02	1.2007E-01
10	7.8064E-02	3.2414E-02	1.1669E-01
15	7.5633E-02	3.1432E-02	1.1315E-01
20	7.3051E-02	3.0408E-02	1.0947E-01
25	7.0301E-02	2.9330E-02	1.0559E-01
30	6.7370E-02	2.8191E-02	1.0149E-01
35	6.4259E-02	2.6986E-02	9.7150E-02
40	6.0969E-02	2.5711E-02	9.2559E-02
45	5.7502E-02	2.4362E-02	8.7703E-02
50	5.3861E-02	2.2935E-02	8.2567E-02
55	5.0046E-02	2.1427E-02	7.7137E-02
60	4.6062E-02	1.9832E-02	7.1396E-02
65	4.1912E-02	1.8147E-02	6.5329E-02
70	3.7603E-02	1.6366E-02	5.8917E-02
75	3.3140E-02	1.4483E-02	5.2138E-02
80	2.8538E-02	1.2494E-02	4.4979E-02
85	2.3797E-02	1.0390E-02	3.7403E-02
90	1.8918E-02	8.1636E-03	2.9389E-02
95	1.3912E-02	5.8095E-03	2.0914E-02
100	8.8328E-03	3.3369E-03	1.2013E-02
105	5.8069E-03	2.1241E-03	7.6468E-03
110	3.6828E-03	1.3135E-03	4.7287E-03
115	2.1436E-03	7.4426E-04	2.6793E-03
120	1.0637E-03	3.5736E-04	1.2865E-03
125	3.7522E-04	1.2278E-04	4.4201E-04
130	0.0000E 00	1.5602E 02	0.0000E 00

TABLE IX. PAGE 3 OF SUMMARIZATION OF PROGRAM AGDA OUTPUT

THIOKOL-ELKTON
ADVANCED GRAIN DESIGN COMPUTER PROGRAM

COMPLETE SOLID PROPELLANT ROCKET MOTOR EVALUATION TEST CASE

THEORETICAL ANALYSIS BY F.E.MOORE
PROGRAMMING ANALYSIS BY D.H.FREDERICK

WEB BURN PCT	BURNING SURFACE (SQ-IN)	CHAMBER VOLUME (CU-IN)	PROP. VOLUME (CU-IN)	PROP. CG (IN)	PROPELLANT INERTIA TENSOR I-XX (SQ-FT*CU-IN)	I-YY (SQ-FT*CU-IN)	I-ZZ (SQ-FT*CU-IN)
0	5574.66	17151.03	38743.06	9.986	93500.6	93500.6	73154.8
5	5701.89	19011.64	36882.45	10.114	90655.6	90655.6	71385.5
10	5662.43	20901.43	34992.66	10.248	87634.9	87634.9	69447.8
15	5526.67	22747.39	33146.70	10.384	84521.2	84521.2	67365.9
20	5404.55	24546.06	31348.03	10.519	81318.8	81318.8	65146.9
25	5420.16	26330.97	29563.12	10.658	77984.9	77984.9	62773.9
30	5440.68	28122.73	27771.36	10.803	74488.9	74488.9	60232.1
35	5453.31	29919.56	25974.53	10.953	70828.9	70828.9	57522.7
40	5461.95	31719.94	24174.15	11.107	67002.6	67002.6	54646.6
45	5466.61	33522.22	22371.87	11.265	63008.6	63008.6	51606.0
50	5466.34	35324.93	20569.16	11.425	58844.7	58844.7	48403.2
55	5462.09	37126.86	18767.23	11.584	54508.0	54508.0	45040.8
60	5452.42	38926.37	16967.72	11.741	49996.1	49996.1	41523.6
65	5437.26	40721.74	15172.35	11.889	45308.7	45308.7	37856.2
70	5415.02	42510.87	13383.22	12.021	40444.2	40444.2	34046.0
75	5385.84	44291.97	11602.12	12.124	35399.6	35399.6	30100.9
80	5351.81	46059.71	9834.38	12.173	30184.3	30184.3	26035.4
85	5323.25	47817.55	8076.54	12.126	24784.6	24784.6	21850.3
90	5301.46	49567.61	6326.48	11.903	19195.9	19195.9	17549.6
95	5269.46	51309.21	4584.88	11.298	13415.4	13415.4	13128.6
100	5227.27	53026.60	2867.49	9.612	7492.2	7492.2	8644.1
MAX	5701.89	53026.60	38743.06	12.173	93500.6	93500.6	73154.8
MIN	5227.27	17151.03	2867.49	9.612	7492.2	7492.2	8644.1
AVG	5438.34	35269.35	20624.73	11.140	55739.0	55739.0	45593.2
100+	4445.55						
105	2450.99	54001.86	1892.23		4789.8	4789.8	5820.2
110	1801.36	54691.78	1202.31		2974.1	2974.1	3763.7
115	1294.28	55192.89	701.20		1694.9	1694.9	2230.8
120	878.68	55545.79	348.30		820.8	820.8	1125.6
125	509.63	55771.24	122.85		282.7	282.7	403.2
130	167.18	55878.48	15.61		2.8	0.4	0.8

PER CENT PROPELLANT (0-100 PCT WEB) BY VOLUME = 64.18

PER CENT PROPELLANT (100-130 PCT WEB) BY VOLUME = 5.13

TABLE X. PAGE 1 OF NEW PROGRAM AGDA OUTPUT

(The max., min., and average values refer only to O→100 pct web.
The 100 + surface area is the surface just after web burnout.)

THIOKOL-ELKTON
ADVANCED GRAIN DESIGN COMPUTER PROGRAM

COMPLETE SOLID PROPELLANT ROCKET MOTOR EVALUATION TEST CASE

THEORETICAL ANALYSIS BY P.E.MOORE
PROGRAMMING ANALYSIS BY D.H.FREDERICK

WEB BURN	BURNING SURFACE	PROP. WEIGHT	SYSTEM WEIGHT	SYSTEM CG	PROPELLANT INERTIA TENSOR I-XX	I-YY	I-ZZ
PCT	(SQ-IN)	(LBS)	(LBS)	(IN)	-------(SQ-FT*LBS)-------		
0	5574.66	2448.56	3154.32	7.604	5909.2	5909.2	4623.4
5	5701.89	2330.97	3036.73	7.610	5729.4	5729.4	4511.6
10	5662.43	2211.54	2917.30	7.609	5538.5	5538.5	4389.1
15	5526.67	2094.87	2800.63	7.601	5341.7	5341.7	4257.5
20	5404.55	1981.20	2686.96	7.583	5139.3	5139.3	4117.3
25	5420.16	1868.39	2574.15	7.555	4928.6	4928.6	3967.3
30	5440.68	1755.15	2460.91	7.515	4707.7	4707.7	3806.7
35	5453.31	1641.59	2347.35	7.461	4476.4	4476.4	3635.4
40	5461.95	1527.81	2233.57	7.389	4234.6	4234.6	3453.7
45	5466.61	1413.90	2119.66	7.294	3982.1	3982.1	3261.5
50	5466.34	1299.97	2005.73	7.172	3719.0	3719.0	3059.1
55	5462.09	1186.09	1891.85	7.017	3444.9	3444.9	2846.6
60	5452.42	1072.36	1778.12	6.819	3159.8	3159.8	2624.3
65	5437.26	958.89	1664.65	6.569	2863.5	2863.5	2392.5
70	5415.02	845.82	1551.58	6.253	2556.1	2556.1	2151.7
75	5385.84	733.25	1439.01	5.854	2237.3	2237.3	1902.4
80	5351.81	621.53	1327.29	5.349	1907.6	1907.6	1645.4
85	5323.25	510.44	1216.20	4.706	1566.4	1566.4	1380.9
90	5301.46	399.83	1105.59	3.883	1213.2	1213.2	1108.9
95	5269.46	289.76	995.52	2.820	847.9	847.9	829.7
100	5227.27	181.23	886.99	1.439	473.5	473.5	546.3
MAX	5701.89	2448.56	3154.32	7.610	5909.2	5909.2	4623.4
MIN	5227.27	181.23	886.99	1.439	473.5	473.5	546.3
AVG	5438.34	1303.48	2009.24	6.338	3522.7	3522.7	2881.5
100+	4445.55						
105	2480.99	119.59	825.35	0.761	302.7	302.7	367.8
110	1801.36	75.99	781.75	0.261	188.0	188.0	237.9
115	1294.28	44.32	750.08	-0.119	107.1	107.1	141.0
120	878.68	22.01	727.77	-0.394	51.9	51.9	71.1
125	509.63	7.76	713.52	-0.567	17.9	17.9	25.5
130	167.18	0.99	706.75	-0.648	0.2	0.0	0.0

TABLE XI. PAGE 2 OF NEW PROGRAM AGDA FINAL OUTPUT

(This page includes the weight of inert parts as well as propellant density to obtain actual weight, CG travel, etc.)

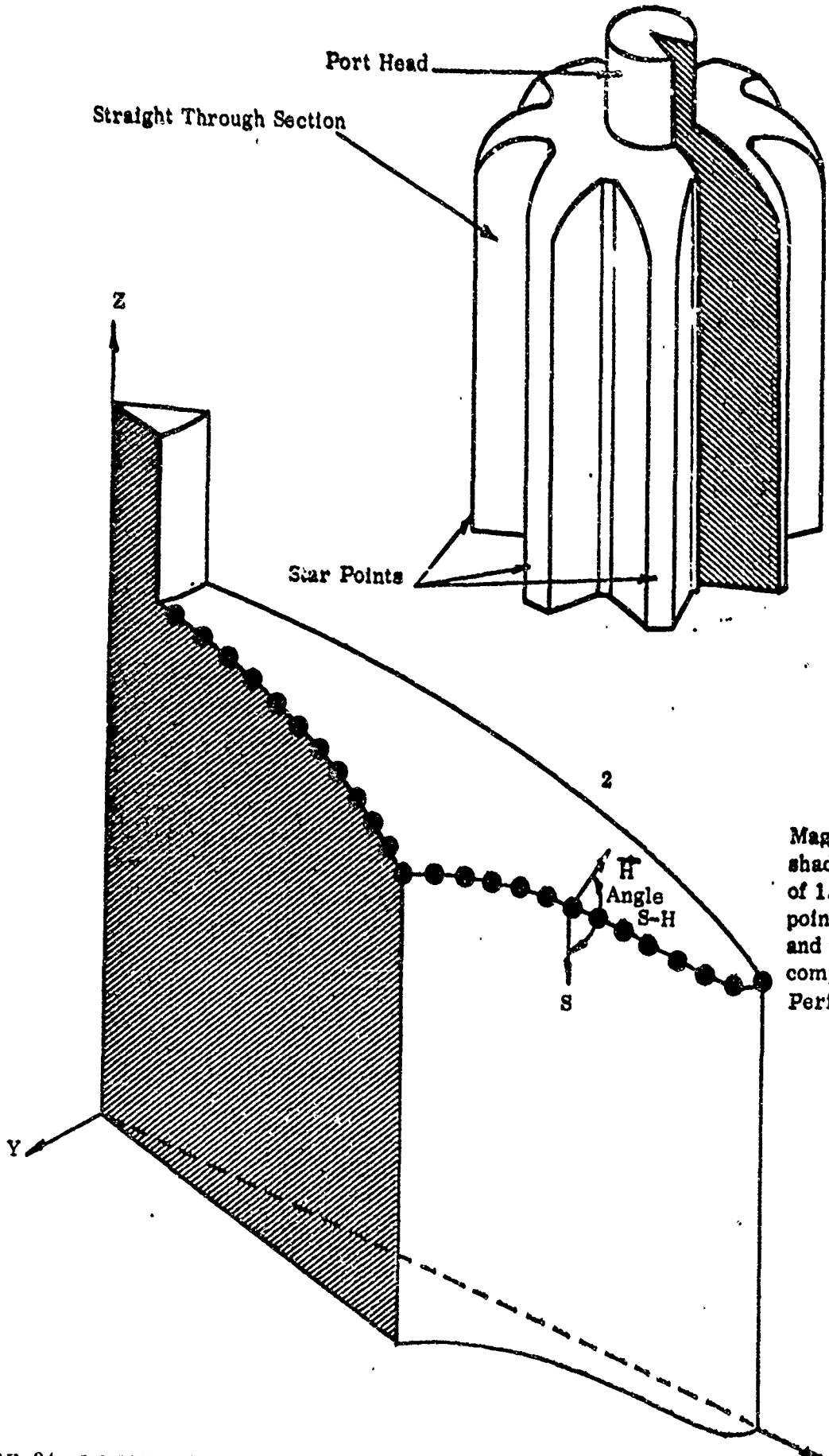

FIGURE 34. LOCATION WITHIN A SOLID PROPELLANT ROCKET MOTOR OF THE PERIPHERY POINTS.

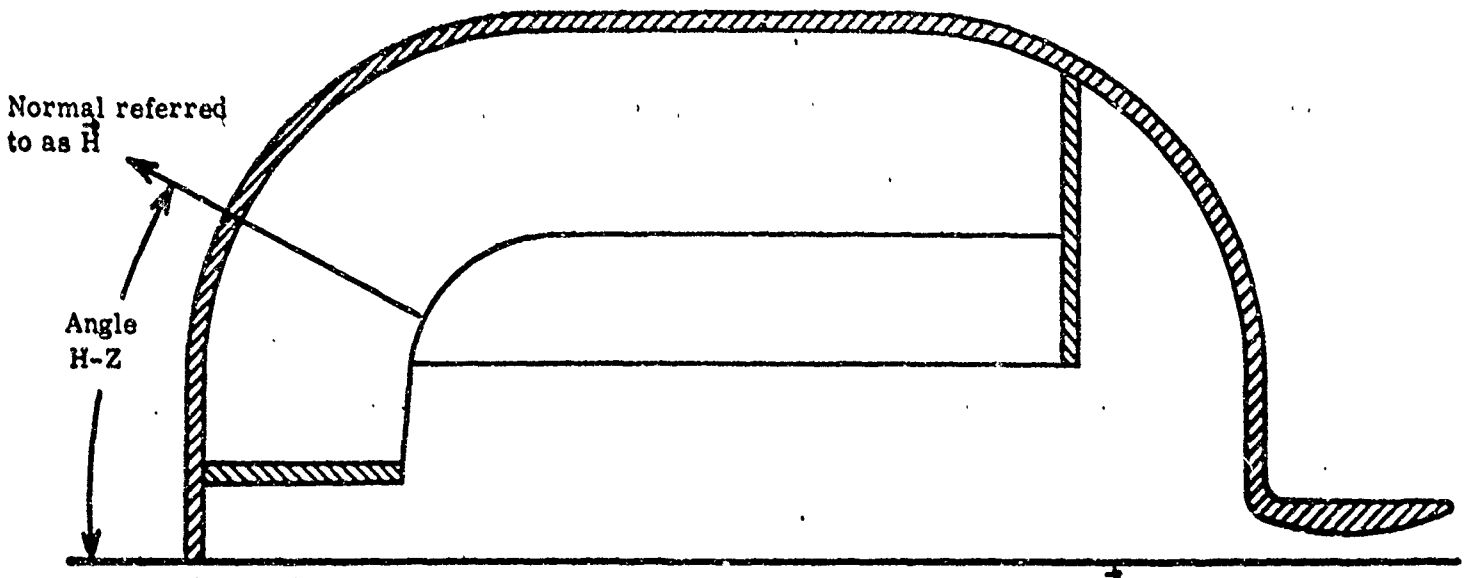

Longitudinal cross section of rocket motor which reveals the normal $\vec{H}$ and the angle Z-H

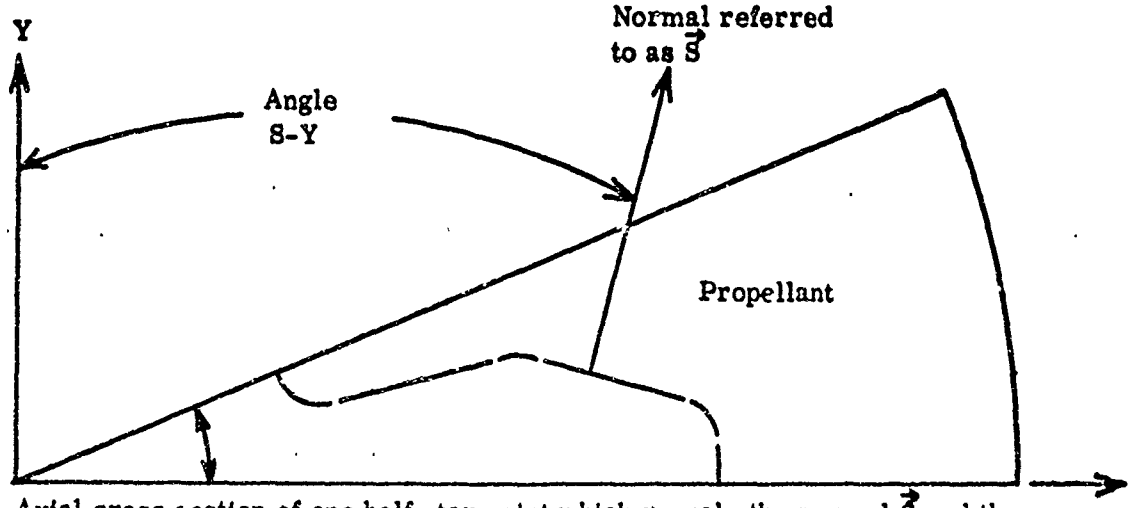

Axial cross section of one half star point which reveals the normal $\vec{S}$ and the angle S-Y

The angle S-H is simply the angle between normals $\vec{H}$ and $\vec{S}$. Reference back to Figure 34 will show a three dimensional illustration of both $\vec{S}$ and $\vec{H}$ and the angle S-H

FIGURE 36. DEFINITION OF NORMALS $\vec{S}$ AND $\vec{H}$ TOGETHER WITH THEIR ASSOCIATED ANGLES

of propellant weight, etc. Case weight and payload weight, if specified to the program, are used in conjunction with the computed propellant center of gravity travel to compute the C.G. travel of the entire system.

e. Nonuniform Temperature Example

The importance of considering the effect of a nonuniform grain temperature may, perhaps, be shown best through an example problem. The rocket motor chosen for consideration is of the "broken back" star classification. A cross section of one half star point of this rocket motor together with its (relatively severe) thermal gradient is shown in Figure 36.

This rocket motor was evaluated, both graphically and by program AGDA, for two temperature conditions:

1) Uniform grain temperature

2) Variable grain temperature

Computer output from these two temperature conditions is shown in Tables XII and XIII. The graph shown in Figure 37 compares the computer output with that obtained graphically. As may be seen from the figure, this comparison is quite good. The greater percentage of difference for the two calculational techniques in the variable temperature case is to be expected. Any small errors associated with the graphical analysis of the nonuniform temperature case are cumulative, while those obtained from the uniform temperature case are not.

Again with reference to Figure 37, there is a considerable difference in the shape of the surface web curve for the uniform versus nonuniform grain

A-4899

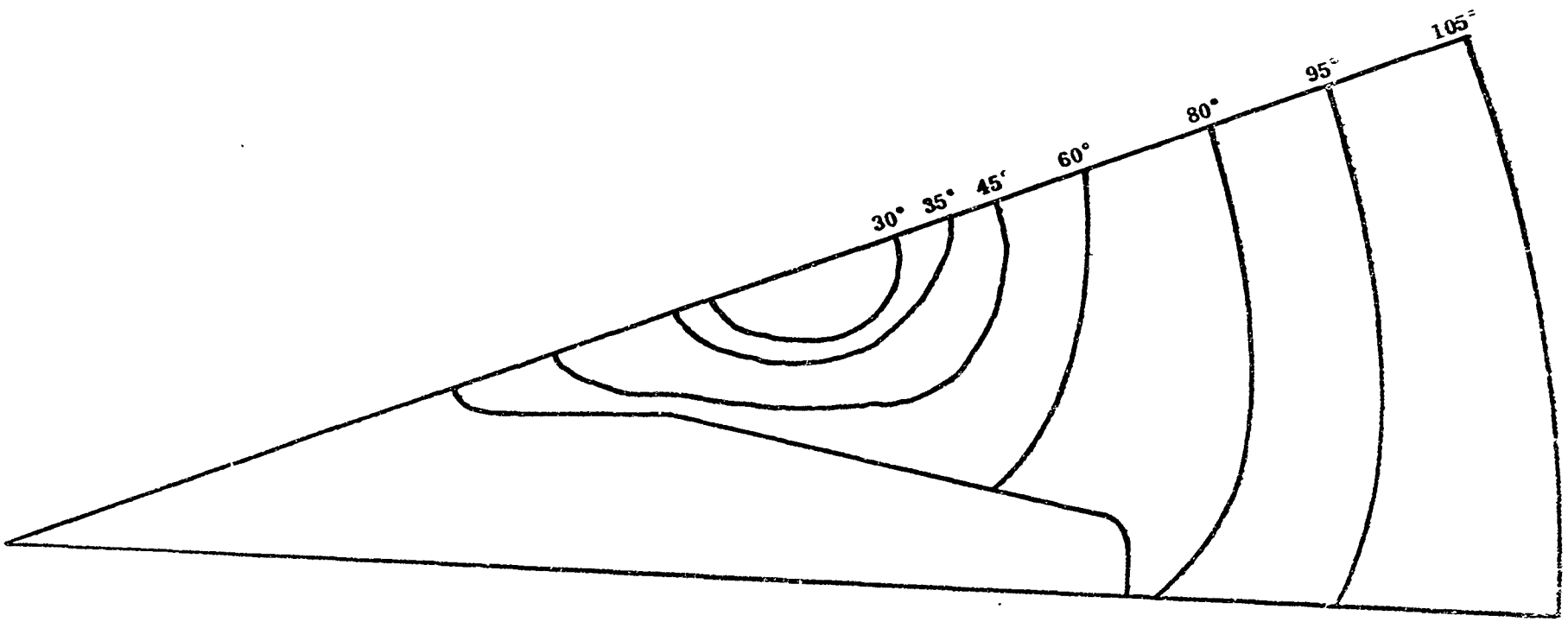

FIGURE 36. GRAIN TEMPERATURE PROFILE USED IN THE VARIABLE TEMPERATURE TEST CASE

THIOKOL-ELKTON
ADVANCED GRAIN DESIGN COMPUTER PROGRAM

STRAIGHT THRU SECTION BROKEN BACK STAR VARIABLE TEMP OPTION DISABLED

THEORETICAL ANALYSIS BY F.E.MOORE
PROGRAMMING ANALYSIS BY D.H.FREDERICK

WEB BURN	BURNING SURFACE	CHAMBER VOLUME	PROP. VOLUME	PROP. CG	PROPELLANT INERTIA TENSOR I-XX	I-YY	I-ZZ
PCT	(SQ-IN)	(CU-IN)	(CU-IN)	(IN)	------(SQ-FT*CU-IN)------		
0	2634.05	6556.54	17370.08	7.850	28072.6	28072.6	36323.3
5	2666.59	7430.92	16495.70	7.850	27138.3	27138.3	35452.4
10	2620.76	8310.01	15616.61	7.850	26163.4	26163.4	34505.8
15	2580.06	9159.67	14766.95	7.850	25173.5	25173.5	33495.6
20	2445.54	9978.20	13948.42	7.850	24171.6	24171.6	32425.8
25	2426.25	10781.46	13145.16	7.850	23145.0	23145.1	31289.4
30	2409.74	11579.18	12347.44	7.850	22085.2	22085.2	30080.0
35	2393.22	12371.46	11555.16	7.850	20991.5	20991.5	28796.8
40	2376.71	13158.30	10768.33	7.850	19863.8	19863.8	27439.3
45	2360.20	13939.68	9986.94	7.850	18701.9	18701.9	26007.2
50	2343.68	14715.61	9211.01	7.850	17505.7	17505.7	24500.3
55	2327.17	15486.10	8440.52	7.850	16275.3	16275.3	22918.7
60	2310.65	16251.14	7675.48	7.850	15010.8	15010.8	21262.7
65	2294.14	17010.73	6915.89	7.850	13712.4	13712.4	19532.7
70	2277.62	17764.87	6161.75	7.850	12380.5	12380.5	17729.5
75	2251.11	18513.56	5413.06	7.850	11015.4	11018.4	15853.7
80	2247.56	19256.12	4670.51	7.850	9618.9	9618.9	13908.0
85	2243.14	19995.82	3930.80	7.850	8186.2	8186.2	11886.7
90	2248.46	20735.90	3190.72	7.850	6712.1	6712.1	9783.1
95	2260.42	21478.62	2448.00	7.850	5192.4	5192.4	7591.2
100	2279.00	22225.26	1701.36	7.850	3624.2	3624.2	5306.9
MAX	2666.59	22225.26	17370.08	7.850	28072.6	28072.6	36323.3
MIN	2243.14	6556.54	1701.36	7.850	3624.2	3624.2	5306.9
AVG	2378.86	14604.72	9321.90	7.850	16892.4	16892.4	23147.1
100+	2276.10						
105	1350.28	22743.75	1182.87		2535.6	2535.6	3721.3
110	1052.03	23136.73	789.89		1706.1	1706.1	2510.8
115	803.97	23438.12	488.51		1063.3	1063.3	1569.1
120	584.86	23666.32	260.30		571.3	571.3	845.6
125	375.92	23821.76	104.86		232.1	232.1	344.5
130	157.53	23908.10	18.52		3.3	0.5	0.7

PER CENT PROPELLANT (0-100 PCT WEB) BY VOLUME = 65.49

PER CENT PROPELLANT (100-130 PCT WEB) BY VOLUME = 7.11

TABLE XII. FINAL PAGE OF OUTPUT, TEST CASE 1

THIOKOL-ELKTON

ADVANCED GRAIN DESIGN COMPUTER PROGRAM

Straight Thru Section Broken Back Star Variable Temp Option Employed With

Grain Temp Shown in Figure 36

THEORETICAL ANALYSIS BY F.E.MOORE

PROGRAMMING ANALYSIS BY D.H.FREDERICK

WEB BURN	BURNING SURFACE	CHAMBER VOLUME	PROP. VOLUME	PROP. CG	PROPELLANT INERTIA TENSOR I-XX	I-YY	I-ZZ
PCT	(SQ-IN)	(CU-IN)	(CU-IN)	(IN)	------(SQ-FT*CU-IN)------		
0	2634.05	6555.75	17370.87	7.850	27254.5	27254.5	34686.2
5	2690.68	7314.03	16612.59	7.850	26418.0	26418.0	33678.5
10	2728.19	8090.19	15836.43	7.850	25529.7	25529.7	32987.5
15	2737.88	8864.80	15061.82	7.850	24603.9	24603.9	32019.9
20	2696.69	9646.74	14279.88	7.850	23625.4	23625.4	30955.3
25	2711.24	10437.38	13489.24	7.850	22590.5	22590.5	29787.6
30	2794.84	11239.82	12686.80	7.850	21500.9	21500.9	28524.2
35	2856.82	12084.50	11842.12	7.850	20322.6	20322.6	27131.5
40	2904.70	12976.34	10950.28	7.850	19036.4	19036.4	25570.8
45	2945.73	13914.81	10011.82	7.850	17641.5	17641.5	23857.9
50	2995.13	14895.57	9031.05	7.850	16138.2	16138.2	21970.5
55	3036.35	15930.37	7996.25	7.850	14503.6	14503.6	19882.3
60	3078.53	17011.65	6914.97	7.850	12740.9	12740.9	17590.8
65	3057.88	18150.32	5776.30	7.850	10833.7	10833.7	15075.8
70	2812.41	19301.47	4625.15	7.850	8832.5	8832.5	12387.1
75	2587.47	20403.53	3523.09	7.850	6822.3	6822.3	9624.3
80	2298.65	21461.11	2465.51	7.850	4812.5	4812.5	6811.6
85	1517.49	22270.76	1655.86	7.850	3257.3	3257.3	4629.0
90	1151.91	22844.63	1082.00	7.850	2147.5	2147.5	3060.2
95	854.19	23279.67	647.95	7.850	1298.0	1298.0	1858.6
100	624.34	23595.26	331.36	7.850	669.9	669.9	961.7
MAX	3078.53	23595.26	17370.87	7.850	27254.5	27254.5	34686.2
MIN	624.34	8855.75	331.36	7.850	669.9	669.9	961.7
AVG	2461.20	15250.84	8675.77	7.850	14789.5	14789.5	19678.8
100+	606.85						
105	377.39	23811.58	115.04		234.5	234.5	337.8
110	103.60	23916.80	9.82		20.1	20.1	29.1
115	0.00	23926.62	0.00		0.0	0.0	0.0
120	0.00	23926.62	0.00		0.0	0.0	0.0
125	0.00	23926.62	0.00		0.0	0.0	0.0
130	0.00	23926.62	0.00		0.0	0.0	0.0

PER CENT PROPELLANT (0-100 PCT WEB) BY VOLUME = 71.22

PER CENT PROPELLANT (100-130 PCT WEB) BY VOLUME = 1.38

TABLE XIII. COMPUTER OUTPUT FOR VARIABLE TEMPERATURE TEST CASE

temperature cases. It is conceivable that everything from a "slightly off target" to a major catastrophe could result from firing such a rocket motor with severe thermal gradient. These effects would be especially pronounced if the propellant selected had a higher than average temperature sensitivity coefficient (π_K).

III. EFFECT OF STRAIN ON BURNING RATE

The effect of strain on propellant structural integrity has received considerable attention in the past. However, only limited effort has been directed toward determining whether a propellant under strain will burn predictably and the extent that burning rate will vary as a function of the induced strain.

Coy,[3] using an ammonium perchlorate-polyurethane propellant, measured approximately 1.5 percent increase in burning rate for each percent strain. (Coy concluded that this strain-burning rate relationship was produced by the formation of a liquid phase at the propellant burning surface.)

Other tests on plastisol propellants which were conducted at Atlantic Research Corporation* showed a definite increase in burning rate but at much higher strain levels than those used by Coy (on the order of 100 percent). In contrast to the work of Coy at ARC, the Longhorn Division[4] of the Thiokol Chemical Corporation static fired a Nike-Hercules motor that had experienced a severe slump problem. The slump (time-dependent strain due to gravity force) had progressed to the extent that the opposite star points in the grain almost joined. When the motor was static tested, the measured burning rate was no different from that measured in laboratory control tests. Therefore, it was concluded that, at least for this particular formulation, burning rate was unaffected by strain.

*Private communication with Cortland Robinson of Atlantic Research Corporation

In these studies, each of which dealt with a single type of propellant, no general criteria for all propellants could be established. It was the main purpose of this study to determine whether such criteria existed and, if possible, to determine the means by which they could be established.

TECHNICAL APPROACH

1. Propellants

The first propellant investigated was an HA/MAPO hydrocarbon propellant (designated Hydrocarbon "A" in this report). Depending on the results obtained with this propellant, other propellants or propellant systems were to be considered for evaluation. Before the end of the program, three other propellants were studied: HB/epoxy (Hydrocarbon "B"), a polyurethane, and a plastisol.

The standard JANAF physical properties of those propellants tested are given below:

Propellant Type	JANAF Modulus, ϵ3.2, psi**	Maximum Stress, psi	Strain at Maximum Stress, ϵ3.2, in/in**
Hydrocarbon"A"	590	100	0.24
Polyurethane	545	77	0.25
Hydrocarbon "B" (Mod.)*	1565	113	0.17
Plastisol	400	90	0.20

*This material was purposely formulated at a high epoxy-to-carboxy ratio in order to achieve a higher modulus material. The normal values for this formulation are 600 psi, 80 psi, and 0.25 in./in., respectively.

**The value 3.2 refers to the effective gauge length used in the determination of the physical properties shown.

2. Tests and Procedures

Two distinct areas were to be investigated at the beginning of this program. One area was concerned with measuring the change in burning rate of specimens with induced uniform strain fields ranging from 0 to 12 1/2 percent at pressures of 500, 900, and 1200 psi. However, the strain levels induced across the face of a grain by firing or thermal sources are nonuniform because of the various geometries encountered in solid propellant grain designs. Therefore, a second type of test in which a nonuniform strain distribution was produced in a propellant sample was planned. The burning rate of this type of sample was to be determined at various positions within the sample under different strain concentrations and compared with the uniform strain data for possible correlation with actual motor firings. The uniform strain field tests were given the greater initial attention since it was felt that the results obtained would elucidate some of the experimental problems that might be encountered in the more complex nonuniform strain field tests.

When the uniform strain field tests on hydrocarbon "A" were completed, it was found that virtually no difference existed between the linear burning rate of the unstrained strands and those strained up to 12 1/2 percent. In the light of the conflict that existed between these results and those of Coy and ARC, it was conjectured that strain does not affect burning rate directly but instead affects a material property which, in turn,can be related to changes in burning rate. A quantitative parameter, which might be directly related to burning rate, is the change in volume with strain. This property, referred to here as Poisson's ratio, is defined as the ratio of the lateral strain, ϵ_2, to the longitudinal strain, ϵ_1, in a material subjected to a uniaxial tensile stress.

When a material is stretched, the cross-sectional area changes as well as length. Poisson's ratio, ν, is the parameter relating these changes in dimension

$$\nu = -\frac{\epsilon_2}{\epsilon_1} = \frac{\text{Percent Change in Width}}{\text{Percent Change in Length}} = \frac{\Delta W/W_o}{\Delta L/L_o} \tag{2.1}$$

If a material is incompressible, an elongation would result in changing the cross-sectional area but not the volume. Since linear burning rate is independent of cross-sectional area, no change in burning rate would be expected. On the other hand, if the material is compressible and incurred a change in volume as a result of elongation, the resulting change in density should cause a change in the burning rate.

It can be shown that if the volume of a material remains constant when subjected to very small strains, ν is a constant and equals 0.50. Generally, materials increase in volume when subjected to a tensile strain, resulting in a ν less than 0.50. For most materials ν lies between 0.2 and 0.5 and approaches 0.50 for rubbers or liquids.

When a material is subjected to a strain sufficiently large to prohibit the use of infinitesimal strain theory, ν is no longer a constant but a function of the strain:

$$\nu = \frac{1}{\alpha - 1}\left[1 - \left(\frac{V}{V_o}\right)^{-1/2} \alpha^{-1/2}\right] \tag{2.2}$$

where ν = Poisson's ratio

α = Principal extension ratio $(1 + \epsilon_1)$

V = Volume

V_o = Original volume

If the material is incompressible, i.e., $V/V_0 = 1$, equation (2.2) reduces to:

$$\nu_l = \frac{1}{\epsilon_1}\left[1 - (1 + \epsilon_1)^{-1/2}\right] \tag{2.3}$$

where $\nu/\nu_l \leq 1$ (2.4)

It can be seen from equation (2.2) that the lower the value of ν, the greater the volume increase and hence the greater the density change due to the strain, ϵ_1. Therefore, it can be expected that the burning rate of the material which displays the greatest departure from incompressibility would be most affected by strain. The dimensionless ratio ν/ν_l, henceforth referred to as the "volumetric change index," is representative of the departure from incompressibility. To test this hypothesis the linear burning rates of the four candidate materials were determined over the pressure ranges mentioned above. In addition, the volumetric change index was determined as a function of strain for the same materials. To accomplish this an apparatus for the experimental determination of ν was developed, based on fundamental concepts previously devised under corporate funding.

A discussion of the methods and equipment used for the three procedures and a discussion of the results are given below.

a. Uniform Strain Field Tests

The burning of the propellant was accomplished in a standard Autoclave Engineering Company strand burner (see Figure 38). The strand burner consisted of a 3-inch-diameter by 12-inch-deep cylindrical burning chamber. The sample holder was lowered into this chamber. In addition to supporting the strand, the sample holder

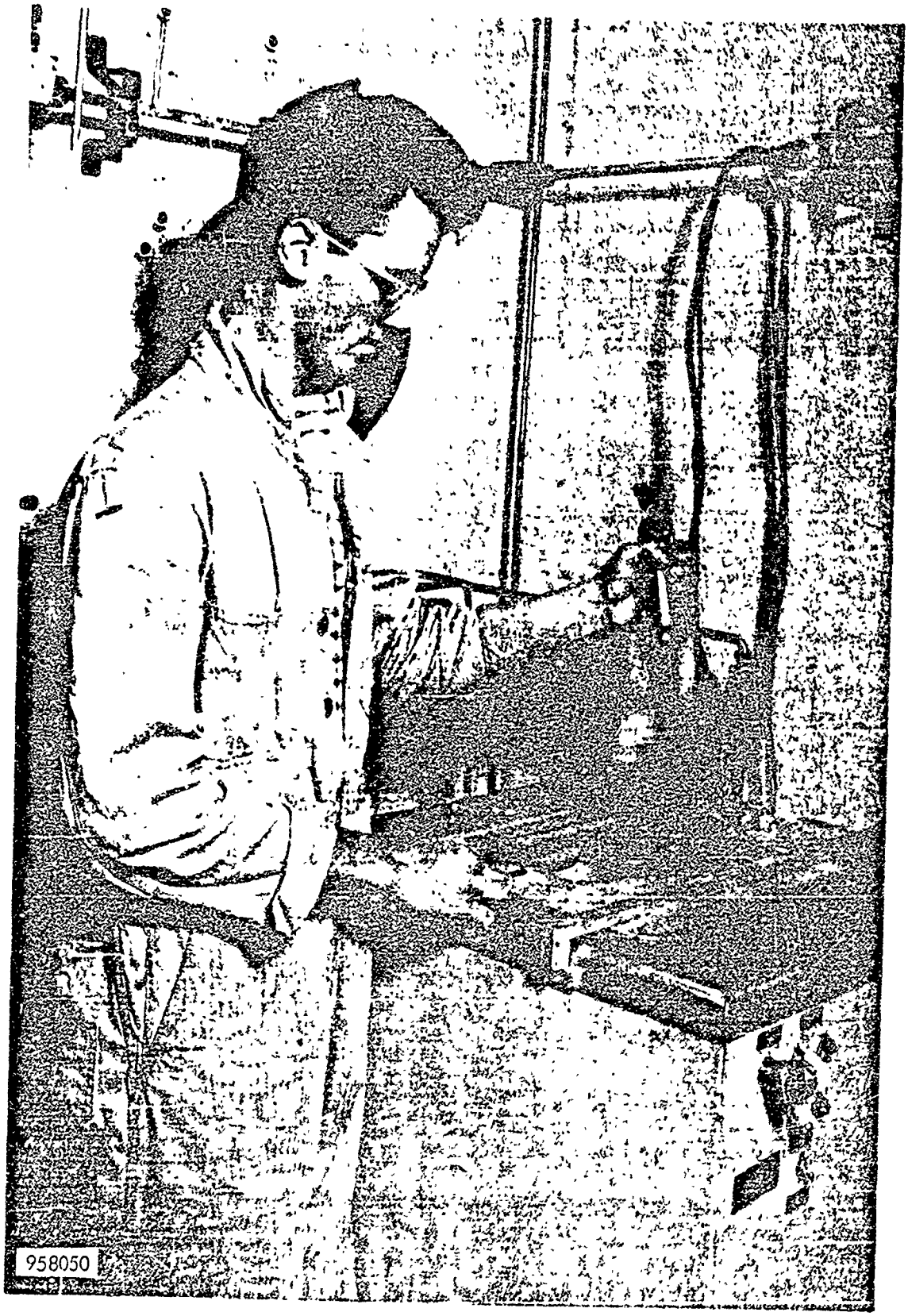

FIGURE 38. PROPELLANT STRAND BURNER

provided the means for igniting the propellant. The burner was also equipped with three clocks; one clock measured the time to burn through the first half of the strand; another measured the time to burn through the last half; and the third clock measured total burning time and provided a check on the other two. The bomb was pressurized with nitrogen by a reciprocating booster pump. The maximum allowable pressure for the bomb was 10,000 psia. Any pressure buildup in the bomb during burning was absorbed by a 1750-milliliter surge tank. Burning rates can be measured to an accuracy of $\pm$ .005 in./min.

The specimen consisted of a 1/4-inch by 1/4-inch by 6-inch strand of propellant. The specimen ends were inserted through two Teflon collars and bonded with Armstrong A-1 cement. In this form it was similar to the end bonded tensile specimen[5] developed at the Thiokol-Redstone Division. Four constant strain devices were revised to provide a means for achieving the desired strain levels in the strand. Each device was capable of independently straining two strands. Once the desired strain level was achieved, the sample was coated on all sides with Armstrong A-1 cement. This procedure is shown in Figure 39. The cured adhesive bonded to the strand;and since the coating was stiff, the strain level in the grain was maintained. In addition, the cement acted as an inhibitor to prevent side burning during firing.

Three wires were placed through the strands spaced 2-1/2 inches apart in the direction of burning. These wires were connected to the three clocks of the strand burner. The circuitry was designed so that as the propellant burned and the wires were severed, they started and stopped the timers, causing the burning time

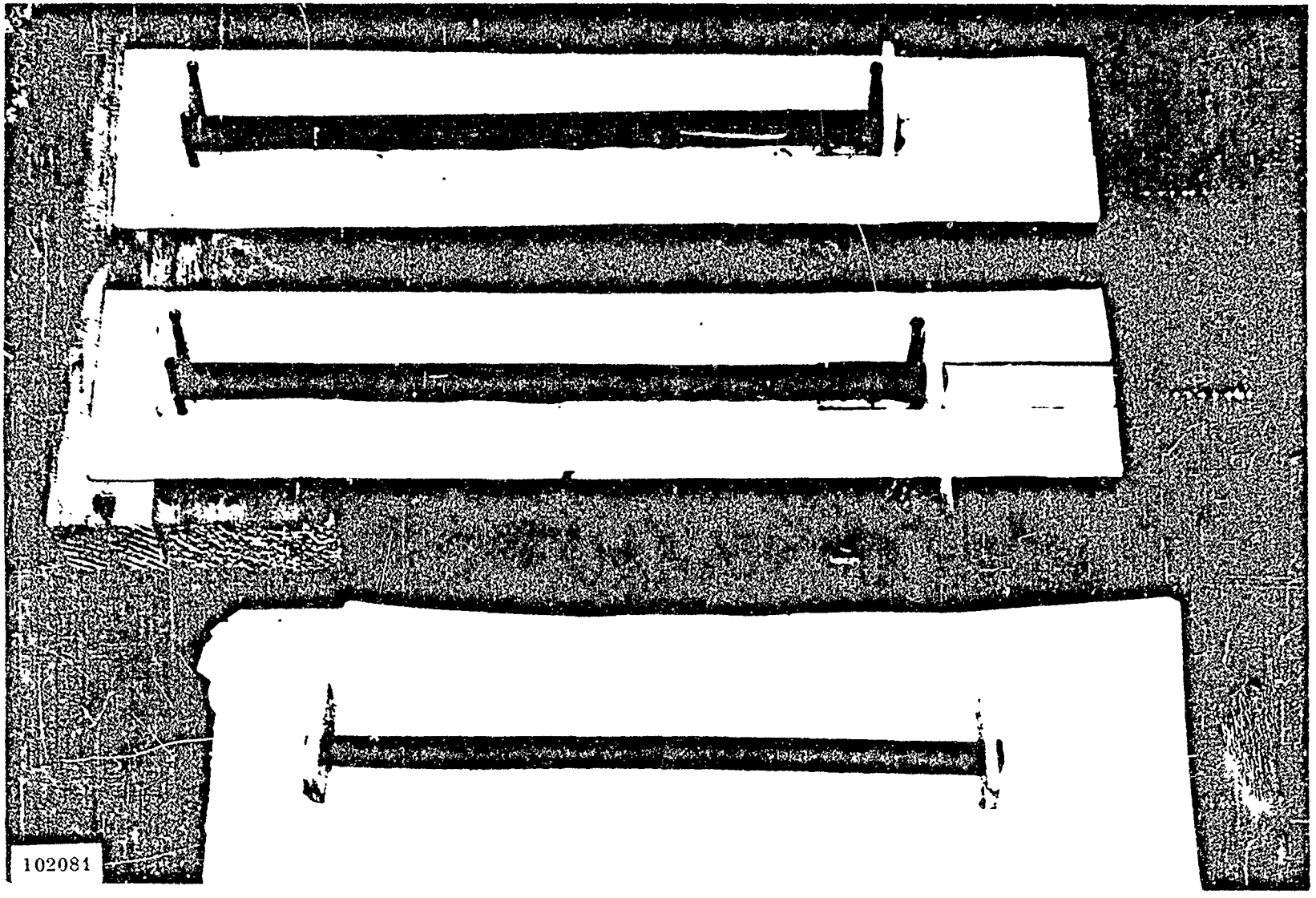

FIGURE 39. METHOD OF PREPARING STRAINED PROPELLANT STRANDS

between each wire to be recorded. One additional wire was inserted through the propellant near the top of the strand, which acted as an igniter.

b. Nonuniform Strain Field Test

The apparatus necessary to induce a nonuniform strain field into solid propellant sample is shown in Figure 40. A triangular sample of propellant 2 inches by 2 inches by 2 inches by 1 inch thick was cast into a vise made of 1-inch thick Plexiglas to make a direct bond between vise wall and the sample. When the sample cured, its face was covered with a birefringent coating 1/8 inch thick with a thin film of reflective paint at the interface between the coating and the propellant. In this manner, the strain levels in the sample could be determined by PhotoStress (reflective photoelasticity technique). When the strain geography in the sample for a particular amount of vise wall displacement was known, a new sample could be similarly prepared without the birefringent coating and paint. The sample might then be compressed by the vise to achieve the previously determined strain pattern. An igniter wire can be inserted in the 1/4-inch-diameter groove at the lower portion of the vise.

The bomb assembly (which has been utilized previously to study the effect of defects on burning) consisted of two basic parts: a windowed container and an internal assembly to hold the sample (see Figures 41 and 42). The bomb has a window and a vented stainless steel cylinder. Two 1-inch-thick by 1/2-inch-wide by 5-inches-long Herculite windows held in place with steel plate and screws were located on opposite sides of the bomb. An outlet through the side of the bomb near the bottom provided a means for pressurizing the bomb. Two other connections provided a means for pressure gauge connection and a safety blow-out disk.

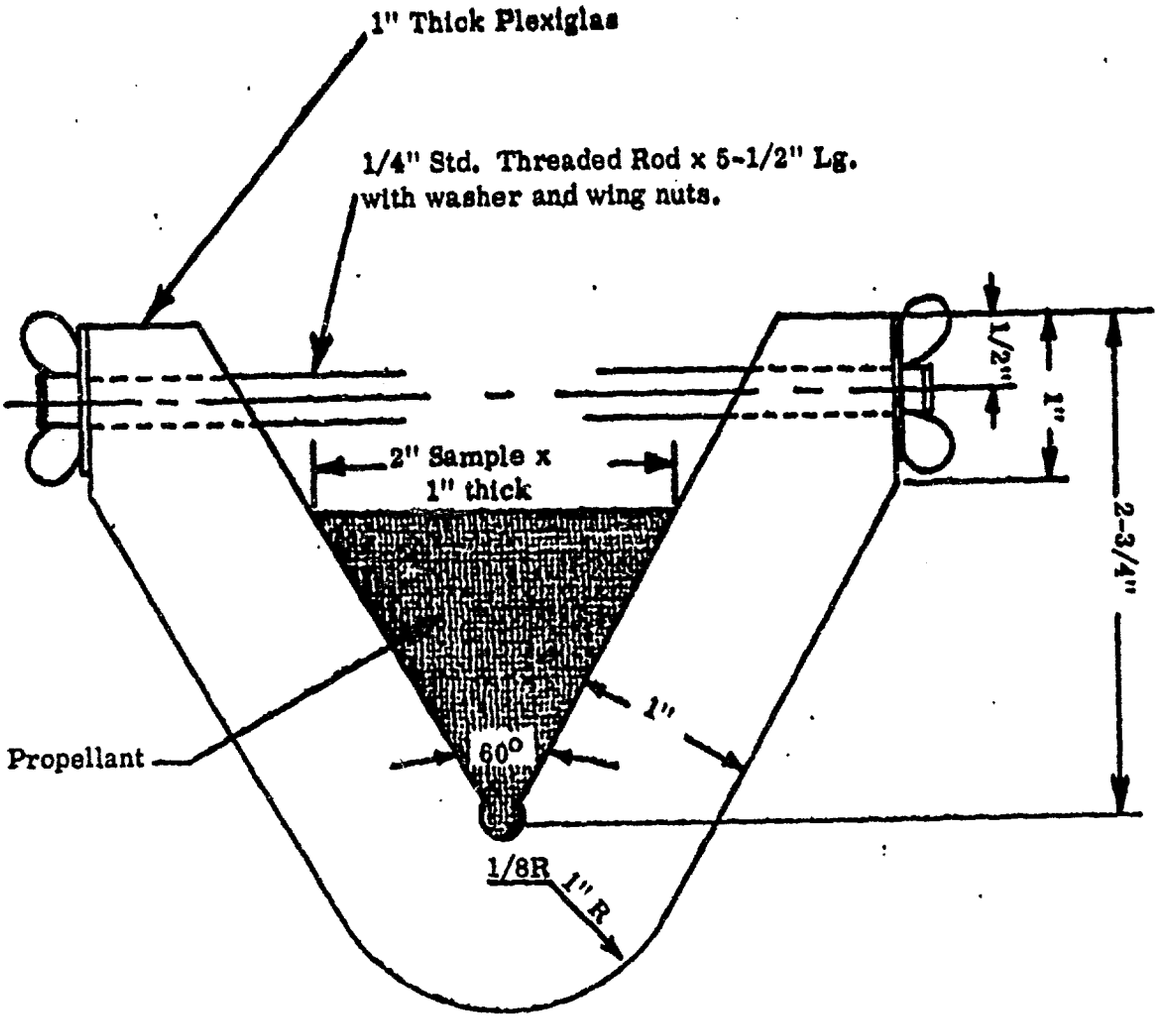

FIGURE 40. TEST JIG FOR NON-UNIFORM STRAIN VERSUS BURNING RATE TEST

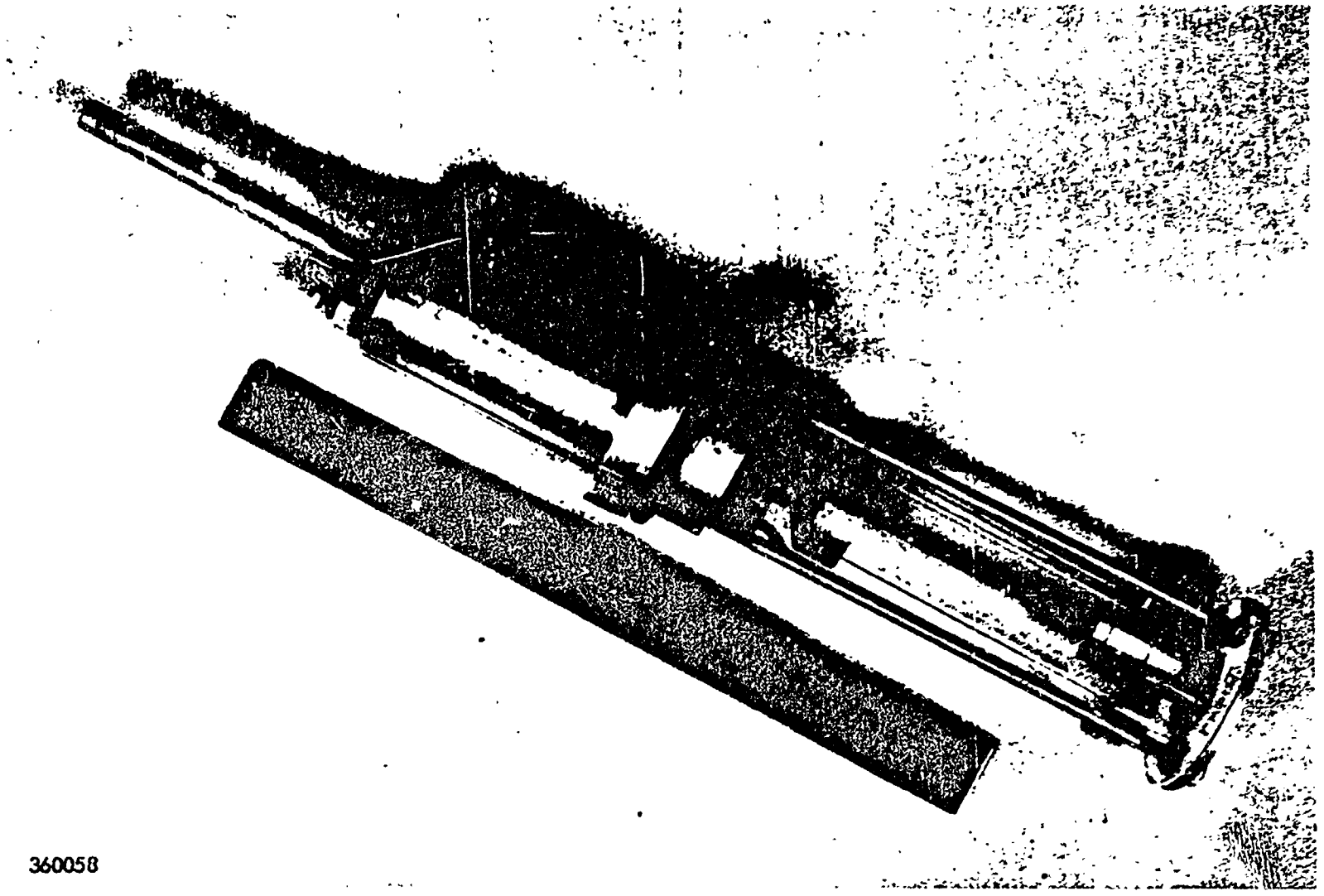

360058

FIGURE 41. WINDOW BOMB INTERNAL ASSEMBLY

FIGURE 42. WINDOW BOMB TEST ARRANGEMENT

The specimen can be mounted on the internal assembly so that it can be viewed through the bomb window. The system can then be sealed and pressurized with nitrogen to the desired pressure level and ignited.

A Wollensak Fastax 16mm high speed camera can be used to photograph the surface of the propellant as it burns. The propellant should provide sufficient illumination to permit good resolution; however, a standard photo flash unit can be used to obtain a picture of the specimen before ignition. Timing reference marks superimposed on the film can be used to provide for burning rate measurements.

c. Poisson's Ratio Test

An apparatus for the determination of the volumetric changes of propellant has been developed and consists of a point light source, an end-bonded cylindrical tensile specimen,[6] a 10X lens, an Instron tensile tester, and a sheet of graph paper. This is shown schematically in Figure 43. A specimen of known diameter was placed in the path of the point light source. The image was magnified ten times by means of the lens and projected on the graph paper. The highly magnified diameter was measured and the volumetric changes are calculated from the measured lateral and longitudinal strains, using equation 2.2. It should be mentioned that since the optics of this device are still in the preliminary stage of development, it was necessary that the average of at least five tests were reported. The preparation of samples must be performed with extreme care to assure uniaxial stress conditions during deformation.

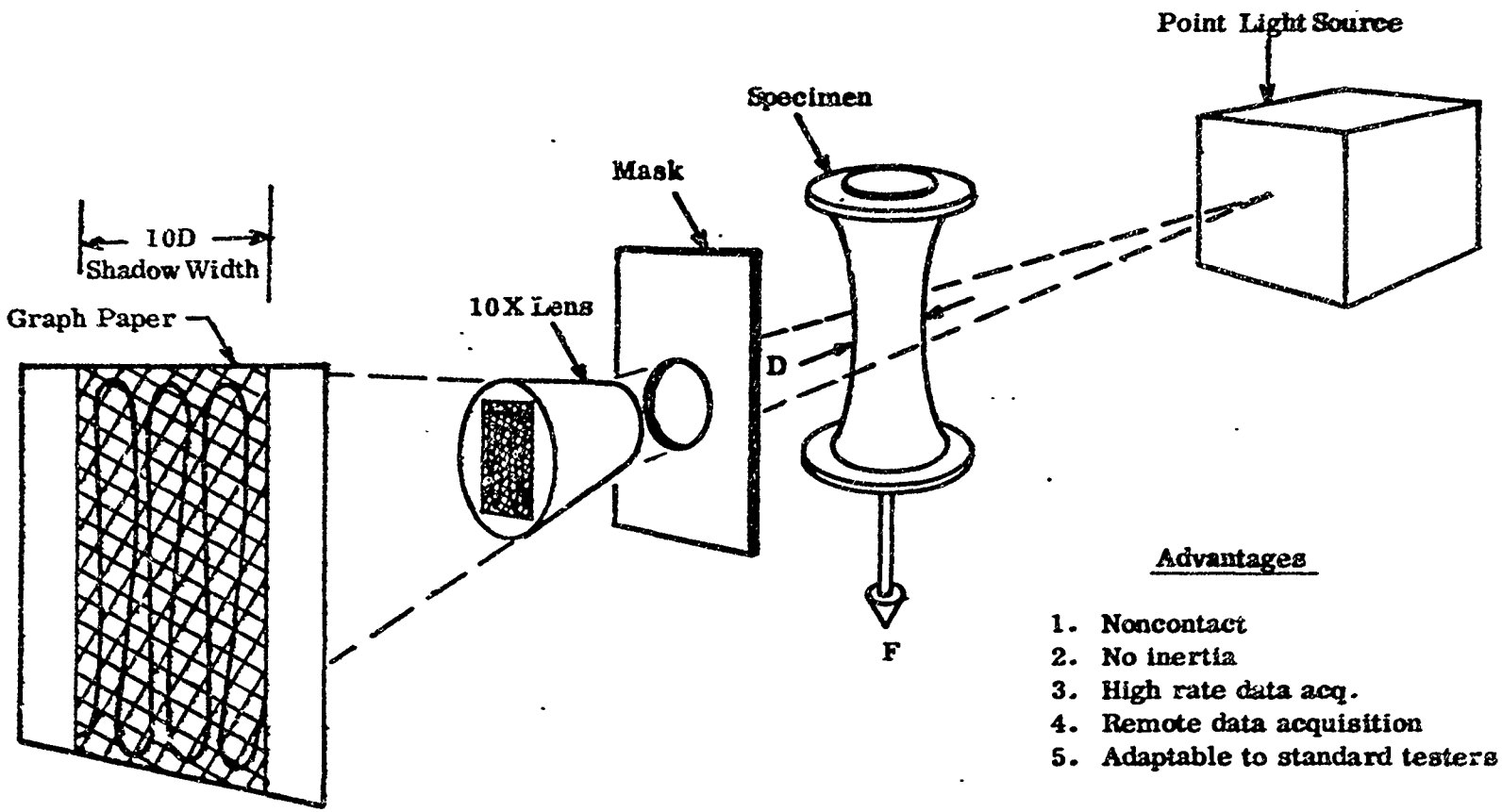

FIGURE 43. APPARATUS FOR MEASURING CROSS SECTIONAL AREA OF A SPECIMEN DURING A TENSILE TEST

d. Discussion of Results

The results of the linear burning rate versus strain tests are given in Tables XIV through XXIV and Figure 44 for the four propellants tested. It can be seen from the graph that the influence of strain on linear burning rate is different for the four formulations. The data for hydrocarbon "A" show virtually no difference between burning rates of the unstrained strands and those strained up to 12 1/2 percent. This independence of strain on burning rate for this particular propellant supports the Longhorn Division[4] results on the slumped Nike-Hercules motor.

It was originally intended to obtain data at 0, 4, 8 and 16 percent strain and 500, 900 and 1200 psi burning test pressure. It became increasingly difficult to achieve 16-percent strain in the type of specimen used without sample rupture. For hydrocarbon "A" the maximum strain achieved was 12 1/2 percent. For the other materials even this was not possible, and 10-percent strain was used. In addition, since virtually all propellants experience a linear, log-log, pressure-burning rate trace, it was decided to use 500 and 1500 psi rather than 500, 900 and 1200 psi. This was also done to permit a wider spread in the data. Therefore, some of the results are reported at different strains and pressures.

The data for the polyurethane propellant show an increase of 4.0 percent in burning rate at 1000 psi and 0.10 in./in. strain. The burning rate of the modified hydrocarbon "B" increased 9.1 percent at 0.10 in./in. strain and 1500 psi, and the plastisol exhibited an increase in burning rate of 27 percent at 0.10 in./in. and 1500 psi.

TABLE XIV

BURNING RATE OF HYDROCARBON "A" (0% STRAIN)

Test Number	Average Pressure, psi		Burning Rate, in/sec	
1		578		0.416
2		565		0.405
3		582		0.397
4		550		0.427
5		565		0.422
6		558		0.406
7		563		0.406
8		565		0.405
	Aver.	565	Aver.	0.410
1		1000		0.521
2		1000		0.543
3		1008		0.550
4		1008		0.539
5		1005		0.500
6		1012		0.515
7		1000		0.527
	Aver.	1005	Aver.	0.527
1		1313		0.570
2		1345		0.569
3		1325		0.577
4		1313		0.577
5		1345		0.587
	Aver.	1328	Aver.	0.576

TABLE XV

BURNING RATE OF HYDROCARBON "A" (4% STRAIN)

Test Number	Average Pressure, psi		Burning Rate, in/sec	
1		588		0.416
2		593		0.404
3		563		0.414
4		550		0.391
5		565		0.404
6		565		0.389
	Aver.	570	Aver.	0.403
1		1008		0.508
2		1015		0.594
3		1010		0.541
4		1008		0.511
5		1001		0.508
6		1000		0.589
7		1000		0.595
	Aver.	1006	Aver.	0.549
1		1313		0.576
2		1318		0.569
3		1313		0.556
4		1325		0.587
5		1325		0.588
6		1325		0.587
7		1325		0.582
	Aver.	1320	Aver.	0.578

TABLE XVI

BURNING RATE OF HYDROCARBON "A" (8% STRAIN)

Test Number		Average Pressure, psi		Burning Rate, in/sec
1		575		0.388
2		563		0.407
3		563		0.394
4		563		0.415
5		563		0.404
6		563		0.394
7		550		0.396
8		563		0.410
9		563		0.411
	Aver.	563	Aver.	0.402
1		1120		0.568
2		998		0.585
3		1000		0.529
4		1120		0.542
5		1120		0.575
6		1000		0.494
7		1000		0.483
8		1000		0.497
	Aver.	1045	Aver.	0.532
1		1313		0.563
2		1313		0.553
3		1338		0.587
4		1313		0.578
5		1318		0.558
6		1313		0.550
	Aver.	1318	Aver.	0.565

TABLE XVII

BURNING RATE OF HYDROCARBON "A" (13-1/2% STRAIN)

Test Number	Average Pressure, psi	Burning Rate, in/sec
1	575	0.404
2	575	0.442
3	575	0.401
4	563	0.401
5	563	0.404
6	587	0.407
7	575	0.390
8	562	0.393
	Aver. 572	Aver. 0.405
1	975	0.488
2	963	0.478
3	950	0.475
4	950	0.472
5	950	0.521
6	950	0.514
7	963	0.529
8	975	0.497
	Aver. 960	Aver. 0.484
1	1300	0.586
2	1300	0.545
3	1300	0.535
4	1300	0.534
5	1300	0.555
6	1300	0.547
7	1300	0.539
8	1300	0.562
	Aver. 1300	Aver. 0.550

TABLE XVIII

BURNING RATE OF POLYURETHANE PROPELLANT (0% STRAIN)

Test Number	Average Pressure, psi	Burning Rate, in./sec
1	575	0.160
2	550	0.157
3	538	0.157
4	538	0.157
5	500	0.158
	Aver.	0.1578
6	1075	0.159
7	1075	0.161
8	1088	0.163
9	1075	0.163
10	1063	0.163
	Aver.	0.1616

TABLE XIX

BURNING RATE OF POLYURETHANE PROPELLANT (10% STRAIN)

Test Number	Average Pressure, psi	Burning Rate, in./sec
1	538	0.160
2	530	0.159
3	530	0.161
	Aver.	0.160
5	1068	0.166
6	1050	0.170
7	1075	0.168
8	1063	0.167
	Aver.	0.168

TABLE XX

LINEAR BURNING RATE OF HYDROCARBON "B" (MOD) (0% STRAIN)

Test Number	Average Pressure, psi	Burning Rate, in./sec
1	565	0.246
2	550	0.247
	Aver.	0.247
3	1565	0.396
4	1560	0.396
5	1565	0.396
	Aver.	0.396

TABLE XXI

LINEAR BURNING RATE OF HYDROCARBON "B" (MOD) (5% STRAIN)

Test Number	Average Pressure, psi	Burning Rate, in./sec
1	563	0.264
2	550	0.256
3	550	0.255
4	550	0.256
	Aver.	0.258
5	1550	0.409
6	1600	0.411
7	1600	0.412
8	1575	0.415
	Aver.	0.412

TABLE XXII

LINEAR BURNING RATE OF HYDROCARBON "B" (MOD) (10% STRAIN)

Test Number	Average Pressure, psi	Burning Rate, in./sec
1	650	0.269
2	675	0.287
3	675	0.285
4	650	0.274
	Aver.	0.281
5	1600	0.418
6	1590	0.437
7	1595	0.443
	Aver.	0.432

TABLE XXIII

BURNING RATE OF PLASTISOL PROPELLANT (0% STRAIN)

Test Number	Average Pressure, psi	Burning Rate, in./sec
1	578	0.321
2	582	0.322
3	550	0.317
4	565	0.323
5	565	0.317
6	565	0.320
	Aver.	0.320
1	1650	471
2	1665	472
3	1625	479
4	1636	481
	Aver.	475

TABLE XXIV

BURNING RATE OF PLASTISOL PROPELLANT (10% STRAIN)

Test Number	Average Pressure, psi	Burning Rate, in./sec
1	565	0.453
2	565	0.447
3	570	0.435
	Aver.	0.445
1	1675	0.594
2	1645	0.613
3	1650	0.602
4	1650	0.591
	Aver.	0.600

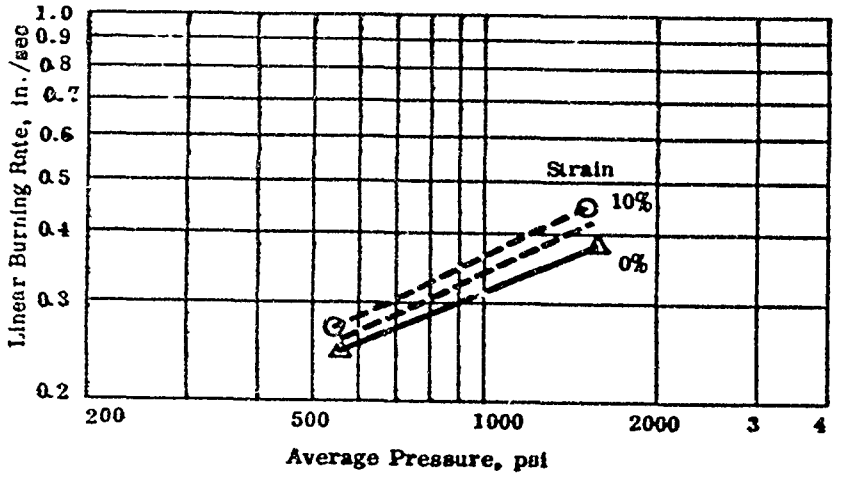

HYDROCARBON "B" (MOD)

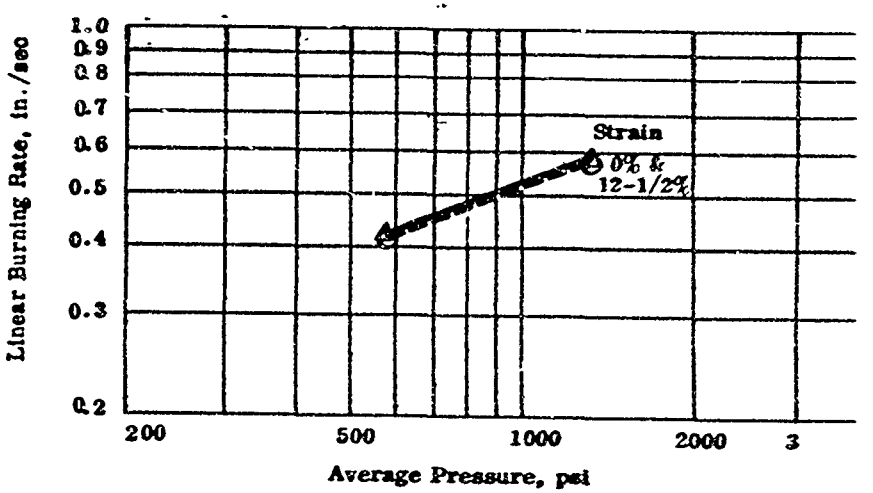

HYDROCARBON "A"

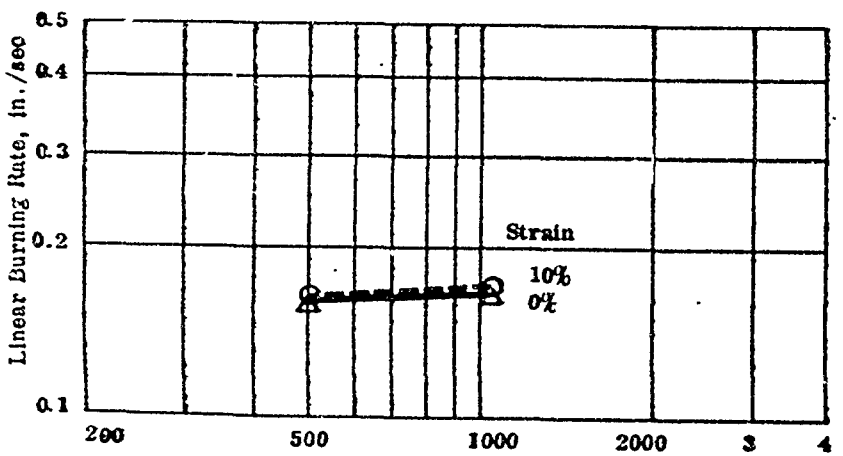

POLYURETHANE

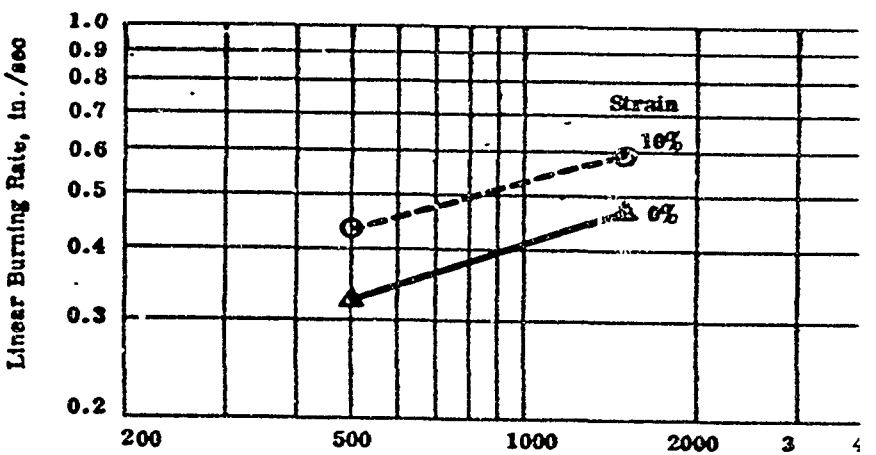

PLASTISOL

FIGURE 44. LINEAR BURNING RATE VERSUS PRESSURE

It can be seen that the curves for the strained condition are not necessarily parallel to their respective unstrained curves, thus indicating a different pressure dependence for each case. It appears that strain may increase the pressure dependence, although the data are inconclusive.

Consideration was given to the "mass burning rate" in addition to the linear burning rate. When a strain is imposed on a strand, it will permit an increase in time necessary to burn the propellant completely (i.e., a 10-percent strain will produce a 10-percent longer burning time for an incompressible material). The mass burning rate is thus reduced by the time increase required to consume the sample. Therefore, mass burning rate is a direct function of the reciprocal of the strain for the incompressible case. The mass burning rate calculations were based on the following relationship:

$$\dot{w} = rA\rho$$

where $\dot{w}$ = Mass burning rate, lb/sec

r = Linear burning rate (taken from experimental data), in./sec

A = Burning surface area, $in.^2$

ρ = Material density, $lb/in.^3$

The value of A changes with strain and was calculated from the Poisson's ratio data. From this value a new density of the material was computed. The combination of the linear burning rate (r), area (A), and density (ρ) of the material in the strained condition permitted the calculations of the mass burning rate, $\dot{w}$.

The computed mass burning rate shown in Tables XXV through XXVIII and Figure 45 experienced a decrease with strain for all propellants except the plastisol. This is not necessarily inconsistent since it is conceivable that strain can increase the burning rate to a degree which will completely offset the time to burn the additional length of the specimen.

It should be mentioned here that the burning rate calculations were based on three assumptions:

1) Perfect homogeneity exists throughout the strained sample. This would indicate that the dewetting action due to strain was also uniform along the length of the sample. This is probably not true, and localized areas of dewetting probably exist. This assumption affects the calculation of the density in the deformed state, and the linear burning rate is not really constant throughout the length of the strand. However, the linear rates measured include the gross summation of such areas, and the results should approximate the actual behavior.

2) The assumption is also made that the dimensions of the strand are 1/4 inch by 1/4 inch along the entire length and that after straining the new cross section is uniform also. Where this nonuniformity does not enter into the determinations of linear burning rate, it does affect the mass burning rate calculations.

3) The mass of the inhibitor does not influence the mass burning rate. This assumption was verified in the linear burning rate studies by comparison with control data on uninhibited strands. The difference was felt to be negligible.

These factors in conjunction with the nature of the plastisol propellant, limit the reliability of mass burning rate results obtained in this indirect manner.

TABLE XXV

MASS BURNING RATE VERSUS STRAIN, HYDROCARBON "A"

Percent Strain	Density (ρ), lbs/in.^{3}	Area (A), in.^{2}	Volume, in.^{3}	Linear Burning Rate, in.sec	Pressure, psi	$\dot{w}$, lbs/sec	M, lbs
0	0.0631	0.0625	0.3125	0.410	500	1.62×10^{-3}	19.70×10^{-3}
				0.527	1000	2.08×10^{-3}	19.70×10^{-3}
				[illegible]576	1300	2.27×10^{-3}	19.70×10^{-3}
4	0.0631	0.0601	0.3125	0.403	500	1.47×10^{-3}	18.95×10^{-3}
				0.549	1000	2.00×10^{-3}	18.95×10^{-3}
				0.578	1300	2.10×10^{-3}	18.95×10^{-3}
8	0.0631	0.0579	0.3125	0.402	500	1.36×10^{-3}	18.24×10^{-3}
				0.532	1000	1.30×10^{-3}	18.24×10^{-3}
				0.565	1300	1.91×10^{-3}	18.24×10^{-3}
12-1/2	0.0631	0.0555	0.3120	0.405	500	1.26×10^{-3}	17.49×10^{-3}
				0.484	1000	1.51×10^{-3}	17.49×10^{-3}
				0.550	1300	1.71×10^{-3}	17.49×10^{-3}

TABLE XXVI

MASS BURNING RATE VERSUS STRAIN, POLYURETHANE PROPELLANT

Percent Strain	Density (ρ), lbs/in.^{3}	Area (A), in.^{2}	Volume, in.^{3}	Linear Burning Rate, in./sec	Pressure, psi	$\dot{w}$, lbs/sec	M, lbs
0	0.598	0.0625	0.3125	0.158	500	0.59×10^{-3}	18.68×10^{-3}
				0.161	1500	0.60×10^{-3}	18.68×10^{-3}
10	0.05425	0.0570	0.3135	0.160	500	0.49×10^{-3}	16.98×10^{-3}
				0.168	1500	0.52×10^{-3}	16.98×10^{-3}

TABLE XXVII

MASS BURNING RATE VERSUS STRAIN, HYDROCARBON "B" (MOD)

Percent Strain	Density (ρ), lbs/in.^{3}	Area (A), in.^{2}	Volume, in.^{3}	Linear Burning Rate, in./sec	Pressure, psi	$\dot{w}$, lbs/sec	M, lbs
0	0.0625	0.0625	0.3125	0.247	500	0.96×10^{-3}	19.6×10^{-3}
				0.396	1500	1.55×10^{-3}	19.6×10^{-3}
5	0.0592	0.0595	0.3140	0.258	500	0.91×10^{-3}	18.6×10^{-3}
				0.412	1500	1.45×10^{-3}	18.6×10^{-3}
10	0.0562	0.0565	0.3165	0.281	500	0.89×10^{-3}	17.8×10^{-3}
				0.432	1500	1.37×10^{-3}	17.8×10^{-3}

TABLE XXVIII

MASS BURNING RATE VERSUS STRAIN, PLASTISOL PROPELLANT

Percent Strain	Density (ρ), lbs/in.^{3}	Area (A), in.^{2}	Volume, in.^{3}	Linear Burning Rate, in./sec	Pressure, psi	$\dot{w}$, lbs/sec	M, lbs
0	0.0592	0.0625	0.3125	0.320	500	1.18×10^{-3}	18.5×10^{-3}
				0.475	1500	1.76×10^{-3}	18.5×10^{-3}
10	0.0522	0.0581	0.3220	0.445	500	1.35×10^{-3}	16.8×10^{-3}
				0.600	1500	1.82×10^{-3}	16.8×10^{-3}

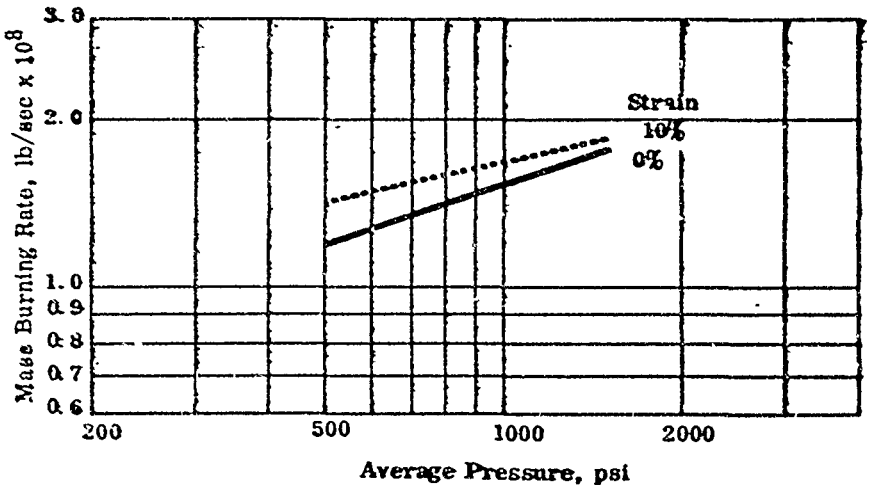

PLASTISOL

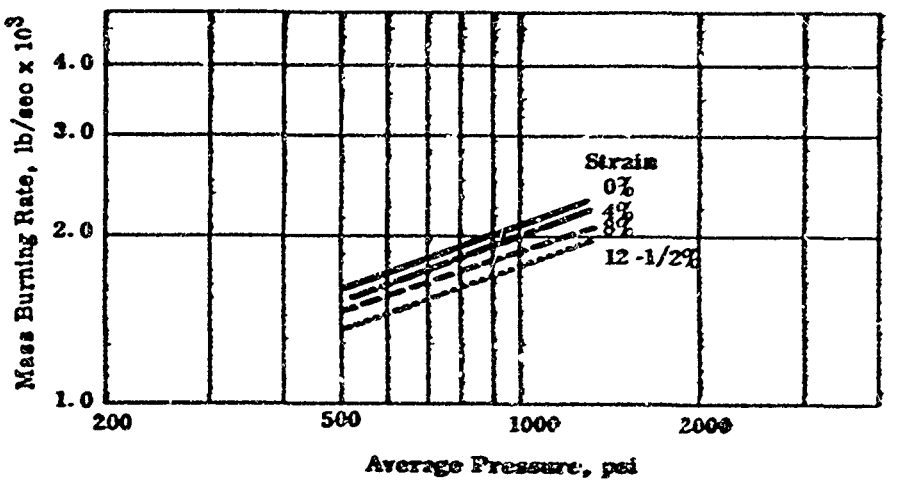

HYDROCARBON "A"

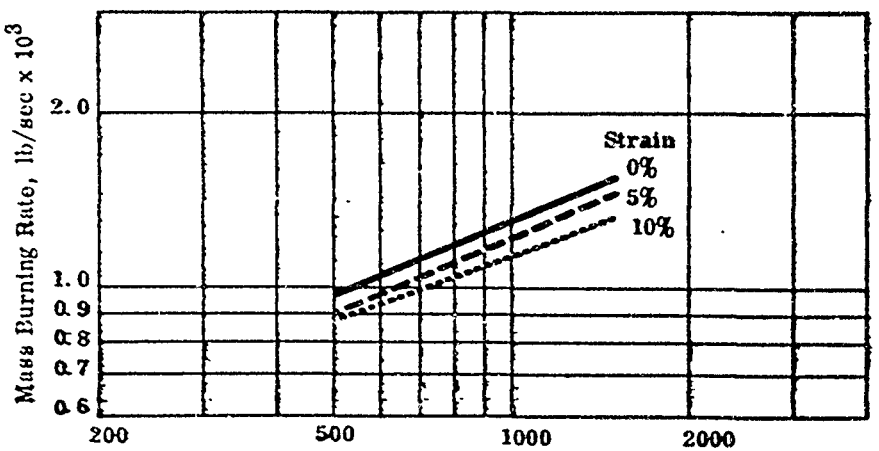

HYDROCARBON "B" (MOD)

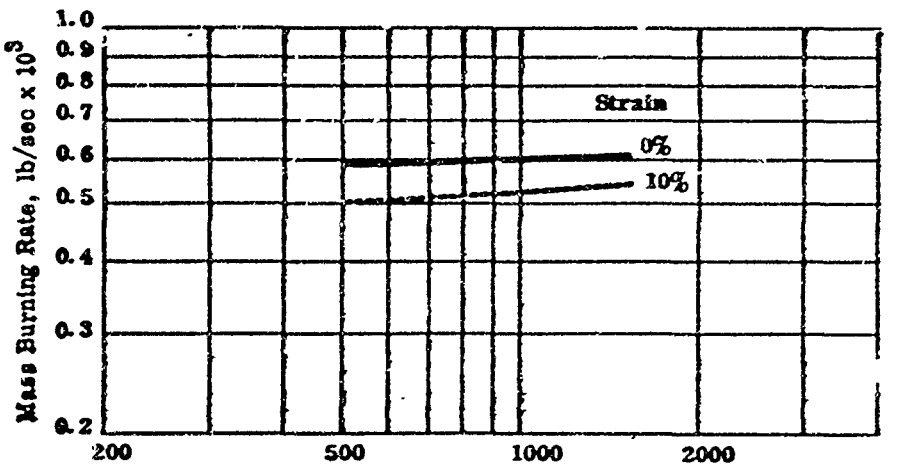

POLYURETHANE

FIGURE 45. MASS BURNING RATE VERSUS PRESSURE

The different degrees that the various materials were affected by strain initiated the effort to determine whether a criterion for these changes in burning rate could be established based on the change in volume due to strain (Poisson's ratio) rather than strain "per se." The value of the expression for an incompressible material (equation 2.3) was calculated for strain values for the four propellants determined experimentally. The results are shown in Figure 46 and Table XXIX. It can be seen that the departure of the Poisson's ratio for the individual propellants from the incompressible material curve is in direct sequence with the degree of influence of strain on burning rate. The data for hydrocarbon "A," which showed virtually no effect of strain on burning rate, follow quite closely the curve for an incompressible material, indicating that this particular formulation exhibits a negligible change in density due to strain. On the other hand, the plastisol, which displayed the departure from the incompressible curve, also had the most strain-sensitive burning rate. In order to examine this behavior more closely, the percent increase in linear burning rate, $\Delta r/r_o$, is compared with the volumetric change index, ν/ν_i, at the various pressures and strains tested. The results are shown on page 135.

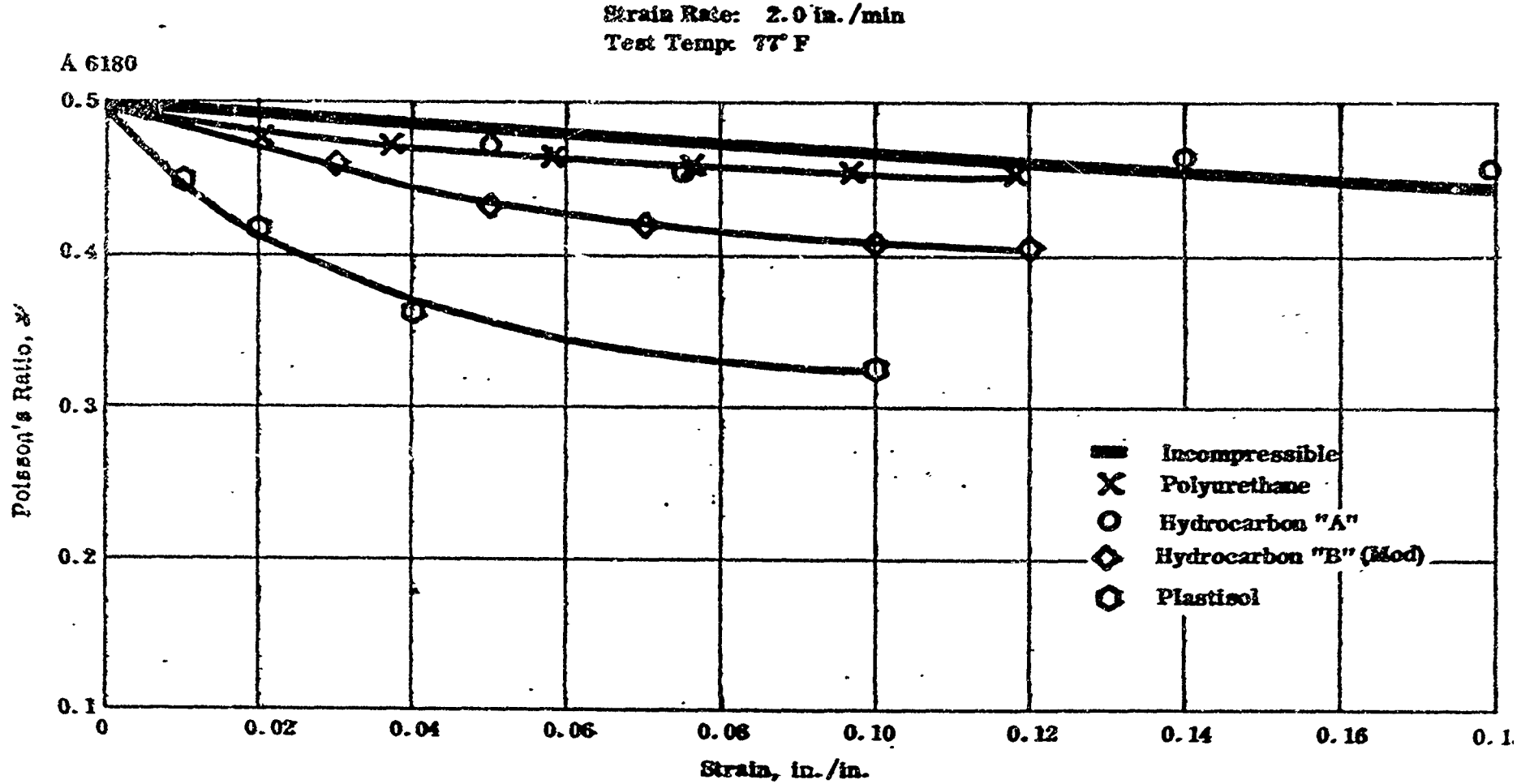

FIGURE 46. POISSON'S RATIO VERSUS STRAIN

TABLE XXIX

POISSON'S RATIO VERSUS STRAIN

TEST TEMPERATURE: 77°F

Percent Strain	Poisson's Ratio, Incompressible Material, ν_i	Poisson's Ratio, ν			
		Polyurethane	Hydrocarbon "B"	Plastisol	Hydrocarbon "A"
2	0.493	0.479	0.478	0.450	0.496
4	0.485	0.470	0.445	0.365	0.485
6	0.479	0.465	0.425	-	0.473
8	0.472	0.460	0.416	-	0.469
10	0.465	0.453	0.409	0.325	0.465
12	0.459	0.451	0.4 5	-	0.462
14	0.45				0.454
18	0.441				0.446

LINEAR BURNING RATE AND VOLUMETRIC CHANGE DATA

Propellant	Strain (ϵ_1), %	Pressure, psi	Percent Increase in Linear Burning Rate due to Strain, $\Delta r/r_o$	Volumetric Change Index (v/v_i) x 100	$\Delta r/r_o + (v'/v_i)$
Hydro-carbon "A"	4	500	-1.7	100.0	101.7
		1320	0.35		100.35
	8	500	1.95	99.36	101.31
		1320	1.20		100.56
	12 1/2	500	1.219	100.7	101.92
		1320	2.777		103.48
Poly-urethane	10	500	1.394	97.42	98.81
		1000	3.96		101.38
Hydro-carbon "B" (Mod)	5	500	4.453	90.25	94.70
		1500	4.040		94.29
	10	500	13.77	87.96	101.7
		1500	9.09		97.05
Plastisol	10	500	39.06	69.89	109.0
		1500	26.32		96.2

An interesting relationship appears to exist between the two parameters at the 10-percent strain level, i.e.:

$$\Delta r/r_o + (v/v_i) \approx \text{constant} \approx 100 \qquad (2.5)$$

Since only the 0 and 10-percent strain effects were obtained on all but hydrocarbon "A," it is not possible at this time to determine whether this relationship is consistent at intermediate strain values. This, perhaps, could be a subject for future study.

Dr. Landel of JPL was contacted to determine the value of Poisson's ratio at 10-percent strain for the material tested by Coy.* The value of Poisson's ratio for that particular material was 0.415. The rise in burning rate, $\Delta r/r_o$, was 14 percent and ν/ν_1 equaled 88 percent; he correlation, at least for linear burning rate, is thus further substantiated. From the above table it appears that equation 2.4 is valid with an accuracy of $\pm$ 0.05.

A similar table for mass burning rate is shown below.

MASS BURNING RATE AND VOLUMETRIC DATA

Propellant	Strain (ϵ_1), %	Pressure, psi	Percent Change in Mass Burning Rate Due to Strain, $\Delta \dot{w}/\dot{w}_o$	Volumetric Change Index, $(\nu)\nu_1) \times 100$	$\Delta \dot{w}/\dot{w}_o + (\nu)\nu_1)$
Hydro-carbon "A"	4	500	-9.259	100.00	90.74
		1320	-7.488		92.51
	8	500	-16.049	99.36	83.311
		1320	-15.86		83.50
	12 1/2	500	-22.22	100.7	78.48
		1320	-24.67		76.03
Poly-urethane	10	500	-16.214	97.42	81.206
		1000	-13.816		83.604
Hydro-carbon "B"	5	500	-5.906	90.25	84.34
		1500	-6.266		83.98
	10	500	-7.564	87.96	80.40
		1500	-11.434		76.53
Plastisol	10	500	+13.94	69.89	83.83
		1500	+3.53		73.42

*Dr. Landel was contacted for this information since Coy had since left the employ of JPL. Dr. Landel had been consulted before to this as to the advisability of pursuing the Poisson's ratio approach.

Unlike the previous case, the expression $\Delta \dot{w}/\dot{w}_o \div (\nu/\nu_i)$ is not a constant but changes with strain. For the case of hydrocarbon "A," which approximates an incompressible material, the relationship decreases with strain. It can be expected that for an incompressible material such as hydrocarbon "A," decrease in value of this expression with strain will be maximum. Also, as the material deviates from incompressibility the values of $\Delta \dot{w}/\dot{w}_o$ will approach zero and then become positive. This can be seen from the values for the plastisol. The data would indicate that the strain dependence of $\Delta\dot{w}/\dot{w}$ is slightly more pressure sensitive than that for $\Delta r/r_o$. The correlation is thus more complex than that for $\Delta r/r_o$, and additional work at more pressures and strains is necessary before any definite criteria for mass burning can be established.

The attempt to develop a test specimen suitable for measuring burning rate in a nonuniform strain field was unsuccessful. The contributing factors were:

1) The mass of the propellant sample had to be relatively small due to the limitations set up by the dimensions of the window bomb. This created problems in the Photo-Stress analysis, since the fringe patterns were so close together that an accurate correlation of the burning rate with position was difficult, especially at higher strains.

2) The size of the sample also requires that extreme care be taken in the selection of the PhotoStress plastic. The end effects at the outer perimeter of the specimen, due to relative reinforcement of plastic and material, at times extended across the entire specimen.

3) The PhotoStress plastics used all broke away from the vise grip walls at very low strains. The most promising material used was a Hysol #2085 PhotoStress plastic with a modulus of approximately 660 psi.

4) The technique in its present form could not assure that the strain patterns induced in the sample would not be altered as the sample material was consumed. The most promising specimen evaluated was the wedge.

For this reason, along with the more promising results being generated in the uniform strain field studies, it seemed advisable that the latter effort in this area be discontinued in January 1963 until a better definition of uniform strain effects could be achieved.

IV. PROPELLANT SLUMP ANALYSIS

Propellant structural integrity must be of prime concern to engineers associated with the design and development of solid propellant rocket motors since failure of a motor system may, in many instances, be traced to deficiencies in the design and/or physical properties of the propellant charge. Effort in this area during the past year has been directed toward the development of a means by which the effects of internal pressurization, thermal shrinkage, and axial acceleration loads upon propellant physical integrity could be predetermined. Since any propellant structural investigation must consider the complex time-dependent (or viscoelastic) properties of the material being examined, a limited amount of time and effort was expended in the area of propellant characterization. The second phase of the program concerned the development of a method for analyzing structural problems in axisymmetric grains having arbitrary end geometries and straight-through ports.

Subsection A specifies a means of analytically characterizing the viscoelastic properties of a solid propellant by linear differential operators and the time-dependent elastic modulus, E(t). The method and its accuracy are illustrated by examining the time-dependent properties of a typical hydrocarbon propellant (TP-H-1011).

Subsection B presents a technique for resolving structural problems in axisymmetric grain designs subject to loadings of pressure, temperature, and axial acceleration. The analysis is formulated in terms of two stress functions, Φ and Ψ, and a coupled pair of governing elliptic partial differential equations. The solution is sought through a finite difference approximation to the governing system. The pertinent boundary conditions,

together with their corresponding finite difference forms, are specified. A digital computer program based upon the above formulation, which is being completed, is discussed.

A. CHARACTERIZATION OF PROPELLANT TIME-DEPENDENT MATERIAL PROPERTIES

Problems associated with predetermining the structural integrity of solid propellant rocket motors defy resolution for many reasons. Among these are difficulties associated with the inherently complex mechanisms that govern the response of composite solid propellants to broad spectrum environmental and operational loads. That is, present composite solid propellants are members of a wide class of polymeric materials whose structural characteristics are typified by both elastic and viscous response when subjected to given tensile, shear, or compressive forces. If propellant structural designs are to be reliable, they must necessarily take into account the complex physical properties that these highly loaded polymers exhibit.

1. Determination of Linear Viscoelastic Model Constants from Uniaxial Creep and Stress Relaxation Tests

In classical elasticity where linearity, isotropy, and homogeneity are usually assumed, the relationship between stress and strain in a Hookean body is given by

$$\sigma = E\epsilon \tag{3.1}$$

For a linear viscoelastic material (i.e., a material that satisfies Boltzmann's superposition principle) it can be inferred that the Laplace transformed stresses

are related to the Laplace transformed strains by an analogous equation of the form[8]

$$\sigma(s) = s\,E(s)\,\epsilon(s) \tag{3.2}$$

The transformed elastic modulus E(s) is usually associated with the transfer function of a generalized Maxwell mechanical model, as illustrated in Figure 47. This association arises naturally from the isothermal viscoelastic stress-strain law that governs the response of an incompressible linear viscoelastic solid to a uniaxial force. This relationship may be expressed by either hereditary integrals or the following linear differential operator form[6]

$$P\sigma(t) = Q\epsilon(t) \tag{3.3}$$

where

$$P = \sum_{i=0}^{n} P_i \frac{\partial^i}{\partial t^i}$$

and

$$Q = \sum_{i=0}^{n} Q_i \frac{\partial^i}{\partial t^i}$$

The employment of (3.3) in solutions to propellant structural problems has been limited because of the inherent difficulties that the determination of the so-called "model constants" presented.[9] These constants are not available explicitly but may be obtained implicitly from experimental uniaxial stress relaxation or constant stress (creep) data wherein both stress and strain are known functions of time.[8,11]

An accurate knowledge of propellant relaxation times in the millisecond range is essential to the meaningful use of equation (3.3). In the past, stress relaxation

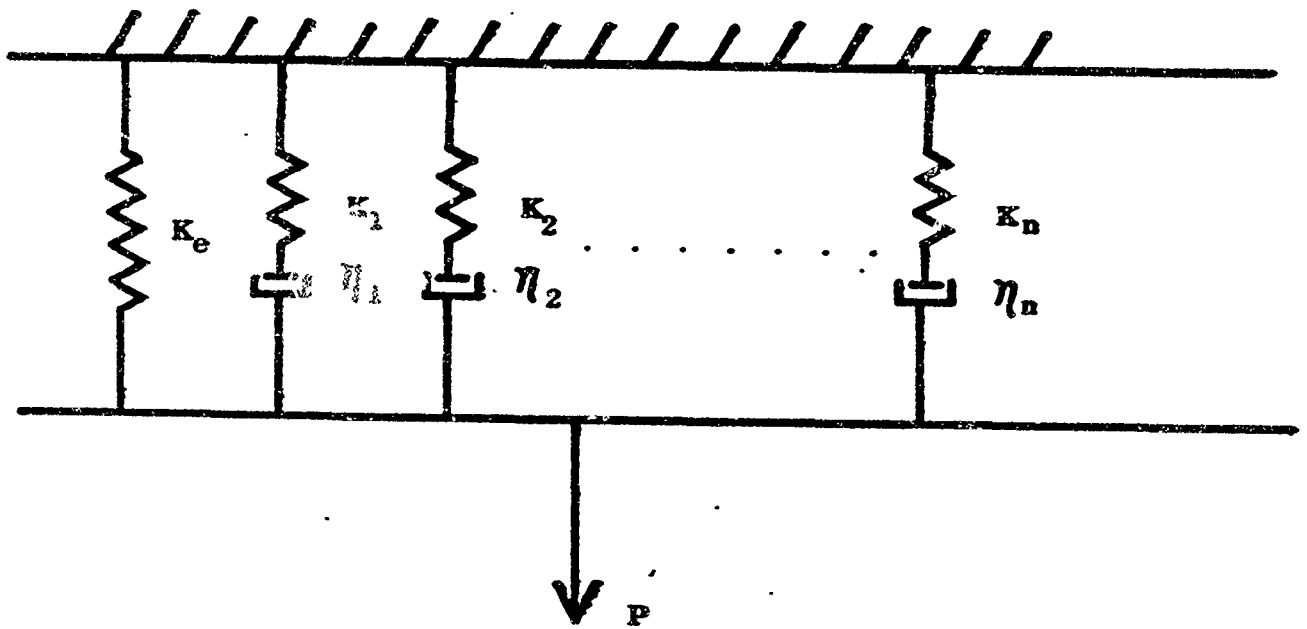

FIGURE 47. n - ELEMENT WIECHERT MODEL

data were unavailable from a reliable experimental apparatus capable of measuring stress decay at short times while eliminating transient dynamic effects in the experimental system for these times. Difficulties that resulted have been resolved at Thiokol during the past year.[10] Many experimental problems, such as those mentioned above, were overcome; and the measurement of stress response for finite input strain histories has progressed so that now error in empirical data does not contribute significantly to the over-all error in the analytical formulation of stress analysis solutions based upon differential operators.

In a tensile relaxation test having a finite loading time, the input strain may be characterized by (see Figure 48)

$$\epsilon(t) = A_o t - A_o (t-t_1)\, u(t-t_1) \tag{3.4}$$

In this case, the time-dependent relaxation modulus, as determined from the transfer function of the mechanical system illustrated in Figure 47, may be represented as a function of time as

$$E(t) = C_{n+2} + \sum_{i=1}^{n} C_i e^{-\alpha_i t} \tag{3.5}$$

where n is some conveniently chosen integer.

The time-dependent stress as measured during the relaxation test may be characterized as*

*See Appendix IV

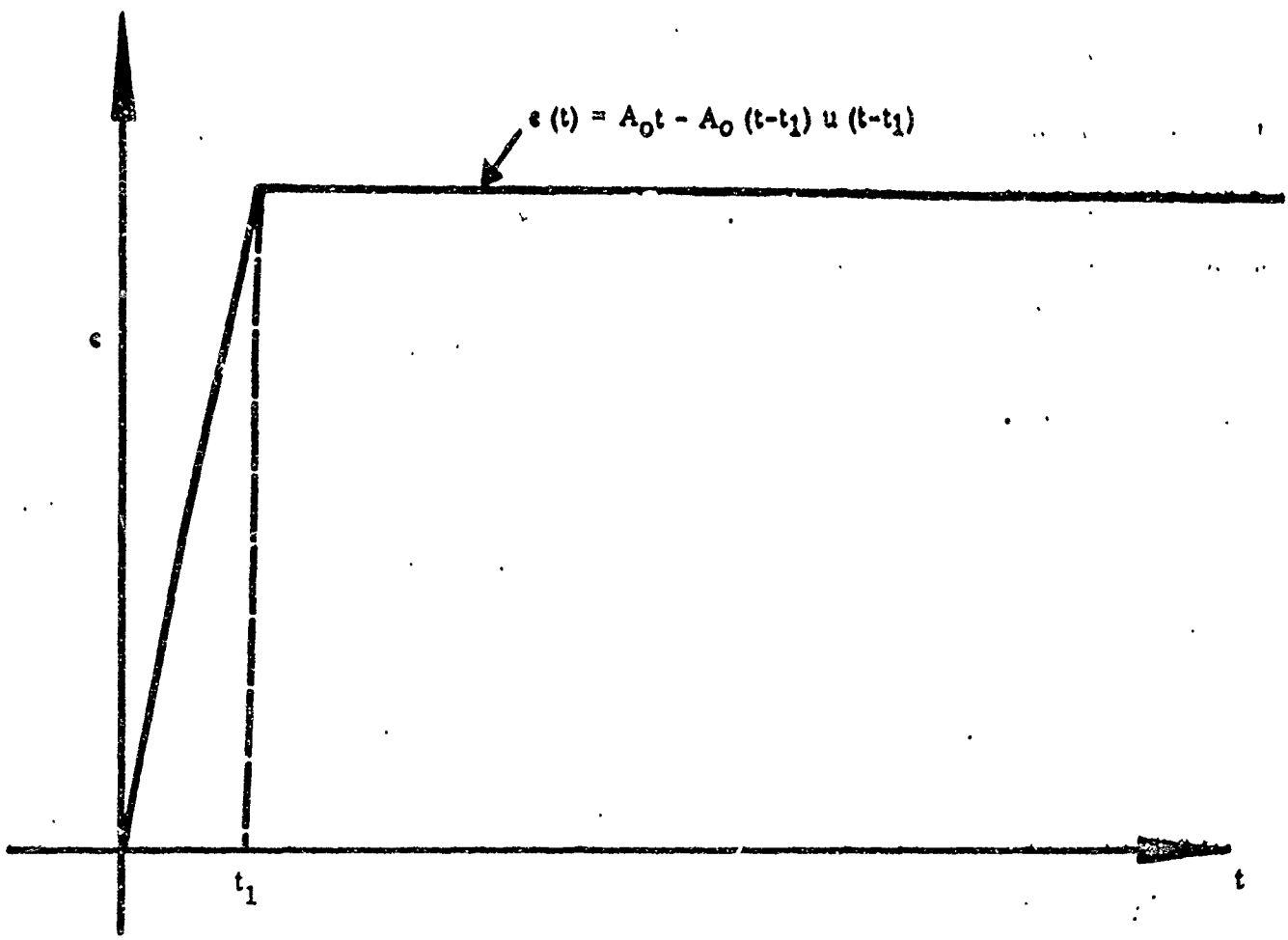

FIGURE 48. INPUT STRAIN VERSUS TIME

$$\sigma(t) = A_o \left[A_{n+2} t + A_{n+1} + \sum_{i=1}^{n} A_i e^{-\alpha_i t} \right]$$

$$- A_o \left[A_{n+2}(t-t_1) + A_{n+1} + \sum_{i=1}^{n} A_i e^{-\alpha_i (t-t_1)} \right] \cdot u(t-t_1) \qquad (3.6$$

where the A_i's in (3.6) are related to the C_i in (3.5) by

$$C_{n+2} = A_{n+2}$$

$$\sum_{i=1}^{n} \frac{C_i}{\alpha_i} = A_{n+1} \qquad (3.7$$

$$-\frac{C_i}{\alpha_i} = A_i$$

For $t > t_1$

$$\sigma(t) = A_o \left(A_{n+2} t_1 + \sum_{i=1}^{n} A_i \left[1 - e^{\alpha_i t_1} \right] e^{-\alpha_i t} \right) \qquad (3.$$

If the stress response in relaxation is known for $t > t_1$ and (3.8) is fit to these data, it can be deduced* that the relaxation modulus, (3.5), and the material constants, P_i, Q_i, are specified in that C_i, P_i, Q_i can be determined.

Difficulties inherent in the fitting of Prony type series (3.8) to experimental data have been emphasized elsewhere[8] and will not be considered here. However, the fitting of (3.8) to data where the decay factors α_i have not been prescribed previously gives rise to a system of transcendental equations that must be solved by unwieldly algebraic techniques.[9] This problem may be averted by employing a collocation method due to Schapery,[12] which, in essence, states that in fitting viscoelastic data it is

*See Appendix IV.

sufficient, in a least squares sense, to specify the decay factors as

$$\alpha_i = \frac{1}{2t_i} \tag{3.9}$$

2. Time Dependent Characterization of TP-H-1011

The analysis given above has been used to investigate the time-dependent mechanical properties of TP-H-1011, a hydrocarbon solid propellant used in the Minuteman propulsion system. Typical data from uniaxial stress relaxation tests conducted on this propellant are illustrated in Figures 49, 50, and 51.

The 80°F isothermal temperature tests disclosed that the response of TP-H-1011 could be adequately represented if the constants C_i, P_i, and Q_i were specified as

P_i		Q_i		C_i	
P_6 =	1	Q_6 =	9,794.4	C_6 =	7.38
P_5 =	505.55	Q_5 =	522,234.5	C_5 =	77.8
P_4 =	2780.5	Q_4 =	1,474,683.6	C_4 =	119.8
P_3 =	1402.9	Q_3 =	501,832.026	C_3 =	153.9
P_2 =	70.132	Q_2 =	16,563.32	C_2 =	434.6
P_1 =	0.347	Q_1 =	55.522	C_1 =	8,720.7
P_0 =	1.5×10^{-4}	Q_0 =	0.023	C_0 =	145.0

This specification is equivalent to the use of a 13- element Wiechert model (n = 6). The accuracy of the method is best illustrated by considering Figure 52 where data (stress) from a relaxation test are compared with the results obtained from the analytical characterization.

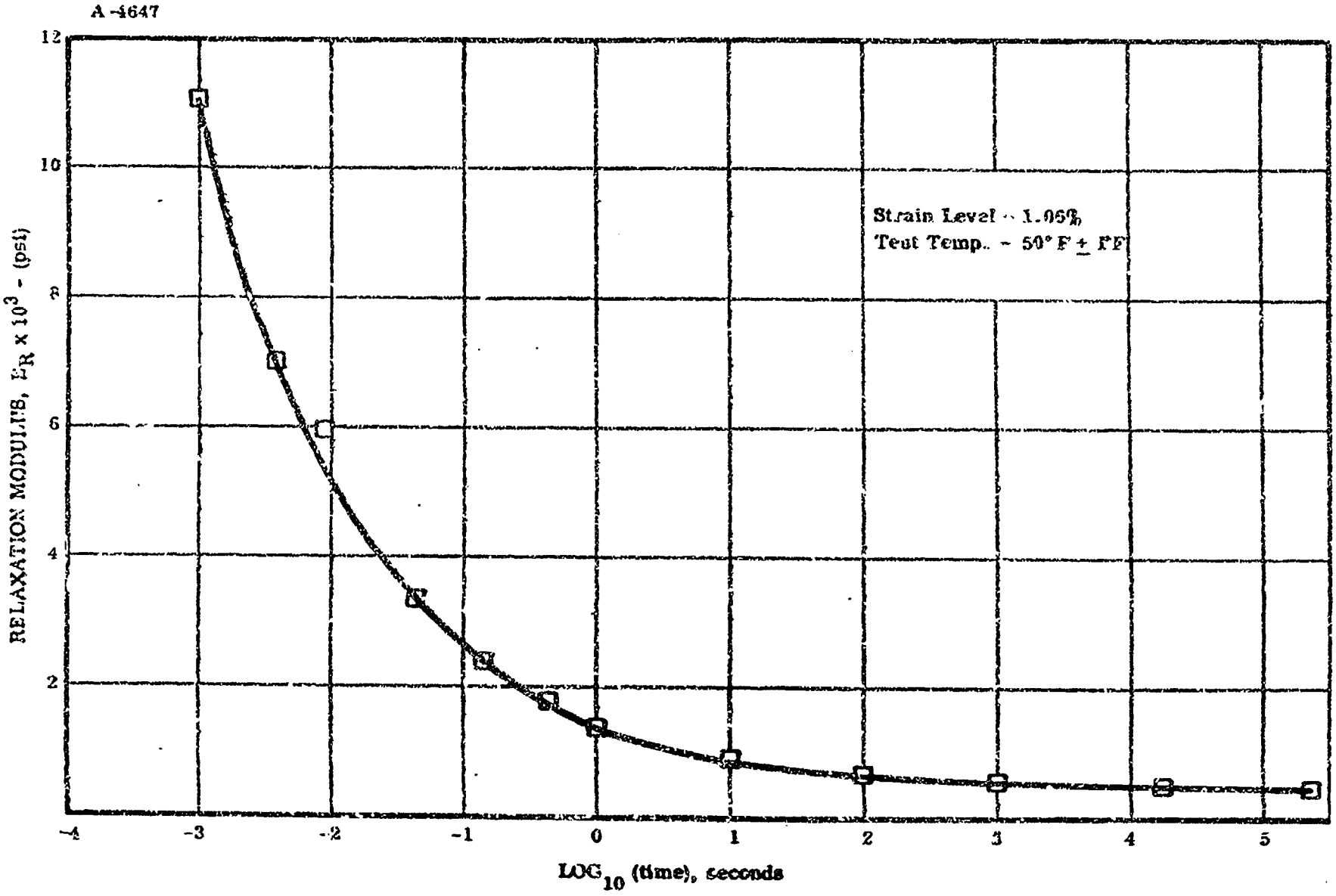

FIGURE 48. RELAXATION MODULUS VERSUS LOG(TIME), TP-H-1011

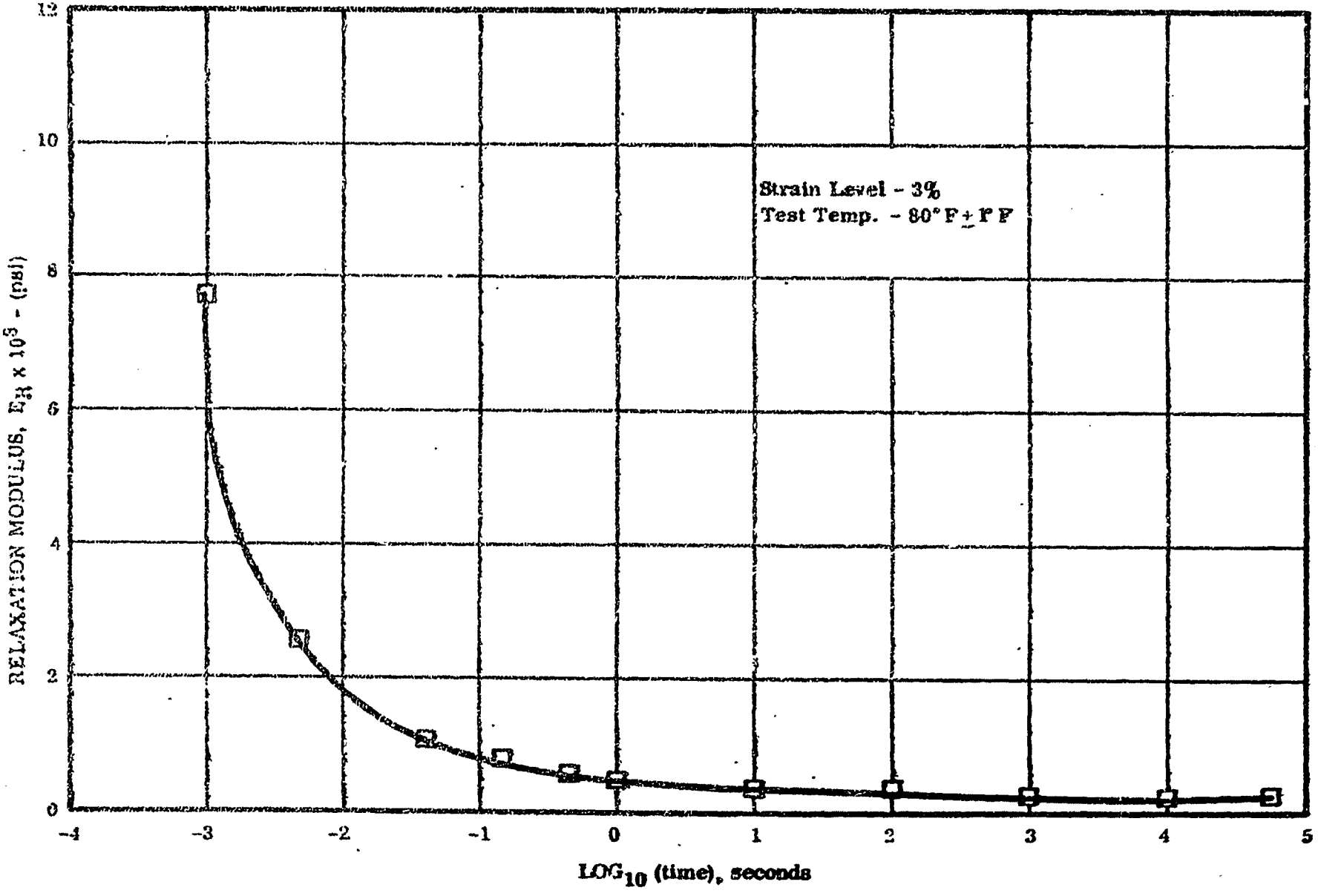

FIGURE 50. RELAXATION MODULUS VERSUS LOG (TIME), TP-H-1011

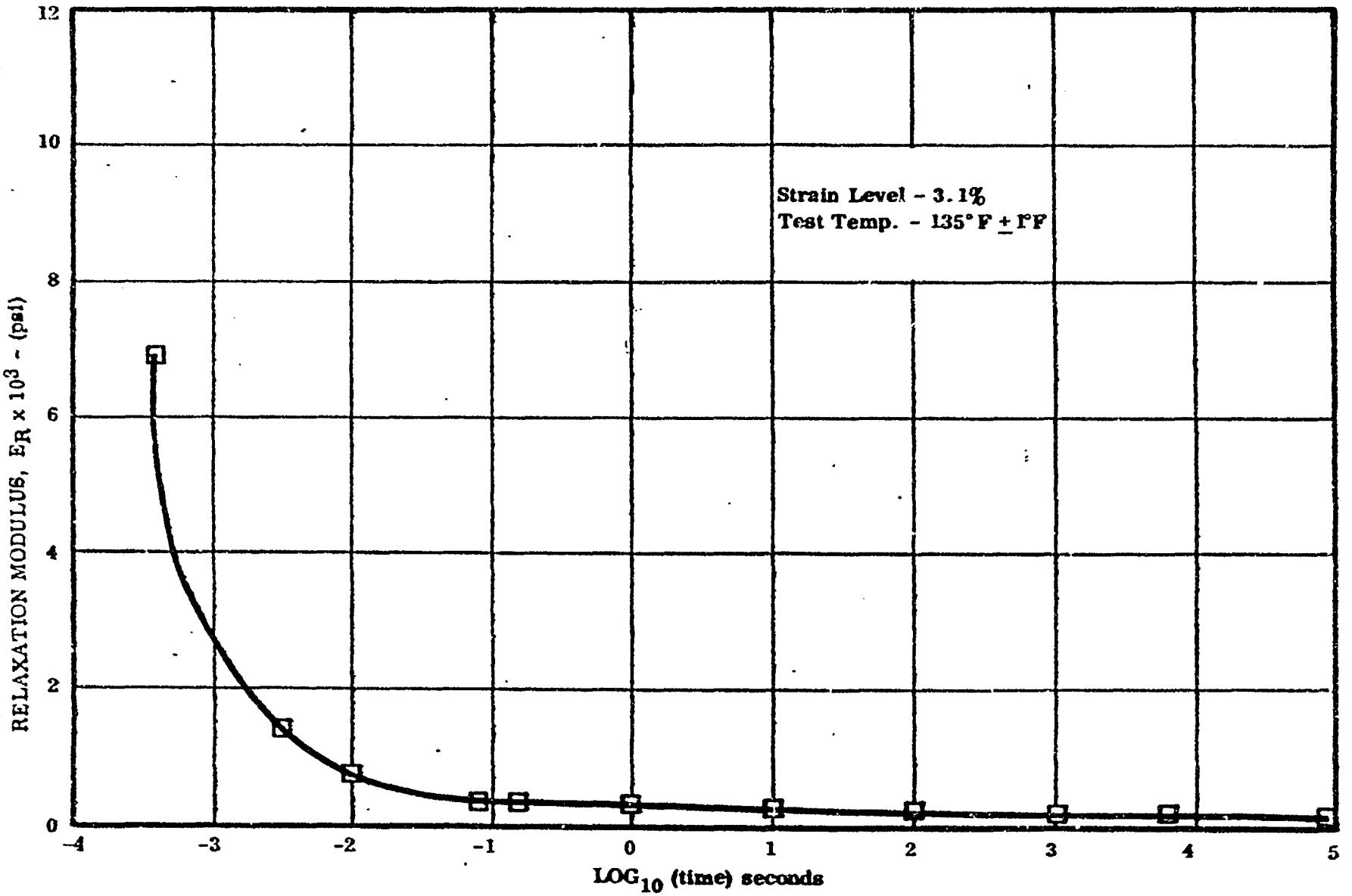

FIGURE 51. RELAXATION MODULUS VERSUS LOG (TIME), TP-H-1011

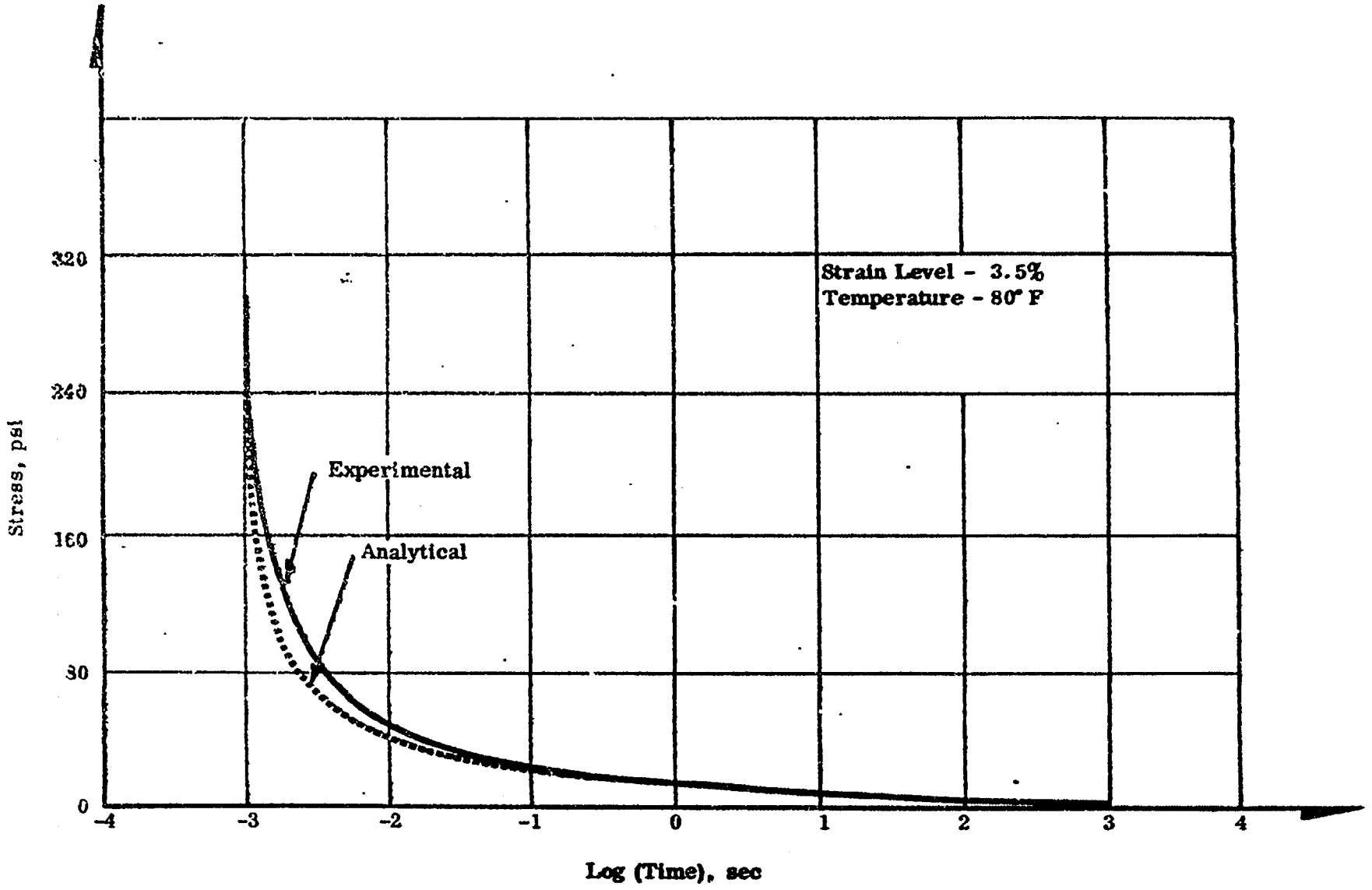

FIGURE 52. STRESS VERSUS LOG (TIME),TP-H-1011

Although these results are fragmentary, they provide basic information concerning the variation of modulus with time. This information is necessary to extend the elastic results of the finite difference elastic analysis described in subsection B.

B. STRESS ANALYSIS OF AXISYMMETRIC GRAIN DESIGNS HAVING ARBITRARY END GEOMETRIES AND STRAIGHT-THROUGH PORTS

Solid propellant rocket motors are exposed to a wide range of loadings during operation and storage. Basic among these are loadings due to internal pressure and acceleration during operation and propellant changes in volume due to thermal shrinkage (expansion) during cure and subsequent storage.

Principal effort in this area has been directed toward the development of an elastic analysis for axisymmetric grain designs having arbitrary end geometries and straight-through ports. The propellant charge is assumed to be linear elastic, isotropic, and homogeneous and bonded to a rigid case on its outer periphery head and aft ends. The stresses, strains, and displacements to be determined are those induced by either internal pressurization, uniform thermal shrinkage, or a constant acceleration load applied in the axial direction.

The initial step in any structural analysis of a solid propellant rocket grain is to obtain a solution of the elastic field equations subject to given boundary conditions and a prescribed external loading. In particular, if the grain is axisymmetric and the prescribed loads are rotationally symmetric, the governing system is considerably simplified. In this case, the analyst has several methods[13] at his disposal from which

he may seek the solution. However, such methods present inherent difficulties that may be traced to the basic need for satisfying the mixed boundary conditions typical of this class of problems. An approximate numerical technique originally developed by Southwell[14] and more recently extended to the analysis of solid propellant rocket grains by Parr[15, 16, 17] was found to be especially applicable to the solution of t' problem.

1. Stress Functions

Elastic bodies having forms that are solids of revolution and loaded so that axial symmetry is maintained in the resulting deformation have been shown to be amenable to numerical solution using stress functions and relaxation techniques.[14, 18] In particular, for the conditions described above, if two functions, Φ and Ψ, of the spacial coordinates r and z (but not θ) are defined in such a way that they satisfy the differential system

$$\begin{aligned} \frac{\partial^2 \Phi}{\partial r^2} - \frac{1}{r}\frac{\partial \Phi}{\partial r} + \frac{\partial^2 \Phi}{\partial z^2} &= 0 \\ \frac{\partial^2 \Psi}{\partial r^2} - \frac{1}{r}\frac{\partial \Psi}{\partial r} + \frac{\partial^2 \Psi}{\partial z^2} &= \frac{\partial^2 \Phi}{\partial z^2} \end{aligned} \tag{4.1}$$

the equilibrium and compatibility conditions are satisfied if the stresses are defined by

$$\sigma_r = \frac{1}{r}\left[\frac{\partial \Phi}{\partial r} + \frac{\partial \Psi}{\partial r}\right] - \frac{1}{r^2}\left[\Psi + (1-\nu)\Phi\right] \tag{4.2}$$

$$\sigma_\theta = \nu \frac{\partial \Phi}{\partial r} + \frac{1}{r^2}\left[\Psi + (1-\nu)\Phi\right] \tag{4.3}$$

$$\sigma_z = -\frac{1}{r}\frac{\partial \Psi}{\partial r} + z I_z \tag{4.4}$$

and

$$\tau_{rz} = \frac{1}{r}\frac{\partial \Psi}{\partial z} \tag{4.5}$$

I_z is the effective body force due to acceleration and is equal to the load in g's multiplied by the mass density of the propellant.

The associated strains and displacements, expressed as functions of Φ, Ψ, and their partial derivatives may be obtained from the axisymmetric stress-strain and strain-displacement relations of elasticity. For brevity they are not delineated here.

The relations (4.1)-(4.5) and their corresponding strains and displacements may be generalized to include the effects of an axial acceleration and propellant expansion due to thermal shrinkage during cure (see references 16 and 18).

2. Formulation of Problem in Terms of Dimensionless Quantities

Using standard notation[16, 19] we define (see Figures 53 and 54).

$$\begin{aligned}
\rho &= \frac{r}{b} & \sigma_\rho &= \frac{\sigma_r}{E} & \epsilon_\rho &= \epsilon_r \\
\eta &= \frac{z}{b} & \sigma_\theta &= \frac{\sigma_\theta}{E} & \epsilon_\theta &= \epsilon_\theta \\
Z &= \frac{bI_z}{E} & \sigma_\eta &= \frac{\sigma_z}{E} & \epsilon_\eta &= \epsilon_z \\
\Phi &= b^2 E \Phi & \tau_{\rho\eta} &= \frac{\tau_{rz}}{E} & \gamma_{\rho\eta} &= \gamma_{rz} \\
\Psi &= b^2 E \Psi & u_\rho &= \frac{u}{b} & u_\eta &= \frac{w}{b}
\end{aligned} \tag{5.1}$$

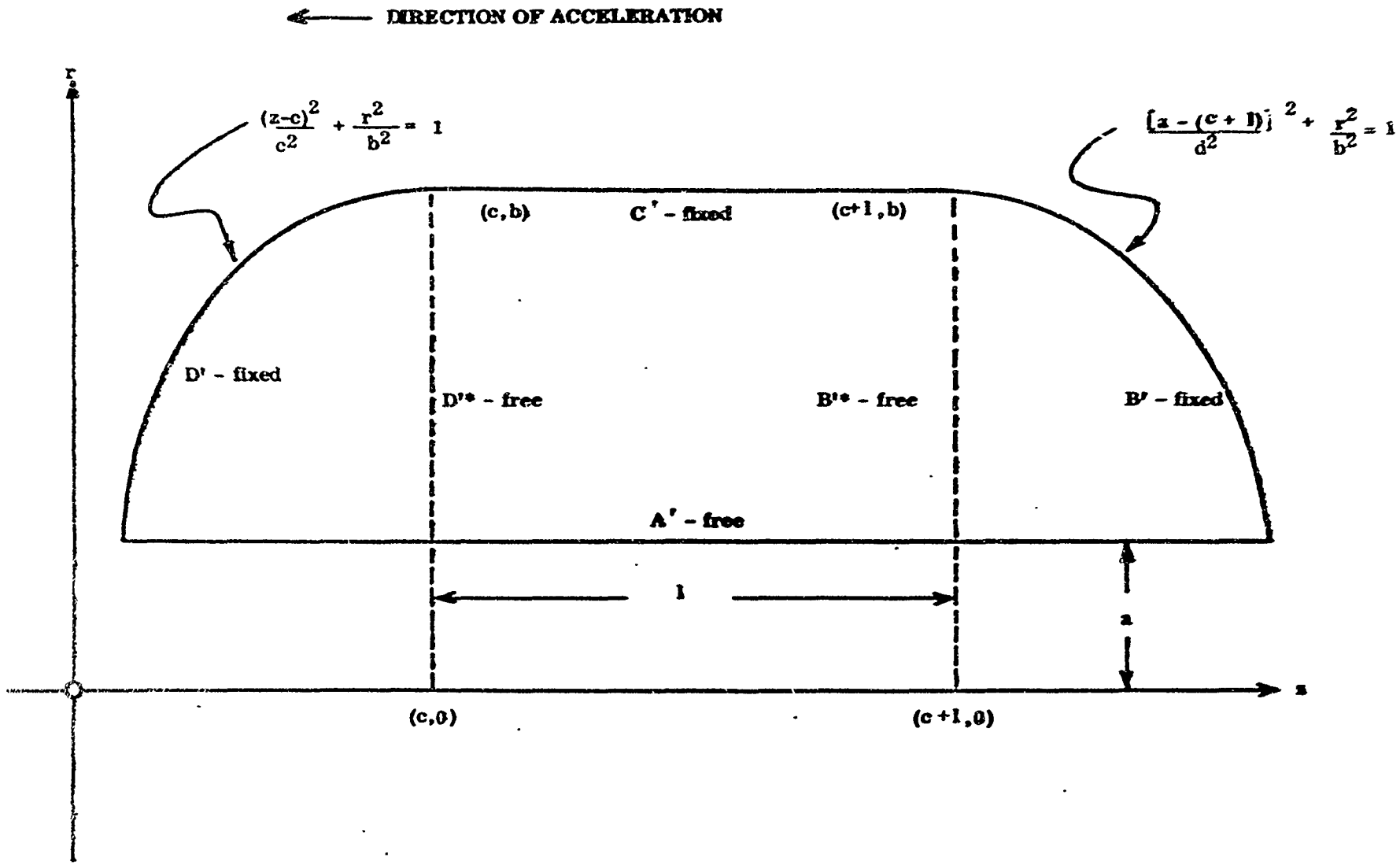

FIGURE 53. AXIAL CROSS SECTION OF CYLINDRICAL GRAIN WITH ARBITRARY HEAD AND AFT END

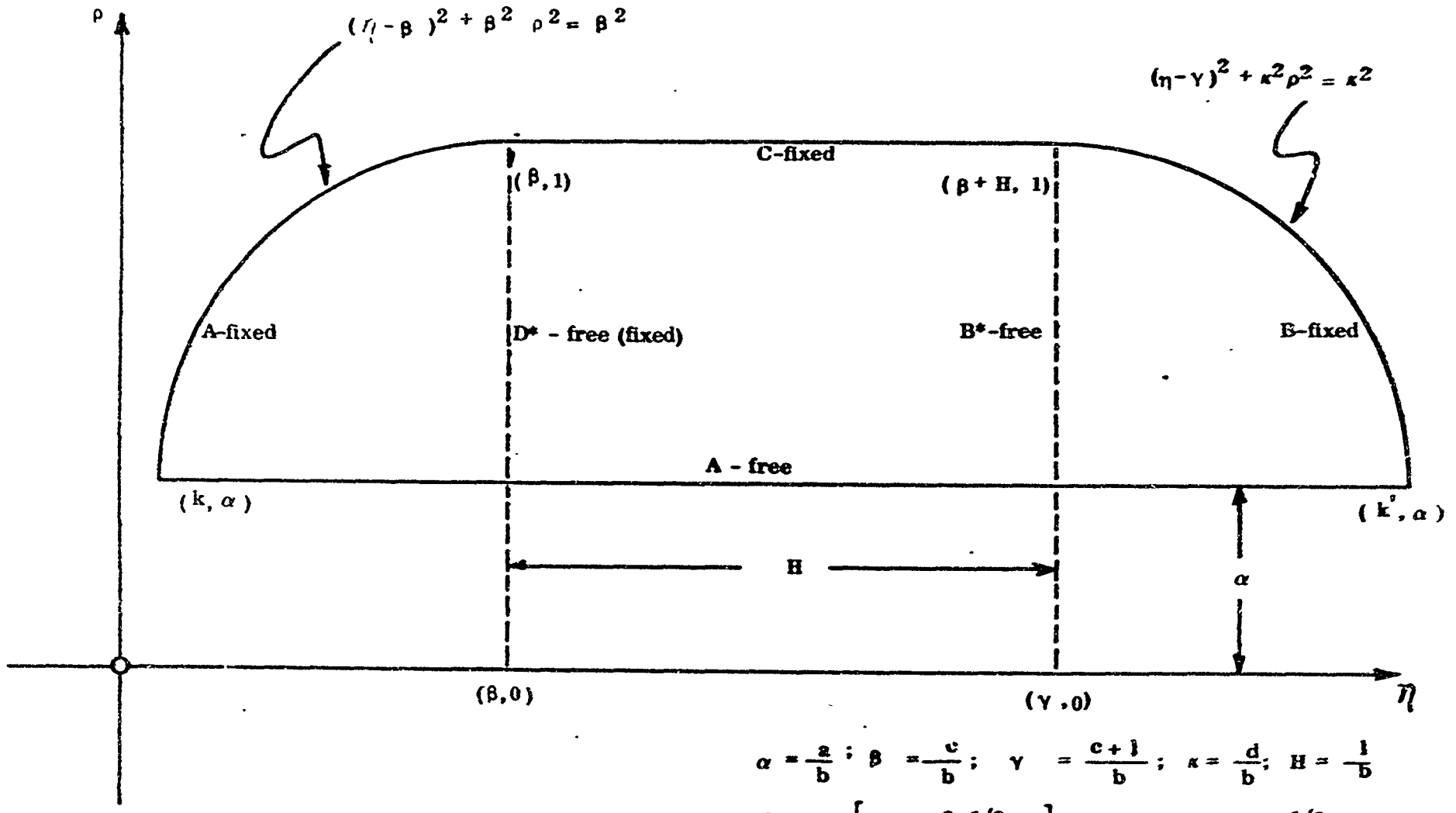

$$\alpha = \frac{a}{b}\ ;\ \beta = \frac{c}{b}\ ;\ \gamma = \frac{c+1}{b}\ ;\ \kappa = \frac{d}{b};\ H = \frac{1}{b}$$

$$k = \beta\left[(1-\alpha^2)^{1/2}+1\right]\ ;k' = \kappa\ (1-\alpha^2)^{1/2}+\gamma$$

FIGURE 54. NONDIMENSIONAL COORDINATE SYSTEM

in order that the governing system (4.1), stresses (4.2)-(4.5), strains and displacements may be expressed in a more compact nondimensional form. These may now be written as

$$\frac{\partial^2 \phi}{\partial \rho^2} - \frac{1}{\rho}\frac{\partial \phi}{\partial \rho} + \frac{\partial^2 \phi}{\partial \eta^2} = 0$$
$$\frac{\partial^2 \psi}{\partial \rho^2} - \frac{1}{\rho}\frac{\partial \psi}{\partial \rho} + \frac{\partial^2 \psi}{\partial \eta^2} = \frac{\partial^2 \phi}{\partial \eta^2} \qquad (5.2)$$

and

$$u_\rho = \frac{(1+\nu)}{\rho}\left[\psi + (1-\nu)\phi\right] - \nu\rho\eta Z + \mu\delta \qquad (5.3)$$

$$u_\eta = -\frac{\nu Z}{2}\left\{\left[f(\eta)\right]^2 - \rho^2\right\} - (1+\nu)\int_\rho^{\rho = f(\eta)}\left[\frac{1}{\rho}\frac{\partial \psi}{\partial \eta} - \frac{(1-\nu)}{\rho}\frac{\partial \phi}{\partial \eta}\right] d\rho \qquad (5.4)$$

$$\epsilon_\rho = \frac{(1+\nu)}{\rho}\left\{\frac{\partial \psi}{\partial \rho} + (1-\nu)\frac{\partial \phi}{\partial \rho} - \frac{1}{\rho}\left[\psi + (1-\nu)\phi\right]\right\} - \nu\eta Z + \delta \qquad (5.5)$$

$$\epsilon_\zeta = \frac{(1+\nu)}{\rho^2}\left[\psi + (1-\nu)\phi\right] - \nu\eta Z + \delta \qquad (5.6)$$

$$\epsilon_\eta = -\frac{(1+\nu)}{\rho}\left[\frac{\partial \psi}{\partial \rho} + \nu\frac{\partial \phi}{\partial \rho}\right] + \eta Z + \delta \qquad (5.7)$$

$$\sigma_\rho = \frac{1}{\rho}\left[\frac{\partial \phi}{\partial \rho} + \frac{\partial \psi}{\partial \rho}\right] - \frac{1}{\rho^2}\left[\psi + (1-\nu)\phi\right] \qquad (5.8)$$

$$\sigma_\theta = \frac{\nu}{\rho}\frac{\partial \phi}{\partial \rho} + \frac{1}{\rho^2}\left[\psi + (1-\nu)\phi\right] \qquad (5.9)$$

$$\sigma_\eta = -\frac{1}{\rho}\frac{\partial \psi}{\partial \rho} + \eta Z \qquad (5.10)$$

$$\tau_{\rho\eta} = \frac{1}{\rho}\frac{\partial \psi}{\partial \eta} \qquad (5.11)$$

$$\gamma_{\rho\eta} = \frac{2(1+\nu)}{\rho}\frac{\partial \psi}{\partial \eta} \qquad (5.12)$$

3. Boundary Conditions

The simultaneous solution of (5.2), subject to the boundary conditions and loadings described above and illustrated in Figure 54, constitutes a description of the stress-strain-displacement state of the propellant charge. The boundary conditions associated with this formulation may be quite arbitrary and may consist of specified stresses on free boundaries (A, B*, D*, and specified displacements on fixed boundaries (B, C, D). General boundary conditions for the grains illustrated in Figure 54 are delineated below. For a loading by an internal pressure, $P_i(z)$, it was assumed that free surfaces were subjected to a dimensionless normal force, $\pi_i(\eta)$, where

$$\pi_i(\eta) = \frac{P_i(z)}{E} \tag{6.1}$$

Although the analysis described below may be readily extended to include variable internal pressure, $P_i(z)$ was assumed to be constant with axial position for the cases considered here.

Side A ($\rho = \alpha$)

On this free boundary the normal radial stress and shearing stresses are specified as:

Acceleration and Thermal Loadings

$$\sigma_\rho = 0 \tag{6.2}$$

$$\tau_{\rho\eta} = 0 \tag{6.3}$$

Pressure Loading

$$\sigma_\rho = -\pi_i(\eta) \tag{6.4}$$

$$\tau_{\rho\eta} = 0 \tag{6.5}$$

Side B ($\rho = f_1(\eta)$)

On this fixed boundary the radial and axial displacements are identically zero for all loadings; therefore, the boundary conditions for Side B are:

Acceleration, Thermal, and Pressure Loading

$$u_\rho = 0 \tag{6.6}$$

$$u_\eta = 0 \tag{6.7}$$

Side B* ($\eta = \beta + H$)

A flat aft end of a motor was designated as a free boundary; as such, the boundary conditions are:

Acceleration and Thermal Loadings

$$\sigma_{\eta_1} = 0 \tag{6.8}$$

$$\tau_{\rho\eta} = 0 \tag{6.9}$$

Pressure Loading

$$\sigma_\eta = -\pi_2(\eta) \tag{6.10}$$

$$\tau_{\rho\eta} = 0 \tag{6.11}$$

Side C ($\rho = 1$)

On this fixed boundary the radial and axial displacements, as in the case of Side B, are identically zero for all load' specified above; hence, the boundary conditions for this side are:

Acceleration, Thermal, and Pressure Loadings

$$u_\rho = 0 \tag{6.12}$$

$$u_\eta = 0 \tag{6.13}$$

Side D $[\rho = f_2(\eta)]$

The boundary conditions are the same as those for Side B; namely,

Acceleration, Thermal and Pressure Loading

$$u_\rho = 0 \tag{6.14}$$

$$u_\eta = 0 \tag{6.15}$$

Side D* ($\eta = \beta = 0$)

On a flat head-end boundary, η was specified as zero. This boundary was either fixed or free. For a fixed end condition, the displacements are zero for all loadings; hence,

Acceleration, Thermal and Pressure Loadings

$$u_\rho = 0 \tag{6.16}$$

$$u_\eta = 0 \tag{6.17}$$

If D* is free, the boundary conditions take the form of specified stresses, which are:

Acceleration and Thermal Loadings

$$\sigma_\eta = 0 \tag{6.18}$$

$$\tau_{o\eta} = 0 \tag{6.19}$$

Pressure Loadings

$$\sigma_\eta = \pi_3(\eta) \tag{6.20}$$

$$\tau_{\rho\eta} = 0 \tag{6.21}$$

Corner Points

At corner points, the boundary conditions for each pair of adjoining boundaries must be satisfied.

The stress functions ϕ and ψ must satisfy not only the governing differential equations but also the boundary conditions specified by (6.2)-(6.21). In most instances, these general boundary conditions, when coupled with their respective representations (5.2)-(5.12), will be used as stated. However, in certain instances (e.g., on curved boundaries) the use of these conditions is not desirable from a numerical analysis standpoint. To obtain numerical representations that are "nice," recourse must be made to physical intuition and algebraic manipulation of the various relations of classical elasticity.

4. Finite Difference Formulation of Solution

a. Governing System

The five-point nodal molecule in Figure 55 illustrates that the central finite difference representation of (5.2) in relation to node 0 is

$$\frac{h}{2\rho_o}(\phi_4 - \phi_2) + \phi_1 + \phi_2 + \phi_3 + \phi_4 - 4\phi_o = 0$$

$$\frac{h}{2\rho_o}(\psi_4 - \psi_2) + \psi_1 + \psi_2 + \psi_3 + \psi_4 - 4\psi_o - \phi_1 - \phi_3 + 2\phi_o = 0 \qquad (7.1)$$

If one or more points of a nodal molecule lie outside the boundary of the grain, alterations must be made in (7.1). Such points, aptly termed fictitious, are present for both boundary and interior nodes when these nodes are separated from adjacent nodes by a boundary.

If the curved segment (head end) of the boundary lies to the left of the mid-section, as it does in Figure 54, three possibilities are applicable to the nodes centered in the interior:

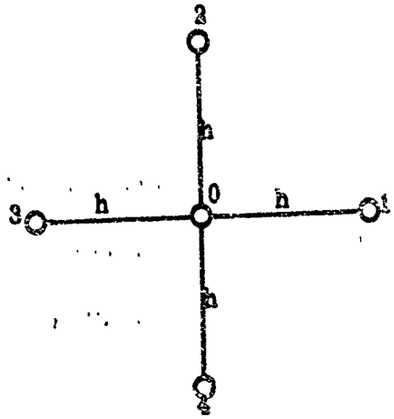

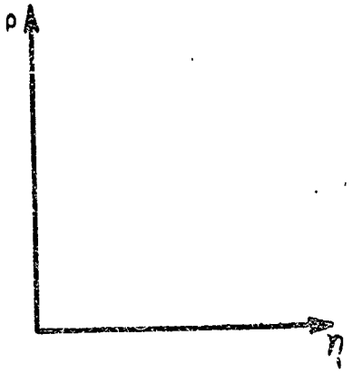

$$\left(\frac{\partial X}{\partial \rho}\right)_0 = \frac{X_2 - X_4}{2h}$$

$$\left(\frac{\partial X}{\partial \eta}\right)_0 = \frac{X_1 - X_3}{2h}$$

$$\left(\frac{\partial^2 X}{\partial \rho^2}\right)_0 = \frac{X_2 + X_4 - 2X_0}{h^2}$$

$$\left(\frac{\partial^2 X}{\partial \eta^2}\right)_0 = \frac{X_1 + X_3 - 2X_0}{h^2}$$

$$\left(\frac{\partial^2 X}{\partial \rho^2}\right)_0 + \left(\frac{\partial^2 Y}{\partial \eta^2}\right)_0 = \frac{X_1 + X_2 + X_3 + X_4 - 4X_0}{h^2}$$

FIGURE 55. FINITE DIFFERENCE MOLECULE

1) Nodes 2 and 3 are fictitious,

2) Node 3 is fictitious, or

3) Node 2 is fictitious.

Similarly, if the curved segment (aft end) of the boundary lies to the right of the mid-section, as it does in Figure 54, three possibilities are again applicable to the nodes centered in the interior. However, if node 2 is fictitious, possibility (3) above is applicable, and only the distinct cases need consideration:

1) Node 1 is fictitious, or

2) Nodes 1 and 2 are fictitious.

The five distinct possibilities are illustrated in Figure 56.

The first case is identified by (1) in Figure 56. Without loss of generality it may be assumed that ϕ and ψ can be expanded about node 0 in a two-dimensional Taylor series of the form

$$X = X_0 + (\eta - \eta_0)\left(\frac{\partial X}{\partial \eta}\right)_0 + (\rho - \rho_0)\left(\frac{\partial X}{\partial \rho}\right)_0 + \frac{(\eta-\eta_0)^2}{2!}\left(\frac{\partial^2 X}{\partial \eta^2}\right)_0 + (\rho-\rho_0)(\eta-\eta_0)\left(\frac{\partial^2 X}{\partial \rho \partial \eta}\right)_0 + \frac{(\rho-\rho_0)^2}{2!}\left(\frac{\partial^2 X}{\partial \rho^2}\right)_0 + \cdots \tag{7.2}$$

The fictitious nodes 2 and 3 must be replaced by their corresponding boundary nodes, A and B. The points 1, A, 4, and B have coordinates $(\eta_0 + h, \rho_0)$, $(\eta_0 - \delta_A h, \rho_0)$, $(\eta_0, \rho_0 - h)$ and $(\eta_0, \rho_0 + \delta_B h)$, respectively. When these are substituted into (7.2) (after terms having factors of h greater than three are truncated), four

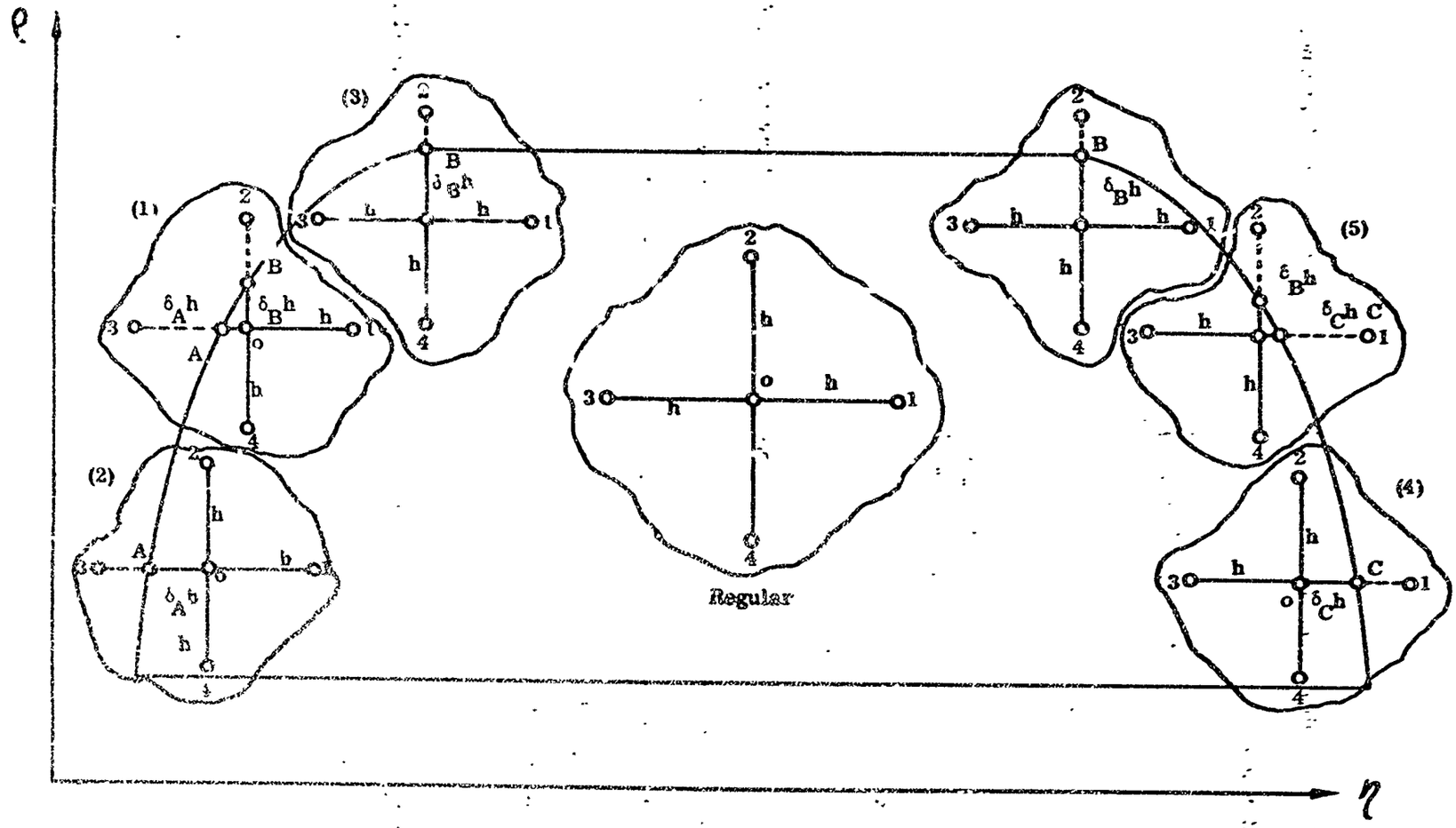

FIGURE 86. IRREGULAR INTERIOR NODES

linear equations result in terms of the first and second derivatives of X with respect to ρ and η at node 0.

$$X_1 = X_o + h \left(\frac{\partial X}{\partial \eta}\right)_o + \frac{h^2}{2}\left(\frac{\partial^2 X}{\partial \eta^2}\right)_o$$

$$X_A = X_o - \delta_A h \left(\frac{\partial X}{\partial \eta}\right)_o + \frac{(\delta_A h)^2}{2}\left(\frac{\partial^2 X}{\partial \eta^2}\right)_o \qquad (7.3)$$

$$X_4 = X_o - h \left(\frac{\partial X}{\partial \rho}\right)_o + \frac{h^2}{2}\left(\frac{\partial^2 X}{\partial \rho^2}\right)_o$$

$$X_B = X_o + \delta_B h \left(\frac{\partial X}{\partial \rho}\right)_o + \frac{(\delta_B h)^2}{2}\left(\frac{\partial^2 X}{\partial \rho^2}\right)_o \qquad (7.4)$$

When these systems, (7.3)-(7.4), are solved for the first and second derivatives of X and these, in turn, are substituted for the corresponding derivatives of ϕ and ψ in (2.2), the finite difference representation of the governing system is

$$K_1 \phi_1 + K_2 \phi_B + K_3 \phi_A + K_4 \phi_4 + K_5 \phi_o = 0$$

$$K_1 \psi_1 + K_2 \psi_B + K_3 \psi_A + K_4 \psi_4 + K_5 \psi_o \qquad (7.5)$$

$$-K_1 \phi_1 - K_2 \phi_A + K_6 \phi_o = 0$$

where the K_i's are constants that must be computed for each interior node of type (1). In this instance the K_i's were

$$K_1 = \frac{2}{1 + \delta_A} \qquad (7.6)$$

$$K_2 = \frac{2\rho_o - h}{\rho_o \delta_B (1 + \delta_B)} \qquad (7.7)$$

$$K_3 = \frac{K_2}{\delta_A} \qquad (7.8)$$

$$K_4 = \frac{2\rho_o + \delta_A h}{\rho_o (1 + \delta_B)} \tag{7.9}$$

$$K_5 = \frac{h(1 - \delta_B)}{\rho_o} - \frac{2(\delta_A + \delta_B)}{\delta_A \delta_B} \tag{7.10}$$

$$K_6 = \frac{2}{\delta_A} \tag{7.11}$$

In a similar manner, finite difference expressions for the governing system for irregular interior nodes of types (2), (3), (4), and (5) may be derived. These were:

Type (2)

$$\begin{aligned} &K_1 \phi_1 + \left[1 - \frac{h}{2\rho_o}\right] \phi_2 + K_3 \phi_A + \left[1 + \frac{h}{2\rho_o}\right] \phi_4 - \left[2 + K_6\right] \phi_o = 0 \\ &K_1 \psi_1 + \left[1 - \frac{h}{2\rho_o}\right] \psi_2 + K_3 \psi_A + \left[1 + \frac{h}{2\rho_o}\right] \psi_4 \\ &\quad - \left[2 + K_6\right] \psi_o - K_1 \phi_1 - K_3 \phi_A + K_6 \phi_o = 0 \end{aligned} \tag{7.12}$$

Type (3)

$$\begin{aligned} &\phi_1 + K_2 \phi_B + \phi_3 + K_4 \phi_4 + K_7 \phi_o = 0 \\ &\psi_1 + K_2 \psi_B + \psi_3 + K_4 \psi_4 + K_7 \psi_o \\ &\quad - \phi_1 - \phi_3 + 2\phi_o = 0 \end{aligned} \tag{7.13}$$

Type (4)

$$\begin{aligned} &K_3^* \phi_c + \left[1 - \frac{h}{2\rho_o}\right] \phi_2 + K_1^* \phi_3 + \left[1 + \frac{h}{2\rho_o}\right] \phi_4 - \left[2 + K_6^*\right] \phi_o = 0 \\ &K_3^* \psi_c + \left[1 - \frac{h}{2\rho_o}\right] \psi_2 + K_1^* \psi_3 + \left[1 + \frac{h}{2\rho_o}\right] \psi_4 \\ &\quad - \left[2 + K_6^*\right] \psi_o - K_3^* \phi_c - K_1^* \phi_3 + K_6^* \phi_o = 0 \end{aligned} \tag{7.14}$$

Type (5)

$$K_3^* \phi_o + K_2 \phi_B + K_1^* \phi_3 + K_4 \phi_4 + K_5^* \phi_o = 0 \tag{7.1.}$$

$$K_3^* \psi_o + K_2 \psi_B + K_1^* \psi_3 + K_4 \psi_4 + K_5^* \psi_o$$

$$- K_1^* \phi_3 - K_3^* \phi_o + K_6^* \phi_o = 0$$

where

$$K_7 = -\frac{2}{\delta_B} - 2 + \frac{h(1 - \delta_B)}{\rho_o \delta_B} \tag{7.1}$$

K_1^* indicates that the string 0-1 has been cut by a boundary at C; therefore, A must be replaced by C and δ_A by δ_C. For a fully loaded head end and/or a partially loaded conical aft end (see Figures 57-60), similar expressions could be derived for use in computations at irregular interior nodes created by these additional curved boundaries.

b. Stresses, Strains, and Displacements

The finite difference forms of the equations used to calculate the stresses, strains, and displacements, (5.3)-(5.12), are (see Figure 56):

Regular Interior Nodes

$$(u_\rho)_o = \frac{(1+\nu)}{\rho_o}\left[\psi_o + (1-\nu)\phi_o\right] - \nu\rho_o \eta_o Z + \rho_o \delta \tag{7.1}$$

$$(u_\eta)_o = \frac{-\nu Z}{2}\left\{\left[f(\eta_o)\right]^2 - \rho_o^2\right\} - (1+\nu)\int_{\rho}^{\rho = f(\eta_o)}\left[\frac{1}{\rho}\frac{\partial \psi}{\partial \eta} - \frac{(1-\nu)}{\rho}\frac{\partial \phi}{\partial \eta}\right] d\rho \tag{7.1}$$

$$(\varepsilon_\rho)_o = \frac{(1+\nu)}{2h\rho_o^2}\left\{\rho_o(\psi_2 - \psi_4) + \rho_o(1-\nu)(\phi_2 - \phi_4)\right. \tag{7.1}$$

$$\left. - 2h\left[\psi_o + (1-\nu)\phi_o\right]\right\} - \nu\eta_o Z + \delta$$

$$(\varepsilon_\theta)_o = \frac{(1+\nu)}{\rho_o^2}\left[\psi_o + (1-\nu)\phi_o\right] - \nu\eta_o Z + \delta \tag{7.1}$$

A-6597

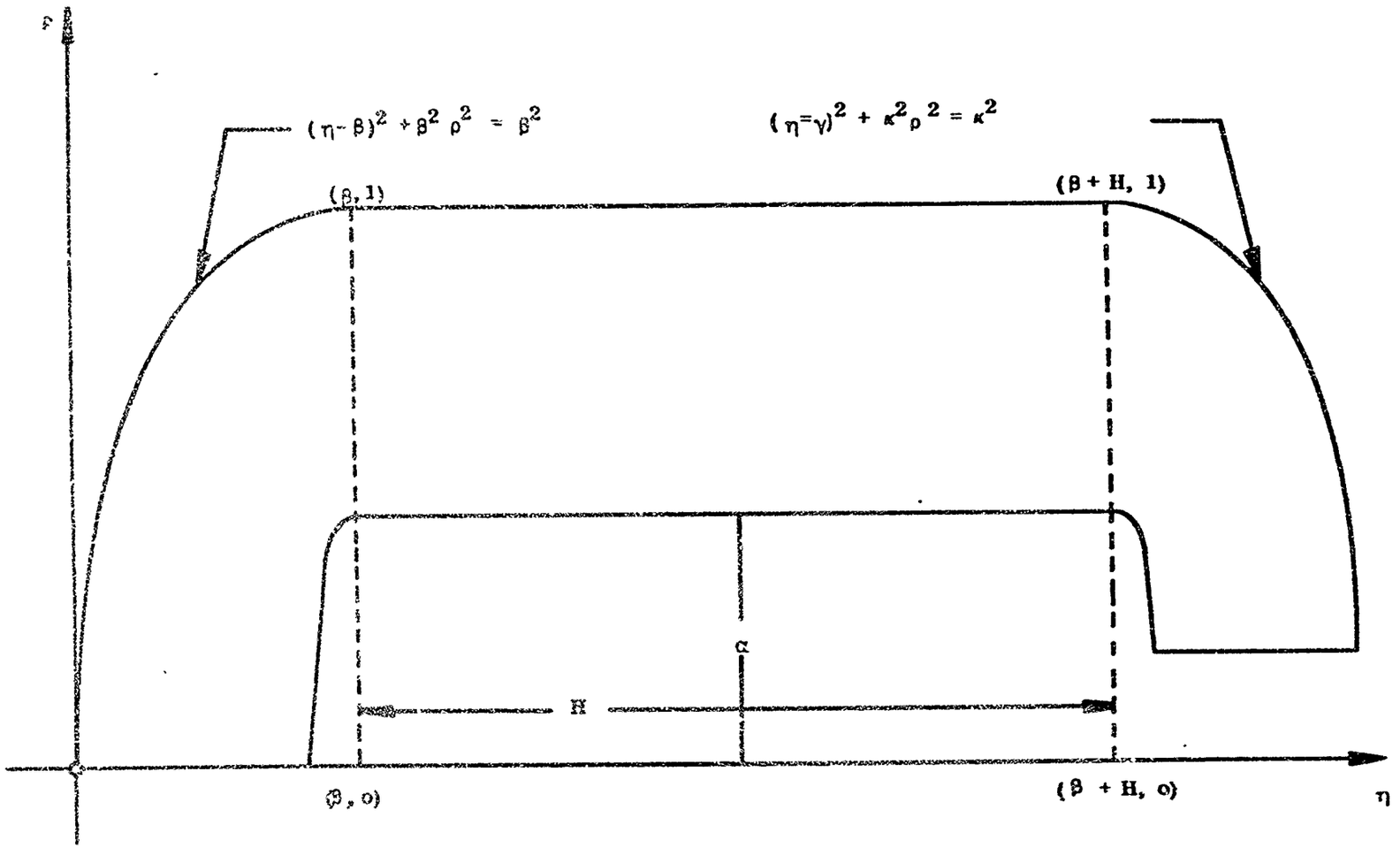

FIGURE 57. CYLINDRICAL GRAIN WITH FULLY LOADED HEAD END AND CONICAL AFT END

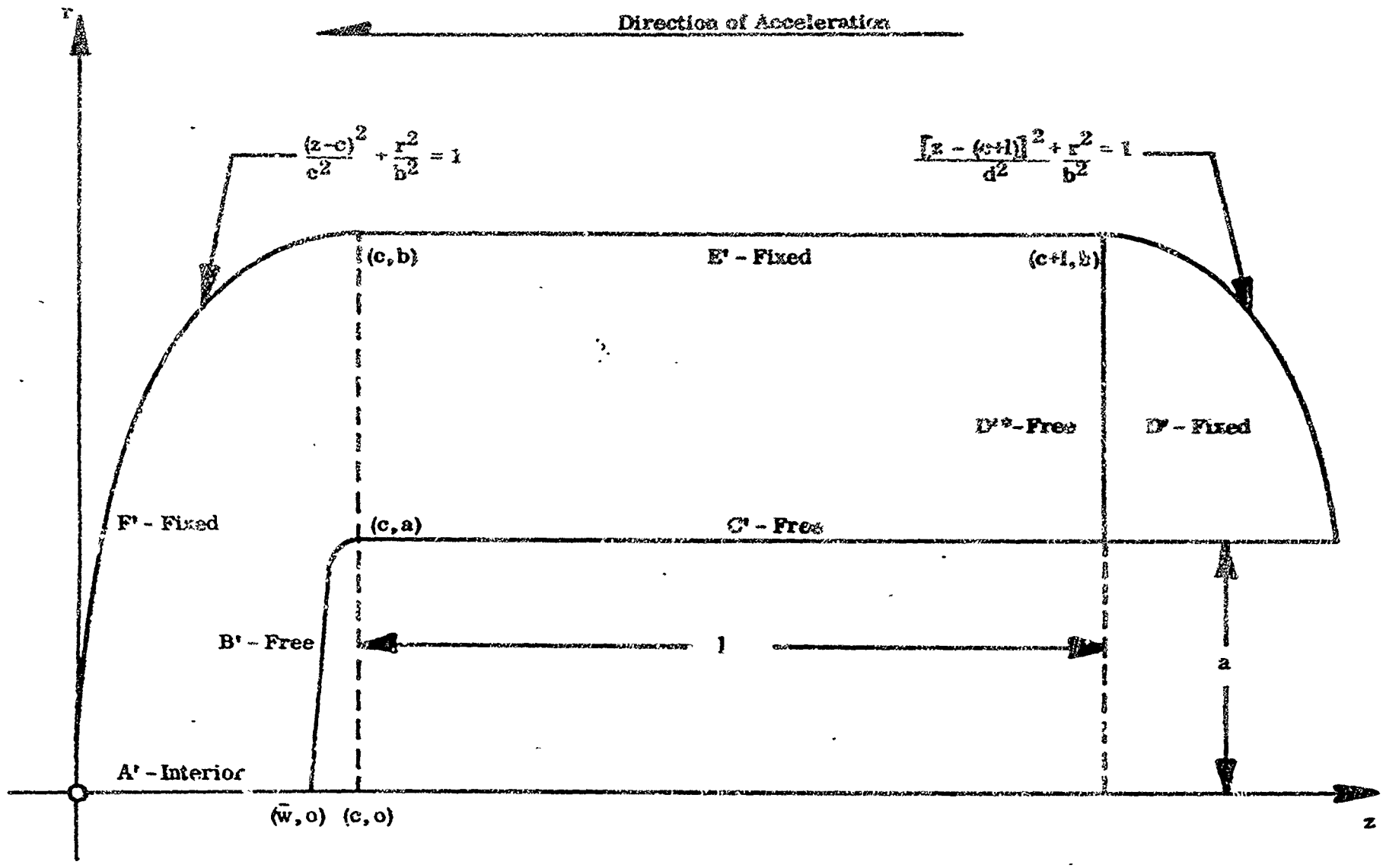

FIGURE 58. AXIAL CROSS SECTION OF FULLY LOADED CYLINDRICAL GRAIN WITH ARBITRARY HEAD AND AFT END

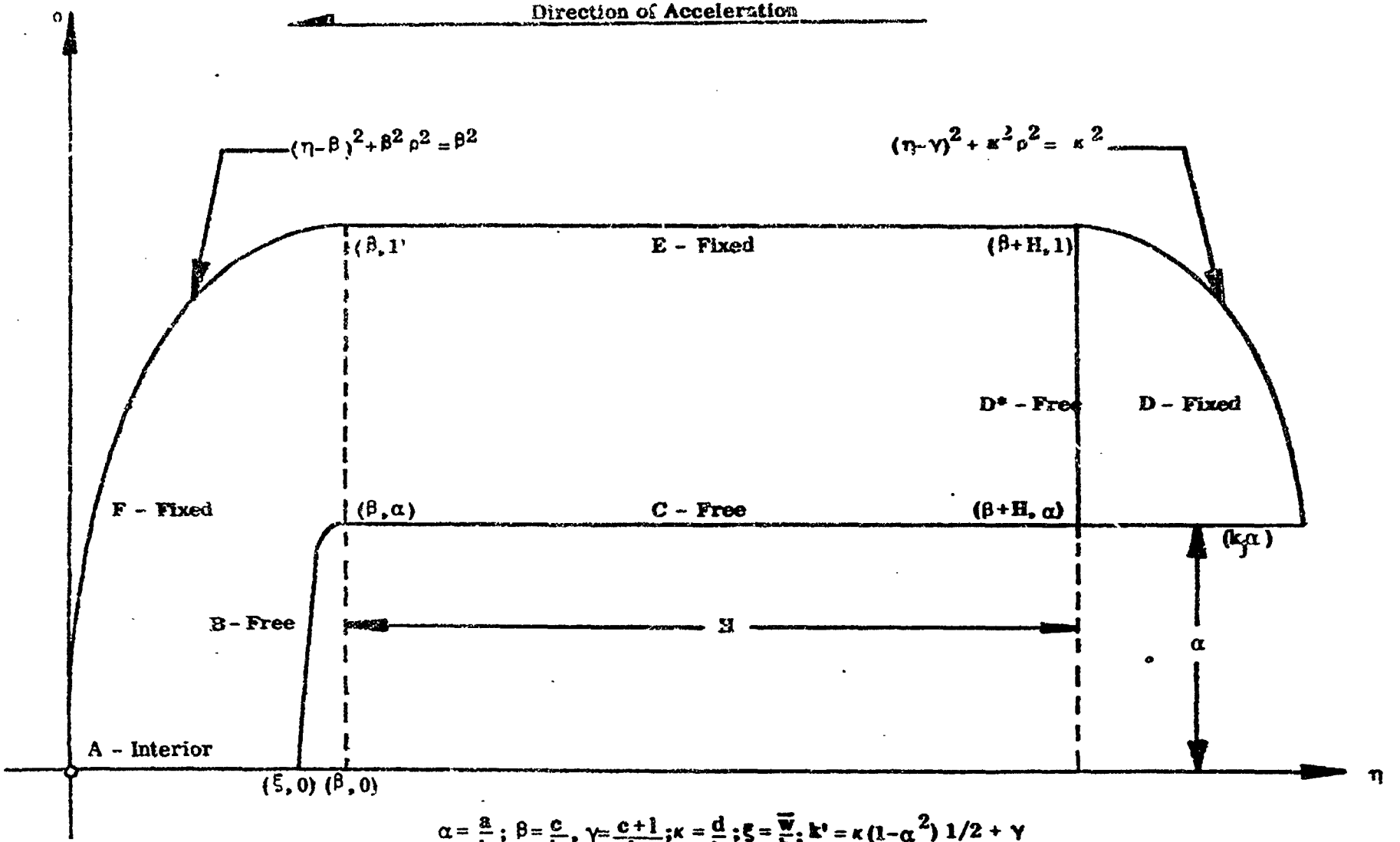

$$\alpha=\frac{a}{b};\ \beta=\frac{c}{b},\ \gamma=\frac{c+1}{b};\kappa=\frac{d}{b};\xi=\frac{\bar{w}}{b};\ k'=\kappa(1-\alpha^2)\,1/2+\gamma$$

FIGURE 59. NONDIMENSIONAL COORDINATE SYSTEM

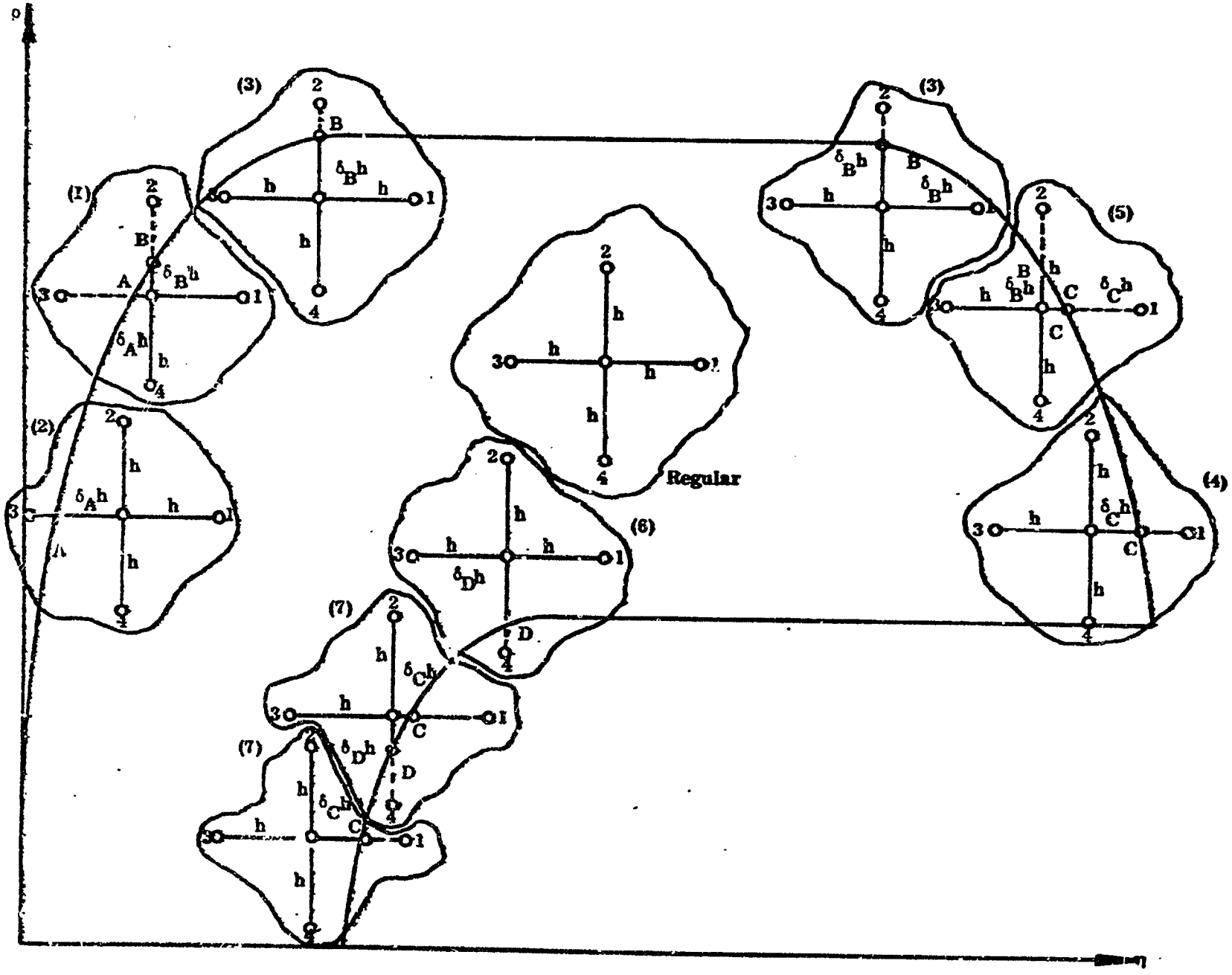

FIGURE 60. IRREGULAR INTERIOR NODES

$$(\epsilon_\eta)_o = -\frac{(1+\nu)}{2h\rho_o}\left[\psi_2 - \psi_4 + \nu(\phi_2 - \phi_4)\right] + \eta_o z + \delta \tag{7.21}$$

$$(\sigma_\rho)_o = \frac{1}{2h\rho_o}\left[\phi_2 - \phi_4 + \psi_2 - \psi_4\right] - \frac{1}{\rho_o^2}\left[\psi_o + (1-\nu)\phi_o\right] \tag{7.22}$$

$$(\sigma_\theta)_o = \frac{\nu}{2h\rho_o}\left[\phi_2 - \phi_4\right] + \frac{1}{\rho_o^2}\left[\psi_o + (1-\nu)\phi_o\right] \tag{7.23}$$

$$(\sigma_\eta)_o = -\frac{1}{2h\rho_o}\left[\psi_2 - \psi_4\right] + \eta_o z \tag{7.24}$$

$$(\tau_{\rho\eta})_o = \frac{1}{2h\rho_o}\left[\psi_1 - \psi_3\right] \tag{7.25}$$

$$(\gamma_{\rho\eta})_o = \frac{2(1+\nu)}{h\rho_o}\left[\psi_1 - \psi_3\right] \tag{7.26}$$

c. Boundary Conditions

In addition to satisfying the governing differential system at each point in the interior, the stress functions must also be compatible with the boundary conditions (see IV-B-2) imposed by the loading and particular geometry being considered. The finite difference form of these constraints may be expressed as:

Side A ($\rho = \alpha$)

The constraints that all considered loadings place on the stress function on this boundary are summarized by two relations:

$$\phi_2 + \psi_2 - \left\{1 + (1-\nu)\frac{h}{\alpha}\left[1 + \frac{h}{2\alpha}\right]\right\}\phi_o + h\alpha\pi_1\left[1 + \frac{h}{2\alpha}\right] = 0 \tag{7.27}$$

$$\psi_o = 0 \tag{7.28}$$

This finite difference form of the boundary conditions for Side A and those for Sides B* and D*, below, are the same as those given by Parr[16] for the free boundaries of the flat-end cylinders that he studied.

Side B $\left[\rho = f_1(\eta)\right]$

On this fixed boundary the displacements are identically zero; and, using (6.6) and (7.17), one condition that the stress functions must satisfy is

$$\frac{(1+\nu)}{\rho_o}\left[\psi_o + (1-\nu)\,\phi_o\right] - \nu\rho_o\,\eta_o\,Z + \rho_o\,\delta = 0 \qquad (7.29$$

When applied to (7.18), the second boundary condition, (6 7), does not present a form that is very tractable from a numerical analysis standpoint. However, since u_η is invariant with respect to arc length on this boundary,

$$\frac{\partial u_\eta}{\partial s} = 0 \qquad (7.30$$

but

$$\frac{\partial u_\eta}{\partial s} = \frac{\partial u_\eta}{\partial \eta}\,\frac{d\eta}{ds} + \frac{\partial u_\eta}{\partial \rho}\,\frac{d\rho}{ds} \qquad (7.31$$

Hence, using (7.30) and (7.31)

$$\frac{\partial u_\eta}{\partial \eta} = -\frac{\partial u_\eta}{\partial \rho}\,\frac{d\rho}{d\eta} \qquad (7.32$$

now

$$\frac{\partial u_\eta}{\partial \eta} = \varepsilon_\eta = -\frac{(1+\nu)}{\rho}\left[\frac{\partial \psi}{\partial \rho} + \nu\frac{\partial \phi}{\partial \rho}\right] + \eta Z + \varepsilon \qquad (7.33$$

$$\frac{\partial u_\eta}{\partial \rho} = \gamma_{\rho\eta} - \frac{\partial u_\rho}{\partial \eta} \qquad (7.34$$

$$\gamma_{\rho\eta} = \frac{2(1+\nu)}{\rho}\,\frac{\partial \psi}{\partial \eta} \qquad (7.35$$

and

$$\frac{\partial u_\rho}{\varepsilon\,\eta} = \frac{(1+\nu)}{\rho}\left[\frac{\partial \psi}{\partial \eta} + (1-\nu)\,\frac{\partial \phi}{\partial \eta}\right] - \nu\rho Z \tag{7.36}$$

On this boundary

$$\frac{d\rho}{d\eta} = \frac{\gamma-\eta}{\kappa^2\rho} \tag{7.37}$$

By applying (7.33)-(7.37) to (7.34), a more tractable boundary condition is obtained; namely,

$$\frac{\partial \psi}{\partial \rho} + \nu\frac{\partial \phi}{\partial \rho} - \left\{\frac{\varepsilon \psi}{\partial \eta} - (1-\nu)\,\frac{\partial \phi}{\partial \eta}\right\}\cdot\frac{\gamma-\eta}{\kappa^2\rho}$$
$$- \frac{\rho Z}{\kappa^2(1+\nu)}\left[\kappa^2\eta + \nu(\gamma-\eta)\right] - \frac{\rho\delta}{1+\nu} = 0 \tag{7.38}$$

Using backward differences, in finite difference form (7.38) may be expressed as

$$\delta_{Ch}\left[\psi_o - \psi_4 + \nu(\phi_o - \phi_4)\right]$$
$$- \delta_{Bh}\left[\psi_o - \psi_3 + (\nu-1)\left\{\phi_o - \phi_3\right\}\right]\frac{(\gamma-\eta_o)}{\kappa^2\rho_o} \tag{7.39}$$
$$- \frac{\delta_{Bh}\,\delta_{Ch}\,\rho_o Z}{\kappa^2(1+\nu)}\left[\kappa^2\eta_o + \nu(\gamma-\eta_o)\right] - \frac{\delta_{Bh}\,\delta_{Ch}}{1+\nu} = 0$$

The equations (7.29) and (7.39) are the most useful form of finite difference relations that can be formulated for Side B.

Side B* ($\eta = \beta + H$)

$$\frac{h}{2\rho_o}(\phi_4 - \phi_2) + \phi_2 + \phi_4 - 2\phi_o + 2\psi_3 - 2\psi_o = 0 \tag{7.40}$$

$$\psi_o = \left[\frac{\rho_o^2 - \alpha^2}{2}\right]\left[\pi_2 + (\beta + H)\,Z\right] \tag{7.41}$$

Side C ($\rho = 1$)

Since $u_\rho = 0$ on this fixed boundary, the first relation that the stress functions must satisfy (see 7.29) is

$$\psi_o + (1 - \nu)\,\phi_o - \frac{\nu \eta_o Z}{1+\nu} + \frac{\delta}{1+\nu} = 0 \qquad (7.42)$$

u_η is also identically zero on this boundary; and the fact that axial displacement is invariant with respect to η here implies that ϵ_η is also zero. Thus, after (7.1) is used to eliminate the fictitious values ϕ_2, ψ_2 in (7.21), the second condition that the stress functions must satisfy is

$$\psi_1 + \psi_3 + \psi_4 - \left[\frac{3-4\nu}{1-\nu}\right]\psi_o + \nu\phi_4 + \frac{\delta}{1+\nu}\left\{\frac{\nu}{1-\nu} + \frac{h}{2}\left[2-h\right]\right\} + \frac{\eta_o Z}{1+\nu}\left\{\frac{h}{2}\left[2-h\right] - \frac{\nu^2}{1-\nu}\right\} = 0 \qquad (7.43)$$

Side D $\rho = f_2(\eta)$

The Side D displacements are zero, as on Side B; therefore, after the geometric terms are replaced by those of Side D and subscript 1 is substituted for the subscript 2, the boundary conditions (see 7.29 and 7.39) are:

$$\frac{(1+\nu)}{\rho_o}\left[\psi_o + (1-\nu)\,\phi_o\right] - \nu\rho_o\,\eta_o Z + \rho_o\delta = 0 \qquad (7.44)$$

$$\delta_A h\left[\psi_o - \psi_4 + \nu(\phi_o - \phi_4)\right] - \delta_B h\left[\psi_o - \psi_1 + (\nu-1)\left\{\phi_o - \phi_1\right\}\right]\cdot\frac{(\beta - \eta_o)}{\beta^2\,\rho_o} - \frac{\delta_A h\;\delta_B h\;\rho_o Z}{\kappa^2\,(1+\nu)}\left[\kappa^2\,\eta_o + \nu(\beta - \eta_o)\right] - \frac{\delta_A h\;\delta_B h}{1+\nu}\,\delta = 0 \qquad (7.45)$$

Side D* $\eta = \theta = 0$

Fixed End Conditions:

Equation (5.28), when coupled with (7.17), gives the first condition

$$\frac{(1+\nu)}{\rho_o} \psi_o + (1-\nu)\,\phi_o + \rho_o\,\delta = 0 \tag{7.46}$$

Since u_η is invariant with respect to ρ on this boundary

$$\frac{\partial u_\eta}{\partial \rho} = 0 \tag{7.47}$$

Now the strain-displacement equation that relates the shearing strain $\gamma_{\rho\eta}$ and the displacements u_ρ and u_η is given by

$$\gamma_{\rho\eta} = \frac{\partial u_\rho}{\partial \eta} + \frac{\partial u_\eta}{\partial \rho} \tag{7.48}$$

When (7.47), (5.3), and (5.12) are employed and the fictitious nodes ϕ_3, ψ_3 are eliminated by using (7.1), the second boundary condition takes the form

$$\phi_1 - 2\phi_o - 2\psi_1 + (1-2\nu)\left[\phi_1 + \phi_2 + \phi_4 - 4\phi_o + \frac{h}{2\rho_o}(\phi_4 - \phi_2)\right] - \frac{2\rho_o^2}{1+\nu}\left[\delta + \nu h Z\right] = 0 \tag{7.49}$$

Free End Conditions:

When (5.10) is integrated along this boundary, ψ is known at each nodal point and for all loadings on this boundary is given by

$$\psi_o = \frac{(\rho_o^2 - \alpha^2)}{2}\,\pi_3 \tag{7.50}$$

From equations (6.21) and (7.25):

$$\psi_1 - \psi_3 = 0 \tag{7.51}$$

The result of eliminating ψ_3, using (7.1), is

$$\frac{h}{2\rho_o}(\phi_4 - \phi_2) + \phi_2 + \phi_4 - 2\phi_o + 2\psi_1 - 2\psi_o = 0 \qquad (7.52$$

The relations (7.50) and (7.52) are the most useful forms of the boundary conditions for D* when this side is unconstrained.

Corner Nodes

At adjoining boundaries the satisfaction of the boundary conditions defined above consists mainly of algebraic manipulations of these equations. A complete list is given below.

$$\left[\eta = \beta + H,\ \rho = \alpha\right] \qquad (7.53)$$

$$\psi_o = 0$$

$$\phi_2 - \left\{1 + (1-\nu)\ \frac{h}{\alpha}\left[1 + \frac{h}{2\alpha}\right]\right\}\phi_o + h\left[\frac{2\alpha + h}{2}\right]\left[\pi_2 + (\beta + H)\,Z\right] + h\alpha\left[1 + \frac{h}{2\alpha}\right]\pi_1 = 0 \qquad (7.54)$$

$$\left[\eta = k',\ \rho = \alpha\right]$$

$$\psi_o = 0 \qquad (7.55$$

$$\phi_o = \frac{\alpha^2}{1-\nu^2}\left[\nu k' Z - \delta\right] \qquad (7.56$$

$$\left[\eta = \beta + H,\ \rho = 1,\ \kappa = 0\right]$$

$$\psi_o = \left[\frac{1-\alpha^2}{2}\right]\left[\pi_2 + (\beta + H)\,Z\right] \qquad (7.57$$

$$\phi_o = \frac{1}{1-\nu^2}\left[\nu(\beta + H)\,Z + \kappa' - \frac{(1-\alpha^2)}{2(1-\nu)}\left[\pi_2 + (\beta + H)\,Z\right]\right] \qquad (7.58$$

$$\left[\eta = \beta + H,\ \rho = 1,\ \kappa \neq 0\right]$$

$$\psi_1 + \psi_2 + \psi_4 - \frac{3 - 4\nu}{1 - \nu}\ \psi_o + \nu\phi_4 \tag{7.59}$$

$$+ \frac{\delta}{1+\nu}\ \frac{\nu}{1+\nu} + \frac{h}{2}\ 2 - h + \frac{(\beta + H)\ Z}{1+\nu}\ \frac{h}{2}\ 2 - h - \frac{\nu^2}{1-\nu} = 0$$

$$\phi_o = \frac{1}{1-\nu^2}\ \nu(\beta + H)\ Z - \delta - \frac{\psi_o}{1-\nu} \tag{7.60}$$

Fixed End Condition:

$$\phi_1 - 2\,\phi_o - 2\,\psi_1 + (1 - 2\nu)\ \phi_1 + \phi_2 + \phi_4 \tag{7.61}$$

$$- 4\,\phi_o + \frac{h}{2}\ (\phi_4 - \phi_2) - \frac{2}{1+\nu}\ \delta + \nu h\ Z \quad = 0$$

$$\phi_o = - \frac{1}{1-\nu}\ \frac{\delta}{1+\nu} + \psi_o \tag{7.62}$$

Free End Condition:

$$\eta = \frac{(1 - \alpha^2)}{2}\ \pi_3 \tag{7.63}$$

$$\frac{h}{2}\ (\phi_4 - \phi_2) + \phi_2 + \phi_4 - 2\,\phi_o + 2\,\psi_1 - 2\ \psi_o \quad = 0 \tag{7.64}$$

$$\eta = \delta\ ,\ \rho = 1, \beta \neq o$$

$$\psi_1 + \psi_3 + \psi_4 - \frac{3 - 4\nu}{1 - \nu}\ \psi_o + \nu\phi_4 \tag{7.65}$$

$$+ \frac{\delta}{1+\nu}\ \frac{\nu}{1-\nu} + \frac{h}{2}\ 2 - h + \frac{\beta Z}{1+\nu}\ \frac{h}{2}\ 2 - h - \frac{\nu^2}{1-\nu} = 0$$

$$\phi_o = \frac{1}{1-\nu}\ \nu\beta Z - \delta - \frac{\psi_o}{1-\nu} \tag{7.66}$$

$$\eta = k,\ \rho = \alpha$$

$$\psi_o = 0 \tag{7.67}$$

$$\phi_o = \frac{\alpha^2}{1-\nu^2}\ \nu k\ Z - \delta \tag{7.68}$$

$$\left[\eta = 0,\ \rho = \alpha\right] \tag{7.69}$$

Free End Conditions:

$$\psi_o = 0 \tag{7.70}$$

$$\phi_2 - \left\{1 + (1 - \nu)\ \frac{h}{\alpha}\left[1 + \frac{h}{2\alpha}\right]\right\}\phi_o + h\left[\frac{2\alpha + h}{2}\right]\pi_2 + h\left[\frac{2\alpha + h}{2}\right]\pi_1 = 0 \tag{7.71}$$

Fixed End Condition:

$$\psi_o = 0 \tag{7.72}$$

$$\phi_o = -\ \frac{\alpha^2}{1 - \nu^2}\ \delta \tag{7.73}$$

5. Calculation of Stresses, Strains, and Displacements

(7.17) - (7.26) are the equations used to calculate the stresses, strains, and displacements at regular interior points. The equations used to calculate these quantities at other than regular interior points are listed below.

Irregular Interior Nodes

Since the finite difference relations used to calculate u_ρ and ϵ_θ remain the same for all nodes, they are not specified under the different types below. Also, since several of the relations (7.17)-(7.26) involve derivatives with respect to only one spacial coordinate, the absence of a representation for a stress or strain for any one type of interior point listed below will serve to indicate that the corresponding relation (7.17)-(7.26) is to be used.

Type 1

$$(\epsilon_\rho)_o = \frac{(1+\nu)}{h\rho_o}\left\{\frac{\psi_B}{\delta_B(1+\delta_B)} - \frac{\delta_B\,\psi_4}{1+\delta_B} - \frac{(1-\delta_B)}{\delta_B}\,\psi_o\right.$$

$$+ (1-\nu)\left[\frac{\beta_B}{\delta_B(1+\delta_B)} - \frac{\delta_B}{1+\delta_B}\,\beta_4 - \frac{(1-\delta_B)}{\delta_B}\,\beta_o\right]$$

$$\left. - \frac{h}{\rho_o}\left[\psi_o + (1-\nu)\,\beta_o\right]\right\} - \nu\,\eta_o\,Z + \delta \qquad (8.1)$$

$$(\epsilon_\eta)_o = -\frac{(1+\nu)}{h\rho_o}\left\{\frac{\psi_B}{\delta_B(1+\delta_B)} - \frac{\delta_B}{1+\delta_B}\,\psi_4\right.$$

$$- \frac{(1-\delta_B)}{\delta_B}\,\psi_o + \nu\left[\frac{\beta_B}{\delta_B(1+\delta_B)} - \frac{\delta_B}{1+\delta_B}\,\beta_4\right.$$

$$\left.\left. - \frac{(1-\delta_B)}{\delta_B}\,\beta_o\right]\right\} + \eta_o\,Z + \delta \qquad (8.2)$$

$$(\sigma_\rho)_o = \frac{1}{h\rho_o}\left[\frac{(\beta_B + \psi_B)}{\delta_B(1+\delta_B)} - \frac{\delta_B}{1+\delta_B}\,(\beta_4 + \psi_4)\right.$$

$$\left. - \frac{(1-\delta_B)}{\delta_B}\,(\beta_o + \psi_o)\right] - \frac{1}{\rho_o^2}\left[\psi_o + (1-\nu)\,\beta_o\right] \qquad (8.3)$$

$$(\sigma_\theta)_o = \frac{\nu}{h\rho_o}\left[\frac{\beta_B}{\delta_B(1+\delta_B)} - \frac{\delta_B}{1+\delta_B}\,\beta_4\right.$$

$$\left. - \frac{(1-\delta_B)}{\delta_B}\,\beta_o\right] + \frac{1}{\rho_o^2}\left[\psi_o + (1-\nu)\,\beta_o\right] \qquad (8.4)$$

$$(\sigma_\eta)_o = -\frac{1}{h\rho_o}\left[\frac{\psi_B}{\delta_B(1+\delta_B)} - \frac{\delta_B}{1+\delta_B}\,\psi_4 - \frac{(1-\delta_B)}{\delta_B}\,\psi_o\right] + \eta_o\,Z \qquad (8.5)$$

$$(\tau_{\rho\eta})_o = \frac{1}{h\rho_o}\left[\frac{\delta_A}{1+\delta_A}\,\psi_1 - \frac{\psi_A}{\delta_A(1+\delta_A)} + \frac{(1-\delta_A)\,\psi_o}{\delta_A}\right] \qquad (8.6)$$

$$(\gamma_{\rho\eta})_o = \frac{2(1+\nu)}{h\rho_o}\left[\frac{\delta_A}{1+\delta_A}\,\psi_1 - \frac{\psi_A}{\delta_A(1+\delta_A)} + \frac{(1-\delta_A)}{\delta_A}\,\psi_o\right] \qquad (8.7)$$

Type (2)

$(\tau_{\rho\eta})_o$ - Same as (8.6) (8.8)

$(\gamma_{\rho\eta})_o$ - Same as (8.7) (8.9)

Type (3)

$(\epsilon_\rho)_o$ - Same as (8.1) (8.10)

$(\epsilon_\eta)_o$ - Same as (8.2) (8.11)

$(\sigma_\rho)_o$ - Same as (8.3) (8.12)

$(\sigma_\theta)_o$ - Same as (8.4) (8.13)

$(\sigma_\eta)_o$ - Same as (8.5) (8.14)

Type (4)

$$(\tau_{\rho\eta})_o = \frac{1}{h\rho_o}\left[\frac{\psi_C}{\delta_C(1+\delta_C)} - \frac{\delta_C\ \psi_3}{1+\delta_C} - \frac{(1-\delta_C)}{\delta_C}\ \psi_o\right] \quad (8.15)$$

$$(\gamma_{\rho\eta})_o = \frac{2(1+\nu)}{h\rho_o}\left[\frac{\psi_C}{\delta_C(1+\delta_C)} - \frac{\delta_C}{1+\delta_C} - \frac{(1-\delta_C)}{\delta_C}\ \psi_o\right] \quad (8.16)$$

Type (5)

The equations used to calculate the normal stresses (σ_ρ, σ_θ, σ_η) and normal strains (ϵ_ρ, ϵ_θ, ϵ_η) are the same as those of Type (1) with δ_C replacing δ_A. The equations used to calculate the shearing stress, $\tau_{\rho\eta}$, and the shearing strain, $\gamma_{\rho\eta}$, are equations (8.15) and (8.16), respectively.

6. Method of Numerical Solution

If the finite difference equations that govern the elastic state of the propellant grain are written for each node, the values of the stress functions at each nodal point and, hence, the dimensionless stresses, strains, and displacements at

each nodal point may be obtained from the simultaneous solution of the resulting set of linear equations and the subsequent employment of equations (7.17)-(7.26) and (8.1)-(8.16). For realistic propellant grains, this system may consist of as many as 2500 equations. Although the solution of such a large linear system presents certain difficulties, there are a number of methods by which the solution may be obtained accurately and economically. A two-variable relaxation routine, which has been used extensively in the past by Southwell[18] and Allen,[20] was used in the digital program based upon the analysis described above. The method is fundamentally point iterative and fairly versatile in handling the large linear systems common to axisymmetric stress problems.

Basically, the values of the stress functions at each nodal point must be obtained from a matrix equation of the form

$$\left[C_{i,j}\right] \cdot \left[X_i\right] = \left[R_i\right] \qquad (i = 1, n)\ (j = 1, n) \tag{9.1}$$

where $C_{i,j}$ is the coefficient matrix, $\left[X_i\right]$ is the solution vector with entries $\phi_{i,j}$, $\Psi_{i,j}$ and $\left[R_i\right]$ is the constant or residual vector.

Initially, all entries in the solution vector are set equal to zero. New trial values for the stress functions $\phi_{i,j}$, $\Psi_{i,j}$, at a nodal point $P_{i,j}$ for the (n + 1) iteration are obtained from the formulas

$$\phi_{i,j}^{(n+1)} = \phi_{i,j}^{(n)} + \beta_1 F_{i,j}^{(n)} \tag{9.2}$$

$$\Psi_{i,j}^{(n+1)} = \Psi_{i,j}^{(n)} + \beta_2 G_{i,j}^{(n)}$$

and

$$\phi_{i,j}^{(n+1)} = \phi_{i,j}^{(n)} + \beta_3 F_{i,j}^{(n)} \tag{9.3}$$

$$\psi_{i,j}^{(n+1)} = \psi_{i,j}^{(n)} + \beta_4 G_{i,j}^{(n)}$$

where (9.2) and (9.3) are used for nodal points in the interior and on the boundary, respectively. $F_{i,j}^{(n)}$, $G_{i,j}^{(n)}$ are the residuals obtained by evaluating the governing finite difference relations at $P_{i,j}$ using values of the stress functions $\phi_{i,j}^{(n)}$, $\psi_{i,j}^{(n)}$ from the n^{th} iteration. The β_i are relaxation factors, which, in general, range over $[1, 2)$. For a particular geometry, the convergence of the iterative process is a strong function of ν and the values of β_i that are chosen. As ν decreases in value from 0.5 (incompressible propellant material as measured by Poisson's ratio), the number of iterations needed for convergence decreases. Values of ≈ 1.7 are near optimum for relaxing the interior,[16, 19] while β_3 and β_4 usually vary with the geometry.

The solution, for a given mesh size h, is assumed to be "good" when the absolute value of all residuals is less than a specified number ξ:

$$\left| F_{i,j} \right| < \xi \ , \left| G_{i,j} \right| < \xi \tag{9.4}$$

The value of ξ indicates the degree of accuracy of the solution for a given mesh size. As is common to most iterative methods, the time involved in solving any given problem will be proportional to the accuracy desired.

A description of the complete program and comments on its versatility are presented in subsection 7 below.

7. Description of Computer Program Stress Analysis of Axisymmetric Grain Designs Having Arbitrary End Geometries and Straight-Through Ports

The block diagram in Figure 61 illustrates the digital computer program developed to analyze structural problems in axisymmetric grain designs having arbitrary end geometries and straight-through ports. Although the existing program is not capable of accounting for the addition of a head-end web, with minor modifications it can be readily adapted to handle such configurations for loadings by internal pressure, thermal shrinkage, and axial acceleration. A description of the essential features of the computer program (input, calculations, output) is given below.

Basically, three separate routines comprise the main program:

1) Finite difference input grid generator

2) Relaxation routine

3) Stress-strain-displacement routine

The input grid generator (see Figure 61) specifies the spacial coordinates of all nodal points in the interior and on the boundary. The generator also classifies, by type, both boundary and interior nodes. Since the method of solution is fundamentally point iterative, the generator has also been written so that it specifies the iteration indices upon which the relaxation routine is based.

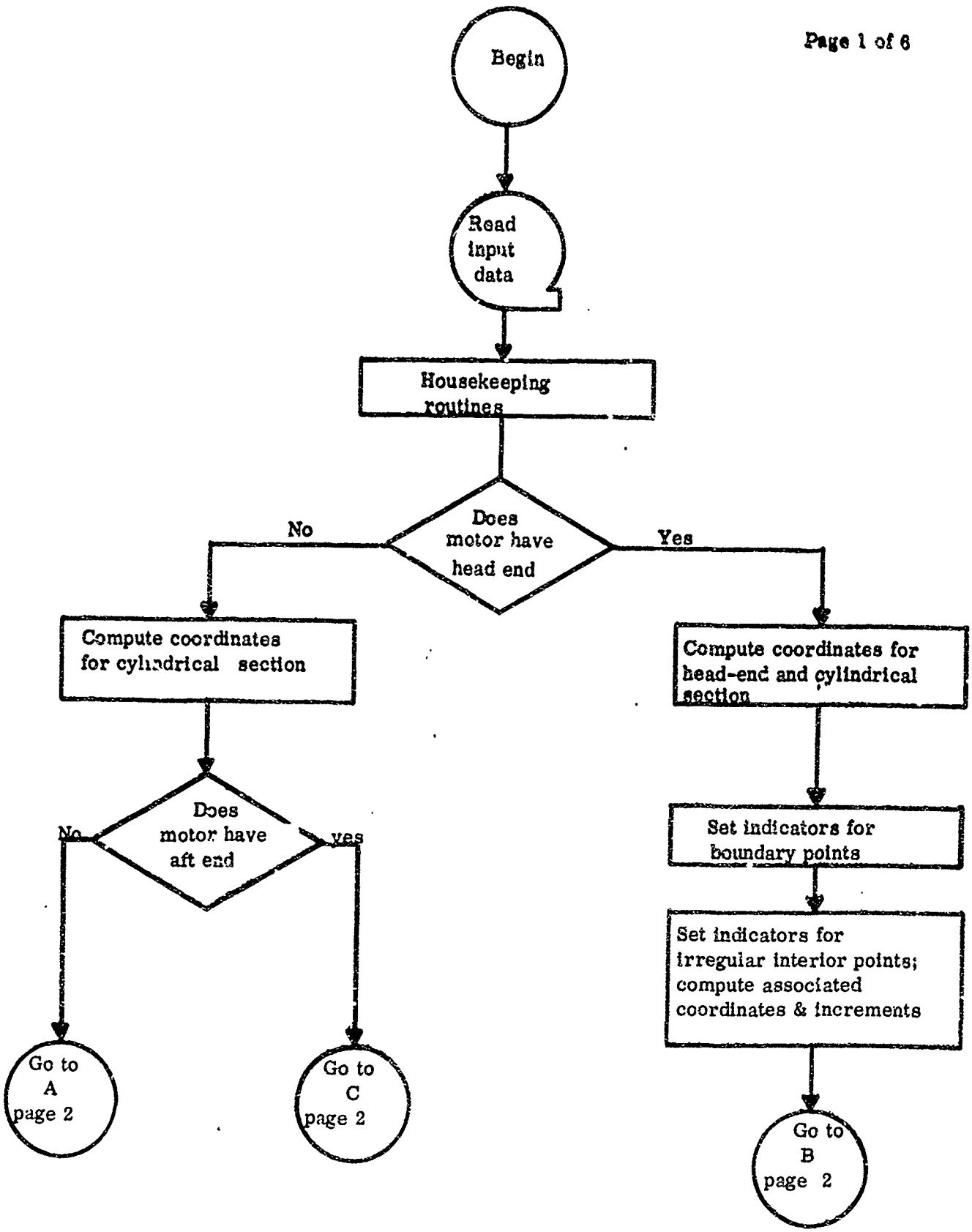

FIGURE 61. BLOCK DIAGRAM - STRESS ANALYSIS OF AXISYMMETRIC GRAIN DESIGNS HAVING ARBITRARY END GEOMETRIES AND STRAIGHT-THROUGH PORTS

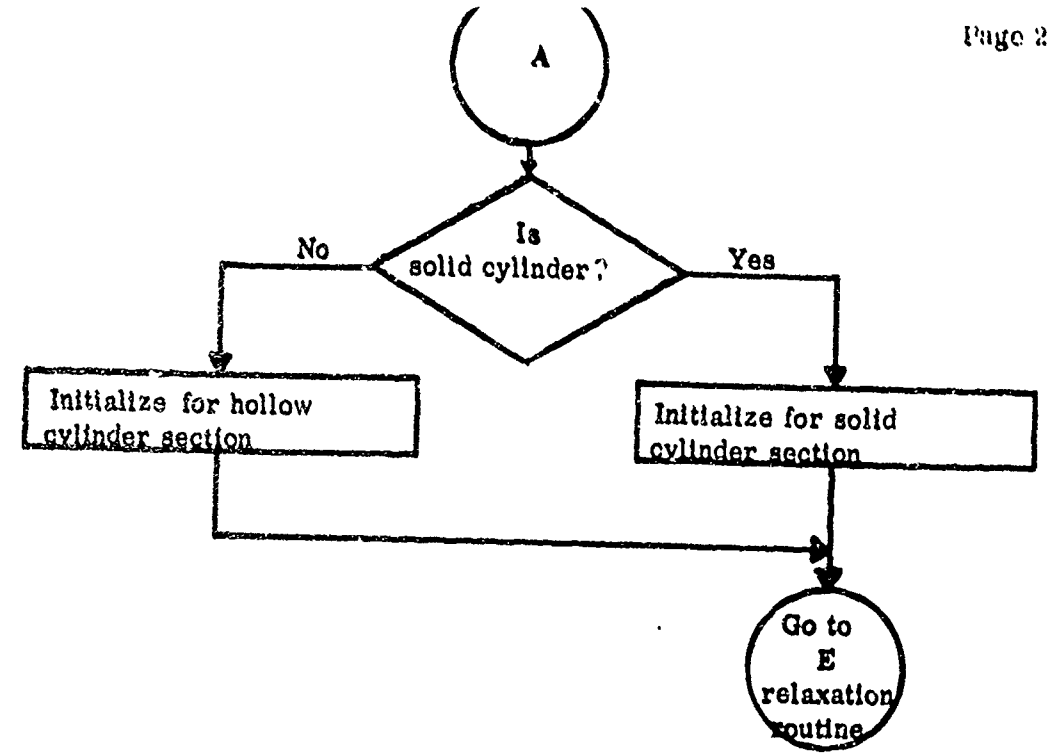

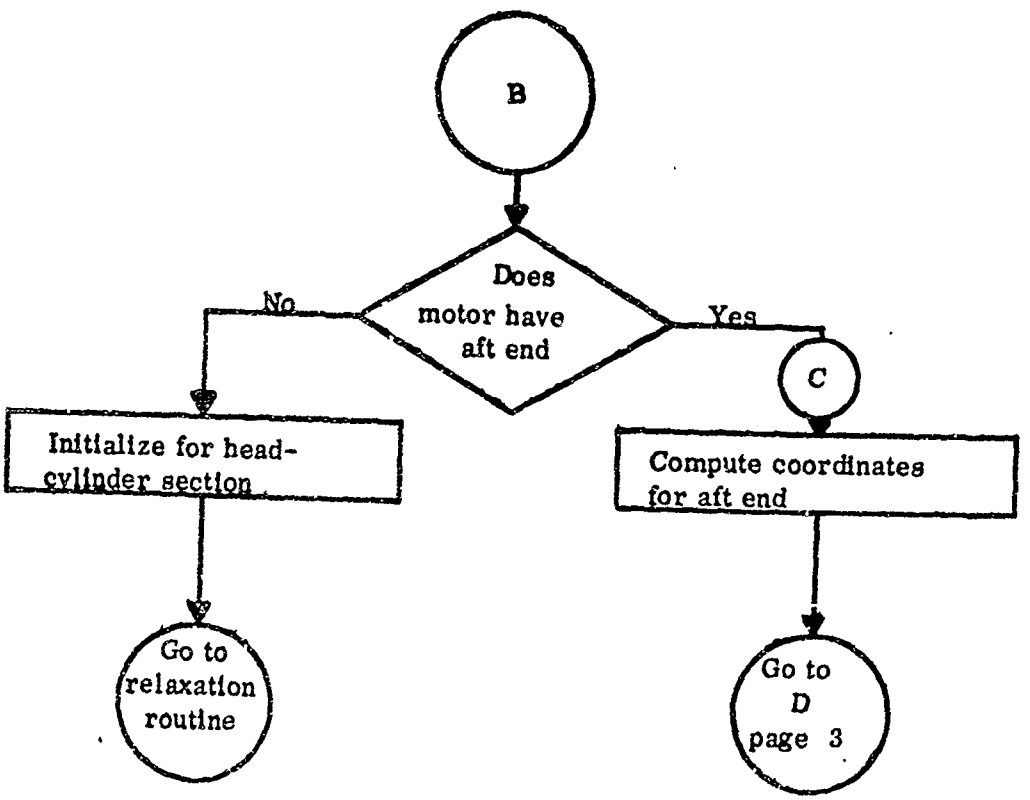

FIGURE 61. CONTINUED

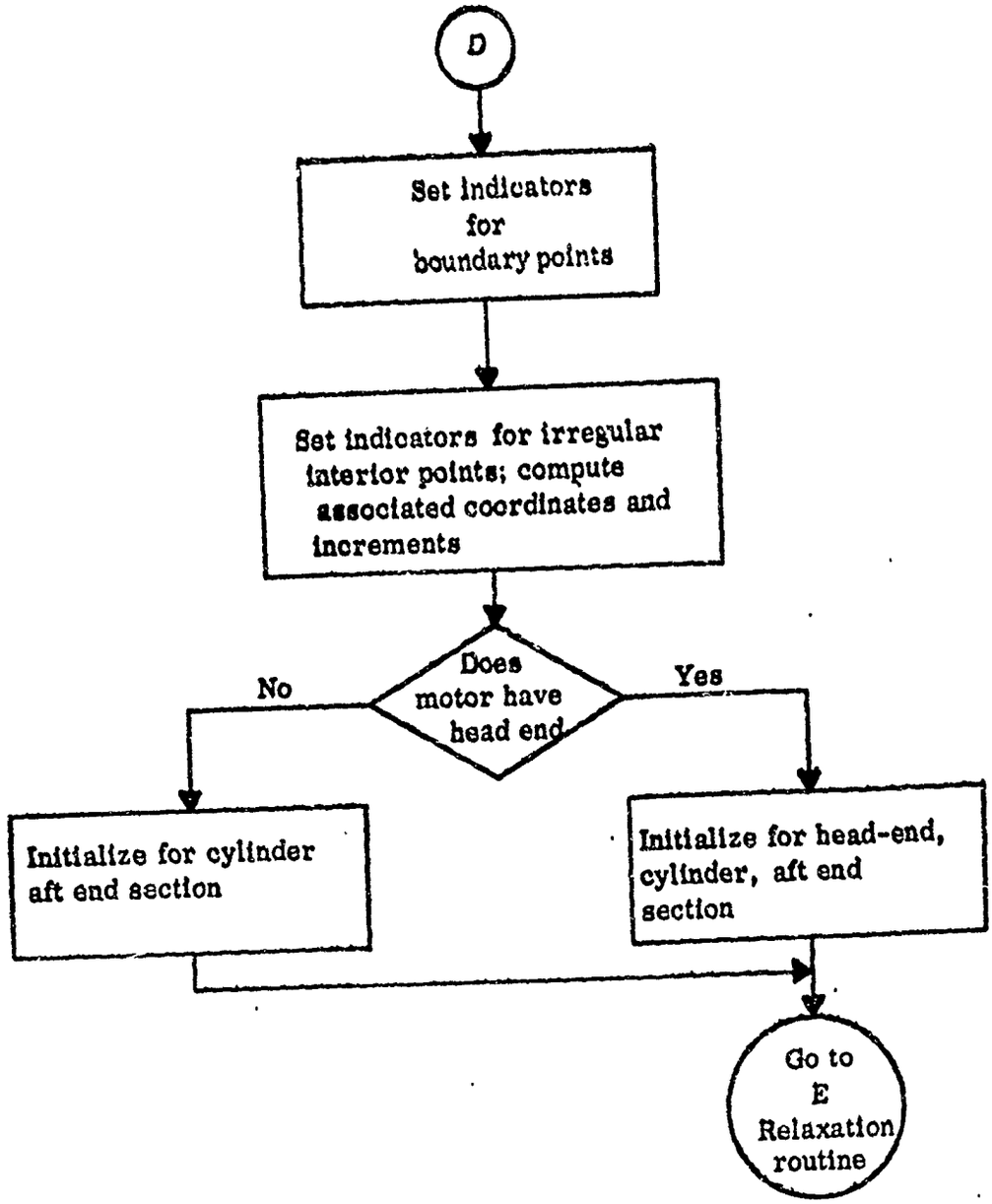

FIGURE 61. CONTINUED

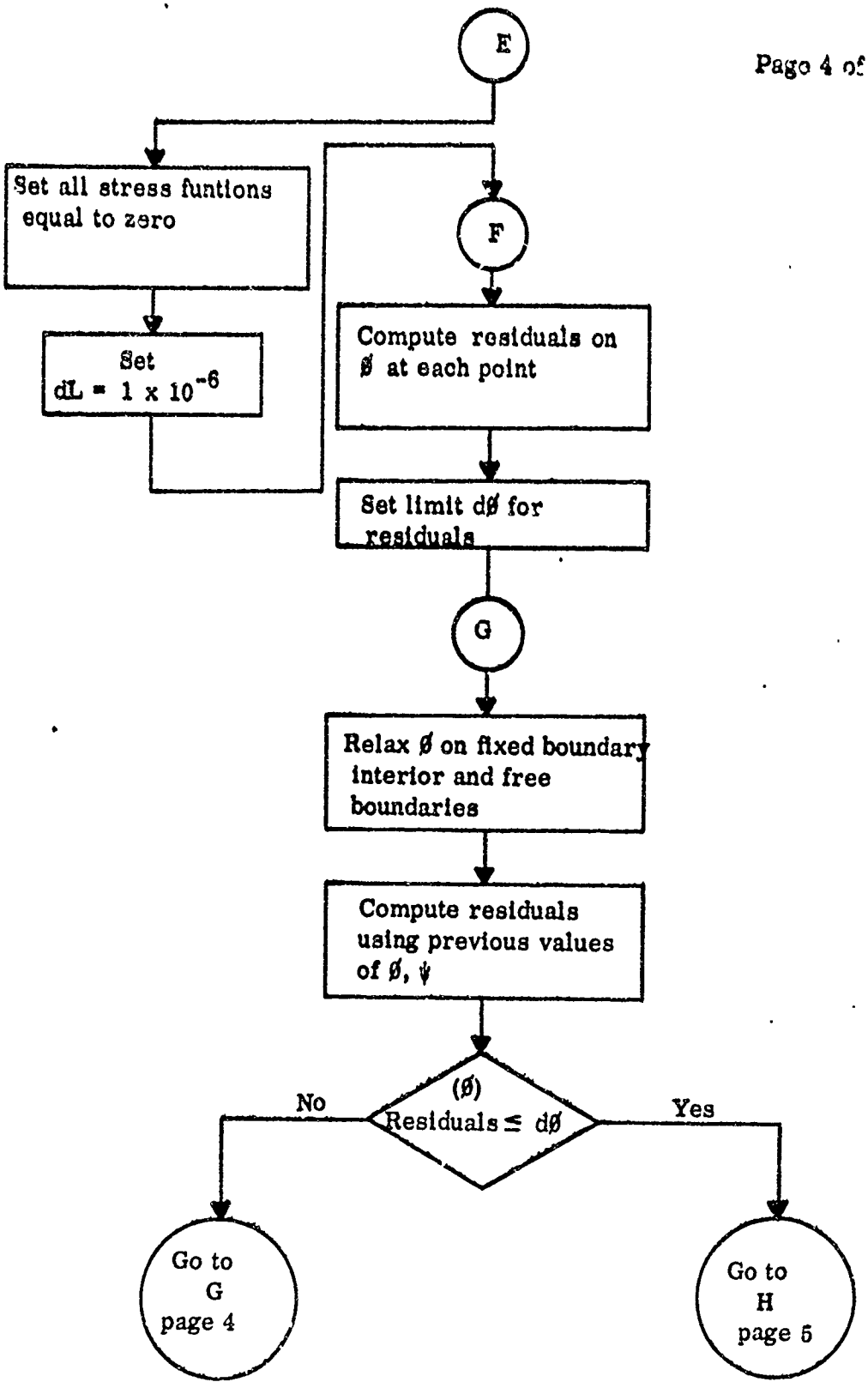

FIGURE 61. CONTINUED

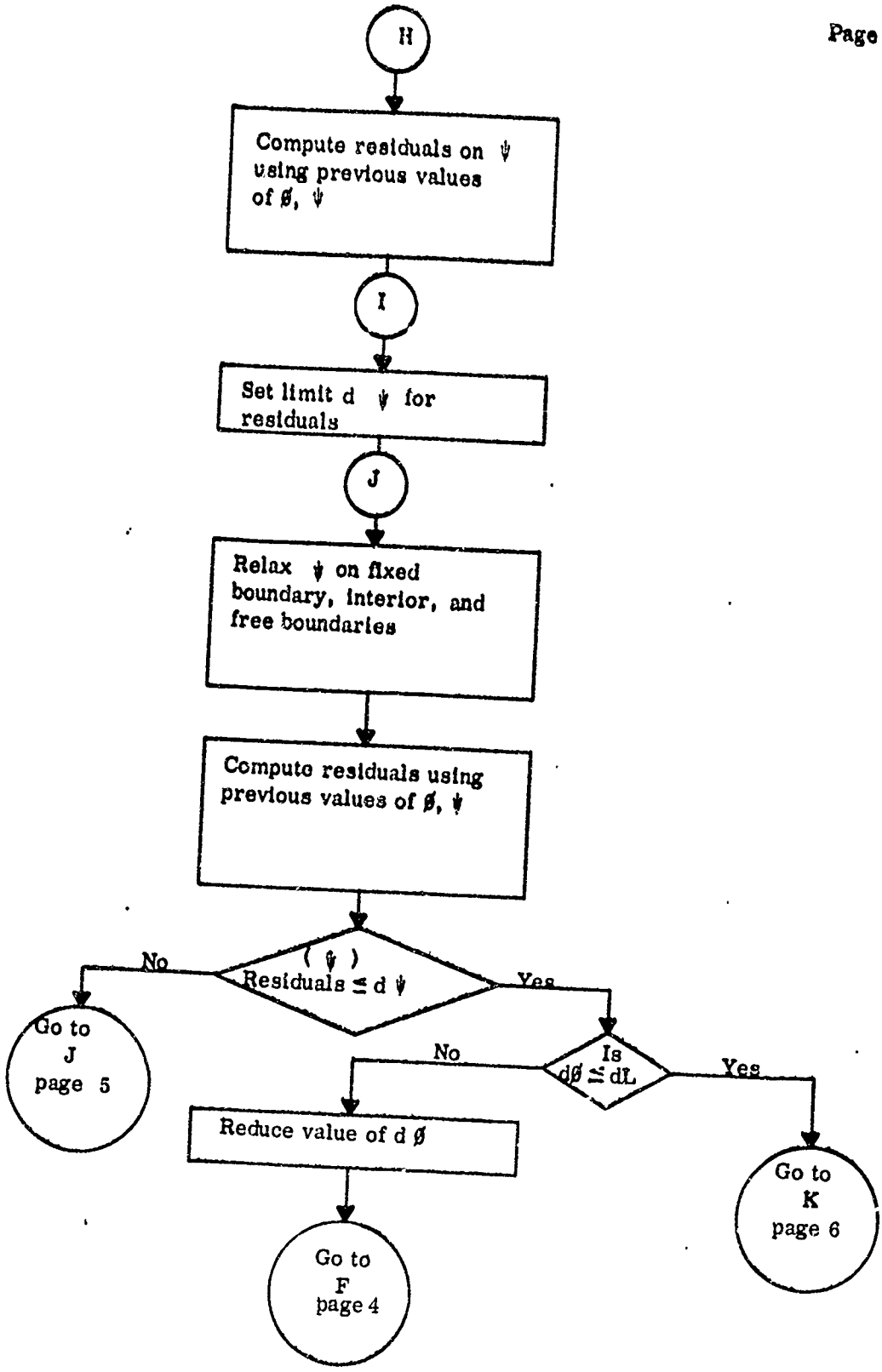

FIGURE 61. CONTINUED

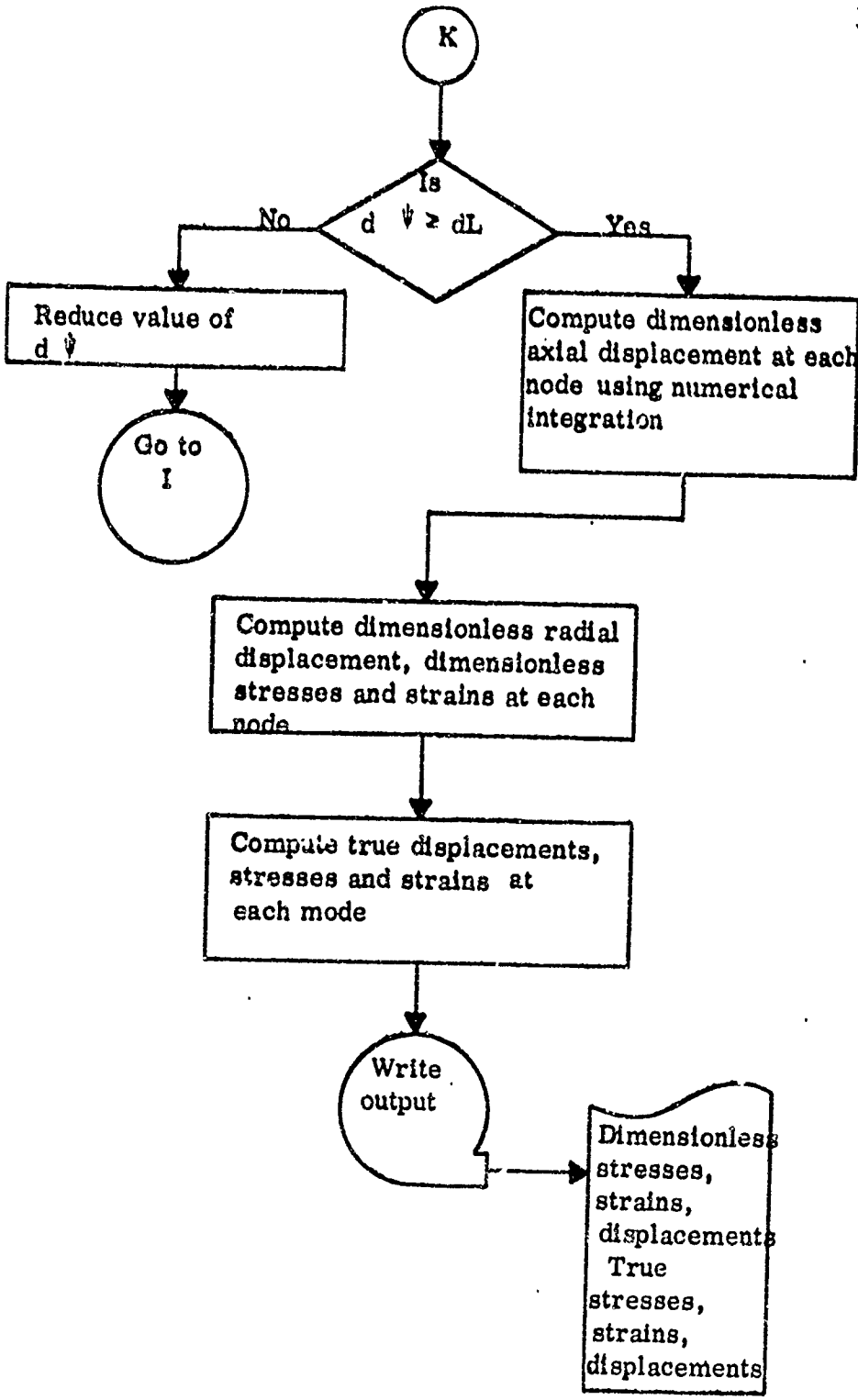

FIGURE 61. CONTINUED

The relaxation routine makes use of systematic over-relaxation to solve for the values of ϕ and ψ at all nodal points. The values of ϕ in the solution vector $[X_i]$ are improved to a certain degree by reduction of the corresponding entries in the residual vector $[R_i]$. These values of ϕ are, in turn, used to improve the values of ψ in the solution vector. This process is continued until all residuals are less than some specified number dL. When all residuals are less than dL, the values of ϕ and ψ which are in storage, are used to calculate the stresses, strains, and displacements at each node.

Since the axial displacement at any nodal point involves evaluating integrals of derivatives of the stress functions ϕ and ψ with respect to the spacial coordinate ρ, numerical integration along a radial line $\rho = \rho_o$ must be employed to calculate u_η. The remaining stresses, strains, and radial displacement at a nodal point are readily obtained by using the appropriate finite difference equations, (7.17)-(7.26) and (8.1)-(8.16), which specify the values of these quantities at each point of the bounded region. Since these expressions involve only first derivatives (see equations 5.3-5.12), these values can be calculated to a considerable degree of accuracy.

The value of the dimensionless stresses, strains, and displacements (u_η, u_ρ, ϵ_ρ, ϵ_θ, ϵ_η, σ_ρ, σ_θ, σ_η, $\tau_{\rho\eta}$, $\gamma_{\rho\eta}$) at each nodal point of the bounded region (see Figure 61) are printed as output.

Although the existing analysis and computer program does not account for the viscoelastic (time-dependent) properties that most propellants exhibit, the results

(true stresses, strains, and displacements), as obtained from the analysis above, may be used directly in analyzing problems involving short and long times by employing the glassy and equilibrium properties of the propellant. The extension to time space of the elastic results obtained from this analysis is being investigated. Apparently, a knowledge of the variance of the elastic solution for a range of the elastic modulus, E(t), is necessary for incorporating the viscoelastic propellant properties into the elastic solution.

This program will be used to investigate the effects of variation in the geometric parameters λ (l/d ratio), α (a/b ratio), and ν (ellipse ratio) upon the stress-strain fields of these grain configurations when they are subjected to loadings by internal pressure, temperature variation, and axial acceleration. These results, in the form of design charts, will provide an additional structural tool to design engineers.

V. CONCLUSIONS AND RECOMMENDATIONS

The technical discussions presented in Sections II, III, and IV outline the results obtained from the studies of heat transfer, influence of strain on burning rate, and propellant slump. Each of these interdependent studies generated specific conclusions, which are given in this section. Recommendations are also presented based on the work accomplished on this contract.

The two-dimensional heat transfer program developed under this contract has extended the capability to predict temperature profiles within propellant grains to situations more closely representing the actual environments experienced by today's propulsion systems. Subject to the characterization by experimental means of the materials being considered by the analysis, the program will handle a wide variation in the temperature dependency of thermal properties. The program has the demonstrated ability to consider either a single thermally symmetric section or an entire motor cross section with the same comprehensive consideration being given to time-dependent and circumferentially variant external environments. The above capabilities and versatility are not known to be available in any other single program throughout the industry.

Apart from the above capabilities, the resolution and apparent accuracy of the results were extremely rewarding. This is not always the situation with numerical solutions of this type. In all instances, expected effects were produced and apparently realistic reproductions of the anticipated thermal profiles resulted.

In these respects, the two-dimensional heat transfer program provides a capability directly applicable to subsequent analysis and programs for ballistic and structural evaluation of grains subjected to adverse environments.

Since satisfactory results were obtained from the two-dimensional heat transfer program and an extended capability was shown, the following recommendations regarding the use and possible extension of the analysis are submitted.

1) Because of the demonstrated success of the numerical approach, the basic analysis might be extended to consider three-dimensional configurations.

2) An experimental program should be undertaken to ascertain the necessary temperature dependency of thermal properties of propellants. A similar effort is required regarding the coefficients for determining the heat of polymerization during cure. Only upon completion of these efforts can the full capability of the program be realized.

3) Since the resolution of program results has been demonstrated, application of these results to areas other than the ballistic analysis should be investigated. Specifically, consideration should be given to the development of a thermal-structural analysis to evaluate stress-strain profile within propellant grains subjected to adverse thermal environments. This analysis, of course, should not be limited to thermal consideration but should also allow for pressure and dynamic loading, since the most realistic situation involves the superposition of all these.

These recommendations are directed toward the development and combination of modular program systems in order to provide an integrated system for complete motor design evaluation.

The following conclusions resulted from the study program to advance the state of the art of solid propellant rocket design by high-speed electronic digital computation techniques:

1) The Advanced Grain Design Analysis has proved to be an extremely effective tool for the rocket design engineer. The method combines conceptual simplicity with extreme computational accuracy and is applicable to a wide class of rocket motor designs.

2) The Advanced Grain Design Analysis (Program AGDA) is the only computer program in existence capable of computing the propellant inertia tensor components as they vary with time.

3) Ability of the Elkton-Moore Method to consider nonuniform thermal gradients throughout the solid propellant grain has been clearly established. This is the only known technique available that is amenable to such considerations.

4) The introduction of engineering-oriented software through the Input Generator has proved to be of tremendous value to computer operations.

Certain areas concerned with computerized grain design by AGDA deserve further consideration. Thiokol recommends further effort as follows:

1) While Program AGDA computes virtually all the geometrically derivable performance parameters, it does not consider such fundamental parameters as chamber pressure, thrust, delivered I_{sp}, or total impulse. Therefore, the most logical extension to Program AGDA would provide a rigorous interior ballistic analysis capable of considering the following effects: erosive burning, pressure variations, nozzle erosion, and ablation.

2) The wide class of solid propellant rocket motors that may be treated by Program AGDA represents only a small fraction of total imaginable rocket motors. Additional classes of rocket motors that might be considered are the dendrite or forked wagon wheel and the conicel.

3) Since Program AGDA is the only solid propellant rocket grain design computer program in the industry today capable of considering geometrically dependent propellant properties, this capability could be extended to include:

   a) Variation in burning rate with three-dimensional grain temperature variations

   b) Variation of burning rate caused by three-dimensional strain distributions

4) The engineering-oriented software created and used with Program AGDA should be applied to other programs requiring large amounts of input evolving from complicated geometric configurations. Specifically, multi-dimensional heat transfer and stress-strain analyses are envisioned. Further, the output of such programs should be adapted so that it is usable directly by Program AGDA. This would establish a relatively complete solid propellant rocket simulation computer program system capable in the most general sense of forecasting the failure or predicting the performance of a wide variety of solid propellant rocket motors.

5) Future effort should be directed toward establishing methods of semi-automatic or automatic solid propellant grain design. Fruition of such concepts as the solid propellant grain design library, a catalog of solid propellant fuel characteristics, automatic combination and scaling of parts of rocket motors from the solid propellant grain design library, and automatic generation of solid propellant fuel characteristics by consideration of the past history of every solid propellant rocket motor firing using this propellant should be realized.

The results of the study of the influence of strain on burning rate showed that burning rate is affected by strain only when the material ceases to behave as an incompressible material. This condition occurs in filled polymers (such as composite solid propellants) when the tensile strains have reached a level that causes a severing of the oxidizer-binder bond. This phenomenon, also referred to as "dewetting," can

occur at very low strains, as in the case of brittle materials, or at relatively high strains for more viscous material. Therefor all propellants are not affected to the same degree by strain.

The basis for a definite criterion on the effect of strain on burning rate has been shown through the investigation of volumetric change index, and a correlation between percent change in burning rate and a volumetric change index is given. The latter term is a representation of the departure from incompressibility that the material experiences due to strain. For the linear case, an empirical relationship has been shown to exist for the range of strains and pressures and for the propellants tested. The fact that the results obtained here correlated quite well with the data of a study conducted at another agency adds further support to this conclusion. For mass burning, a similar but more complex criterion has been shown to exist. However, both cases require more study before a general correlation for all classes of solid propellants can be established.

From the results achieved in this program, certain areas are recommended for future work.

1) Examine a greater variety of propellants (including double-base types) over wider ranges of strain and pressure to establish a firm correlation among burning rate, strain, and chemical structure.

2) Investigate the effect of temperature upon the relationship between strain and burning rate.

3) Determine the extent to which compressive strains influence burning rate. If a similar correlation could be extended to include compressive as well as tensile strain, a convenient

input for use in grain design computer programs for ballistic performance predictions could be realized. For example, if the thermal history of a motor grain and the thermal expansion properties of the propellant are known, the strain geography can be determined. From this information, along with the knowledge of the strain dependence on the burning rate, the net burning behavior for the motor can be computed. This becomes increasingly important as the burning rates of propellants are increased.

The results achieved here are not limited in their use to the solid propellant industry. The experimental logic employed should also apply to the pyrotechnic industry or to any industry when the control of burning rate is important.

The computer program conceived under this program, 'Stress Analysis of Axisymmetric Grain Designs Having Arbitrary End Geometries and Straight-Through Ports," provides a suitable method for predetermining the response of these grain designs to pressure, thermal, and axial acceleration loads.

It is recommended that this analysis be extended to encompass:

1) A thorough investigation of the effects of the parameters ν , λ (L/D ratio), α (a/b ratio), and ν (ellipse ratio) upon the stress-strain field in axisymmetric grain designs having arbitrary end geometries and straight-through ports

2) A modification of the computer program in order to incorporate the effects of head-end webs and arbitrary aft cutbacks

3) A parameter study to examine the effects of the variables in (1) upon the strain field in motors having fully loaded head ends

4) Verification of the studies in (3) by means of a correlation with actual stresses and strains in experimental models having full head-end webs

5) Incorporation of the above recommendations into engineering design charts

REFERENCES

1. McAdams, W. H., Heat Transmission, McGraw-Hill, New York, 1954, pp. 31-52.

2. Richtmeyer, R. D., Difference Methods for Initial Value Problems, Interscience Publishers, Inc., New York, 1957.

3. Coy, J., Jet Propulsion Laboratory, Quarterly Summary Report 38-4, WASA Contract No. NAS_w-6, July 15, 1961.

4. Personal Communication with Mr. Leo Long, Longhorn Division, Thiokol Chemical Corporation.

5. Cooper, M. H., and Baldwin, J. B., "Development of an End Bonded Tensile Specimen," 20th Meeting Bulletin of the JANAF Physical Properties Panel, Volume I, p. 201.

6. Zandman, F., and Redner, S. S., "A Feasibility of Stress Analysis of Solid Propellant Grain Using the PhotoStress Technique," Thiokol Chemical Corporation, Order No. EB-7255, Contract AF 33(616)-6530, April 1960.

7. Saylak, D., "Design Fabrication and Evaluation of An End Bonded Cylindrical Tensile Specimen for Tensile Testing Composite Rocket Propellant," Bulletin of the First Meeting of the ICRPG Working Group on Mechanical Behavior, CPIA Publication No. 2, 54, December 1962.

8. Williams, M. L., Blatz, P. J., and Schapery, R. A., "Fundamental Studies Relating to Systems Analysis of Solid Propellants," California Institute of Technology, Final Report GALCIT 101, February 1961.

9. Thiokol Chemical Corporation, Elkton Division, "A Research Study to Advance the State-of-the-Art of Solid Propellant Grain Design," Quarterly Progress Report No. 9, E173-62, December 1, 1962.

10. Layton, L. H., and Stoker, J. H., "Determination of Stress Relaxation in a Composite Solid Propellant," Bulletin of the First Meeting of the ICRPG Working Group on Mechanical Behavior, CPIA Publication No. 2, 60, December 1962.

11. Jones, J. W., et al, "Propellant Viscoelastic Characterization in Creep and Stress Relaxation Tests," Bulletin of the 20th Meeting of the JANAF-ARPA-NASA Panel on Physical Properties of Solid Propellants, Volume I, 1961.

12. Schapery, R. A., "A Simple Method of Fitting Viscoelastic Models to Experimental Data," GALCIT SM-61-23A, California Institute of Technology, November 1961.

13. Sokolnikoff, I. S., "Mathematical Theory of Elasticity," Brown University Press, Providence, R. I., 1941.

14. Southwell, R. V., "Some Practically Important Stress-Systems in Solids of Revolution," Proceedings of the Royal Society, Series A, Volume 180, 1942, pp. 367-386.

15. Parr, C. H., and Gillis, G. F., "Deformations of Case-Bonded Solid Propellant Grains Under Axial and Transverse Acceleration Loads," ARS paper No. 2750-63, 1963.

16. Rohm & Haas Company, Quarterly Progress Report on Engineering Research, No. P-61-17, June 1962.

17. Rohm & Haas Company, Quarterly Progress Report on Engineering Research, No. P-62-27, April 1963.

18. Southwell, R. V., "Relaxation Methods in Theoretical Physics," Oxford, 1956.

19. "A Research Study to Advance the State-of-the-Art of Solid Propellant Grain Design," Contract AF 33(615)-6530, Quarterly Progress Report No. 3, Thiokol Chemical Corporation, Elkton Division, April 1963.

20. Allen, D. N., "Relaxation Methods," McGraw-Hill, New York, 1954.

DISTRIBUTION LIST FOR REPORT NO. E92-63

Director
Rocket Research Laboratories
United States Air Force
Edwards, California
Attn: DGSMD, Lt. Harold W. Gale
(3 copies)

Commander
Air Force Flight Test Center
Edwards AFB, California
Attn: Tech. Library Code FTOOT
(10 copies)

Air Force Systems Command
(STLO)
Lewis Research Center (NASA)
Cleveland 35, Ohio
(1 copy)

U. S Department of the Interior
Bureau of Mines
4800 Forbes Avenue,
Pittsburgh 13, Pa.
Attn: M M. Dolinar, Repts Librarian
Explosives Research Lab.
(1 copy)

National Aeronautics & Space Admin.
Lewis Research Center
21000 Brookpark Road
Cleveland 35, Ohio
Attn: Library
(1 copy)

National Aeronautics & Space Admin.
Manned Spacecraft Center
P. O. Box 1537
Houston 1, Texas
Attn: Library
(1 copy)

California Institute of Technology
Pasadena, California
Attn: Dr. Max Williams
(1 copy)

Defense Documentation Center
Arlington Hall Station
Arlington 12, Virginia
(20 copies)

RTD (RTA)
Bolling Air Force Base
Washington 25, D. C
(1 copy)

Central Intelligence Agency
2430 E Street, N. W.
Washington 25, D. C.
Attn: OCD, Standard Dist.
(1 copy)

Office of the Director of Defense
Research and Engineering
Washington 25, D. C.
Attn: D. B. Brooks
Office of Fuels & Lubricants
(1 copy)

National Aeronautics & Space Admin.
Launch Operations Center
Cocoa Beach, Florida
Attn: Library
(1 copy)

National Aeronautics & Space Admin.
George C. Marshall Space Flight Center
Huntsville, Alabama
Attn: Library
(1 copy)

National Aeronautics & Space Admin.
Langley Research Center
Langley Air Force Base
Virginia
Attn: Library
(3 copies)

Scientific and Tech. Info. Facility
P. O. Box 5700
Bethesda, Maryland
Attn: NASA Representative
(2 copies)

National Aeronautics & Space Admin.
Goddard Space Flight Center
Greenbelt, Maryland
Attn: Library
(1 copy)

Arnold Eng. Development Center
Air Force Systems Command
Tullahoma, Tennessee
Attn: AEOIM
(1 copy)

Air Force Rocket Propulsion Lab.
Edwards
California
Attn: DGPS
(1 copy)

Air Force Rocket Propulsion Lab.
Edwards
California
Attn: DGS
(1 copy)

Air Force Missile Test Center
Patrick Air Force Base
Florida
Attn: MTBAT
(1 copy)

National Aeronautics & Space Admin.
Washington 25, D. C.
Attn: Office of Technical Information & Educational Programs, Code ETL
(1 copy)

National Aeronautics & Space Admin.
Washington 25, D. C.
Attn: R. W. Ziem (RPS)
(1 copy)

Air Force Systems Command
Andrews AFB
Washington 25, D. C.
Attn: SCTAP
(1 copy)

Air Force Rocket Propulsion Lab.
Edwards
California
Attn: DGPL
(1 copy)

Air Force Rocket Propulsion Lab.
Edwards
California
Attn: DGR
(1 copy)

Air Force Missile Dev. Center
Holloman AFB, New Mexico
Attn: MDGRT
(1 copy)

Commander
Aeronautical Research Laboratory
Wright-Patterson AFB, Ohio
Attn: AFC, Mr. Karl Scheller
(1 copy)

Director
Special Projects Office
Department of the Navy
Washington 25, D. C.
(1 copy)

DISTRIBUTION LIST FOR REPORT NO. E92-63 (Cont'd)

Aeronautical Systems Division
Wright-Patterson AFB, Ohio
Attn: ASRCEE-1
(1 copy)

Commander
AFSC
Foreign Technology Division
Wright-Patterson AFB, Ohio
Attn: RTD(TD-E3b)
(1 copy)

Commanding Officer
Harry Diamond Laboratories
Washington 25, D. C.
Attn: AMXDO-TIB
(1 copy)

Commanding Officer
Frankford Arsenal
Philadelphia 37, Pennsylvania
Attn: Propellant and Explosives
Section, 1331
(1 copy)

Redstone Scientific Information Center
U. S. Army Missile Command
Redstone Arsenal, Alabama
Attn: Chief, Document Section
(5 copies)

Bureau of Naval Weapons
Department of the Navy
Washington 25, D. C.
Attn: DLI-3
(2 copies)

Bureau of Naval Weapons
Department of the Navy
Washington 25, D. C.
Attn: RMMP-3
(1 copy)

Aeronautical Systems Division
Wright-Patterson AFB, Ohio
Attn: ASRCEM-1
(1 copy)

Commanding Officer
Ballistic Research Laboratories
Aberdeen Proving Ground, Maryland
Attn: BLI
(1 copy)

Commanding Officer
Ordnance Office
Duke Station
Durham, North Carolina
(1 copy)

Commanding Officer
Picatinny Arsenal
Dover, New Jersey
Attn: Library
(1 copy)

Commanding General
White Sands Missile Range
New Mexico
Attn: Technical Library
(1 copy)

Bureau of Naval Weapons
Department of the Navy
Washington 25, D. C.
Attn: RMMP-2
(2 copies)

Bureau of Naval Weapons
Department of the Navy
Washington 25, D. C.
Attn: RMMP-4
(1 copy)

Mr. James MacPherson
Atlantic Research Corporation
Shirley Highway and Edsall Road
Alexandria, Virginia
(1 copy)

DISTRIBUTION LIST FOR REPORT NO. E92-63 (Cont'd)

Bureau of Naval Weapons
Department of the Navy
Washington 25, D. C.
Attn: RRRE-6
(1 copy)

Commander
U. S. Naval Ordnance Laboratory
White Oak
Silver Spring, Maryland
Attn: Library
(2 copies)

Commander
U. S. Naval Ordnance Test Station
China Lake, California
Attn: Technical Library Branch
(2 copies)

Commanding Officer
U. S. Naval Propellant Plant
Indian Head, Maryland
Attn: Technical Library
(1 copy)

Director (Code 6180)
U. S. Naval Research Lab.
Washington 25, D. C.
Attn: H. W. Carhart
(1 copy)

Commanding Officer
U. S. Naval Underwater Ordnance Station
Newport, Rhode Island
Attn: W. W. Bartlett
(1 copy)

Aerojet-General Corporation
11711 South Woodruff Avenue
Downey, California
Attn: Florence Walsh, Librarian
(1 copy)

Commander
U. S. Naval Missile Center
Point Mugu, California
Attn: Technical Library
(2 copies)

Commander
U. S. Naval Ordnance Test Station
China Lake, California
Attn: Code 45
(5 copies)

Superintendent
U. S. Naval Postgraduate School
Naval Academy
Monterey, California
(1 copy)

Commanding Officer
Office of Naval Research
1030 E. Green Street
Pasadena 1, California
(1 copy)

Director
U. S. Naval Research Lab.
Washington 20, D. C.
Attn: Chemistry Division, Code 6130
R. R. Miller
(1 copy)

Aerojet-General Corporation
P. O. Box 296
Azusa, California
Attn: Librarian
(2 copies)

Aerojet-General Corporation
P. O. Box 1947
Sacramento, California
Attn: Technical Information Office
(3 copies)

Aerospace Corporation
P. O. Box 95085
Los Angeles 45, California
Attn: Library-Documents
(1 copy)

Amcel Propulsion Company
Box 3049
Asheville, North Carolina
(1 copy)

Armour Research Foundation of Illinois
Institute of Technology
Technology Center
Chicago 16, Illinois
Attn: C. K. Kersh, Chemistry Division
(1 copy)

Atlantic Research Corporation
Shirley Highway and Edsall Road
Alexandria, Virginia
(2 copies)

Battelle Memorial Institute
505 King Avenue
Columbus 1, Ohio
Attn: Report Library, Room 6A
(1 copy)

The Boeing Company
Aero Space Division
P. O. Box 3707
Seattle 24, Washington
Attn: R. R. Barber, Lib. Ut. Ch.
(1 copy)

Douglas Aircraft Co., Inc.
Santa Monica Division
Santa Monica, California
Attn: Mr. J. L. Waisman
(1 copy)

Allied Chemical Corporation
General Chemical Division
Research Lab., P. O. Box 405
Morristown, New Jersey
Attn: L. J. Wiltrakis, Security Officer
(1 copy)

American Cyanamid Company
1937 W. Main Street
Stamford, Connecticut
Attn: Security Officer
(1 copy)

ARO, Inc.
Arnold Engrg. Dev. Center
Arnold AF Station, Tennessee
Attn: Dr. B. H. Goethert
Director of Engrg.
(1 copy)

Atlantic Research Corporation
Western Division
209 Easy Street
El Monte, California
Attn: H. Niederman
(1 copy)

Chemical Propulsion Information Agency
Applied Physics Laboratory
8621 Georgia Avenue
Silver Spring, Maryland
(3 copies)

The Dow Chemical Company
Security Section
Box 31
Midland, Michigan
Attn: Dr. R. S. Karpiuk, 1710 Building
(1 copy)

E. I. duPont deNemours and Company
Eastern Laboratory
Gibbstown, New Jersey
Attn: Mrs. Alice R. Steward
(1 copy)

Ethyl Corporation
Research Laboratories
1600 West Eight Mile Road
Ferndale, Michigan
Attn: E. B. Rifkin, Assistant Director,
Chemical Research
(1 copy)

General Electric Company
Cincinnati 15, Ohio
Attn: Technical Information Center
(1 copy)

Hercules Powder Company
Allegany Ballistics Laboratory
P. O. Box 210
Cumberland, Maryland
Attn: Library
(2 copies)

Hercules Powder Company
Research Center
Wilmington 99, Delaware
Attn: Dr. Herman Skolnik, Manager
Technical Information Division
(1 copy)

Jet Propulsion Laboratory
4800 Oak Grove Drive
Pasadena 3, California
Attn: L. E. Newlan
Chief, Reports Group
(1 copy)

Lockheed Propulsion Company
P. O. Box 111
Redlands, California
Attn: Miss Belle Berlad, Librarian
(3 copies)

Esso Research and Engineering Co.
Special Projects Unit
P. O. Box 8
Linden, New Jersey
Attn: Mr. D. L. Baeder
(1 copy)

General Dynamics/Convair
San Diego 12, California
Attn: Engrg. Library
K. G. Blair, Ch. Librn.
Mail Zone 50-03
(1 copy)

Allison Division
General Motors Corporation
Indianapolis 6, Indiana
Attn: Plant 8, Tech. Library
Mr. L. R. Smith
(1 copy)

Hercules Powder Company
Kenvil
New Jersey
Attn: Library
(1 copy)

Institute for Defense Analysis
Res. & Eng. Support Division
Attn: Technical Information Office
1825 Connecticut Avenue
Washington 9, D. C.
(1 copy)

Arthur D. Little, Inc.
15 Acorn Park
Cambridge 40, Massachusetts
Attn: W. H. Varley
(1 copy)

Marquardt Corporation
16555 Saticoy Street
Box 2013 - South Annex
Van Nuys, California
(1 copy)

Martin Company
Baltimore 3, Maryland
Attn: Science-Technology
Library - Mail 398
(1 copy)

Martin Company
Orlando, Florida
Attn: Library
(1 copy)

Monsanto Research Corporation
Boston Labs., Everett Station
Boston 49, Massachusetts
Attn: Library
(1 copy)

North American Aviation, Inc.
Space & Information Systems Div.
12214 Lakewood Boulevard
Downey, California
Attn: W. H. Morita
(1 copy)

Rocketdyne
6633 Canoga Avenue
Canoga Park, California
Attn: Library, Dept. 596-306
(3 copies)

Space Technology Laboratory, Inc.
1 Space Park
Redondo Beach, California
Attn: STL Tech. Lib. Doc. Acquisitions
(2 copies)

Thiokol Chemical Corporation
Alpha Division, Huntsville Plant
Huntsville, Alabama
Attn: Technical Director
(2 copies)

Martin Company
Advanced Technology Library
P. O. Box 1176
Denver, Colorado
(1 copy)

Minnesota Mining & Manufacturing Co.
900 Bush Avenue
St. Bush 6, Minnesota
Attn: J. D. Ross
VIA: H. C. Zeman
Security Administrator
(2 copies)

New York University
Dept. of Chemical Engineering
New York 53, New York
Attn: P. F. Winternitz
(1 copy)

Purdue University
Lafayette, Indiana
Attn: M. J. Zucrow
(1 copy)

Rohm and Haas Company
Redstone Arsenal Research Division
Huntsville, Alabama
Attn: Librarian
(1 copy)

Texaco Experiment Incorporated
P. O. Box 1-T
Richmond 2, Virginia
Attn: Librarian
(1 copy)

Thiokol Chemical Corporation
Alpha Division
Space Booster Plant
Brunswick, Georgia
(1 copy)

Thiokol Chemical Corporation
Reaction Motors Division
Denville, New Jersey
Attn: Librarian
(1 copy)

Union Carbide Corporation
Union Carbide Plastics Co. Div.
1 River Road
Bound Brook, New Jersey
Attn: Mr. N. R. Smith
(1 copy)

United Aircraft Corporation
Pratt & Whitney Fla. Res. & Dev. Ctr.
P. O. Box 2691
W. Palm Beach, Florida
Attn: Library
(1 copy)

British Defence Staff
British Embassy
3100 Massachusetts Avenue
Washington, D. C.
Attn: Scientific Information Officer
VIA: Headquarters
Air Force Systems Command
Andrews Air Force Base
Washington 25, D. C.
Attn: SCS-41 (3-1833)
(4 copies)

Commanding Officer
Ammunition Procurement & Supply Agency
Joliet, Illinois
Attn: Engr. Library
(1 copy)

Callery Chemical Company
Research and Development
Callery, Pennsylvania
Attn: Document Control
(1 copy)

Thiokol Chemical Corporation
Wasatch Division
P. O. Box 524
Brigham City, Utah
Attn: Library Section
(2 copies)

United Aircraft Corporation
Corporation Library
400 Main Street
East Hartford, Connecticut
Attn: Dr. David Rix
(1 copy)

United Technology Center
P. O. Box 358
Sunnyvale, California
Attn: Librarian
(1 copy)

Defence Research Member
Candian Joint Staff(W)
2450 Massachusetts Avenue
Washington, D. C.
VIA: Headquarters
Air Force Systems Command
Andrews Air Force Base
Washington 25, D. C.
Attn: SCS-41(3-1833)
(4 copies)

American Machine and Foundry Co.
Mechanics Research Department
7501 North Natchez Avenue
Niles 48, Illinois
Attn: Phil Rosenberg
(1 copy)

Ethyl Corporation
P. O. Box 3091
Istrouma Branch
Baton Rouge, Louisiana
(1 copy)

B. F. Goodrich Aerospace & Defense Products
P. O. Box 157, Rialto, California
Attn: Mr. A. B. Japs, Tech. Manager
Rocket Motor Development
(1 copy)

Hynes Research Corporation
308 Bon Air Avenue
Durham, North Carolina
(1 copy)

National Research Corporation
70 Memorial Drive
Cambridge 42, Massachusetts
Attn: Document Custodian
Document Control Section
(1 copy)

Olin Mathieson Chemical Corporation
Research Library 1-K-3
275 Winchester Avenue
New Haven, Connecticut
Attn: Mail Control Room
Miss Laura M. Kajuti
(1 copy)

Phillips Petroleum Company
145 Chemical Labs. Bldg.
Bartlesville, Oklahoma
Attn: H. M. Fox
(1 copy)

Shell Development Company
4560 Horton Street
Emeryville 8, California
(1 copy)

Thiokol Chemical Corporation
Post Office Box 27
Bristol, Pennsylvania
Attn: R. Morris
(1 copy)

Hercules Powder Company
Bacchus Works
Magna, Utah
Attn: Librarian
(1 copy)

Walter Kidde Company
675 Main Street
Belleville 9, New Jersey
Attn: Security Librarian
(1 copy)

Olin Mathieson Chemical Corporation
Marion, Illinois
Attn: Research Library
Box 508
(1 copy)

Pennsalt Chemicals Corporation
Box 4388
Philadelphia 18, Pennsylvania
Attn: Dr. G. Barth-Wehrenalp
(1 copy)

Rocketdyne, A Division of North
American Aviation, Inc.
Solid Propulsion Operations
P. O. Box 548, McGregor, Texas
Attn: Library
(1 copy)

Southwest Research Institute
Department of Structural Research
8500 Culebra Road
San Antonio 6, Texas
Attn: Dr. Robert C. DeHart, Director
(1 copy)

Wright Aeronautical Division
Curtiss-Wright Corporation
Wood-Ridge, New Jersey
(1 copy)

APPENDIX I

TWO-DIMENSIONAL HEAT TRANSFER PROGRAM

A. Glossary
B. List of Functions and Subroutines (Transfer Vector) Used by Two-Dimensional Heat Transfer
C. Card Input Format (Two-Part Program)
D. Flow Charts
E. Input Format (Revised program for one part loading when grid size is within specified limitations)

APPENDIX I

TWO-DIMENSIONAL HEAT TRANSFER PROGRAM

A. GLOSSARY

B. LIST OF FUNCTIONS AND SUBROUTINES (TRANSFER VECTOR) USED BY TWO-DIMENSIONAL HEAT TRANSFER

C. CARD INPUT FORMAT (TWO-PART PROGRAM)

D. FLOW CHARTS

E. INPUT FORMAT (REVISED PROGRAM FOR ONE-PART LOADING WHEN GRID SIZE IS WITHIN SPECIFIED LIMITATIONS)

APPENDIX I

A. GLOSSARY

Symbol	Identification	Dimensions	FORTRAN
A	Experimental Constant for Heat of Polymerization	None	EN1
B	Experimental Constant for Heat of Polymerization	None	EN2
C_p	Specific Heat	BTU/lb-°R	CP
E	Heat Flux	BTU/hr-ft^2	E
F_o	Shape Factor	None	GEOM
h_g	Internal Film Coefficient	BTU/hr-ft^2-°R	HGC
h_o	External Film Coefficient	BTU/hr-ft^2-°R	HGCS
$K_{i,j}$	Thermal Conductivity	BTU-ft/hr-ft^2-°R	THRCON
n	Experimental Constant for Heat of Polymerization	None	EN3
$P_{j,k}$	Polymer Fraction	None	ALF(4)
Q	Heat of Polymerization	BTU/lb	HOP
R	Gas Constant	BTU/lb-°R	R
$r_{i,j}$	Radius	In.	ALF(5)
T_c	Internal Convective Temp.	°R	TEIN
$T_{i,j}$	Initial Temp.	°R	ALF(1)
T_o	External Convective Temp.	°R	TECON
T_{rad}	Radiant Temp.	°R	TERAD

A. GLOSSARY (Continued)

Symbol	Identification	Dimensions	FORTRAN
Δr	Forward Difference in Radial Direction	In	ALF(3)
$\Delta \theta$	Time Increment	Min	DELTAT
$\Delta \phi$	Forward Difference in Circumferential Direction	Rad	ALF(2)
θ	Time	Min	TIME
ρ	Density	lb/ft^3	RHO

APPENDIX I

B. LIST OF FUNCTIONS AND SUBROUTINES (TRANSFER VECTORS) USED BY TWO-DIMENSIONAL HEAT TRANSFER (LISTED SEPARATELY FOR PARTS I AND II)

Main Program - Part I

TAPES*
EXIT**
LOAD*** } Subroutines for Part I (no functions)

Main Program - Part II

SQRTF
COSF
SINF
TAPES*
EXIT** } Subroutines and Functions for Part II

---

*TAPES subroutine is unique to the Elkton IBM-7070 System but can be easily revised to any other system. The tape designation at the Elkton division is as follows:

FORTRAN Tape Designation	Symbolic Representation	Use
1	None	FORTRAN Package
2	IN	Loader
3	LET	Output
4	INTER C	Scratch
5	INTER B	Scratch
6	INTER A	Scratch

This may be revised by altering the equivalence statement to the specifications of another system. As an example, if the input for a system was FORTRAN tape 5 and output was FORTRAN tape 6, the equivalence statement would be as follows:

EQUIVALENCE (NTAPES(2), INTERC), (NTAPES (3), INTER B), (NTAPES (4), INTER A), (NTAPES (5), IN), (NTAPES (6), LET).

**EXIT: The EXIT subroutine is unique to the Elkton system. It is not required for application of the program to the IBM-7090, for instance.

***LOAD: Subroutine LOAD is a routine used to provide for multiple core loads. This will not be needed in the IBM-7090 but the following cards will have to be deleted:

Part I

```
185 CALL LOAD
    END
```

Part II

All the cards that contain DIMENSION, EQUIVALENCE, and COMMON statements.

The program will be compiled as one deck, and not as a two-part program.

SHEET 1

WORD	-
COLUMNS	2-72
FORMAT	1X, 71H
CARD 1	Alphanumeric Information to Identify Problem
SYMBOL	Name

WORD	1	2	3	4	5
COLUMNS	1-5	6-10	11-15	16-20	21-25
FORMAT	I5	I5	I5	I5	I5
CARD 2	Number of Constant Phi Lines	Number of Constant Radius Lines	Number of Printed Outputs		Number of Propellant Bypass Iterations
SYMBOL	NENPHI	NENRAD	NENOP		NADD

WORD	1	2	3	4	5	6	7	8
COLUMNS	1-10	11-20	21-30	31-40	41-50	51-60	61-70	71-80
FORMAT	F10.0	F10.0	F10.0	F10.0	F10.0	F10.0	F10.0	F10.0
CARD 3	Time Increment, min	Total Time, min	Propellant Density, lb/ft^3	Case Density, lb/ft^3	Gas Constant, BTU/lb-°R	Heat of Polymerization, BTU/lb	Propellant Identification	Case Material Identification
SYMBOL	DELTAT	TOT I	RHO I	RHOC	R	HOP	DA	DE

SHEET 2

WORD	1	2	3	4	5
COLUMNS	1-10	11-20	21-30	31-40	41-50
FORMAT	F10.0	F10.0	F10.0	F10 0	F10.0
CARD 4	A Experimental Constants for Heat of Polymerization	B	n	Internal Convective Temperature, °R	Internal Film Coefficient, BTU/hr-ft^2-°R
SYMBOL	EN 1	EN 2	EN 3	TEIN	HGC

WORD	1	2	3	4	5
COLUMNS	1-10	11-20	21-30	31-40	41-50
FORMAT	F10.0	F10.0	F10.0	F10.0	F10.0
CARD 5	Coefficients for Determining Thermal Conductivity of Propellant as a Function of Temperature, °R $K = PA(1) + PA(2)\ T + PA(3)\ T^2 + PA(4)\ T^3 + PA(5)\ T^4$ (BTU-ft/hr-ft^2-°R)				
SYMBOL	PA(1)	PA(2)	PA(3)	PA(4)	PA(5)

WORD	1	2	3	4	5
COLUMNS	1-10	11-20	21-30	31-40	41-50
FORMAT	F10.0	F10.0	F10.0	F10.0	F10.0
CARD 6	Coefficients for Determining Thermal Conductivity of Case Material as a Function of Temperature, °R $K = PB(1)\ \ PB(2)\ T + PB(3)\ T^2 + PB(4)\ T^3 + PB(5)\ T^4$ (BTU-ft/hr-ft^2-°R)				
SYMBOL	PB(1)	PB(2)	PB(3)	PB(4)	PB(5)

SHEET 3

WORD	1	2	3	4	5
COLUMNS	1-10	11-20	21-30	31-40	41-50
FORMAT	F10.0	F10.0	F10.0	F10 0	F10.0
CARD 7	Coefficients for Determining Specific Heat of Propellant as a Function of Temperature. °R $C_p = PC(1) + PC(2)\ T + PC(3)\ T^2 + PC(4)\ T^3 + PC(5)\ T^4$ (BTU/lb-°R)				
SYMBOL	PC(1)	PC(2)	PC(3)	PC(4)	PC(5)

WORD	1	2	3	4	5
COLUMNS	1-10	11-20	21-30	31-40	41-50
FORMAT	F10.0	F10.0	F10.0	F10.0	F10.0
CARD 8	Coefficients for Determining Specific Heat of Case Material as a Function of Temperature, °R $C_p = PD(1) + PD(2)\ T + PD(3)\ T^2 + PD(4)\ T^3 + PD(5)\ T^4$ (BTU/lb-°R)				
SYMBOL	PD(1)	PD(2)	PD(3)	PD(4)	PD(5)

WORD	1	2	3	4	5
COLUMNS	1-5	6-10	11-15	16-20	21-25
FORMAT	I5	I5	I5	I5	I5
CARD 9	0 - One Boundary Zone for Convective Temperature*	0 - One Boundary Zone for External Film Coefficient*	0 - One Boundary Zone for Radiation View Factor*	0 - One Boundary Zone for External Radiant Temperature*	0 - One Boundary Zone for Heat Flux*
SYMBOL	NENCON	NENHG	NENGE	NENRA	NENE

*Phi line separating two external boundary zones.

WORD	1	2	3	4	5	6	7	8
COLUMNS	1-10	11-20	21-30	31-40	41-50	51-60	61-70	71-80
FORMAT	F10.0	F10.0	F10.0	F10.0	F10.0	F10.0	F10.0	F10.0
CARD 10-19	0, Time, min	Coefficients for Determining Radiant Temperature of Zone 1 as a Function of Angle, Radians $T_{RAD} = A + B\phi + C\phi^2 + D\phi^3 + E\phi^4 + F \sin\phi + G \cos\phi$ (°R)						
SYMBOL	TERAD	A	B	C	D	E	F	G

WORD	1	2	3	4	5	6	7	8
COLUMNS	1-10	11-20	21-30	31-40	41-50	51-60	61-70	71-80
FORMAT	F10.0	F10.0	F10.0	F10.0	F10.0	F10.0	F10.0	F10.0
CARD (20-29)*	θ, Time, min	Coefficients for Determining Radiant Temperature of Zone 2 as a Function of Angle, Radians $T_{RAD} = A + B\phi + C\phi^2 + D\phi^3 + E\phi^4 + F \sin\phi + G \cos\phi$ (°R)						
SYMBOL	TERAD1	A	B	C	D	E	F	G

*To be used if NENRA > 0

WORD	1	2	3	4	5	6	7	8
COLUMNS	1-10	11-20	21-30	31-40	41-50	51-60	61-70	71-80
FORMAT	F10.0	F10.0	F10.0	F10.0	F10.0	F10.0	F10.0	F10.0
CARD 30-39	θ, Time, min	Coefficients for Determining External Convective Temperature for Zone 1 as a Function of Angle, Radians $T_{CON} = A + B\phi + C\phi^2 + D\phi^3 + E\phi^4 + F \sin\phi + G \cos\phi$ (°R)						
SYMBOL	TECON	A	B	C	D	E	F	G

SHEET 5

WORD	1	2	3	4	5	6	7	8
COLUMNS	1-10	11-20	21-30	31-40	41-50	51-60	61-70	71-80
FORMAT	F10.0	F10.0	F10.0	F10.0	F10.0	F10.0	F10.0	F10.0
CARD 40-49	θ, Time, min	Coefficients for Determining External Convective Temperature of Zone 2 as a Function of Angle, Radians $T_{CON} = A + B\,\phi + C\,\phi^2 + D\,\phi^3 + E\,\phi^4 + F \sin\phi + G \cos\phi$ (°R)						
SYMBOL	TECON1	A	B	C	D	E	F	G

To be used if NENCON > 0

WORD	1	2	3	4	5	6	7	8
COLUMNS	1-10	11-20	21-30	31-40	41-50	51-60	61-70	71-80
FORMAT	F10.0	F10.0	F10.0	F10.0	F10.0	F10.0	F10.0	F10.0
CARD 50-59	θ, Time, min	Coefficients for Determining F_o of Zone 1 as a Function of Angle, Radians $F_o = A + B\,\phi + C\,\phi^2 + D\,\phi^3 + E\,\phi^4 + F \sin\phi + G \cos\phi$ (Dimensionless)						
SYMBOL	GEOM	A	B	C	D	E	F	G

WORD	1	2	3	4	5	6	7	8
COLUMNS	1-10	11-20	21-30	31-40	41-50	51-60	61-70	71-80
FORMAT	F10.0	F10.0	F10.0	F10.0	F10.0	F10.0	F10.0	F10.0
CARD 60-69	θ, Time, min	Coefficients for Determining F_o of Zone 2 as a Function of Angle, Radians $F_o = A + B\,\phi + C\,\phi^2 + D\,\phi^3 + E\,\phi^4 + F \sin\phi + G \cos\phi$ (Dimensionless)						
SYMBOL	GEOM1	A	B	C	D	E	F	G

WORD	1	2	3	4	5	6	7	8
COLUMNS	1-10	11-20	21-30	31-40	41-50	51-60	61-70	71-80
FORMAT	F10.0	F10.0	F10.0	F10.0	F10.0	F10.0	F10.0	F10.0
CARD 70-79	θ, Time, min.	Coefficients for Determining External Film Coefficients of Zone 1 as a Function of Angle, Radians $h_o = A + B\phi + C\phi^2 + D\phi^3 + E\phi^4 + F \sin\phi + G \cos\phi$ (BTU/hr-ft^2-°R)						
SYMBOL	HGOS	A	B	C	D	E	F	G

WORD	1	2	3	4	5	6	7	8
COLUMNS	1-10	11-20	21-30	31-40	41-50	51-60	61-70	71-80
FORMAT	F10.0	F10.0	F10.0	F10.0	F10.0	F10.0	F10.0	F10.0
CARD 80-89	θ, Time, min	Coefficients for Determining External Film Coefficients of Zone 2 as a Function of Angle, Radians $h_o = A + B\phi + C\phi^2 + D\phi^3 + E\phi^4 + F \sin\phi + G \cos\phi$ (BTU/hr-ft^2-°R)						
SYMBOL	HGOS1	A	B	C	D	E	F	G

To be used if NENHG > 0

WORD	1	2	3	4	5	6	7	8
COLUMNS	1-10	11-20	21-30	31-40	41-50	51-60	61-70	71-80
FORMAT	F10.0	F10.0	F10.0	F10.0	F10.0	F10.0	F10.0	F10.0
CARD 90-99	θ, Time, min	Coefficients for Determining Heat Flux of Zone 1 as a Function of Angle, Radians $E = A + B\phi + C\phi^2 = D\phi^3 + E\phi^4 + F \sin\phi + G \cos\phi$ (BTU/hr-ft^2)						
SYMBOL	E	A	B	C	D	E	F	G

SHEET 7

WORD	1	2	3	4	5	6	7	8
COLUMNS	1-10	11-20	21-30	31-40	41-50	51-60	61 70	71-80
FORMAT	F10.0	F10.0	F10.0	F10.0	F10.0	F10.0	F10.0	F10.0
CARD 100-109	0, Time, min	Coefficient for Determining Heat Flux of Zone 2 as a Function of Angle, radians $F = A + B\,\phi + C\,\phi^2 + D\,\phi^3 + E\,\phi^4 + F \sin\phi + G \cos\phi$ (BTU/hr-ft^2)						
SYMBOL	E 1	A	B	C	D	E	F	G

To be used if NENE > 0

WORD	1	2	3	4	5
COLUMNS	1-5	6-10	11-15	16-20	21-25
FORMAT	I5	I5	I5	I5	I5
CARD	Code - See Sheet 8				Beginning of radial line
SYMBOL	K1	K1	K1	K1	

To be used for each point considered beginning with $\phi = 0$

WORD	1	2	3	4	5	6	7
COLUMNS	1-10	11-20	21-30	31-40	41-50	51-60	61-70
FORMAT	F10.0	F10.0	F10.0	F10.0	F10.0	F10.0	F10.0
CARD	Initial Temperature, °R	$\Delta\phi$, Forward, radians	Δr, Forward, in.	$P_{j,k}$, Polymer Fraction	$r_{j,k}$, in.	If Internal Boundary Δr for Computing Normal Derivative, in.	If Internal Boundary $\Delta\phi$ for Computing Normal Derivative, radians
SYMBOL	ALF						

To be used for each point considered beginning with $\phi = 0$

DEFINITION OF CODE WORD

WORD 1:	COLUMNS 1-5:	00000	- None of the conditions listed below
		00001	- $\phi = 0$
		00002	- $\phi = \phi$ max
WORD 2:	COLUMNS 6-10:	00000	- None of the conditions listed below
		00001	- Internal point
		00002	- Internal surface point
		00003	- Propellant-case interface
		00004	- External surface point
WORD 3:	COLUMNS 11-15:	00000	- None of the conditions listed below
		00001	- Entering propellant on constant ϕ
		00002	- Leaving propellant on constant ϕ
WORD 4:	COLUMNS 16-20:	00000	- None of the conditions listed below
		00001	- Entering propellant on constant r
		00002	- Leaving propellant on constant r
		00003	- Entering and leaving propellant on constant r

D. FLOW CHARTS

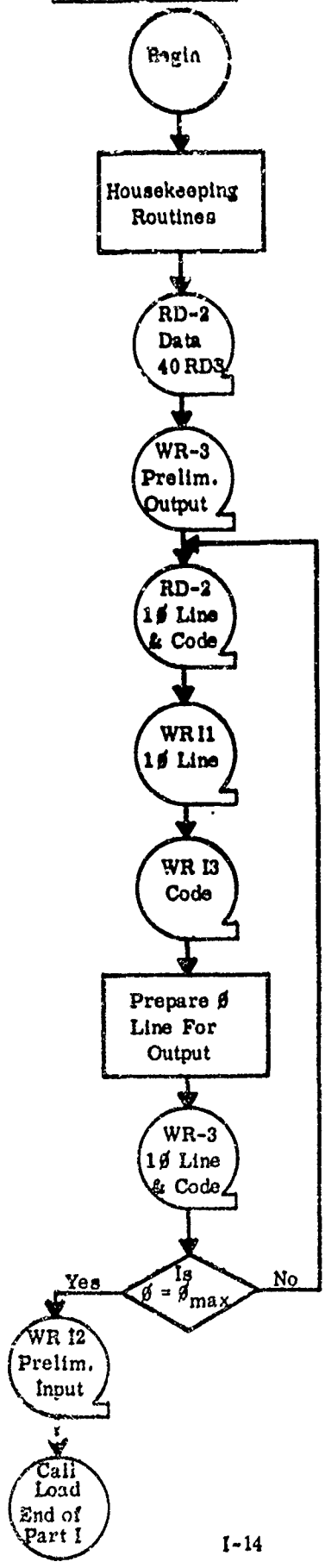

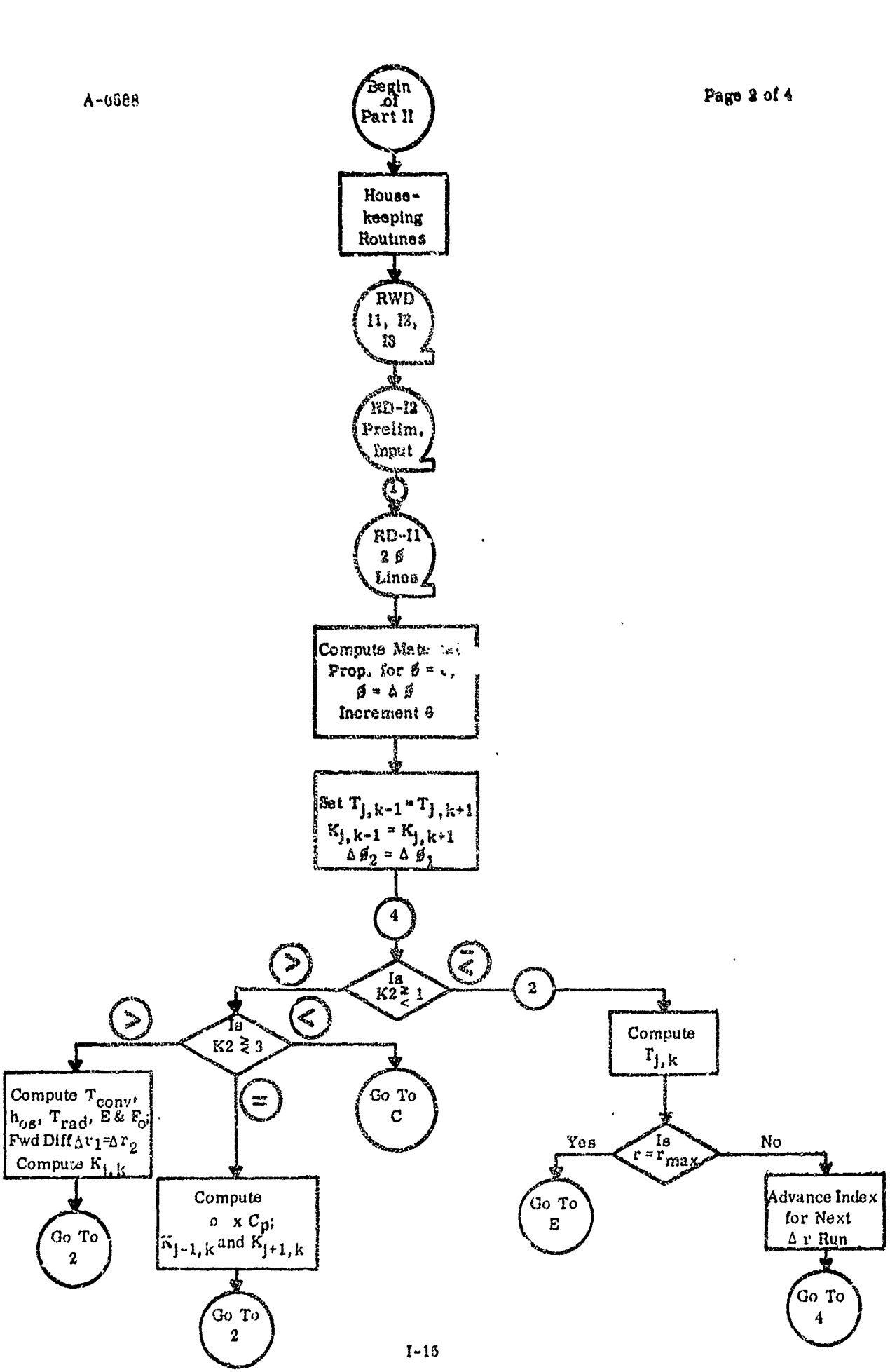
Begin of Part II
House-keeping Routines
RWD I1, I2, I3
RD-I2 Prelim. Input
1
RD-I1 2 ∅ Lines
Compute Mate... Prop. for ∅ = ..., ∅ = Δ ∅ Increment 6
Set $T_{j,k-1} = T_{j,k+1}$ $K_{j,k-1} = K_{j,k+1}$ $\Delta \emptyset_2 = \Delta \emptyset_1$
4
Is K2 ≷ 1
>
<
=
2
Is K2 ≷ 3
Compute T_{conv}, h_{os}, T_{rad}, E & F_o; Fwd Diff $\Delta r_1 = \Delta r_2$ Compute $K_{1,k}$
Go To 2
Compute ρ x C_p; $K_{j-1,k}$ and $K_{j+1,k}$
Go To 2
Go To C
Compute $T_{j,k}$
Is $r = r_{max}$
Yes
No
Go To E
Advance Index for Next Δ r Run
Go To 4

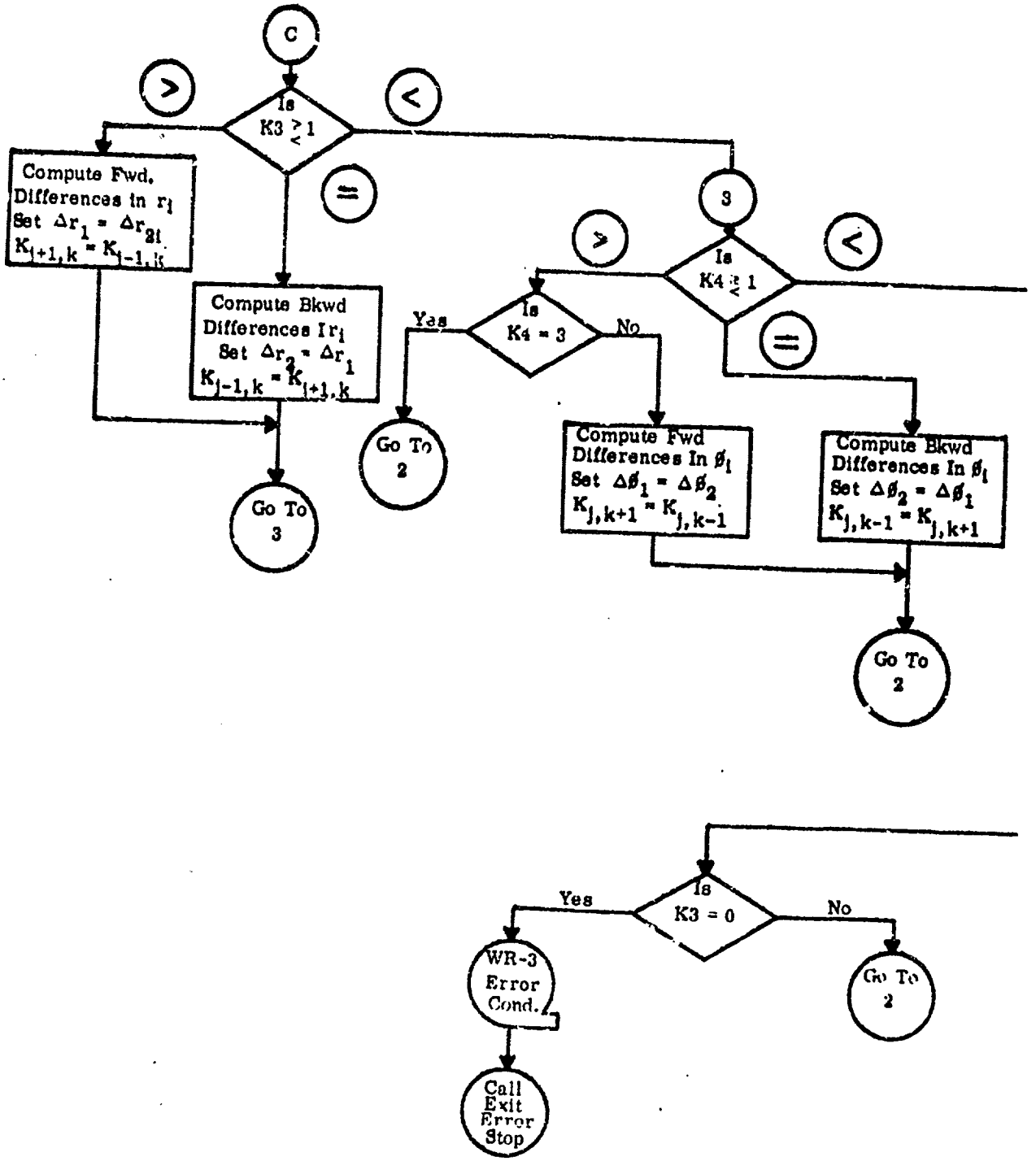
C
Is K3 ≷ 1
>
<
=
Compute Fwd. Differences In r_1
Set $\Delta r_1 = \Delta r_{21}$
$K_{j+1,k} = K_{j-1,k}$
Compute Bkwd Differences In r_1
Set $\Delta r_2 = \Delta r_1$
$K_{j-1,k} = K_{j+1,k}$
Go To 3
Go To 2
3
Is K4 ≷ 1
Is K4 = 3
Yes
No
Compute Fwd Differences In β_1
Set $\Delta\beta_1 = \Delta\beta_2$
$K_{j,k+1} = K_{j,k-1}$
Compute Bkwd Differences In β_1
Set $\Delta\beta_2 = \Delta\beta_1$
$K_{j,k-1} = K_{j,k+1}$
Go To 2
Is K3 = 0
Yes
No
WR-3 Error Cond.
Call Exit Error Stop
Go To 2

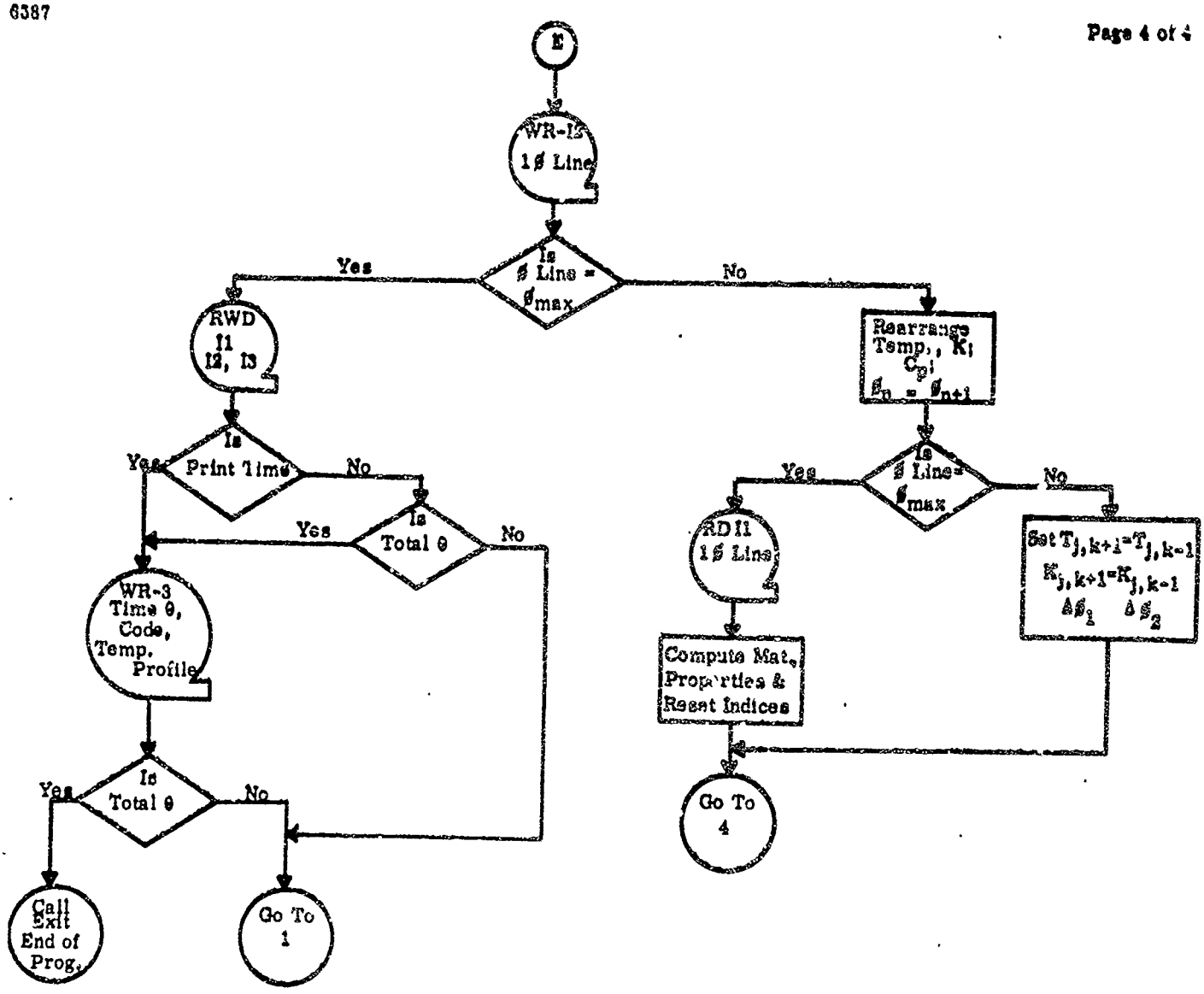
E
WR-I3
1 ϕ Line
Is
ϕ Line =
ϕmax
Yes
No
RWD
I1
I2, I3
Rearrange
Temp., Ki
Cpi
ϕn = ϕn+1
Is
Print Time
Yes
No
Is
Total θ
Yes
No
Is
ϕ Line=
ϕmax
Yes
No
WR-3
Time θ,
Code,
Temp.
Profile
RD I1
1 ϕ Line
Set Tj,k+1=Tj,k-1
Kj,k+1=Kj,k-1
Δϕ1 Δϕ2
Compute Mat.
Properties &
Reset Indices
Is
Total θ
Yes
No
Go To
4
Call
Exit
End of
Prog.
Go To
1

Two-Dimensional Heat Transfer Input Format (Revised)
CPE-70129-A

WORD	1
COLUMNS	2-72
FORMAT	1X, 14A5, A1
CARD 1	Alphabetic Information to Identify Problem.
SYMBOL	Name

WORD	1	2	3	4	5	6	7	8	9	10
COLUMNS	1-5	6-10	11-15	16-20	21-25	26-30	31-35	36-40	41-45	46-50
FORMAT	I5	I5	I5	I5	I5	I5	I5	I5	I5	I5
CARD 2	No. of Constant Radial Lines	No. of Constant circumferential Lines	No. of Printed Outputs	00000- one run 00001- more than one run	No. of Propellent bypass iterations	00000 - One Boundary Zone 000XX - Radial Line Separating Two External Boundary Zones in the following order: Radiant Temp.; Convective Temp.; Shape Factor; Film Coefficient; Heat Flux.				
SYMBOL	NENPHI	NENRAD	NENOP	NRE	NADD	NENCON	NENHG	NENGE	NENRA	NENE

WORD	1-30
COLUMNS	1-60
FORMAT	I2
CARD 3	Each word contains the beginning of each constant radial line.
SYMBOL	NPHIB (30)

WORD	1	2	3	4	5	6	7	8
COLUMNS	1-10	11-20	21-30	31-40	41-50	51-60	61-70	71-80
FORMAT	F10.0	F10.0	F10.0	F10.0	F10.0	F10.0	F10.0	F10.0
CARD 4-7	$\Delta\phi$'s, forward, for each radial line beginning with constant phi line equal to zero.							
SYMBOL	PHIL	(30)						

WORD	1	2	3	4	5	6	7	8
COLUMNS	1-10	11-20	21-30	31-40	41-50	51-60	61-70	71-80
FORMAT	F10.0	F10.0	F10.0	F10.0	F10.0	F10.0	F10.0	F10.0
CARD 8-11	Δr's, forward, for constant circumferential line equal to zero.							
SYMBOL	RIJ	(30)						

WORD	1	2	3	4	5	6	7	8
COLUMNS	1-10	11-20	21-30	31-40	41-50	51-60	61-70	71-80
FORMAT	F10.0	F10.0	F10.0	F10.0	F10.0	F10.0	F10.0	F10.0
CARD 12	Time Increment, min	Total Time, min	Density Propellant, lb/ft^3	Density Case, lb/ft^3	Gas Constant, BTU/lb-R	Heat of Polymerization, BTU/lb	Propellant Identification	Case Material Identification
SYMBOL	DELTAT	TOTI	RHOI	RHOC	R	HOP	DA(2)	DE(2)

WORD	1	2	3	4	5
COLUMNS	1-10	11-20	21-30	31-40	41-50
FORMAT	F10.0	F10.0	F10.0	F10.0	F10.0
CARD 13	A	B	C	Internal Convective Temperature, °R	Internal Film Coefficient, BTU/hr-ft^2-°R
	Experimental Constant for Heat of Polymerization				
SYMBOL	EN1	EN2	EN3	TEIN	HGC

WORD	1	2	3	4	5
COLUMNS	1-10	11-20	21-30	31-40	41-50
FORMAT	F10.0	F10.0	F10.0	F10.0	F10.0
CARD 14	Coefficients for Determining Thermal Conductivity of Propellant as a Function of Temperature, °R $[(BTU-ft)/(hr-ft^2-°R)]$ $K = PA(1) + PA(2)\,T + PA(3)\,T^2 + PA(4)\,T^3 + PA(5)\,T^4$				
SYMBOL	PA(1)	PA(2)	PA(3)	PA(4)	PA(5)

WORD	1	2	3	4	5
COLUMNS	1-10	11-20	21-30	31-40	41-50
FORMAT	F10.0	F10.0	F10.0	F10.0	F10.0
CARD 15	Coefficients for Determining Thermal Conductivity of Case Material as a Function of Temperature, °R $[(BTU-ft)/(hr-ft^2-°R)]$ $K = PB(1) + PB(2)\,T + PB(3)\,T^2 + PB(4)\,T^3 + PB(5)\,T^4$				
SYMBOL	PB(1)	PB(2)	PB(3)	PB(4)	PB(5)

WORD	1	2	3	4	5
COLUMNS	1-10	11-20	21-30	31-40	41-50
FORMAT	F10.0	F10.0	F10.0	F10.0	F10.0
CARD 16	Coefficients for Determining Specific Heat of Propellant as a Function of Temperature, °R $C_p = PC(1) + PC(2)\,T + PC(3)\,T^2 + PC(4)\,T^3 + PC(5)\,T^4$				
SYMBOL	PC (1)	PC (2)	PC (3)	PC (4)	PC (5)

WORD	1	2	3	4	5
COLUMNS	1-10	11-20	21-30	31-40	41-50
FORMAT	F10.0	F10.0	F10.0	F10.0	F10.0
CARD 17	Coefficients for Determining Specific Heat of Case Material as a Function of Temperature, °R $C_p = PD(1) + PD(2)\,T + PD(3)\,T^2 + PD(4)\,T^3 + PD(5)\,T^4$ (BTU/lb-°R)				
SYMBOL	PD (1)	PD (2)	PD (3)	PD (4)	PD (5)

WORD	1	2	3	4	5	6	7	8
COLUMNS	1-10	11-20	21-30	31-40	41-50	51-60	61-70	71-80
FORMAT	F10.0	F10.0	F10.0	F10.0	F10.0	F10.0	F10.0	F10.0
CARD 18-27	0, Time, min	Coefficients for Determining Radiant Temperature of Zone 1 as a Function of Angle, radians $T_{RAD} = A + B\phi + C\phi^2 + D\phi^3 + E\phi^4 + F \sin\phi + G \cos\phi$ (°R)						
SYMBOL		A	B	C	D	E	F	G

WORD	1	2	3	4	5	6	7	8
COLUMNS	1-10	11-20	21-30	31-40	41 50	51-60	61-70	71-80
FORMAT	F10.0	F10.0	F10.0	F10.0	F10.0	F10.0	F10.0	F10.0
CARD 28-37	θ, Time, min	Coefficients for Determining Radiant Temperature of Zone 2 as a Function of Angle, radians $T_{RAD} = A + B\phi + C\phi^2 + D\phi^3 + E\phi^4 + F \sin\phi + G \cos\phi$ (°R)						
SYMBOL		A	B	C	D	E	F	G

To be used if NENRA > 0

WORD	1	2	3	4	5	6	7	8
COLUMNS	1-10	11-20	21-30	31-40	41-50	51-60	61-70	71-80
FORMAT	F10.0	F10.0	F10.0	F10.0	F10.0	F10.0	F10.0	F10.0
CARD 38-47	θ, Time, min	Coefficients for Determining External Convective Temperature for Zone 1 as a Function of Angle, radians $T_{CON} = A + B\phi + C\phi^2 + D\phi^3 + E\phi^4 + F \sin\phi + G \cos\phi$ (°R)						
SYMBOL		A	B	C	D	E	F	G

WORD	1	2	3	4	5	6	7	8
COLUMNS	1-10	11-20	21-30	31-40	41-50	51-60	61-70	71-80
FORMAT	F10.0	F10.0	F10.0	F10.0	F10.0	F10.0	F10.0	F10.0
CARD 48-57	θ, Time, min	Coefficients for Determining External Convective Temperature of Zone 2 as a Function of Angle, radians $T_{CON} = A + B\phi + C\phi^2 + D\phi^3 + E\phi^4 + F \sin\phi + G \cos\phi$ (°R)						
SYMBOL		A	B	C	D	E	F	G

To be used if NENCON > 0

WORD	1	2	3	4	5	6	7	8
COLUMNS	1-10	11-20	21-30	31-40	41-50	51-60	61-70	71-80
FORMAT	F10.0	F10.0	F10.0	F10.0	F10.0	F10.0	F10.0	F10.0
CARD 58-67	θ, Time, min	Coefficients for Determining F_o of Zone 1 as a Function of Angle, radians $F_o = A + B\phi + C\phi^2 + D\phi^3 + E\phi^4 + F \sin \phi + G \cos \phi$ (Dimensionless)						
SYMBOL		A	B	C	D	E	F	G

WORD	1	2	3	4	5	6	7	8
COLUMNS	1-10	11-20	21-30	31-40	41-50	51-60	61-70	71-80
FORMAT	F10.0	F10.0	F10.0	F10.0	F10.0	F10.0	F10.0	F10.0
CARD 68-77	θ, Time, min	Coefficients for Determining Fo of Zone 2 as a Function of Angle, radians $F_o = A + B\phi + C\phi^2 + D\phi^3 + E\phi^4 + F \sin \phi + G \cos \phi$ (Dimensionless)						
SYMBOL		A	B	C	D	E	F	G

To be used if NENGE > 0

WORD	1	2	3	4	5	6	7	8
COLUMNS	1-10	11-20	21-30	31-40	41-50	51-60	61-70	71-80
FORMAT	F10.0	F10.0	F10.0	F10.0	F10.0	F10.0	F10.0	F10.0
CARD 78-87	θ, Time, min	Coefficients for Determining External Film Coefficients of Zone 1 as a Function of Angle, radians $h_o = A + B\phi + C\phi^2 + D\phi^3 + E\phi^4 + F \sin \phi + G \cos \phi$ (BTU/hr-ft^2-°R)						
SYMBOL		A	B	C	D	E	F	G

WORD	1	2	3	4	5	6	7	8
COLUMNS	1-10	11-20	21-30	31-40	41-50	51-60	61-70	71-80
FORMAT	F10.0	F10.0	F10.0	F10.0	F10.0	F10.0	F10.0	F10.0
CARD 88-97	0, Time, min	Coefficients for Determining External Film Coefficient of Zone 2 as a Function of Angle, radians $h_o = A + B\phi + C\phi^2 + D\phi^3 + E\phi^4 + F \sin \phi + C \cos \phi$ (BTU/hr-ft^2-°R)						
SYMBOL		A	B	C	D	E	F	G

To be used if NENHG > 0

WORD	1	2	3	4	5	6	7	8
COLUMNS	1-10	11-20	21-30	31-40	41-50	51-60	61-70	71-80
FORMAT	F10.0	F10.0	F10.0	F10.0	F10.0	F10.0	F10.0	F10.0
CARD 98-107	0, Time, min	Coefficients for Determining Heat Flux of Zone 1 as a Function of Angle, radians $E = A + B\phi + C\phi^2 + D\phi^3 + E\phi^4 + F \sin \phi + G \cos \phi$ (BTU/hr-ft^2)						
SYMBOL		A	B	C	D	E	F	G

WORD	1	2	3	4	5	6	7	8
COLUMNS	1-10	11-20	21-30	31-40	41-50	51-60	61-70	71-80
FORMAT	F10.0	F10.0	F10.0	F10.0	F10.0	F10.0	F10.0	F10.0
CARD 108-117	0, Time, min	Coefficients for Determining Heat Flux of Zone 2 as a Function of Angle, radians $E = A + B\phi + C\phi^2 + D\phi^3 + E\phi^4 + F \sin \phi + G \cos \phi$ (BTU/hr-ft^2)						
SYMBOL		A	B	C	D	E	F	G

To be used if NENE > 0

WORD	1	2	3	4	5	6	7	8	9
COLUMNS	1-5	6-10	11-15	16-20	21-30	31-40	41-50	51-60	61-70
FORMAT	I5	I5	I5	I5	F10.0	F10.0	F10.0	F10.0	F10.0
CARD	Code - See Sheet 9				Initial Temperature, °R	$P_{j,k}$, Polymer Fraction	$r_{j,k}$, in.	If Int. Boundary Δr for Computing Normal Deriv., in.	If Int Boundary $\Delta\phi$ for Computing Normal Deriv, rad.
SYMBOL	NCODE (4)				ALF				

N = Total number of points in grid.

WORD	
COLUMNS	
FORMAT	
CARD	
SYMBOL	

WORD	
COLUMNS	
FORMAT	
CARD	
SYMBOL	

DEFINITION OF CODE WORD

WORD 1:	COLUMNS 1-5:	00000 - None of the conditions listed below 00001 - $\phi' = 0$ 00002 - $\phi' = \phi$ max
WORD 2:	COLUMNS 6-10:	00000 - None of the conditions listed below 00001 - Internal point 00002 - Internal surface point 00003 - Propellant-case interface 00004 - External surface point
WORD 3:	COLUMNS 11-15:	00000 - None of the conditions listed below 00001 - Entering propellant on constant ϕ 00002 - Leaving propellant on constant ϕ
WORD 4:	COLUMNS 16-20:	00000 - None of the conditions listed below 00001 - Entering propellant on constant r 00002 - Leaving propellant on constant r 00003 - Entering and leaving propellant on constant r

APPENDIX II

ELLIPTICAL CASE, CONSTANT WEB

APPENDIX II

ELLIPTICAL CASE, CONSTANT WEB

Quite often a specific mission may require the design of a grain having a neutral trace, a high impulse, and a fairly short burn time. If, in addition, there is a low L/D requirement imposed, the problem becomes one of significantly increased complexity relative to the straightforward task of designing a straight-through star having a neutral trace. Once we become aware of the considerable influence of end effects on the motor performance characteristics, we realize that we must have a progressive head end grain design to counterbalance the inherent regressivity of the aft end. While loading density may also be a problem, we immediately realize that the elliptical case head design will be more effective than that of the spherical design, since the portion of our over-all length relegated to the head and aft ends will be considerably less when using the former. Unfortunately, we have just eliminated the end case design directly amenable to mathematical solution in closed form. Fully aware of the worth of a uniform thickness head-end web, we endeavor to find a generalized mathematical relationship between the surface which is normal to, and a fixed distance from, our elliptical case for purposes of head-end evaluation.

An iterative scheme was derived and implemented for the calculation of points on this resulting nonelliptical surface. The following is a presentation of the derivation by Mr. W. G. Andrews. For this purpose it is sufficient to consider an axial cross section, as shown in the figure that follows.

A-6601

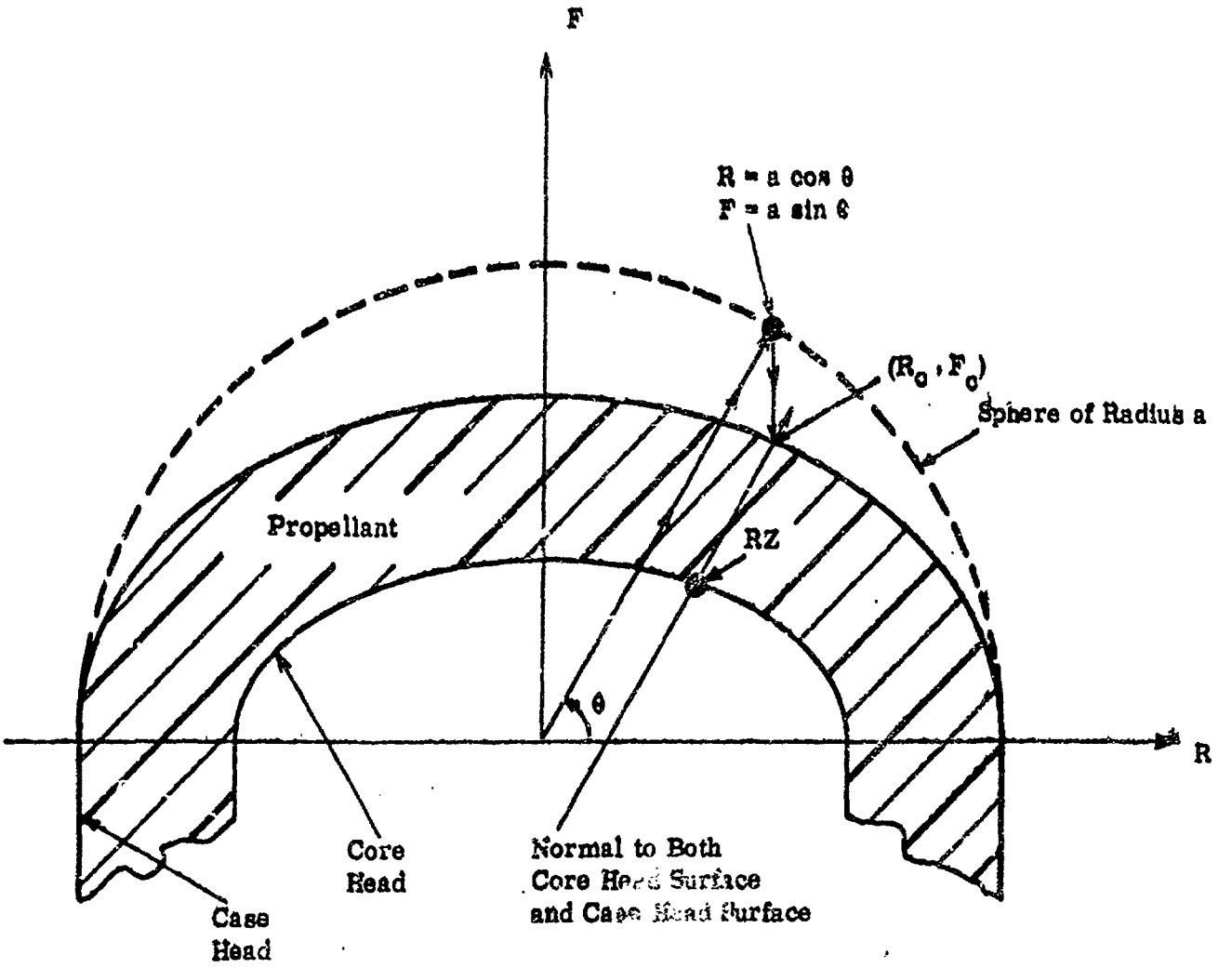

CROSS SECTION OF SOLID PROPELLANT ROCKET HEAD END
TO ILLUSTRATE MATHEMATICAL CONSTRUCTION OF A CORE HEAD SURFACE

If

$$\frac{R_c^2}{a^2} + \frac{Z_c^2}{b^2} = 1 \qquad a \geq b$$

is the elliptical case equation, then the equations of the ellipse in parametric form are given by,

$$R_c = a \cos \theta$$

$$0 \leq \theta \leq \pi$$

$$Z_c = b \sin \theta,$$

where θ is the eccentric angle of the point, $P(R_c, Z_c)$, on the ellipse.

Differentiating these parametric equations, it is seen that

$$\frac{dR_c}{d\theta} = -a \sin \theta$$

$$\frac{dZ_c}{d\theta} = b \cos \theta.$$

Hence the slope of the tangent line to the ellipse at any point $(R_c, Z_c) = (a \cos \theta, b \sin \theta)$ is given by,

$$m = \frac{dZ_c}{dR_c} = -\frac{b \cos \theta}{a \sin \theta}.$$

It follows that the slope of the normal is

$$m = \frac{a \sin \theta}{b \cos \theta}.$$

Applying the two-point slope formula

$$\frac{a \sin \theta}{b \cos \theta} = \frac{Z - b \sin \theta}{R - a \cos \theta} .$$

Let

$$\frac{R - a \cos \theta}{b \cos \theta} = \frac{Z - b \sin \theta}{a \sin \theta} = t.$$

Then

$$R - a \cos \theta = b \cos \theta \cdot t = R - R_c$$

$$Z - b \sin \theta = a \sin \theta \cdot t = Z - Z_c$$

and

$$D^2 = (Z - Z_c)^2 + (R - R_c)^2$$

$$D^2 = (a \sin \theta \cdot t)^2 + (b \cos \theta \cdot t)^2,$$

where D is the constant web thickness.

This implies that

$$t = \pm \frac{D}{(a^2 \sin^2 \theta + b^2 \cos^2 \theta)^{1/2}} .$$

Since $c^2 = a^2 - b^2$, where c is the distance from the center of the ellipse to the focus, the expression inside the radical simplifies to

$$t = \pm \frac{D}{(a^2 - c^2 \cos^2 \theta)^{1/2}} .$$

An examination of the equations,

$$R = (a + bt) \cos \theta \qquad 0 \leq \theta \leq \pi$$

$$Z = (b + at) \sin \theta$$

indicates that the minus sign in the above expression for t is applicable for the given range of θ, and in fact for $0 \leq \theta \leq 2\pi$.

It is clear that the coordinates of any point of the burning surface are given in terms of the auxiliary variable θ by the equations,

$$R = a - \frac{bD}{(a^2 - c^2 \cos^2 \theta)^{1/2}} \cos \theta$$

$$Z = b - \frac{aD}{(a^2 - c^2 \cos^2 \theta)^{1/2}} \sin \theta \,. \qquad 0 \leq \theta \leq \pi$$

It follows that any attempt to solve $R = h(\theta)$ or $Z = g(\theta)$ for θ will ultimately lead to the evaluation of a fourth degree equation in $\cos \theta$.

The preceding analysis includes the special case of the sphere ($a = b$) and it follows that analytical expressions for surface area, volume, etc., can be obtained from the parametric equations, although these expressions will in general be complex.

Implementation of the above functional relationships in the Advanced Grain Design Analysis Program was accomplished by the determination of bounding values of θ on the eccentric circle,

$$R^2 + Z^2 = a^2 \,.$$

Following the standard program technique for the analysis of the head end web surface regression pursuant to construction of a core head mesh, an initial value of R on the core head is obtained (zero initially). The angle associated with this coordinate on the eccentric circle is then determined from

$$\theta_1 = \cos^{-1}\left(\frac{R}{a}\right) \,.$$

If the R coordinate value is then incremented by a web thickness and the respective angle is evaluated from

$$\theta_2 = \cos^{-1} \frac{(R + D)}{a} ,$$

it is immediately evident that the desired angle, θ, is bounded by the relationship (see the figure on page II-2),

$$\theta_1 \geq \theta \geq \theta_2 .$$

Since the actual bounds on θ have been determined, it is an extremely simple matter to calculate the precise value of the angle, to any desired degree of accuracy, by use of the "Method of False Position" (iteration technique).

Worthy of note is the fact that in this specification of the bounds on θ in terms of the known parametric values, for complete generality the range of evaluation is an absolute minimum.

APPENDIX III

PICTORIAL DEMONSTRATION OF THE INSIGNIFICANCE OF SURFACE NORMAL BENDING RESULTING FROM A NONUNIFORM GRAIN TEMPERATURE

A-4807

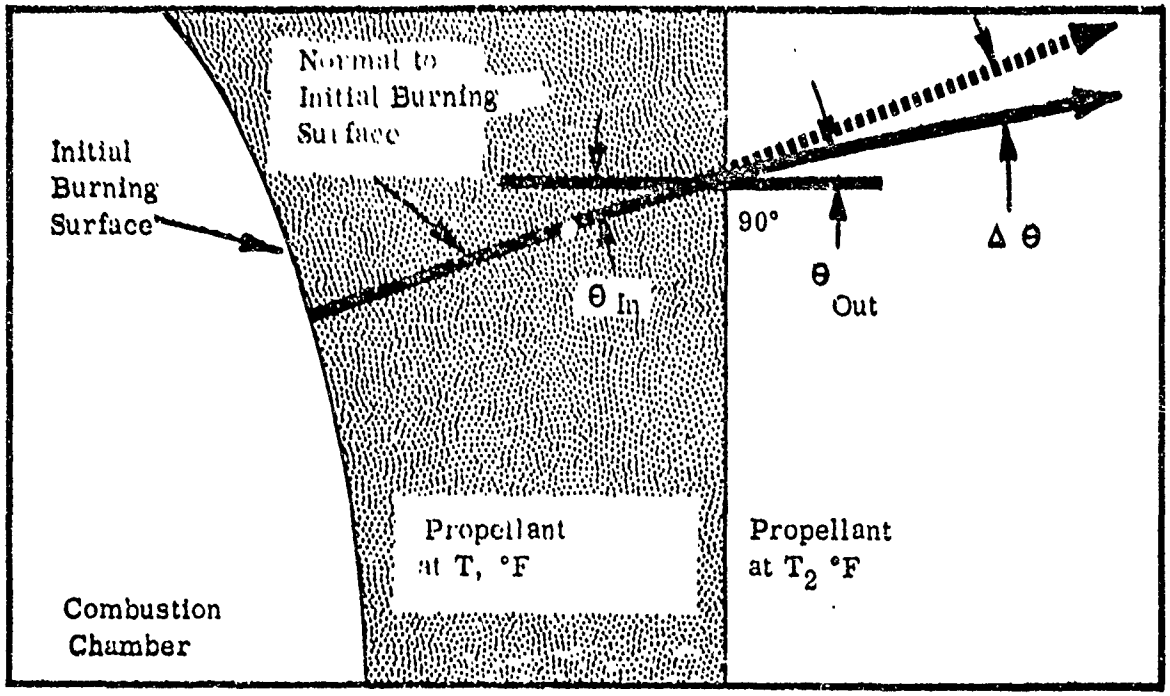

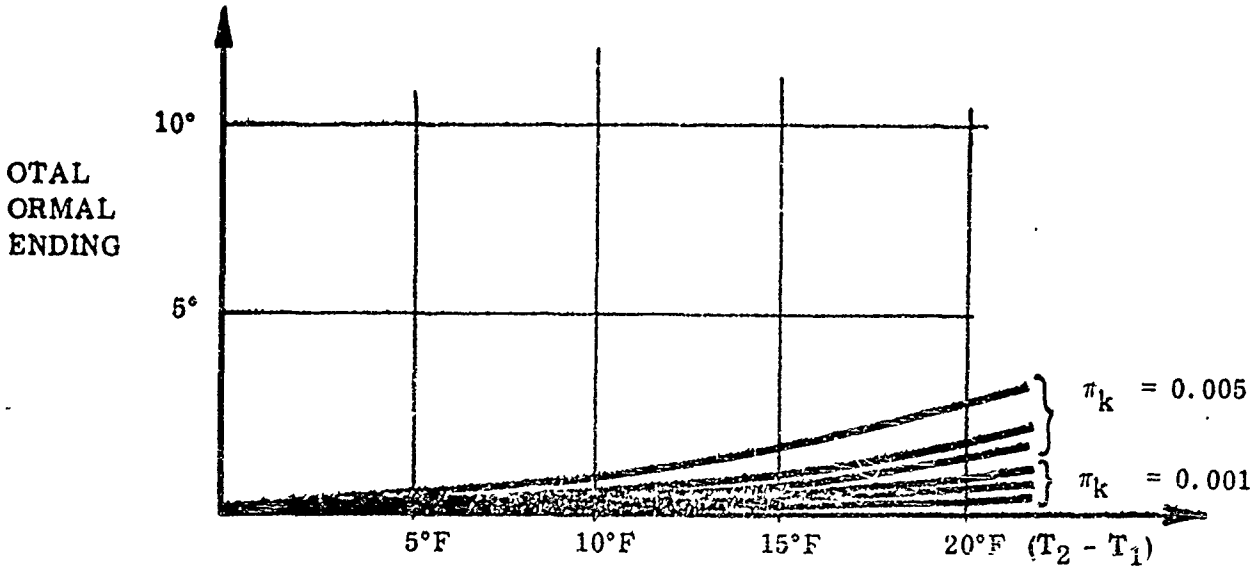

$$\left\{ \begin{matrix} \text{Total} \\ \text{Normal} \\ \text{Bending} \end{matrix} \right\}_{\Delta T} = (\Delta\Theta) = \text{Sin}^{-1} \left\{ (\text{Sin}\,\Theta_{in})\, e^{\pi_k (T_2 - T_1)} \right\} - \Theta_{in}$$

PICTORIAL DEMONSTRATION OF THE INSIGNIFICANCE OF SURFACE NORMAL BENDING RESULTING FROM A NONUNIFORM GRAIN TEMPERATURE

APPENDIX IV

DETERMINATION OF LINEAR VISCOELASTIC MODEL CONSTANTS FROM UNIAXIAL CREEP AND STRESS RELAXATION TESTS

APPENDIX IV

DETERMINATION OF LINEAR VISCOELASTIC MODEL CONSTANTS FROM UNIAXIAL CREEP AND STRESS RELAXATION TESTS

The mathematical model constants in the linear differential operator specification of time-dependent tensile stress, $\sigma(t)$, to the corresponding time-dependent tensile strain, $\epsilon(t)$,

$$\left(\sum_{i=o}^{n} P_i \frac{\partial^i}{\partial t^i}\right) \sigma(t) = \left(\sum_{i=o}^{n} Q_i \frac{\partial^i}{\partial t^i}\right) \epsilon(t) \qquad \text{(IV-1)}$$

are not available explicitly but may be obtained implicitly from experimental data in which both stress and strain are known functions of time. It is clear that (IV-1), after normalizing with respect to P_n', can be written as

$$\left[\frac{\partial^n}{\partial t^n} + P_{n-1}\frac{\partial^{n-1}}{\partial t^{n-1}} + + \ldots\ldots + P_1 \frac{\partial}{\partial t} + P_o\right] \sigma(t) =$$

$$\left[Q_n \frac{\partial^n}{\partial t^n} + Q_{n-1}\frac{\partial^{n-1}}{\partial t^{n-1}} + \ldots\ldots + Q_1 \frac{\partial}{\partial t} + Q_o\right] \epsilon(t) \qquad \text{(IV-2)}$$

In a stress relaxation test, the input strain can be characterized by a ramp type loading function (see the figure that follows) of the form

$$\epsilon(t) = A_o t - A_o (t-t_1)\, u(t-t_1) \qquad \text{(IV-3)}$$

where

$$u(t-t_1) = \begin{cases} 0 & t < t_1 \\ 1 & t \geq t_1 \end{cases}$$

Therefore, the stress-strain relationship (IV-2) may be expressed as

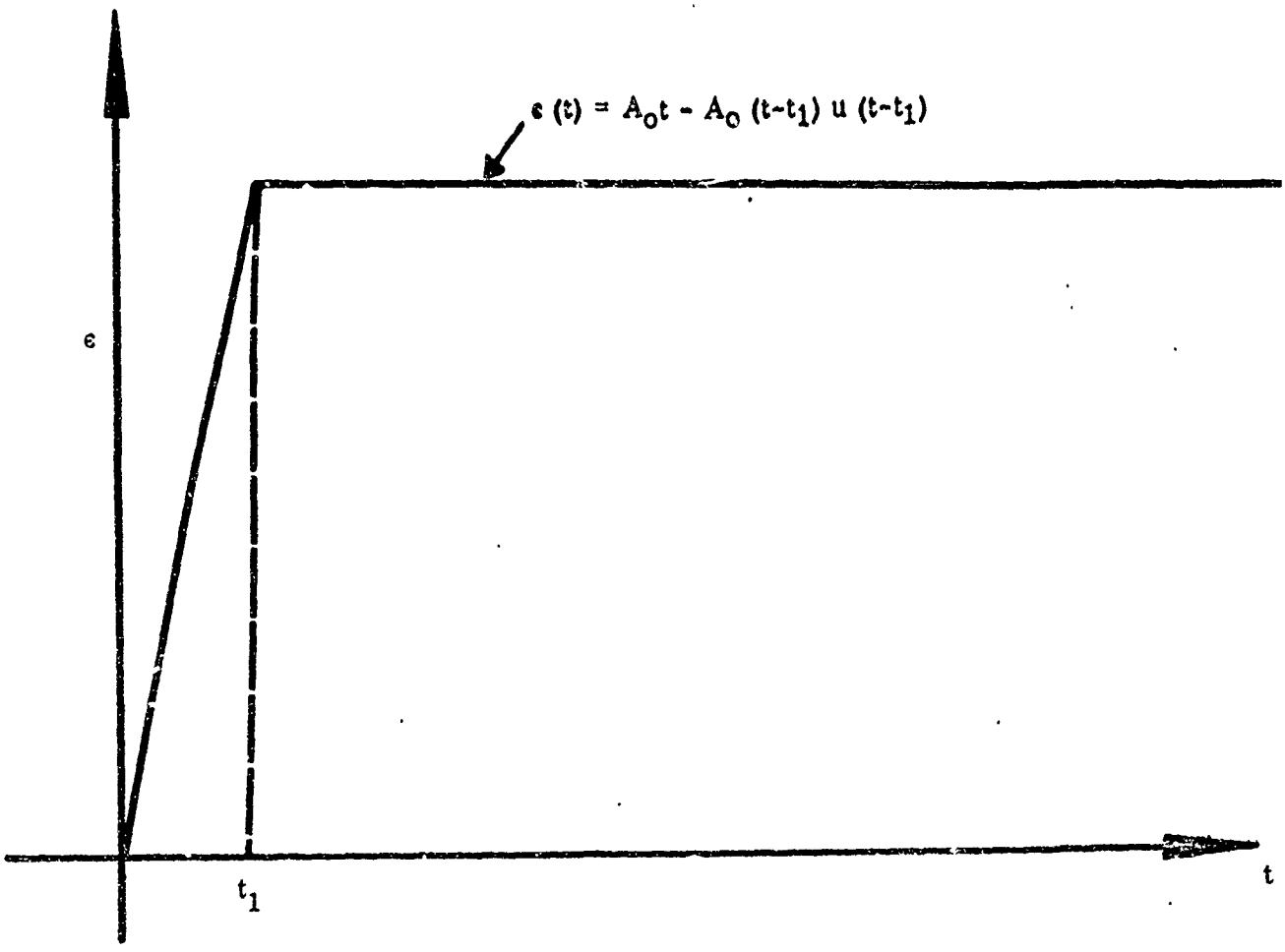

FIGURE 48. INPUT STRAIN VERSUS TIME

$$\left[\frac{\partial^n}{\partial t^n} + P_{n-1}\frac{\partial^{n-1}}{\partial t^{n-1}} + \ldots\ldots + P_1\frac{\partial}{\partial t} + P_o\right]\sigma(t) =$$

$$\left[Q_n\frac{\partial^n}{\partial t^n} + Q_{n-1}\frac{\partial^{n-1}}{\partial t^{n-1}} + \ldots\ldots + Q_1\frac{\partial}{\partial t} + Q_o\right]\left[A_o t - A_o(t-t_1)\cdot u(t-t_1)\right] \qquad \text{(IV-4)}$$

Taking the Laplace transform of (IV-4), it is clear that in s-space

$$\sigma(s) = \left[\frac{Q_n s^n + Q_{n-1}\, s^{n-1} + \ldots\, Q_1 s + Q_o}{s^n + P_{n-1}\, s^{n-1} + \ldots\, P_1 s + P_o}\right]\cdot\left[\frac{A_o}{s^2} - \frac{A_o e^{-t_1 s}}{s^2}\right] \qquad \text{(IV-5)}$$

Without loss of generality, the factors of the denominator in (IV-5) may be assumed to be linear and distinct. Therefore, since the rational function of s is proper, it may be expanded in partial fractions to give

$$\sigma(s) = A_o\left[\frac{A_{n+2}}{s^2} + \frac{A_{n+1}}{s} + \sum_{i=1}^{n}\frac{A_i}{(s+\alpha_i)}\right]\cdot\left[1 - e^{-t_1 s}\right] \qquad \text{(IV-6)}$$

The inversion of (IV-6) via contour integration yields

$$\sigma(t) = A_o\left[A_{n+2}t + A_{n+1} + A_1 e^{\alpha_1 t} + \ldots A_n e^{-\alpha_n t}\right]$$
$$-A_o\left[A_{n+2}(t-t_1) + A_{n+1} + A_1 e^{-\alpha_1(t-t_1)} + \ldots + A_n e^{-\alpha_n(t-t_1)}\right]\cdot\left[u(t-t_1)\right] \qquad \text{(IV-7)}$$

an expression for σ in time space.

If (IV-7) were fit to data obtained from a stress relaxation test, the constants α_1, A_i would be known and the model constants P_i, Q_i could be directly determined from the relations

$$\begin{aligned} P_{n-1} &= K_1^n(\alpha) \\ P_{n-2} &= K_2^n(\alpha) \\ &\vdots \\ P_{n-k} &= K_k^n(\alpha) \end{aligned} \qquad \text{(IV-8)}$$

and

$$Q_n = A_1 K_1^n (\alpha_1 = 0) + A_2 K_1^n (\alpha_2 = 0) + \ldots + A_n K_1^n (\alpha_n = 0)$$

$$\vdots$$

$$+ A_{n+1} K_1^n (\alpha) + A_{n+2} \qquad \text{(IV-9)}$$

$$Q_{n-k} = A_1 K_{k+1}^n (\alpha_1 = 0) + A_2 K_{k+1}^n (\alpha_2 = 0) + \ldots + A_n K_{k+1}^n (\alpha_n = 0)$$

$$+ A_{n+1} K_{k+1}^n (\alpha) + A_{n+2} K_k^n (\alpha)$$

where K_1^n is defined to be a function of (α) in that it is the sum of all products formed by taking the α's i at a time and multiplying them together. The above relations follow immediately when (IV-6) is cleared of fractions and the results are equated to the corresponding polynomials of s in (IV-5). For example, if n=3, then

$$P_2 = (\alpha_1 + \alpha_2 + \alpha_3)$$

$$P_1 = (\alpha_1\alpha_2 + \alpha_1\alpha_3 + \alpha_2\alpha_3) \qquad \text{(IV-10)}$$

$$P_o = (\alpha_1\alpha_2\alpha_3)$$

and

$$Q_3 = A_1 (\alpha_2 + \alpha_3) + A_2 (\alpha_1 + \alpha_3) + A_3 (\alpha_1 + \alpha_2) + A_4 (\alpha_1 + \alpha_2 + \alpha_3) + A_5$$

$$Q_2 = A_1 (\alpha_2\alpha_3) + A_2 (\alpha_1\alpha_3) + A_3 (\alpha_1\alpha_2) + A_4 (\alpha_1\alpha_2 + \alpha_1\alpha_3 + \alpha_2\alpha_3)$$

$$+ A_5 (\alpha_1 + \alpha_2 + \alpha_3) \qquad \text{(IV-11)}$$

$$Q_1 = A_4 (\alpha_1\alpha_2\alpha_3) + A_5 (\alpha_1\alpha_2 + \alpha_1\alpha_3 + \alpha_2\alpha_3)$$

$$Q_o = A_5 (\alpha_1\alpha_2\alpha_3)$$

Rocket Propulsion Laboratory, Edwards AF Base, Calif. Rpt. No. RTD-TDR-63-1049. A RESEARCH STUDY TO ADVANCE THE STATE-OF-THE-ART OF SOLID PROPELLANT GRAIN DESIGN. Summary Report, Oct 1963, 264 pp. incl. illus., tables, and appendixes, 20 refs.

Unclassified Report

A two-dimensional heat transfer analysis was developed for solid propellant motors subjected to a variety of thermal environments. Finite difference equations were developed and incorporated into a numerical solution.

1. Rocket Propellant Grains
2. Combustion
3. Programming (Computers)
4. Heat Transfer
5. Rocket Motors
6. Difference Equations
7. Stresses
8. Laboratory Equipment
9. Deformation
10. Solid Rocket Propellants
11. Design
12. Tensile Properties
13. Viscoelasticity

I. Proj. No. 3059, Task No. 30531

II. Contract AF 33(616)-6530

III. Thiokol Chemical Corp., Elkton Division, Elkton, Md.

IV. Hoebel, J.F., Thompson, R.H., Saylak, D., Andrews, W.G.

V. Secondary Report No. E62-63

VI. In DDC collection.

a advanced grain design analysis computer program at evaluates an extremely wide range of grain con- gurations has been conceived and developed.

nsile strain has been shown to affect solid propellant rning rate in a variable manner. The extent of this fluence is a function of the volumetric change under- ne during tensile deformation.

technique for structurally analyzing axisymmetric ains having arbitrary end geometries and straight- rough ports has been formulated.

Rocket Propulsion Laboratory, Edwards AF Base, Calif. Rpt. No. RTD-TDR-63-1049. A RESEARCH STUDY TO ADVANCE THE STATE-OF-THE-ART OF SOLID PROPELLANT GRAIN DESIGN. Summary Report, Oct 1963, 264 pp. incl. illus., tables, and appendixes, 20 refs.

Unclassified Report

A two-dimensional heat transfer analysis was developed for solid propellant motors subjected to a variety of thermal environments. Finite difference equations were developed and incorporated into a numerical solution

1. Rocket Propellant Grains
2. Combustion
3. Programming (Computers)
4. Heat Transfer
5. Rocket Motors
6. Difference Equations
7. Stresses
8. Laboratory Equipment
9. Deformation
10. Solid Rocket Propellants
11. Design
12. Tensile Properties
13. Viscoelasticity

I. Proj. No. 3059, Task No. 30531

II. Contract AF 33(616)-6530

III. Thiokol Chemical Corp., Elkton Division, Elkton, Md.

IV. Hoebel, J.F., Thompson, R.H., Saylak, D., Andrews, W.G.

V. Secondary Report No. E62-63

VI. In DDC collection

Rocket Propulsion Laboratory, Edwards AF Base, Calif. Rpt. No. RTD-TDR-63-1049. A RESEARCH STUDY TO ADVANCE THE STATE-OF-THE-ART OF SOLID PROPELLANT GRAIN DESIGN. Summary Report, Oct 1963, 364 pp. incl. illus., tables, and appendixes. 20 refs.

Unclassified Report

A two-dimensional heat transfer analysis was developed for solid propellant motors subjected to a variety of thermal environments. Finite difference equations were developed and incorporated into a numerical solution.

1. Rocket Propellant Grains
2. Combustion
3. Programming (Computers)
4. Heat Transfer
5. Rocket Motors
6. Difference Equations
7. Stresses
8. Laboratory Equipment
9. Deformation
10. Solid Rocket Propellants
11. Design
12. Tensile Properties
13. Viscoelasticity

I. Proj. No. 3059, Task No. 30531
II. Contract AF 33(616)-6530
III. Thiokol Chemical Corp., Elkton Division, Elkton, Md.
IV. Hoebel, J.F., Thompson, R.H., Saylak, D., Andrews, W.G.
V. Secondary Report No. E92-63
VI. In DDC collection

Rocket Propulsion Laboratory, Edwards AF Base, Calif. Rpt. No. RTD-TDR-63-1049. A RESEARCH STUDY TO ADVANCE THE STATE-OF-THE-ART OF SOLID PROPELLANT GRAIN DESIGN. Summary Report, Oct 1963, 364 pp. incl. illus., tables, and appendixes. 20 refs.

Unclassified Report

A two-dimensional heat transfer analysis was developed for solid propellant motors subjected to a variety of thermal environments. Finite difference equations were developed and incorporated into a numerical solution.

1. Rocket Propellant Grains
2. Combustion
3. Programming (Computers)
4. Heat Transfer
5. Rocket Motors
6. Difference Equations
7. Stresses
8. Laboratory Equipment
9. Deformation
10. Solid Rocket Propellants
11. Design
12. Tensile Properties
13. Viscoelasticity

I. Proj. No. 3059, Task No. 30531
II. Contract AF 33(616)-6530
III. Thiokol Chemical Corp., Elkton Division, Elkton, Md.
IV. Hoebel, J.F., Thompson, R.H., Saylak, D., Andrews, W.G.
V. Secondary Report No. E92-63
VI. In DDC collection.

n advanced grain design analysis computer program at evaluates an extremely wide range of grain configurations has been conceived and developed.

nsile strain has been shown to affect solid propellant rning rate in a variable manner. The extent of this fluence is a function of the volumetric change under-ne during tensile deformation.

technique for structurally analyzing axisymmetric ains having arbitrary end geometries and straight-rough ports has been formulated.

advanced grain design analysis computer program at evaluates an extremely wide range of grain configurations has been conceived and developed.

nsile strain has been shown to affect solid propellant rning rate in a variable manner. The extent of this fluence is a function of the volumetric change under-e during tensile deformation.

technique for structurally analyzing axisymmetric ins having arbitrary end geometries and straight-ough ports has been formulated.